A STUDY OF THE EFFECT OF MEMBRANE TARGETING ANTIMICROBIAL COMPOUNDS ON IONIC TRANSPORT ACROSS LIPID BILAYER MEMBRANES

A thesis submitted in fulfilment of the requirements for the degree of Doctor of Philosophy

University of Technology Sydney

School of Life Sciences

Faculty of Science

Thomas Berry

2021

CERTIFICATE OF ORIGINAL AUTHORSHIP

I, Thomas Berry declare that this thesis is submitted in fulfilment of the requirements for the award of Doctor of Philosophy, in the School of Life Sciences of the Faculty of Science at the University of Technology Sydney.

This thesis is wholly my own work unless otherwise reference or acknowledged. In addition, I certify that all information sources and literature used are indicated in the thesis. This document has not been submitted for qualifications at any other academic institution. This research is supported by an Australian Government Research Training Program.

Signature: Production Note: Signature removed prior to publication.

Date: 25/04/2021

Acknowledgements

First, I would like to thank my principal supervisor, Dr Charles Crandfield, for his motivation and patience towards me in my development as a researcher, commencing with him allowing me to join his research team as an intern and then seeing my potential to go further. I have appreciated his constant guidance, especially in the final stages of writing this thesis.

Second, thank you to my co-supervisor, Adjunct Professor Dr Bruce Cornell, for his support, especially during the early parts of my PhD which were spent at his lab, Surgical Diagnostics, Pty, Ltd.

I would like to express gratitude towards the people who have helped with developing my understanding of different techniques and completing the necessary experiments I have performed for this study. Thank you to Maryam Parviz for her help with the Dynamic light scattering experiments, to Rufaka Hossain for her help with the Differential scanning calorimetry experiments and to Stephen Holt and Anton LeBrun from ANSTO for their assistance with the Neutron reflectometry experiments. Additional thanks go to Stephen Holt for his help with analysing and editing the results and methods chapters of the Neutron reflectometry experiments.

A special thank you to Dr Naresh Kumar and Dr Mark Willcox from the University of New South Wales for providing the melimine peptides that were used throughout this study. Through their own research of the peptides, I was able to glean substantial insights allowing me to further understand the peptides for this study. I would also like to thank Dr Naresh Kumar and Dr Mark Willcox, along with their research groups, for allowing me to participate with them in additional research leading to the publication of a number of research articles.

I would like to thank Evelyne Deplazes, Alvaro Garcia and Paul Duckworth for the insights they provided during the many discussions of my results.

Lastly, thank you to my parents and family and friends who have supported me behind the scenes in various ways whilst undertaking this work. Their mental and emotional support has been significant in helping me to complete this research study.

Publications arising from this thesis

Berry, T., Dutta, D., Chen, R., Leong, A., Wang, H., Donald, W., Parviz, M., Cornell, B., Willcox, M., Kumar, N., Cranfield, C. G., *Lipid Membrane Interactions of the Cationic Antimicrobial Peptide Chimeras Melimine and Cys-Melimine.* Langmuir, 2018. 34(38): p. 11586-11592.

Alghalayini, A., Garcia, A., **Berry, T.**, Cranfield, C. G., *The Use of Tethered Bilayer Lipid Membranes to Identify the Mechanisms of Antimicrobial Peptide Interactions with Lipid Bilayers*. Antibiotics. 2019. 8(1): p. 12.

Other publications

Nizalapur, S., Kimyon, O., Yee, E., Ho, K., **Berry, T.**, Manefield, M., Cranfield, C. G., Willcox, M., Black, D., Kumar, N., Amphipathic guanidine-embedded glyoxamide-based peptidomimetics as novel antibacterial agents and biofilm disruptors. Organic & Biomolecular Chemistry. 2017. 15(9): p. 2033-2051.

Kuppusamy, R., Yasir, M., **Berry, T.**, Cranfield, C. G., Nizalapur, S., Yee, E., Kimyon, O., Taunk, A., Ho, K., Cornell, B., Manefield, M., Willcox, M., Black, D., Kumar, N., Design and synthesis of short amphiphilic cationic peptidomimetics based on biphenyl backbone as antibacterial agents. European Journal of Medicinal Chemistry. 2017. 143: p. 1702-1722.

Yu, T. T., Nizalapur, S., Ho, K., Yee, E., **Berry, T.**, Cranfield, C. G., Willcox, M., Black, D., Kumar, N., Design, Synthesis and Biological Evaluation of N-Sulfonylphenyl glyoxamide-Based Antimicrobial Peptide Mimics as Novel Antimicrobial Agents. ChemistrySelect. 2017. 2(12): p. 3452-3461.

Nizalapur, S., Ho, K., Kimyon, O., Yee, E., **Berry, T.**, Manefield, M., Cranfield, C. G., Willcox, M., Black, D., Kumar, N., Synthesis and biological evaluation of N-naphthoyl-phenylglyoxamide-based small molecular antimicrobial peptide mimics as novel antimicrobial agents and biofilm inhibitors. Organic & Biomolecular Chemistry. 2016. 14(14): p. 3623-3637.

Cranfield, C. G., **Berry, T.**, Holt, S., Hossain, K. R., Le Brun, A., Carne, S., Al Khamici, H., Coster, H., Valenzuela, S., Cornell, B., Evidence of the Key Role of H3O+ in Phospholipid Membrane Morphology. Langmuir. 2016. 32(41): p. 10725-10734.

Contents

Acknowledgements 3

Publications arising from this thesis 4

Other publications 4

List of Abbreviations 11

List of Figures and Tables 14

Abstract 25

1. Introduction 1

1.1 Antimicrobial Peptides 1

1.1.1 Structure of peptide antimicrobials 1

1.2 Melimine and its derivatives 5

1.2.1 Melimine 5

1.2.2 Cys-melimine 6

1.2.3 Mel4 7

1.2.4 Cys-mel4 7

1.2.5 MelAlanine 7

1.2.6 Summary of melimine and its derivatives 8

1.3 Cell membrane structures and peptide interactions 9

1.3.1 Lipid types 9

1.3.2 Membrane structure 11

1.3.2.1 Gram-positive 11

1.3.3 Interactions of peptides with lipid membranes (modes of action) 12

1.4 Understanding Lipid Membrane Morphology 19

1.4.1 Methods of Researching the Peptide-Lipid Interactions of Lipid Bilayers 21

1.4.2 Measuring bilayer properties 21

1.5 Hypotheses and Aims 34

2 Methods 36

2.1 Peptide synthesis 36

2.2 tBLMs 36

2.2.1 Cartridge assembly 36

2.2.2 Membrane deposition 38

2.2.3 Types of lipids used 39

2.3 Hydropathy Modeling 42

2.4 AC impedance 43

2.4.1 Swept frequency impedance 43

2.4.2 Testing pH effects on membranes 47

2.5 Dynamic light scattering (DLS) 48

2.6 Differential scanning Calorimetry (DSC) 50

2.6.1 DSC data acquisition 50

2.6.2 DSC Data Fitting 51

2.7 Neutron Reflectometry 53
2.7.1 Membrane measurement with PLATYPUS 53
2.7.2 Software 57
2.8 Activation energy 60
2.9 Fluorescence Membrane dipole measures 62
2.9.1 Extrusion of liposomes 62
2.9.2 Dipole potential measurements 62
2.9.3 Ratio of intensities analysis 63
3 Results 64
3.1 Melimine modelling 64
3.1.1 Melimine 64
3.1.2 Cys-melimine 67
3.1.3 Mel4 70
3.1.4 Cys-mel4 72
3.1.5 MelAlanine 74
3.2 Fluoroscopy with RH-421 dye 76
3.2.1 Melimine 76
3.2.2 Cys-melimine 80
3.2.3 Mel4 81
3.2.4 Cys-mel4 82

3.2.5 MelAlanine 83

3.3 Dynamic light scattering (DLS) 85

3.3.1 Fusogenic properties of melimine and its derivatives 85

3.4 Electrical Impedance Spectroscopy (EIS) 88

3.4.1 Melimine 88

3.4.2 Cys-melimine 91

3.4.3 Mel4 95

3.4.4 Cys-mel4 97

3.4.5 MelAlanine 100

3.4.6 Membranes with bacterial lipids 102

3.4.7 Melimine with changes in pH 108

3.5 EIS - Arrhenius plots 112

3.5.1 Melimine 112

3.5.2 Cys-melimine 113

3.5.3 Mel4 114

3.5.4 Cys-mel4 115

3.5.5 MelAlanine 116

3.6 Neutron Reflectometry 119

3.6.1 Melimine 119

3.6.2 Cys-melimine and mel4 121

3.6.3 Cys-mel4 and melAlanine 122
3.7 Differential scanning calorimetry 125
3.7.1 Melimine 125
3.7.2 Cys-melimine 127
3.7.3 Mel4 129
3.7.4 Cys-mel4 131
3.7.5 MelAlanine 133
3.7.6 Summary 136
4 Discussion 137
4.1 Melimine and its derivatives: membrane interactions 139
4.1.1 Impact of the peptide structure 139
4.1.2 Fusogenic properties 140
4.1.3 Fluorescent dipole meaurements 141
4.1.4 pH-induced membrane response 143
4.1.5 Lipid phase transition disruption 143
4.1.6 Ion traversal energy barrier of membranes 145
4.2 Model for Membrane Disruption 147
4.2.1 Membrane penetration 147
4.2.2 Peptide charge 148
4.2.3 Summary 148

4.3 Antimicrobial properties 149

5 Conclusions 150

References 152

List of Abbreviations

α-helices	alpha helices
β-sheet	beta sheets
AC	alternating current
AMP's	antimicrobial peptides
ANOVA	analysis of variance
ANSTO	Australian nuclear science and technology organisation
BLMs	black lipid membranes
CholPEG	cholesterol-pentaethyleneglycol
C_m	capacitance
CPP	critical packing parameter
C_s	counter electrode capacitor
C_{th}	tethering electrode capacitor
DLP	double-length reservoir half-membrane spanning diphytanyl ethylene glycol tethers
DLS	dynamic light scattering
DMPC	1,2-dimyristoyl-sn-glycero-3-phosphocholine
DOPC	1,2-dioleoyl-sn-glycero-3-phosphocholine
DPEPC	diphytanyldietherphosphatidylcholine
DPTL	2,3-di-O-phytanyl-sn-glycerol-1-tetraethylene glycol-DL-a-lipoic acid ester lipid

DSC	differential scanning calorimetry
EIS	electrochemical impedance spectroscopy
FminP	frequency of the minimum phase
GDPE	glyceroldiphytanylether
G_m	conductance
HPLC	high-performance liquid chromatography
KCl	potassium chloride
LPS	lipopolysaccharide
Lyso PC	1-oleoyl-2-hydroxy-sn-glycero-3-phosphocholine
MBC	minimum bactericidal concentration
MIC	minimum inhibitory concentration
NaCl	sodium chloride
NMR	nuclear magnetic resonance
OPEP	optimized potential for efficient structure prediction
PBS	phosphate-buffered saline
PC	phosphatidylcholine
PEG	poly(ethyleneglycol)
PminP	phase of the minimum phase
POPC	1-palmitoyl-2-oleoyl-sn-glycero-3-phosphocholine
POPG	1-Palmitoyl-2-oleoyl-sn-glycero-3-phosphoglycerol

Q	scattering vector
QCM-D	quartz crystal microbalance with dissipation
SA	structural alphabet
SEM	standard error of the mean
SLB	supported lipid bilayer
SLD	scattering length density
spacers	benzyl-disulfide-tetra-ethyleneglycol-OH
SPR	surface plasmon resonance
SUVs	small unilamellar vesicles
tBLMs	tethered bilayer lipid membranes
tethers	(tetra-ethyleneglycol)n=2 C20-phytanyl

Amino acids

Alanine (A)	Leucine (L)
Arginine (R)	Lysine (K)
Asparagine (N)	Proline (P)
Cysteine (C)	Serine (S)
Glutamine (Q)	Threonine (T)
Glycine (G)	Tryptophan (W)
Isoleucine (I)	Valine (V)

List of Figures and Tables

Figure 1.1.1.1: Structures of α-helical and β-sheet peptides. (Figure from Whitman, D. 2013) [15] 2

Figure 1.1.1.3: Thio-ether bridge linking two functional groups. This bridge forms a connection between two residues in a peptide, turning the peptide into a ring-like structure. R1 and R2 represent two different amino acids within the peptide sequence. 4

Figure 1.1.1.4: Peptide wheel of a cyclotide showing the disulphide of the cysteine functional groups. (Figure Ireland, D et al. 2006) [28] 4

Table 1.2: Comparison of the properties of melimine and its derivatives. 8

Figure 1.3.1.1: The headgroups of lipids containing phosphate. 10

Figure 1.3.1.2: The headgroups of lipids that do not contain phosphate moieties. 10

Figure 1.3.3: Differences between the outer membrane structures between Gram-positive and Gram-negative bacteria. A Gram-positive bacteria, seen here with the plasma membrane and peptidoglycan barrier. B Gram-negative bacteria with additional lipopolysaccharide outer membrane. (Figure from Martínez-Carmona et al. 2018) [62] 12

Figure 1.3.2.1: Barrel stave model. (Figure from Alghalayini et al. 2019) [67] Peptides insert into the membrane-like the wooden staves of a barrel. 13

Figure 1.3.2.2: Carpet model. (Figure from Alghalayini et al. 2019) [67] Peptides are accumulating on the surface of the membrane before acting in a detergent-like manner. 14

Figure 1.3.2.3: Two theories of the interdigitated peptide toroidal pore model. a) Combination of lipids and peptides within the bilayer, forming a toroidal pore. (Figure from Alghalayini et al. 2019) [67] b) Expanding toroidal pore through increasing radii and an increasing number of lipids in the pore. (Figure from Alghalayini et al. 2019) [67] 16

Figure 1.3.2.4: The critical packing parameter (CPP) model. As peptides interact and insert into the lipid bilayer, the CPP of the lipids is influenced, causing a shift of the lipids into or out of

the toroidal pores leading to changes in the radius of the pores. (Figure from Alghalayini et al. 2019) [67].....17

Figure 1.4: Representation of the critical packing parameter affecting lipid shape and bilayer formation. A Cylindrical lipid shape leading to a lipid bilayer. B Cone-like lipid structure leading to micelle formation. C Inverted cone-like lipid structure leading to hexagonal reverse micelle formation. 20

Figure 1.4.2.1: Patch clamping. An extracellular pipette is used to create a seal around a section of a cell to measure the cell's resistance. (Figure used with permission from https://www.ipmc.cnrs.fr/~duprat/neurophysiology/patch.htm, © Franck Aguila, CNRS [94]) 23

Figure 1.4.2.2: Black lipid membrane. The membrane seen here is suspended between two substrates. The residual solvent can also be seen within the newly formed membrane. (Image from https://en.wikipedia.org/wiki/Model_lipid_bilayer [95]).....23

Figure 1.4.2.1.1: Representation of a Langmuir trough. Lipids are afloat on the surface of the water in the trough, with their hydrophilic headgroups partially submerged. The hydrophobic tails, on the other hand, are extended upward away from the water's surface. By applying pressure to the lipids, a monolayer can be formed (Figure from Ndeye Rokhaya et al. 2013) [97]. 25

Figure 1.4.2.1.2: Light microscope image of the membrane formed by Tamm and McConnell. (Figure from Tamm and McConnell, 1985) [96]. In this image, the predominantly white area shows the lipid membrane and the dark circles scattered throughout show holes in the membrane where there are no lipids present.....26

Figure 1.4.2.1.3: Artistic representation of the structure of a tBLM. (Figure adapted from Cranfield et al. 2015) [101] This representation depicts a lipid bilayer formed around the ends of tethering molecules. The structure of the tethering molecules is phytanyl-terminated ethylene glycol chains, which secure the bilayer in place. One end extends into the bilayer while the other end is secured to a gold substrate via disulphide bonds. Between the tethering molecules are spacer molecules consisting of benzyl-disulfide-tetra-ethyleneglycol-OH, which provide lateral spacing between the tethering molecules. 28

Figure 1.4.2.1.4: Image by Deng *et al., 2008,* [107], showing the formation of a supported lipid bilayer (SLB) forming around cholesterol on a glass substrate with lipids from small unilamellar vesicles (SUVs). 30

Figure 2.2.1.1: Structures of the tethering and the spacer molecules. The two sulphur moieties on each compound provide the mechanism of attachment to the gold surface via sulphur-gold coordination. The benzene ring attached to the sulphur atoms provides lateral spacing between each compound. The hydrophobic phytanyl group (highlighted in red) is submerged within the lipid bilayer, tethering the membrane in place.....37

Figure 2.2.1.2: A, An assembled tBLM cartridge from both top and bottom view. Here, the gold electrodes can be seen. B, A cross-sectional cartoon view of one well within the tBLM cartridge. Here, yellow shows the location of the gold electrodes. Tether molecules adhere to the bottom gold electrode, with the lipid bilayer forming on these tethers between the two gold layers. Any added solutions flow through the cartridge from left to right in this depiction....38

Figure 2.2.3.1: Structures of the lipids used in forming many of the tBLMs in this study. This includes diphytanyldietherphosphatidylcholine (DPEPC) and glyceroldiphytanylether (GDPE). 40

Figure 2.2.3.2: Structures of other lipids used in forming membranes within tBLMs of this study. This includes 1-palmitoyl-2-oleoyl-sn-glycero-3-phosphocholine (POPC), 1-Palmitoyl-2-oleoyl-sn-glycero-3-phosphoglycerol (POPG) and Lipid A. 41

Figure 2.4.1.1: Depiction of a tBLM and an example of an equivalent circuit. (Figure from Cranfield, C.G. et al., 2014) [135] The gold and the membrane are represented by capacitors, with the membrane containing an additional resistive element. 44

Figure 2.4.1.2: The constant phase element seen with the two arrow symbols is connected in series to the resistor/capacitor network and a resistor representing the electrolyte solution. ..44

Figure 2.4.1.3: Both A and B represent typical Bode plots. A depicts a characteristic impedance versus frequency plot with a log-log scale. Changes in the slope and of these plots allow for the identification of resistive or capacitive elements across a tBLM architecture. The resistive elements have an ideal slope of ‘0’, and capacitive elements have an ideal slope of ‘-1’ [137,

138]. Changes in the slope and magnitude of the impedance plot at each frequency correlate with changes in different parts of the membrane and the two gold electrodes. These changes can be modelled using an equivalent circuit (e.g. Figure 2.4.1.1). B shows a typical phase versus frequency plot on a linear-log scale. This type of plot denotes the admittance of the system and identifies the capacitive (90° phase) and resistive (0° phase) elements of the system through comparing the phase relationship between the excitation signal and the measured response [139]. Thus, the plot allows for the identification of the membrane seen through a low phase angle due to the membrane being a bypass resistor. If a change occurs in the region of the minimum phase (depicted by a cross on the plotted curve above), a change has occurred in either the membrane conductance or capacitance and/or the tethering electrode capacitance. Horizontal shifts to the phase plot in the region of the cross denote a change in the frequency of the minimum phase (FminP); this portrays changes in G_m and/or C_m. A vertical shift indicates a change in the phase of the minimum phase (PminP), describing changes in the C_{th} and/or C_m (Figure from Cranfield et al., 2015) [140]. 46

Figure 2.5: Structure of a 1-oleoyl-2-hydroxy-sn-glycero-3-phosphocholine (Lyso PC) lipid. 48

Figure 2.6.1: Structure of 1,2-dimyristoyl-sn-glycero-3-phosphocholine (DMPC) lipid.....50

Figure 2.7.1.1: Setup of the Platypus time-of-flight neutron reflectometer. The incident beam of neutrons enters from the right, passing through the four disc choppers before reaching the sample stage and ended up at the detector. Figure from James, M. et al. [147].....53

Figure 2.7.1.2: Comparison of DOPC. A, DOPC lipid in its normal hydrogenated state. B, The hydrogens have been replaced with deuterium. 56

Figure 2.7.2: Schematic of a cross-sectional area of a tBLM, showing the separation of the layers used for the modelling of neutron scattering data for each of the lipid bilayers. 59

Figure 3.1.1.1: Local structure prediction profile for melimine. Here, the SA fragments of four amino acid residues in length showed the predictions for the structural conformations. The colours represent the three different conformations, helical conformation (red), random coil conformation (blue) and an extended (non-specific) conformation (green). Image collected using PEP-FOLD 2.0 software package [132, 159-162]. 65

Figure 3.1.1.2: Example of the model visualisation of melimine (one of 10 model outputs) A, a cartoon version of the model depicting α-helical structures. B, ball and stick model showing side amino acid chains. Image collected using PEP-FOLD 2.0 software package [132, 159-162]. 66

Figure 3.1.1.3: Depiction of the hydrophilicity and hydrophobicity of melimine [166]. The peptide has more hydrophobic residues at the N-terminus and more hydrophilic residues at the C-terminus....67

Figure 3.1.2.1: Local structure prediction profile for cys-melimine. The colours represent the three different conformations, helical conformation (red), random coil conformation (blue) and an extended (non-specific) conformation (green). Image collected using PEP-FOLD 2.0 software package [132, 159-162]....68

Figure 3.1.2.2: Example of the model visualisation of cys-melimine (one of 10 model outputs) A, a cartoon version of the model depicting α-helical structures. B, ball and stick model showing side amino acid chains. Image collected using PEP-FOLD 2.0 software package [132, 159-162]....69

Figure 3.1.2.3: Depiction of the hydrophilicity and hydrophobicity of cys-melimine [166]. .69

Figure 3.1.3.1: Local structure prediction profile for mel4. The colours represent the three different conformations, helical conformation (red), random coil conformation (blue) and an extended (non-specific) conformation (green). Image collected using PEP-FOLD 2.0 software package [132, 159-162]. 70

Figure 3.1.3.2: Example of the model visualisation of mel4 (one of 10 model outputs) A, a cartoon version of the model depicting α-helical structure. B, ball and stick model showing side amino acid chains. Image collected using PEP-FOLD 2.0 software package [132, 159-162]. 71

Figure 3.1.3.3: Depiction of the hydrophilicity and hydrophobicity of mel4 [166]. 71

Figure 3.1.4.1: Local structure prediction profile for cys-mel4. The colours represent the three different conformations, helical conformation (red), random coil conformation (blue) and an

extended (non-specific) conformation (green). Image collected using PEP-FOLD 2.0 software package [132, 159-162]. 72

Figure 3.1.4.2: Example of the model visualisation of cys-mel4 (one of 10 model outputs) A, a cartoon version of the model depicting α-helical structure. B, ball and stick model showing side amino acid chains. Image collected using PEP-FOLD 2.0 software package [132, 159-162]. 73

Figure 3.1.4.3: Depiction of the hydrophilicity and hydrophobicity of cys-mel4 [166]. 73

Figure 3.1.5.1: Local structure prediction profile for melAlanine. The colours represent the three different conformations, helical conformation (red), random coil conformation (blue) and an extended (non-specific) conformation (green). Image collected using PEP-FOLD 2.0 software package [132, 159-162]..... 74

Figure 3.1.5.2: Example of the model visualisation of melAlanine (one of 10 model outputs) A, a cartoon version of the model depicting α-helical structures. B, ball and stick model showing side amino acid chains. Image collected using PEP-FOLD 2.0 software package [132, 159-162]..... 75

Figure 3.1.5.3: Depiction of the hydrophilicity and hydrophobicity of melAlanine [166]. 75

Figure 3.2.1.1: Intensity profile of melimine and PBS at an equivalent volume. Average of five scans at a concentration of 10 μM melimine. Dotted lines show the corresponding intensities at 440 nm and 540 nm, at which where the ratios were calculated. 77

Figure 3.2.1.2: Comparison of the intensity ratios between the PBS control and melimine at increasing concentrations. Average of five scans. Error bars denote the standard deviation.. 78

Figure 3.2.1.3: Comparison of the change in the RH-421 fluorescence of melimine and its derivatives at 10 μM against a PBS control at equivalent volume. The error bars represent the standard error of the mean (SEM). One-way ANOVA was conducted determining the statistical difference in terms of a P-value. (*P<0.05, **P<0.01). 79

Figure 3.2.2: Comparison of the intensity ratios between the PBS control and cys-melimine. Average of five scans. Error bars denote the standard deviation..... 80

Figure 3.2.3: Comparison of the intensity ratios between the PBS control and mel4. Average of five scans. Error bars denote the standard deviation. 81

Figure 3.2.4: Comparison of the intensity ratios between the PBS control and mel4. Average of five scans. Error bars denote the standard deviation. 82

Figure 3.2.5: Comparison of the intensity ratios between the PBS control and mel4. Average of five scans. Error bars denote the standard deviation. 83

Table 3.2: Summary of the ANOVA analysis comparing each of the peptides to the PBS control. 84

Figure 3.3.1.1: Comparison of the size of the LysoPC lipid spheroids. The average diameters of the lipid spheroids are shown after the addition of each peptide in comparison to the diameter of lipid spheroids with no peptide. The error bars denote the standard deviation from n=15 measurements. 86

Figure 3.3.1.2: An analysis of variance (ANOVA) was undertaken on this data set, performed using Prism 7.03 (GraphPad Software Inc., La Jolla, CA) [****P-value <0.0001), ***P-value <0.001] Error bars denote the standard deviation from n = 15 measurements. 87

Table 3.4: The minimum inhibitory concentrations and the minimum bactericidal concentrations for each peptide derivative used in this study. Various strains of both Gram-positive and Gram-negative bacteria were used. (Table from Berry et al. [40]). 88

Figure 3.4.1: EIS plots for melimine in diphytanyl lipid tBLMs. A, Bode plot of before and after the addition of melimine (n = 3) showing a fit of the data points; the error bars denote the standard error of the mean (SEM) for each measurement. B, conductance response in diphytanyl lipid tBLM to the peptide melimine in diphytanyl lipid tBLM (n = 3). The error bars denote the SEM. C, capacitance response in diphytanyl lipids to the peptide melimine (n=3). The error bars denote the SEM. 90

Figure 3.4.2.1: EIS plots for cys-melimine in diphytanyl lipid tBLMs. A, Bode plot before and after the addition of cys-melimine (n = 3), showing a fit of the data points. The error bars denote the SEM. B, conductance response of diphytanyl lipids to the peptide cys-melimine (n = 3).

The error bars denote the SEM.C, capacitance response of diphytanyl lipids to the peptide cys-melimine (n = 3). The error bars denote the SEM. 92

Figure 3.4.2.2: EIS plots for cys-melimine in negatively charged tBLMs. A, Bode plot of 10% POPG tBLMs before and after the addition of cys-melimine, showing a fit of the data points. The error bars denote the SEM. B, Conductance response of varying concentrations of negatively charged POPG lipids to the peptide cys-melimine. C, Capacitance response of varying concentrations of negatively charged POPG lipids to the peptide cys-melimine. The 0% POPG and 20% POPG profiles show overlapping data points. 94

Figure 3.4.3.1: EIS plots for mel4 in diphytanyl lipid tBLMs. A, Bode plot of before and after the addition of mel4 (n = 3), showing a fit of the data points. The error bars denote the SEM. B, Conductance response of diphytanyl lipids to the peptide mel4 (n=3). The error bars denote the SEM. C, Capacitance response of diphytanyl lipids to the peptide mel4 (n=3). The error bars denote the SEM. 96

Figure 3.4.3.2: Conductance response of diphytanyl lipids to the peptide mel4 (n = 3) repeated at a higher concentration of 30 μM. The error bars denote the SEM. 97

Figure 3.4.4: EIS plots for cys-mel4 in diphytanyl lipid tBLMs. A, Bode plot of before and after the addition of cys-mel4 (n = 3), showing a fit of the data points. The error bars denote the SEM, B, Conductance response of diphytanyl lipids to the peptide cys-mel4 (n = 3). The error bars denote the SEM. C, Capacitance response of diphytanyl lipids to the peptide cys-mel4 (n = 3). The error bars denote the SEM. 99

Figure 3.4.5: EIS plots for melAlanine in diphytanyl lipid tBLMs. A, Bode plot of before and after the addition of melimine (n = 3). The error bars denote the SEM. B, Conductance response of diphytanyl lipids to the peptide melAlanine (n = 3). The error bars denote the SEM. C, Capacitance response of diphytanyl lipids to the peptide melAlanine (n = 3). The error bars denote the SEM.....101

Figure 3.4.6.1.1: EIS plots for cys-melimine in *E.coli* lipid tBLMs. A, Bode plot of before and after the addition of cys-melimine (n = 3), showing a fit of the data points. The error bars denote the SEM B, Conductance response of *E.coli* lipids to the peptide cys-melimine (n = 3). The

error bars denote the SEM. C, Capacitance response of *E.coli* lipids to the peptide cys-melimine (n=3). The error bars denote the SEM. 103

Figure 3.4.6.1.2: EIS plots for melimine in *E.coli* lipid tBLMs. A, Bode plot of before and after the addition of melimine (n = 3), ... 104

Figure 3.4.6.2.1: EIS plots for lipopolysaccharide tBLMs A, Baseline conductance of four lipopolysaccharide membranes. The variation across each well showed no repeatability. B, Bode plot of membrane 4 depicts a phase minima at high frequencies, with a fitted data curve. 106

Figure 3.4.6.2.2: A, Conductance response of Lipid A membranes to the peptide melimine. B, Capacitance response of Lipid A membranes to the peptide melimine. 108

Figure 3.4.7.1: Conductance response of melimine at pH ~ 5,7,9 in zwitterionic membranes (n = 2). The error bars denote the SEM. 109

Figure 3.4.7.2: Capacitance response of melimine at pH ~ 5,7,9 in zwitterionic membranes (n = 2). The error bars denote the SEM. 110

Figure 3.4.7.3: Conductance response of melimine at pH ~ 5,7,9 in negatively charged membranes (n = 2). 111

Figure 3.4.7.4: Capacitance response of melimine at pH ~ 5,7,9 in negatively charged membranes (n = 2). The error bars denote the SEM. 111

Figure 3.5.1: Arrhenius plot comparing diphytanyl membranes with and without 10 μM melimine. Measurements were completed in parallel, with n=3 for both sets of measurements. The error bars denote the SEM. 113

Figure 3.5.2: Arrhenius plot comparing diphytanyl membranes with and without 10 μM cys-melimine. Measurements were completed in parallel, with n=3 for both sets of measurements. The error bars denote the SEM. 114

Figure 3.5.3: Arrhenius plot comparing diphytanyl membranes with and without 10 μM mel4. Measurements were completed in parallel, n=3 for both sets of measurements. The error bars denote the SEM. 115

Figure 3.5.4: Arrhenius plot comparing diphytanyl membranes with and without 10 μM cys-mel4 comparing the natural log conductance versus the reciprocal of absolute temperature. Measurements were completed in parallel, n=3 for both sets of measurements. The error bars denote the SEM. 116

Figure 3.5.5: Arrhenius plot comparing diphytanyl membranes with and without 10 μM melAlanine. Measurements were completed in parallel, n=3 for both sets of measurements. The error bars denote the SEM. 117

Table 3.5: Percentage change of the activation energies of ion traversal after the addition of melimine and its derivatives. 118

Figure 3.6.1: Reflectivity data profiles showing the different contrast scans of melimine in D_2O and H_2O for both up spin and down spin neutron measurements. Reflectivity has been plotted against Q, the scattering vector, defined in Section 2.7.1. 120

Figure 3.6.2.1: Reflectivity data profiles showing the different contrast scans of cys-melimine in D_2O and H_2O for both up spin and down spin neutron measurements. Reflectivity has been plotted against Q, the scattering vector. 121

Figure 3.6.2.2: Reflectivity data profiles showing the different contrast scans of mel4 in D_2O and H_2O for both up-spin and down-spin neutron measurements. Reflectivity has been plotted against Q, the scattering vector. 122

Figure 3.6.3.2: Reflectivity data profiles showing the different contrast scans of melAlanine in D_2O, H_2O and GMW contrast measurements. Reflectivity has been plotted against Q, the scattering vector. 124

Figure 3.7.1.1: Thermogram of DMPC vesicles, showing an increase in the heat capacity coinciding with the pre-transition and the main phase transition. 125

Figure 3.7.1.2: Thermogram of the main phase transition of DMPC lipid vesicles with and without 10 μM melimine. 126

Figure 3.7.1.3: Thermogram of the pre-transition of DMPC lipid vesicles with and without 10 μM melimine..... 127

Figure 3.7.2.1: Thermogram of the main phase transition of DMPC lipid vesicles with and without 10 μM cys-melimine..... 128

Figure 3.7.2.2: Thermogram of the pre-transition of DMPC lipid vesicles with and without 10 μM cys-melimine. 129

Figure 3.7.3.1: Thermogram of the main phase transition of DMPC lipid vesicles with and without 10 μM mel4. 130

Figure 3.7.3.2: Thermogram of the pre-transition of DMPC lipid vesicles with and without 10 μM mel4..... 131

Figure 3.7.4.1: Thermogram of the main phase transition of DMPC lipid vesicles with and without 10 μM cys-mel4..... 132

Figure 3.7.4.2: Thermogram of the main phase transition of DMPC lipid vesicles with and without 10 μM cys-mel..... 133

Figure 3.7.5.1: Thermogram of the main phase transition of DMPC lipid vesicles with and without 10 μM melAlanine..... 134

Figure 3.7.5.2: Thermogram of the main phase transition of DMPC lipid vesicles with and without 10 μM melAlanine..... 135

Table 3.7: Summary of the enthalpies and transition temperatures of melimine and its derivatives..... 136

Table 4.1: Summary of the results in response to each peptide at 10 μM. Green boxes indicate a marked difference compared to a no-peptide control. Red boxes indicate little or no difference compared to control. 138

Abstract

The novel synthetic cationic peptide *melimine* is a chimera of two natural peptides, *melittin* and *protamine*. This peptide has a broad spectrum of antibacterial activity against both gram-positive and gram-negative bacteria while having no toxicity in mammalian cells. Melimine was initially synthesised as a coating for contact lenses as a way of reducing keratitis, inflammation of the cornea. However, its antibacterial effects also have further potential use as an antimicrobial coating for other biomaterial surfaces.

This peptide has been studied along with four peptide derivatives to determine the effects that peptide hydrophobicity, charge and size have on the peptides' antibacterial properties through studying their peptide-membrane interactions. Melimine has previously been shown to reduce the integrity of membranes, observed through the leakage of dye from bacterial membranes. The membrane-peptide interactions were compared using advanced lipid membrane biophysical techniques, including in-silico structural modelling, fluorescent membrane dipole measures, differential scanning calorimetry, neutron reflectometry, dynamic light scattering and electrical impedance spectroscopy and Arrhenius measures of their interactions with tethered bilayer lipid membranes (tBLMs).

Through analysing the results obtained from these biophysical techniques, the peptide-membrane interactions of melimine and its derivatives were compared against known modes lipid membrane interactions of antimicrobial compounds. These interactions included the barrel-stave model, carpet model, interdigitated toroidal pore model, critical packing parameter model and other surfactant-like properties. The five peptides showed minimal peptide-membrane interactions and an inability to span a lipid bilayer, leading to a postulation that these five peptides do not conform to having one of these aforementioned modes of action in killing bacteria.

The limited peptide-membrane interactions of the five cationic peptides contrast with their known antibacterial activity against bacteria. This suggests that melimine and its derivatives may interact with other components of bacterial cell membranes; this could include extracellular components, such as porin channels. This research highlights that the assumption that cationic peptides adhere to established membrane disruption models for their antimicrobial

activity requires reconsideration. This study emphasises the need for an alternative model of the antibacterial effects of cationic peptides such as melimine and its derivatives.

1. Introduction

1.1 Antimicrobial Peptides

Novel antimicrobial peptides are a strategy for new chemotherapies to counteract the increasing incidence of antimicrobial drug resistance. A significant example of this rising drug resistance is seen with penicillin. Since its discovery in 1928 by Fleming [1], and its effectiveness was proven by Florey and colleagues [2-4], penicillin has been widely used as an anti-microbial compound. However, its effectiveness, along with that of other antimicrobial analogues, has slowly been decreasing over the past 80-90 years [5-7]. Bacteria that have resistance to antibiotics were estimated to have killed 700,000 people in 2017, with predictions that this will increase [8].

An alternative to penicillin can be found in natural antibacterial compounds, in particular, antimicrobial peptides (AMP's), where these peptides are found as a part of immune defence in many species of animals [9-12]. AMPs differ from traditional antibiotics in that most AMPs target bacterial cell membranes instead of disrupting vital cell processes usually used by antibiotics, such as preventing protein synthesis within cells [13] or the inactivation of enzymes that control the production of the cell wall in gram-positive bacteria [14]. In this study, when discussing antimicrobial peptides, the specific focus was on those peptides that target membranes.

1.1.1 Structure of peptide antimicrobials

Antimicrobial peptides consist of a variety of different types of molecules. The peptides are categorised based on their atomic structure, as well as their mode of action or interactions with a lipid bilayer. Structures include the secondary peptide structures such as alpha helices (α-helices) and beta sheets (β-sheet) (Figure 1.1.1.1), as well as thio-ether rings. These structures represent the different ways in which the segments of the peptides form into three-dimensional structures with the different patterns of hydrogen bonds between the residues of the sequences.

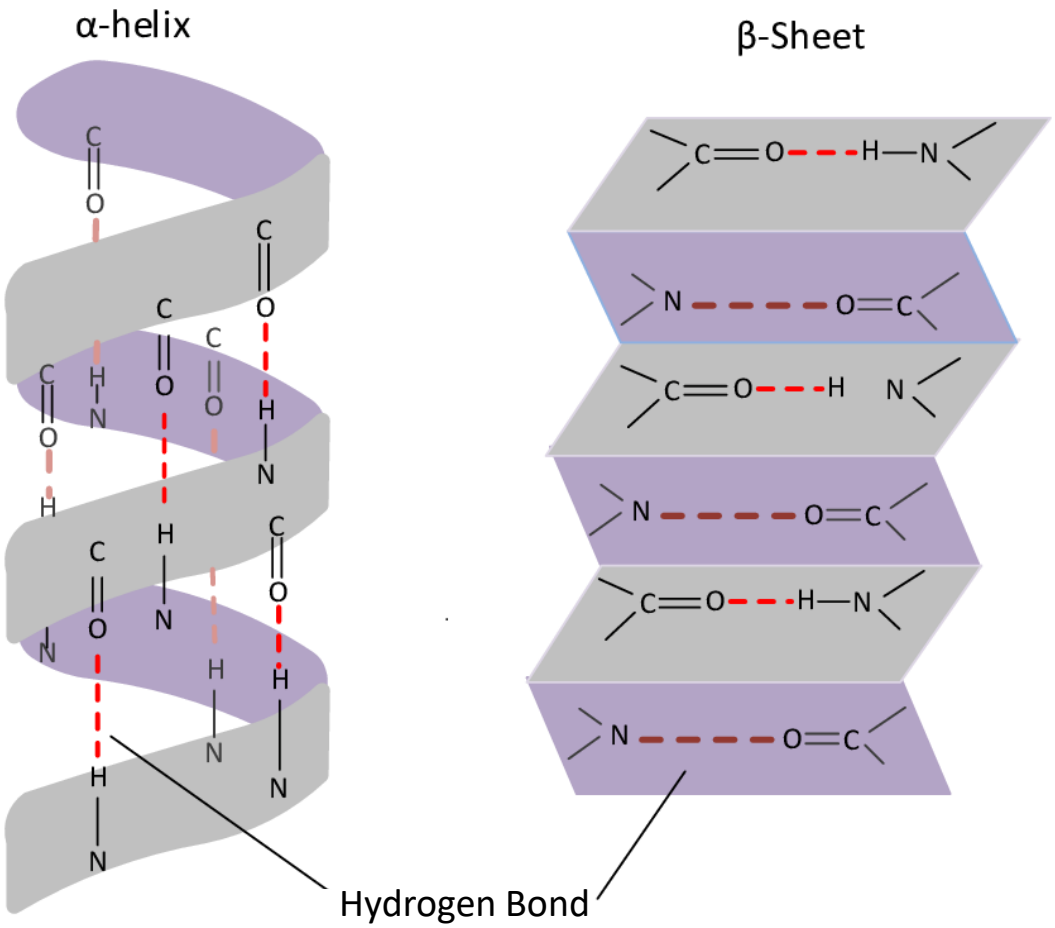

Figure 1.1.1.1: Structures of α-helical and β-sheet peptides. (Figure from Whitman, D. 2013) [15]

1.1.1.1 α-helix

The secondary structure known as an α-helix consists of a right-hand helix in which the N-H groups of the amino acids link via hydrogen bonds with the C=O groups within a neighbouring amino acid in an opposing section of the coil of the peptide chain sequence (Figure 1.1.1.1). Peptides with an α-helix structure tend to be more membrane disruptive due to their ability to traverse the hydrophobic regions of lipid bilayers [16]. In α-helical peptides, the outer regions of the helix contain amino acid residues that are either hydrophobic or hydrophilic, with one face typically being hydrophobic in nature and the other usually being hydrophilic [17]. The hydrophobic portion of the helical peptides align themselves away from the surrounding water,

facing the hydrophobic acyl chains of the lipids when interacting with lipid bilayers. This process also aligns the hydrophilic side of the helix with the water molecules surrounding the lipid bilayer [18, 19].

1.1.1.2 β-sheet

Within the β-sheet structure, the segments of the amino acid chains are stretched out, forming into β-strands. These strands form hydrogen bonds with neighbouring strands that bond laterally, which form into the β-sheet conformation, see Figure 1.1.1.1

Sidechains extending from the β-strands, containing amino acid residues, may be arranged such that the two alternate faces of the β-sheet are hydrophobic and hydrophilic. This arrangement allows for one face of the β-sheet to be more hydrophobic, with the other face being more hydrophilic [18]. This provides an advantage when interacting with a lipid bilayer, allowing it to associate with the inner core of the bilayer as well as the surrounding water molecules [20].

1.1.1.3 Thio-ether rings

Some peptides can form into ring-like structures called thio-ether rings or thio-ether bridges, sharing a common thio-ether group [21-23]. Thio-ethers are a variation of an ether, whereby it contains sulphur atoms instead of oxygen atoms between two functional groups; see Figure 1.1.1.3. These structures have been called lantibiotics and vary from other AMP's due to their specificity towards particular lipid types instead of a general attraction to a lipid bilayer surface due to electrostatic attraction. The lantibiotic *duramycin* has been shown to inhibit phospholipase A2 in lipid bilayers containing phosphatidylethanolamine lipids compared to bilayers containing phosphatidylcholine lipids [24]. The lantibiotic *nisin* has also shown a similar specificity towards lipid II. The addition of nisin caused a 50% leakage of dye in lipid vesicles containing lipid II. In contrast, in lipid vesicles that did not contain lipid II, a 50% leakage was not observed even after increasing the concentration of nisin by 1000 times [25].

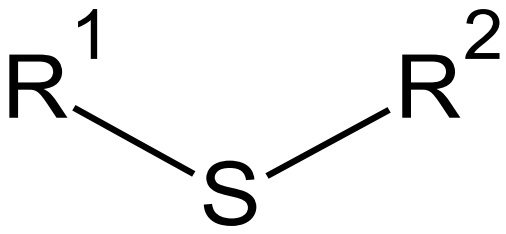

Figure 1.1.1.3: Thio-ether bridge linking two functional groups. This bridge forms a connection between two residues in a peptide, turning the peptide into a ring-like structure. R1 and R2 represent two different amino acids within the peptide sequence.

1.1.1.4 Cyclotides

Another peptide group that shares a similar structure are cyclotides, Figure 1.1.1.4. These peptides form into knotted ring-like structures that are bound together with disulphide bonds, where there are two sulfurs between the two cysteine functional groups instead of one [26, 27].

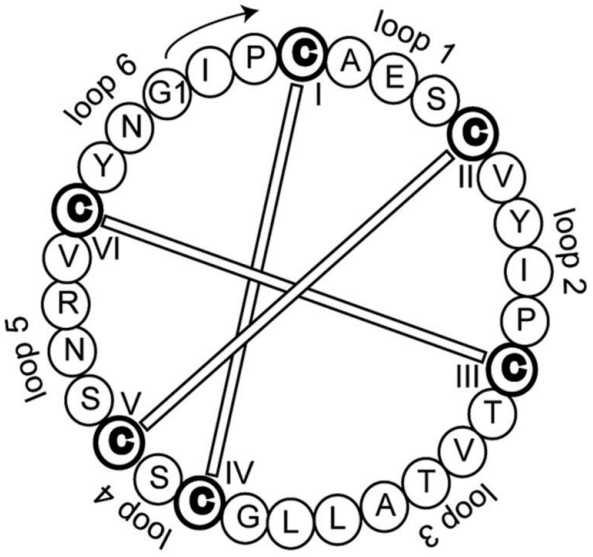

Figure 1.1.1.4: Peptide wheel of a cyclotide showing the disulphide of the cysteine functional groups. (Figure Ireland, D et al. 2006) [28]

1.2 Melimine and its derivatives

1.2.1 Melimine

The antimicrobial peptide *melimine* is a synthetic peptide [29] that is a chimera of two natural peptides, melittin and protamine. It was designed to exhibit a broad spectrum of antibacterial activity against both gram-positive and gram-negative bacteria [29]. This was observed after the addition of melimine caused a decrease in the membrane integrity of the cytoplasmic membrane, as observed through the measurement of diSC3-5 dye release in both types of bacteria [30].

This peptide is cationic and consists of 29 amino acids seen below:

T L I S W I K N K R K Q R P R V S R R R R R R G G R R R R

The arginine residues within the melimine, in particular, give it a strong positive charge, providing the peptide with a net charge of +16 at pH 7. It is believed that its positive charge encourages a stronger affinity for negatively charged bacterial membranes [31].

The C-terminus of the peptide is dominated by hydrophilic arginine residues (R). While the N-terminus of the melimine peptide has amino acids, tryptophan (W), Leucine (L) and Isoleucine (I) which all have a hydrophobic nature and these hydrophobic residues increase the likelihood of the N- terminus anchoring in a hydrophobic membrane, especially with the presence of the tryptophan [32].

While exhibiting bactericidal properties, melimine is found to not induce bacterial resistance after repeated exposure below inhibitory concentrations in both gram-positive and gram-negative bacteria [29]. Melimine has further been shown to have no toxicity in mammalian cells through its inability to cause lysis of red blood cells [29]. This peptide has also been shown to have heat stability, resulting in no change in its bactericidal ability against both gram-positive and gram-negative bacteria after autoclaving at 121^{0}C for 15 min [29].

A similar hybrid peptide has also been produced, a chimera of cecropin and melittin named CEME, which is effective against both gram-positive and gram-negative bacteria [33, 34]. Unlike CEME, the aim of melimine's development was as a coating for contact lenses to reduce keratitis, inflammation of the cornea, in humans without losing its bactericidal effects [29, 35].

It was then further shown that it might have potential use as a broad-spectrum antimicrobial coating for other biomaterial surfaces [36]. This binding was achieved through using two different types of azide linkers, namely 4-azidobenzoic acid and 4-fluoro-3-nitrophenyl azide. These two compounds promote binding between glass and melimine through amide bond formation and carbon-nitrogen bonds for each azide compound, respectively [36]. Clinical trials have subsequently been performed using melimine as an antimicrobial surface coating on contact lenses [35, 37, 38]. Findings from these trials have shown that melimine has induced corneal staining after being used to coat contact lenses [37].

From the primary melimine sequence, four other peptides have also been designed and synthesised, namely, cys-melimine, mel4, cys-mel4 and melAlanine. Each of these peptide derivatives was designed with a set role in mind. Mel4 was derived to be truncated while still maintaining a similar net charge, the two cysteine derivatives were synthesised to assist in surface attachment, and melAlanine was synthesised as a negative control peptide. The sequences of each peptide are compared below.

1.2.2 Cys-melimine

A cysteine moiety was added to the N-terminus of melimine to create *cys-melimine*.

CTLISWIKNKRKQRPRVSRRRRRRGGRRRR

This peptide was designed to increase the potential for melimine to be used as a surface binding agent through the attachment of cysteine-modified melimine on maleimide-functionalised glass [39]. This addition of cysteine also permits its use on surgical instruments such as scalpels and needles through coordination binding with metal surfaces via the thiol group of this amino acid [36].

1.2.3 Mel4

A truncated version of melimine designated *mel4* was produced, composed mostly of lysine and arginine residues [35].

KNKRKRRRRRRGGRRRR

This truncated peptide results in a relatively higher proportion of the positively charged lysine and arginine residues. It maintains a net charge close to that of melimine, allowing for similar interactions with the negatively charged bacterial membranes. This molecule was produced to identify if bactericidal effects can be maintained with a smaller peptide. Mel4 was also used in the same clinical trials as melimine [35, 37, 38]. From these clinical trials, mel- exhibited less corneal staining than melimine, possibly due to the absence of tryptophan residues [38].

1.2.4 Cys-mel4

A cysteine moiety was added to the N-terminus of mel4 to create *cys-mel4.* Similar to cys-melimine, the cysteine moiety allows for surface binding.

CKNKRKRRRRRRGGRRRR

1.2.5 MelAlanine

M*elAlanine* is of a similar size and sequence to melimine but has had six of the arginine residues replaced with alanines [40].

TLISWIKNKRKQRPRVSAAAAAAGGRRRR

This replacement of amino acid residues reduces the net charge of the peptide, permitting a comparison of the effect that the charged groups would have within the peptide.

1.2.6 Summary of melimine and its derivatives

Peptide	Size-Molecular weight (g mol^{-1})	Net charge at pH 7	Sequence
Melimine	3786.47	+16	TLISWIKNKRKQRPRVSRRRRRRGGRRRR
Cys-melimine	3889.62	+15.9	CTLISWIKNKRKQRPRVSRRRRRRGGRRRR
Mel4	2348.79	+14	KNKRKRRRRRRGGRRRR
Cys-mel4	2451.93	+13.9	CKNKRKRRRRRRGGRRRR
MelAlanine	3275.82	+10	TLISWIKNKRKQRPRVSAAAAAAGGRRRR

Table 1.2: Comparison of the properties of melimine and its derivatives.

1.3 Cell membrane structures and peptide interactions

The peptides listed in Section 1.2 were designed to have a broad spectrum antimicrobial range, targeting both gram-negative and gram-positive bacteria. This section outlines both the membrane structures these peptides are designed to target and the possible types of interactions that these peptides may have with those membranes. A variety of membranes can be found within all life, with vast differences between species. One such distinction can be found between eukaryotic membranes and bacterial membranes.

Even within the bacterial domain, the lipid constitution of membranes is not consistent within each family and species but are variable depending on environmental influences and conditions [41] such as temperature [42], salt concentration [43] and pH [44, 45].

1.3.1 Lipid types

Within bacterial lipid membranes, a variety of lipids can be found, including phospholipids, sulfolipids, glycolipids and ornithine lipids. Examples of the commonly occurring bacterial phospholipids include phosphatidylglycerol [46-48], phosphatidylinositol [49-51], phosphatidylethanolamine [47, 52, 53], phosphatidylserine, and cardiolipin [47, 54, 55] (see Figure 1.3.1.1). [46, 56-61]. Glycolipids contain a carbohydrate covalently bonded to the glycerol or sphingosine lipid backbone [41]. Sulfolipids contain a head group which possess a functional group, containing sulphur, the position of which can vary between each suflolipid type, being bound to either a carbon atom or an oxygen atom within the glycerol lipid backbone [41]. Ornithine lipids contain the amino acid ornithine as the head group connected to the glycerol lipid backbone [41] (see Figure 1.3.1.2).

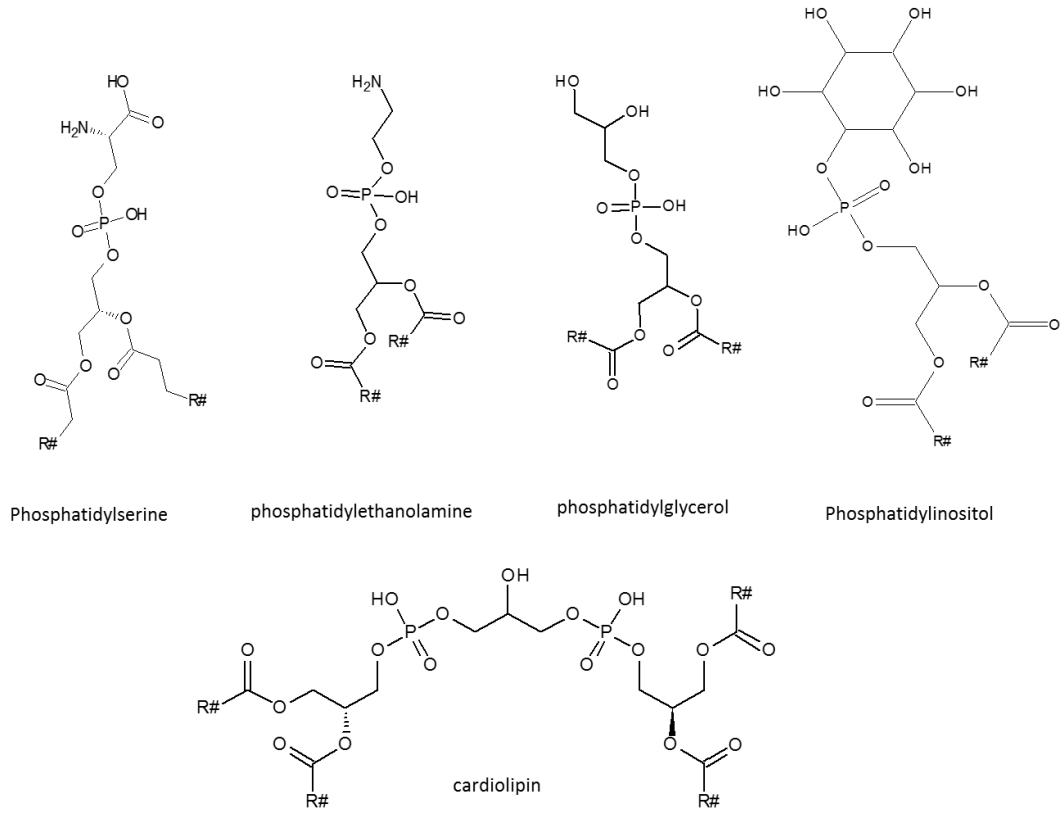

Figure 1.3.1.1: The headgroups of lipids containing phosphate.

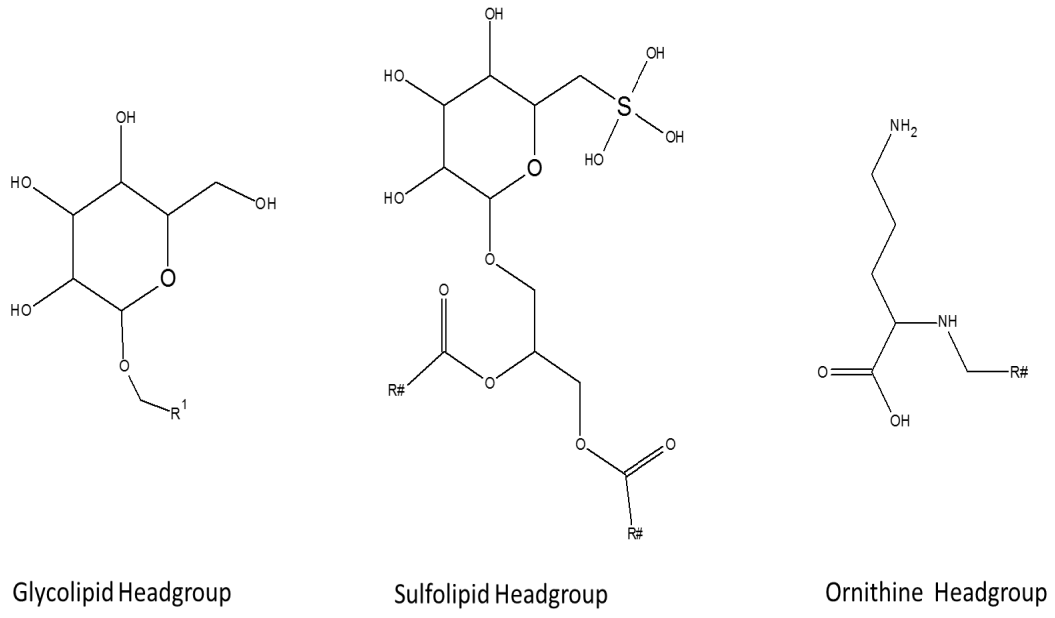

Figure 1.3.1.2: The headgroups of lipids that do not contain phosphate moieties.

1.3.2 Membrane structure

Traditionally, bacteria are divided into either gram-positive or gram-negative types based on the results of the Gram stain test. This test separates bacterial species by their intrinsic variations in the thickness of the peptidoglycan barrier and by the presence of an additional outer membrane surrounding the peptidoglycan barrier. These differences are explained in more detail in Section 1.3.3 and 1.3.4 below. In this test, a crystal violet dye is used to stain the bacteria where the peptidoglycan interacts with the dye resulting in a violet colour being produced. As Gram-positive bacteria have a more prevalent peptidoglycan layer, they are able to retain the staining dye better than Gram-negative bacteria.

1.3.2.1 Gram-positive

Within Gram-positive bacterial, there are two main membrane structures, the plasma membrane and a thick peptidoglycan barrier consisting of polymers of sugars and amino acids which helps to reinforce the cell structure, see Figure 1.3.3 A below. The peptidoglycan barrier in Gram-positive bacteria is thicker than the barrier present in Gram-negative bacteria. Interspersed in and around these layers are various teichoic acids, lipoids and peptidoglycan chains forming chelating and tethering structures, holding the membranes together.

1.3.2.2 Gram-negative

Within Gram-negative bacteria, similar structures are present. Both the plasma membrane and the peptidoglycan barrier can be found, along with the chelating and tethering structures. The presence of the peptidoglycan barrier is altered, however, as it has a decreased thickness. These types of bacteria also contain an additional outer membrane. This additional membrane is composed of various phospholipids present in both the distal and proximal leaflets. Furthermore, the distal leaflet also contains lipopolysaccharide (LPS), seen below in Figure 1.3.3 B.

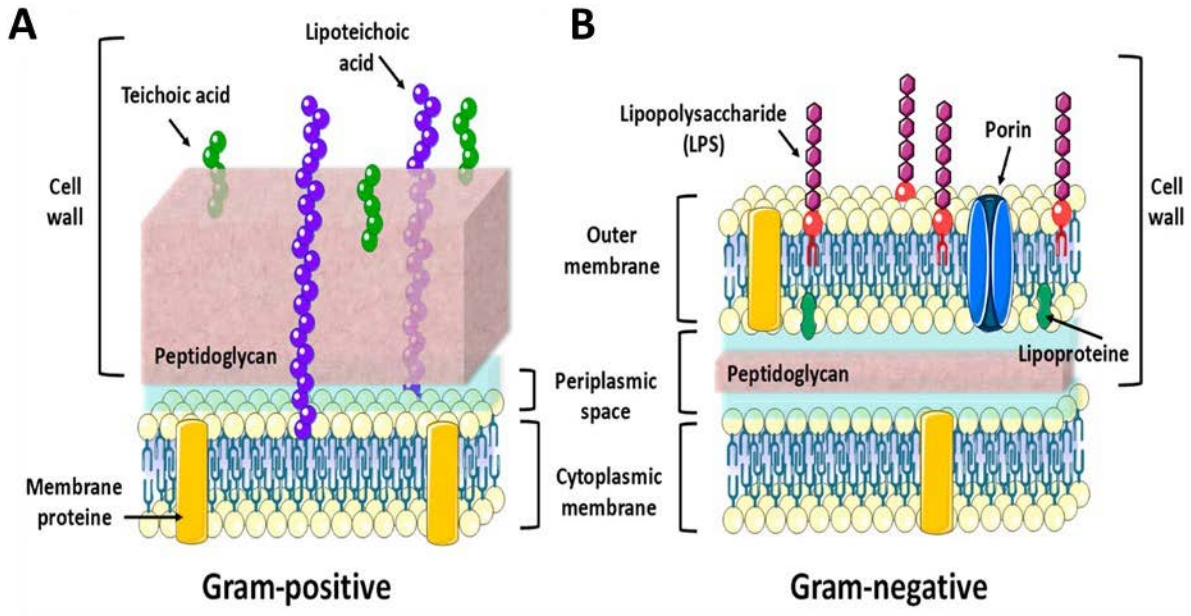

Figure 1.3.3: Differences between the outer membrane structures between Gram-positive and Gram-negative bacteria. **A** Gram-positive bacteria, seen here with the plasma membrane and peptidoglycan barrier. **B** Gram-negative bacteria with additional lipopolysaccharide outer membrane. (Figure from Martínez-Carmona et al. 2018) [62]

1.3.3 Interactions of peptides with lipid membranes (modes of action)

The mode of action of antimicrobial compounds can be separated into a variety of types, such as pore modulators, pore formers and lytic compounds [19]. Pore modulators can either affect the opening or closing of pre-existing pores within a membrane causing changes in the transport of ions across a lipid bilayer. Pore formers are able to insert into a membrane and forcefully form a pore in the surrounding lipids. Lytic compounds cause a reaction whereby rupture of the cell wall or membrane causes a disintegration of the cell. Depending on the secondary structure, the mode of action of each family of different peptides will be different, with a higher probability of membrane disruptive peptides having an α-helical secondary structure [16]. Through identifying the types of interactions that peptides have with lipid bilayers will help to develop an understanding of the mode of action of melimine and its derivatives.

1.3.3.1 Barrel stave model

The barrel stave model describes the action of groups of peptides inserting into a lipid bilayer and bundling together to create an ionic conductive pore. It has been reported that this group of peptides form clusters that resemble the wooden staves of a barrel, giving rise to its name [18, 63, 64] (Figure 1.3.2.1). This pore type was first characterised by Ehrenstein and Lecar [63] by studying amphipathic α-helical peptides, *alamethicin* and *suzukacillin*.

Barrel stave-like transmembrane pore formation involves the following steps; at first, there is a grouping of peptide monomers onto the membrane surface where the peptides form into alpha-helices upon binding with the membrane [65]. Once on the surface of the membrane, the hydrophobic regions of the peptides begin to align with the inner hydrophobic core of the lipid bilayer, and the hydrophilic regions face the surrounding water [64]. This process is then followed by the insertion of the peptide towards the hydrophobic core of the membrane, with the hydrophilic regions of the peptides forming the inner section of the pore. The insertion begins with the peptides as either monomers or grouped as oligomers [66]. As more peptides insert themselves into the membrane, the pore size is continuously increased, resulting in increased leakage of the cell contents, typically leading to cell death [19].

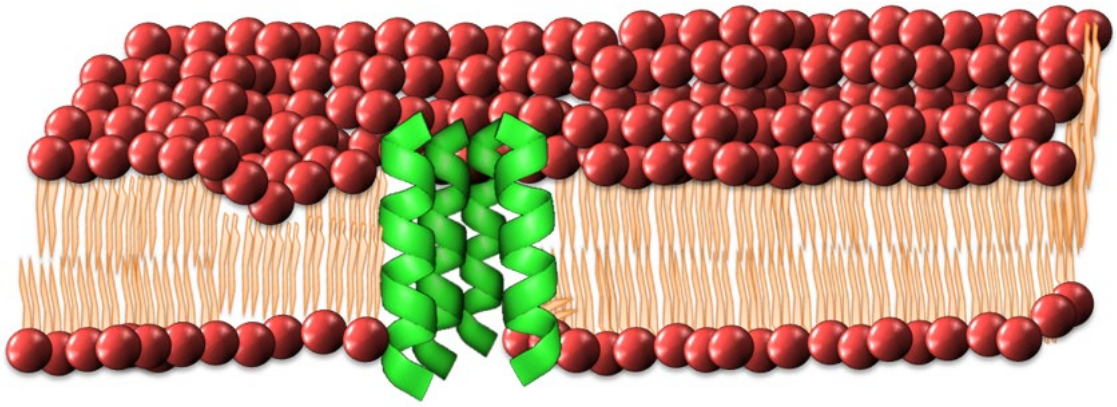

Figure 1.3.2.1: Barrel stave model. (Figure from Alghalayini et al. 2019) [67] Peptides insert into the membrane-like the wooden staves of a barrel.

1.3.3.2 Carpet model

The carpet model was first proposed by Pouny et al. [68] to describe the mode of action of a particular peptide, *dermaseptin*. This model has since been hypothesised to include various other types of peptides, including *ovispirin* and *melittin* from bee venom [18], with melittin exhibiting characteristics from both barrel stave and carpet models [18]. This model describes the accumulation of peptides at the lipid bilayer water interface adjacent to the phospholipid head groups. (Figure 1.3.2.2) This process is caused by an electrostatic attraction to the lipid head groups, whereby the peptides lie parallel to the surface [18, 19]. For these peptides, the positive charges are attracted to the negatively charged head group regions of the lipids [19]. The peptide accumulation on the surface resembles a carpet layer on the membrane surface. This carpet-like layer accumulates on the surface of the membrane until a critical concentration of peptides have been reached, whereby the peptides are thought to act in concert in a detergent-like manner, disrupting the curvature of the lipid bilayer leading to a collapse of the membrane through the formation of micelles [17].

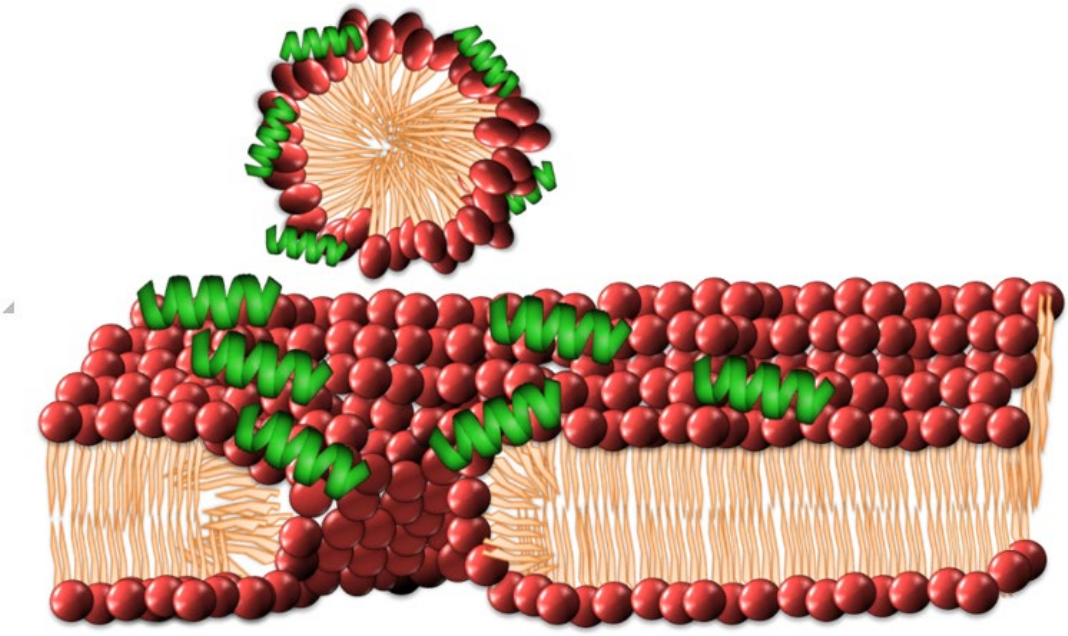

Figure 1.3.2.2: Carpet model. (Figure from Alghalayini et al. 2019) [67] Peptides are accumulating on the surface of the membrane before acting in a detergent-like manner.

1.3.3.3 Interdigitated peptide toroidal pore model

As more studies were undertaken, an increasing number of antimicrobial peptides were shown not to conform to the barrel-stave pore model, namely magainins, protegrins and melittin [64, 69-72]. An alternative method to the barrel stave pore was put forth by Matsuzaki et al. [69]. This new method branched off from the barrel-stave model. It incorporated the barrel staves as well as lipids into one structure, incorporating the existing toroidal pore structures that are already present within the membrane itself.

In this interdigitated model put forth by Matsuzaki et al. [69], the barrel-stave-like peptides are more spread out, allowing for the presence of the lipid headgroups to be present between each peptide. The lipids within the bilayer undergo random flip-flop motions, switching between the two leaflets of the bilayer, shown in Figure 1.3.2.3. When peptides insert into a lipid bilayer, the interaction between the peptides and the lipids undergoing the flip-flop motion leads to the formation of a pore that traverses the membrane. This process causes the monolayer leaflets to bend due to the intrusion of the peptides, with the lipid head groups rotating down towards the centre of the membrane. As this rotation continues, the two leaflets eventually form a continuous connection through the pore and are stabilised with both lipids and peptides. This final structure results in the peptides remaining associated with the lipid headgroups without associating with the hydrophobic chains in the membrane core [18].

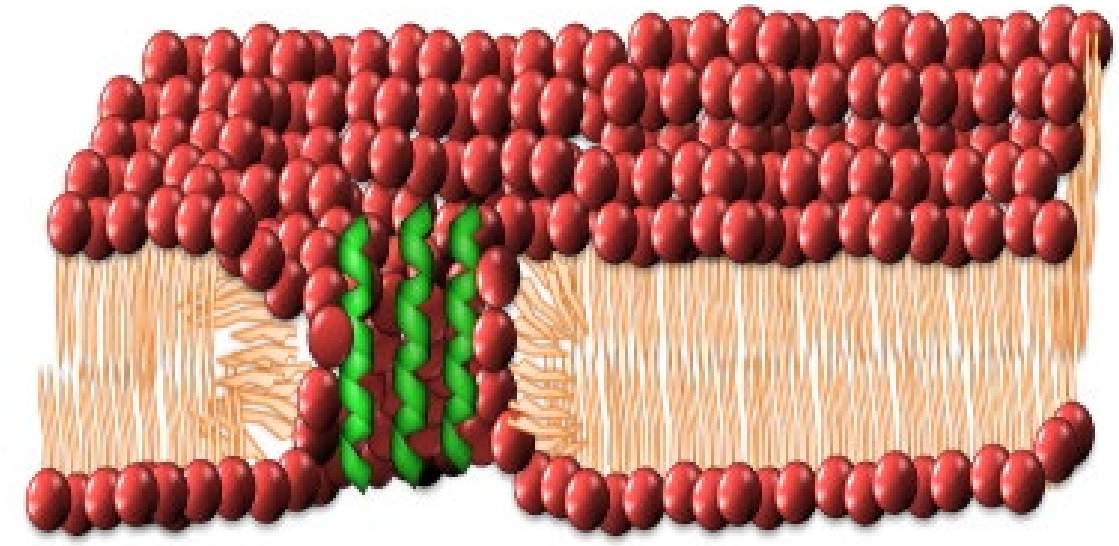

Figure 1.3.2.3: Two theories of the interdigitated peptide toroidal pore model. a) Combination of lipids and peptides within the bilayer, forming a toroidal pore. (Figure from Alghalayini et al. 2019) [67] b) Expanding toroidal pore through increasing radii and an increasing number of lipids in the pore. (Figure from Alghalayini et al. 2019) [67]

1.3.3.4 CPP model

This model describes the insertion of peptides and the interaction with the lipid bilayer through changes to the bilayer geometry where the membrane morphology or *critical packing parameter* (CPP) is altered. These changes can lead to the creation of toroidal pores or changes in the diameter of existing toroidal pores, causing an increase or decrease in membrane conduction [40, 73-75].

Due to the influence of a peptide's shape, the lipid packing is influenced in a way that disrupts the geometry of the lipids within the membrane. This geometrical change leads to an increase or decrease in the CPP of the lipids and bulk membrane. Lipids bound within a membrane do not have much additional space to move, so when the CPP of lipid decreases due to interactions with AMPs, an alternative solution is found. This packing problem of lipids can be resolved through lipids shifting into the toroidal pore regions within the membrane (see Figure 1.3.2.4).

This shift leads to a thinning of the membrane as well as an increase in the radius of the toroidal pores [40, 73]. The increase in the toroidal pore diameter would then be associated with an increase in membrane conduction.

If the insertion of the peptide causes the lipids to become more tightly packed, the CPP of the lipids increases, resulting in the lipids within the toroidal pores moving out of the curved toroidal pore regions. This movement results in a thickening of the membrane and a decrease in the toroidal pore radius, reducing the membrane conduction, see Figure 1.3.2.4. The CPP is described in more detail in Section 1.4 below.

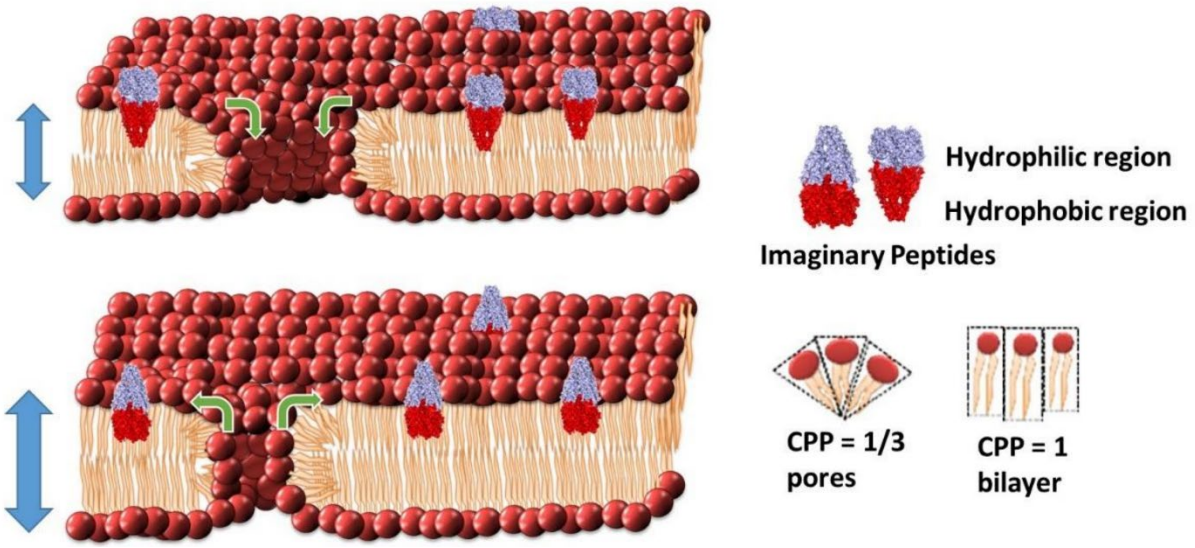

Figure 1.3.2.4: The critical packing parameter (CPP) model. As peptides interact and insert into the lipid bilayer, the CPP of the lipids is influenced, causing a shift of the lipids into or out of the toroidal pores leading to changes in the radius of the pores. (Figure from Alghalayini et al. 2019) [67]

1.3.3.5 Surfactant-like peptides

Other than causing small openings, or closing existing openings, in lipid bilayers, antimicrobial peptides are known to cause lysis or large ruptures of lipid membranes. This has been seen in many peptide types. Giacometti et al. have shown that the peptide *diptericin*, upon the interaction with *E. coli*, both the inner and the outer membranes had an increase in their permeability, resulting in lytic action [76]. The peptide *seminalplasmin*, found in bovine seminal plasma, is suspected of causing lysis through the activation of the autolysis cascade

within bacterial cells, where a response is triggered in the cell that causes its enzymes to self-digest, leading to destruction [17, 77]. Reddy et al. describe some families of natural peptides such as *defensins*, *protegrins* and *dermaseptins*; and synthetic peptides such as *metchnikowin*, *tripticin* and *drosomycin* that all have lytic properties [19]. These peptides cause lysis in various ways. For both defensins and protegrins, the mode of action that disrupts bacterial membranes leading to membrane lysis, is unknown [78, 79]. While dermaseptins cause lytic action to the lipid plasma membrane, it is believed that the process shares similarities with the carpet model [17]. Two prototypic cyclotide peptides, kalata B1 and kalata B2, cause a surfactant-like effect on lipid bilayers containing phosphatidylethanolomine-phospholipids [74]. These two peptides caused a massive alteration in the integrity of the membrane.

The surfactant-like peptides all disrupt cells and their membranes in various ways; while the lytic action is similar to peptides that conform to the carpet model, the exact processes exhibited by these peptides do not conform to the other modes of actions outlined above. As a result, these peptides may not be labelled with an exact mode of action until further research is undertaken.

1.4 Understanding Lipid Membrane Morphology

To understand the possible membrane interactions of melimine and its derivatives, a discussion of the steric properties of bilayers needs to be undertaken. For the intrinsic steric structure of lipid bilayers to be maintained, a specific spatial geometry is required. The relationship between the two main structures of a lipid, i.e., a hydrophobic region at one end of the molecule and the polar head group region, determines this geometry. This relationship was mathematically defined through the *critical packing parameter* model (CPP) proposed by Jacob Israelachvili [80].

The CPP is defined as follows:

$$\boldsymbol{CPP} = \frac{\boldsymbol{V}}{\boldsymbol{A_0 L}}.$$

In this equation, V represents the lipid molecular volume, A_0 is the molecular surface area, and L is the length of an extended hydrocarbon chain. For individual lipids, these three factors dictate the geometry a lipid will take. There are three main types of lipid aggregations; micelles, lipid bilayers, and inverted micelles [80]. If the CPP of the lipid is less than 1, the overall lipid structure might be depicted as being a cone in shape, with a larger head group tapering down towards one or two alkyl (hydrophobic) chains. Lipids with this cone-like structure will generally form into micelles (Figure 1.4 B). If the CPP is of the lipid is greater than 1, the lipid structure will appear to have an inverted cone shape, with the head group smaller than the alkyl chain(s), and will coalesce into a hexagonal reverse micelle structure. For lipids with a CPP value that is approximately 1, these lipids generally have a cylindrical structure. This structure is the most suitable for the formation of lipid bilayers (Figure 1.4 A).

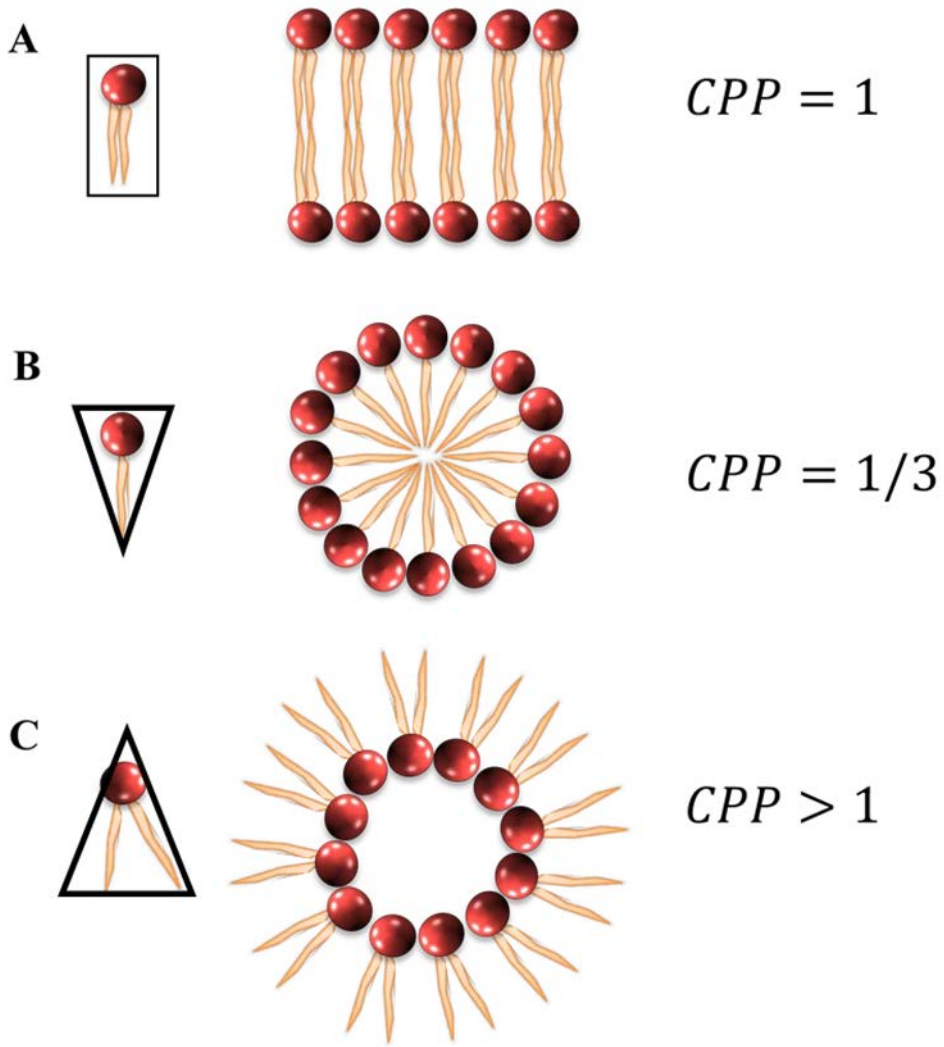

Figure 1.4: Representation of the critical packing parameter affecting lipid shape and bilayer formation. **A** Cylindrical lipid shape leading to a lipid bilayer. **B** Cone-like lipid structure leading to micelle formation. **C** Inverted cone-like lipid structure leading to hexagonal reverse micelle formation.

Recently, we published work that associates changes in a membrane's CPP with the widening of membrane defects (toroidal pores) in the membrane [73]. In this model, increasing the weighted membrane CPP would reduce the size of toroidal pores in a fashion similar to that described in Section 1.1.3.3 above, whereas lowering the overall CPP causes an increase in toroidal pore size and a subsequent increase in basal membrane conduction. Part of this project seeks to identify how and if AMPs can also alter a membrane's weighted CPP and thereby alter

the size of intrinsic membrane defects. In this project, I sought to determine whether this is the main mode-of-action for many antimicrobials.

1.4.1 Methods of Researching the Peptide-Lipid Interactions of Lipid Bilayers

Biological cell membranes are complex structures. They perform a variety of functions, from providing a barrier that blocks unwanted objects and substances interfering with cell activity, to the regulation of metabolic processes and the flow of ions into and out of the cell. These are required for the proper functioning of cellular processes. However, the fluidity and ever-changing nature of these membranes create a complex environment that makes their interactions with proteins, peptides, hormones and the like challenging to study. Current methods for researching lipid membranes include black lipid membranes, patch-clamp electrophysiology, liposomes assays, and tethered bilayer lipid membranes (tBLMs) [81-84].

1.4.2 Measuring bilayer properties

The study of lipid bilayers over the last 80 years has had many advances. Changes and advancements in the characterisation methods have added to this knowledge. The advancements have built upon the understanding of lipid bilayer shape and size of bilayers as well as the structure of lipids. In the pioneering works of Katherine Blodgett and Irving Langmuir in synthesising monolayers of fatty acids onto existing substrates, a doorway was opened into the synthesis of monolayers [85, 86]. From these simplified monolayers, the next step has been to synthesise and recreate cell membranes to produce a product that contains all the physical properties of a cell membrane while reducing the complexities without detracting from the inherent properties exhibited within cells. This process of monolayer synthesis, by Blodgett, now referred to as Langmuir Blodgett films, in itself allowed for firsthand knowledge into lipid film behaviour. However, the technique is hampered, as there is often a low reproducibility, and defects can readily appear in the lipid films produced [87].

Following on from the work of Langmuir and Blodgett were various techniques used to study *bilayer* membranes. One such method was to study liposomes. Liposomes consist of a lipid membrane closed off into a sphere, which encapsulates a small volume of the surrounding

solution [88]. Due to their lipid structure, the liposomes may have chemical or physical instabilities [89]. Their chemical instability is due to the potential hydrolysis of the ester bonds within the lipid structure or the oxidation of unsaturated acyl chains. In some liposome-release assays, a self-quenching fluorescent dye is loaded into the liposome and, upon its release via the actions of a membrane altering drug or chemical, the overall fluorescence of the solution is increased. However, the physical instability is apparent in premature dye leakage from their inner volume when used for drug testing or through aggregation and fusion into larger liposomes [89]. These limitations do not allow for ease of study in comparison to other cell membrane techniques [90].

Another method of studying lipid membranes is through the technique of *patch-clamp electrophysiology*. This involves using an extracellular pipette to create a seal around a small section of a cell membrane [91] (Figure 1.4.2.1). This process results in a seal that has a resistance of 10-100 gigaOhms that can be measured in real-time. The resistance of the seal depends on small variations and dislocations within the membrane that can lead to a variance in the resistance of the seal. If this resistance is too low, there is greater background noise interference during measurements [92]. There are further limitations to this sealing process whereby obtaining a proper seal is affected by the cleanliness of the pipette tip as well as air remaining in the tip during the sealing process. The membrane patch is also easy to rupture due to improper handling of the pipette during measurements, and there are often leaks that occur around the pipette seal [93].

Black lipid membranes (BLMs) are stable artificial membranes that appear as black or grey in optical images due to their inherent thinness, which is of the order of a few nanometers (Figure 1.4.2.2) [84]. The general make-up of these membranes varies from one to another due to inconsistencies during the formation process. Furthermore, a residual solvent can linger in the BLMs once they are formed, and this can alter intrinsic membrane properties can lead to inconsistencies in the acquired data [84].

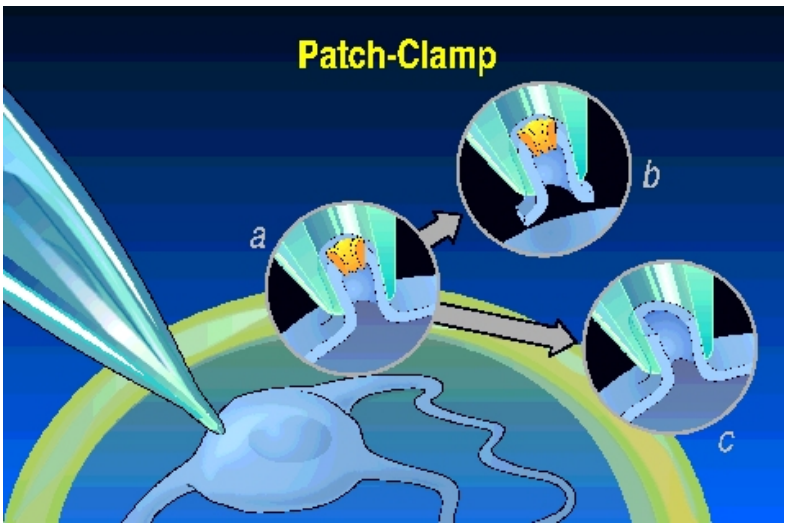

Figure 1.4.2.1: Patch clamping. An extracellular pipette is used to create a seal around a section of a cell to measure the cell's resistance. (Figure used with permission from https://www.ipmc.cnrs.fr/~duprat/neurophysiology/patch.htm, © Franck Aguila, CNRS [94])

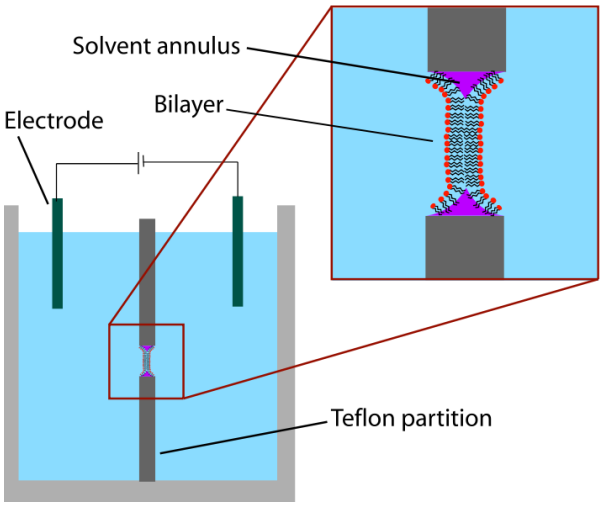

Figure 1.4.2.2: Black lipid membrane. The membrane seen here is suspended between two substrates. The residual solvent can also be seen within the newly formed membrane. (Image from https://en.wikipedia.org/wiki/Model_lipid_bilayer [95])

A newer and more modern technology is found in tethered bilayer lipid membranes (tBLMs). This technology, in conjunction with electrochemical impedance spectroscopy (EIS), can model a membrane in terms of its conduction and thickness. The present study made extensive use of tBLMs to identify the interactions between lipid bilayers and melimine and its derivatives. Due to this, a more detailed description of their development and characteristics is outlined below.

1.4.2.1 Development of tBLMs

The development of tBLMS started with supported bilayers. This was seen in the work of Tamm and McConnell (1985) [96]. They used a Langmuir-Blodgett technique to apply a phospholipid bilayer to a hydrophilic silicon substrate. Once the monolayer had formed on the substrate, the monolayer was then resubmerged into the Langmuir trough horizontally to pass through the air-water interface (Figure 1.4.2.1.1). This was so that the hydrophobic tails were parallel to the surface of the trough to allow the tails to bond to the lipids within the trough. This newly formed lipid bilayer was then secured in place with a glass coverslip to provide additional support for the membrane (Figure 1.4.2.1.2). As a result of using this technique, Tamm and McConnell were able to find that the physical properties present in their supported bilayer were the same as those of other multilayer systems. Therefore these supported bilayers were of good use in several biophysical applications [96].

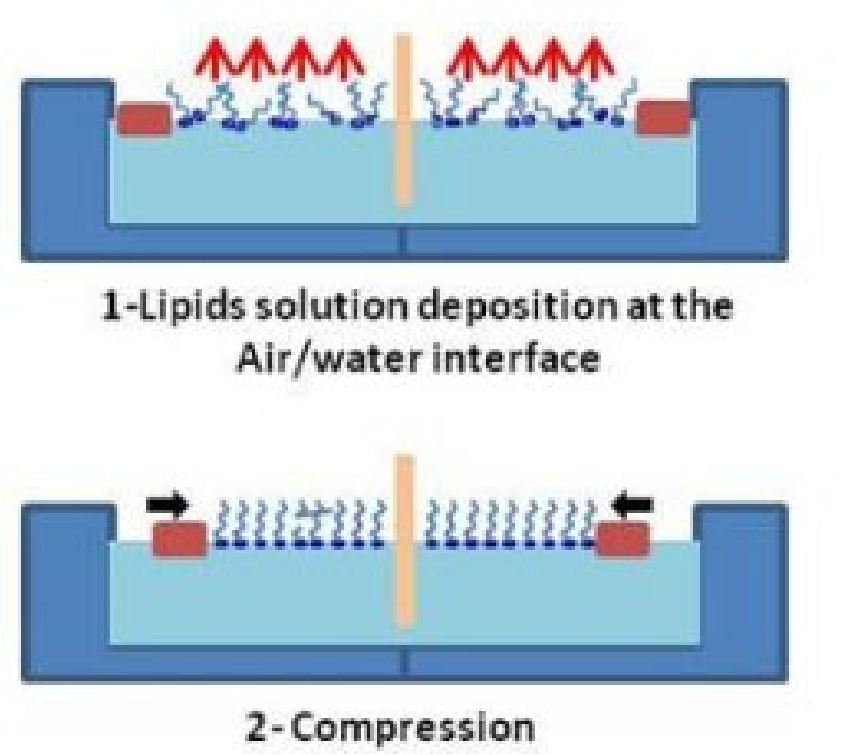

Figure 1.4.2.1.1: Representation of a Langmuir trough. Lipids are afloat on the surface of the water in the trough, with their hydrophilic headgroups partially submerged. The hydrophobic tails, on the other hand, are extended upward away from the water's surface. By applying pressure to the lipids, a monolayer can be formed (Figure from Ndeye Rokhaya et al. 2013) [97].

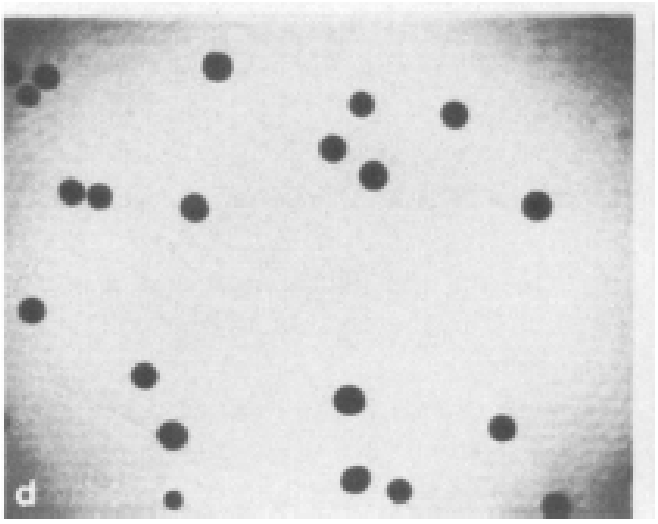

Figure 1.4.2.1.2: Light microscope image of the membrane formed by Tamm and McConnell. (Figure from Tamm and McConnell, 1985) [96]. In this image, the predominantly white area shows the lipid membrane and the dark circles scattered throughout show holes in the membrane where there are no lipids present.

A method to create a supported bilayer involved a separation of the lipid bilayer and the substrate through the use of a second lipid type; this was done in a study by Lang, Duschl and Vogel (1994) [98]. This study used thiolipids as a lower monolayer, attached to the gold substrate through gold-sulfur coordination bonds, with the second monolayer of various lipids layered over the thiolipids forming a complete bilayer.

In a comparative study of tethered membranes by Vockenroth *et al*. (2008) [99], an alternative synthesis method of tBLMs was discussed. The technique involved the fusion of lipids from lipid vesicles onto a monolayer of an anchored thiolipid 2,3-di-O-phytanyl-sn-glycerol-1-tetraethylene glycol-DL-a-lipoic acid ester lipid (DPTL). This thiolipid has two phytanyl chains coupled together via a glycerol linker to a tetra-ethylene oxide spacer. This lower monolayer of DPTL is anchored to a gold substrate via gold-sulfur coordination with the anchoring holding the lipids in place, preventing the lipids from separating from the membrane into the surrounding solution. Vockenroth *et al*. then showed the stability of this tethered bilayer system through repeated EIS measurements at regular intervals for three months at room temperature. The results obtained over the 3 months corresponded well to known values of natural membranes [100].

A new membrane technology emerged in 1997 [82], consisting of a membrane that was raised from the surface of the substrate through the use of double-length reservoir half-membrane spanning diphytanyl (DLP) ethylene glycol tethers. In this method, a lipid bilayer is formed around the hydrophobic region of the DLP that is distal to the substrate. Proximal to the gold substrate, the DLP is firmly attached via sulfur-gold coordination chemistry and separated laterally through the use of polar *spacer molecules* so as not to allow the DLP to form a complete monolayer below the lipids. These *spacer molecules* (benzyl-disulfide-tetra-ethyleneglycol-OH) are shorter than the DLP; therefore, in addition to providing the lateral spacing, a reservoir can form beneath the bilayer in the void created. This reservoir space allows for ions to reside on both sides of the bilayer.

To form a lipid bilayer around the DLP, solvent exchange can be used to permit a relatively quick and easy lipid bilayer formation. The membrane lipids used in this technique are first dissolved in ethanol before being deposited onto the DLP layer on the substrate. Following a short incubation period, the system is then washed with a saline solution. The lipids, via self-assembly, react to the solution with their hydrophobic tail regions retreating from the invading saline solution. As a result of this process, with tail regions that are contained inside with a barrier formed by the hydrophilic head groups, a membrane is formed around the DLP. The lipid bilayer with the incorporated DLP within the membrane allows for a separation from the gold substrate. This reduces the interactions between the membrane and the substrate and permits the formation of a reservoir region into which ions can enter. (Figure 1.4.2.1.3) [82].

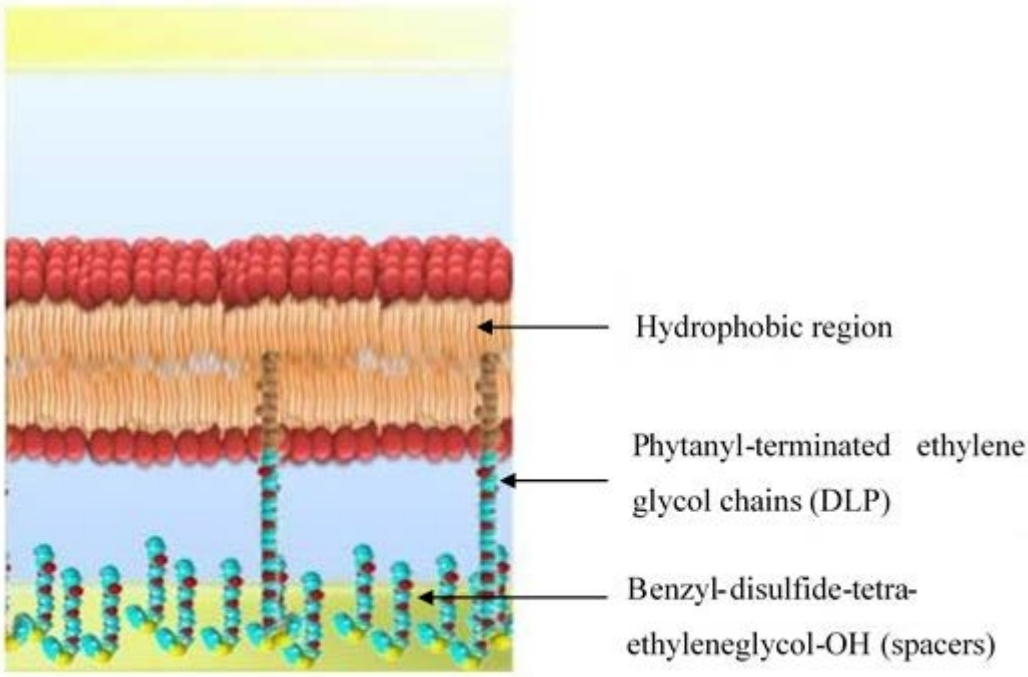

Figure 1.4.2.1.3: Artistic representation of the structure of a tBLM. (Figure adapted from Cranfield et al. 2015) [101] This representation depicts a lipid bilayer formed around the ends of tethering molecules. The structure of the tethering molecules is phytanyl-terminated ethylene glycol chains, which secure the bilayer in place. One end extends into the bilayer while the other end is secured to a gold substrate via disulphide bonds. Between the tethering molecules are spacer molecules consisting of benzyl-disulfide-tetra-ethyleneglycol-OH, which provide lateral spacing between the tethering molecules.

In work by W. Knoll et al. (2000) [102], the research into alternative methods of lipid bilayer structuring was hindered due to the difficulties in maintaining and separating the substrate that the membrane was resting on, from the bulk membrane. This resulted in complete or partial denaturation of the lipid bilayer. To overcome the drawbacks of the early membrane systems, Knoll *et al.* then recommended the use of a tethering layer which was beginning to be developed at the time [82, 98, 103-105]. Knoll et al. put forward two approaches to tethering a bilayer [102]. These two approaches are a top-down approach and a bottom-up approach. The top-down approach involves the transfer of a bilayer formed from a mixture of lipopolymer and lipid components through Langmuir-Blodgett techniques deposited onto a gold or silicon

substrate at the same time. The bottom-up approach is where the layers of the structural elements are added one at a time where the lipopolymer layer is first added to bind to the substrate before the second layer of lipids is added to complete the lipid bilayer.

Since these studies, the main focus in tethered membrane technologies has been to improve on the methods of formation. This has been done through direct improvement on the membrane, through making membranes air-stable, improving methods on membrane-protein interactions or changing the composition of lipids through producing synthetic organic lipids [100, 106-109]. Improvements in the technology have also occurred as a result of expanded methods of characterisation of the membrane structure and formation. This includes physical surface-sensitive techniques such as atomic force microscopy, x-ray photoelectron spectroscopy, surface plasmon resonance spectroscopy [100, 110, 111] and comparing these technologies to already established technologies in lipid bilayer fabrication [110, 112-117].

In 2010, Tun and Jenkins [118] produced a lipid bilayer from a monolayer of DPTL and cholesterol-pentaethyleneglycol (CholPEG). The CholPEG was tethered to a gold-coated silicon substrate as the first layer, with a monolayer of 1,2-di-O-phytanoyl-sn-glycero-2-phosphocholine (DPhyPC) lipid and cholesterol forming the upper leaflet and completing the bilayer. The combination of CholPEG and the addition of the cholesterol within the membrane provided the lipid bilayer with increased stability at higher temperatures. Membranes without the cholesterol, with only DPTL and DPhyPC, had a resistance that was significantly decreased (i.e., were leakier) when measured with EIS at 37^{o}C when compared to room temperature. This increase in temperature affects the phase dynamics of lipids in the fluid phase, and conversely affects membrane stability. When CholPEG and cholesterol were added to the lipid bilayer, results showed a smaller increase in the membrane electrical resistance, suggesting that the membranes were more stable and that the two added components added a sealing effect to the bilayer.

Deng, Y *et al.* [107] created an air-stable supported bilayer in 2008, whereby no solvent was required for the membrane to be stable. This was achieved through the addition of cholesterol to the lower leaflet of the bilayer structure (Figure 1.4.2.1.4). The Cholesterol in the lower leaflet was attached to a glass substrate through poly(ethyleneglycol) (PEG), which increased the stability of the membrane through dehydrating and rehydrating the supported lipid bilayer

(SLB). The SLBs were compared before and after dehydration and rehydration, as seen through fluorescence microscopy performed on the surface of the membranes. During rehydration, areas with a low density of cholesterol resulted in the lipids in those areas being washed from the bilayer, while regions of higher cholesterol density resulted in the membrane retaining lipids.

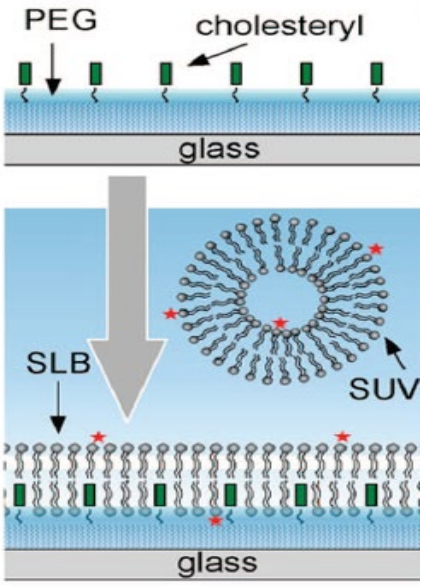

Figure 1.4.2.1.4: Image by Deng *et al., 2008,* [107], showing the formation of a supported lipid bilayer (SLB) forming around cholesterol on a glass substrate with lipids from small unilamellar vesicles (SUVs).

In showing the stability of tBLMs, in a study in 2010 by Wang *et al.* [109], two types of lipid bilayers were compared, tBLMs (bilayers anchored to the gold through polymers) and BLMs (bilayers lying directly on a gold substrate). The fluorescence microscopy used in the study initially showed a uniform signal from fluorescence tagged lipids comprising 5% of the membrane. While undergoing repeated solution exchange, no decrease in the fluorescence intensity was seen for the tBLMs. This was in comparison to the fluorescence images for the BLMs, where a reduction of the fluorescence intensity was observed. This stability, inferred from the undiminished intensity of the fluorescence images for the tBLMs, revealed the robust nature achieved through the tethering structures.

In 2010 Junghans and Köper compared five novel tethering chemistries of varying length, with one tether being wider with an additional tethering point [119]; this work was extended in 2017 by Andersson et al. [120]. The length of the tethers was changed to compare the hydration of the region below the lipid bilayers and the transport of ions across the membranes. They found that increasing the length of the tethers increased the hydration around the anchoring points of the tether. The length of the tethers was balanced against membrane formation, as the longer tethers led to the formation of defects in the lipid bilayers, evidenced from the increased electrical resistance of the membrane. The formation of lipid bilayers on these different tethers indicates that the tBLM architecture could be modified to allow for modifications that can help the membrane to mimic biological membranes, such as protein insertion, without affecting the fundamental structure of the lipid bilayer [120].

1.4.2.2 Lipid membranes as biosensors

Throughout the development of lipid bilayers, the main focus has been to produce a realistic analogue of cell membranes. This is seen in the supported bilayers produced by Tamm and McConnell [96] when they realised that their layers were similar to already known systems in their continuous uniformity and their temperature and pressure stability, and they began comparing their membrane system to other known systems [121-124].

As the structure of tBLMs has a simplistic nature, due to the minimal biological processes occurring within the lipid bilayer structure when compared to a complete cell membrane, it is suitable to be used as a useful analogue of them [102, 110, 111, 113]. In terms of use as a cell membrane analogue, there have been a few studies that have demonstrated the ability of tethered bilayers to act as a biosensor. The very processes that are present in tethered bilayers, measuring ion transfer across the membrane and the incorporation of proteins into the membrane, replicate the processes found in cell membranes without the interference of other biological processes found in nature. This ability to mimic the essential bioprocesses gives tBLMs the potential to be used as an actual biosensor.

When proteins are inserted onto/into membranes, they often require an aqueous phase surrounding the lipid bilayer to maintain proper function [98]. In artificial membranes, a

reservoir is needed below the lipid bilayer as this provides an aqueous region below the membrane, providing space for ionic conductivity on both sides of the membrane and fulfilling the requirement for protein insertion. In supported membranes (untethered), they typically contain a reservoir of water of 1-2 nm [110, 125]. However, a more extensive reservoir can be observed in sparsely tethered membranes, which ranges in size from about 0.8 - 4 nm [82, 125-127]. This increase in the width of the reservoir by a factor of two dramatically increases the volume of water capable of filling the reservoir space.

In using EIS, Tun and Jenkins [118] were able to characterise tBLM processes and behaviour during the insertion of bacteria, both pathogenic and nonpathogenic. They found that in the tBLMs they studied, that a continuous change in both the capacitance and resistance was observed. Through using EIS with tBLMs, and measuring the responses associated with changes in the lytic cycle of pathogens, Tunn and Jenkins reported that there is a potential application of a sensor that could be used to detect human pathogens through detecting the major components of supernatant toxins that are released by pathogens. To this end, Deng *et al.* were able to produce functional microarrays based on tiny membranes that had been tethered to a micro-structured substrate to create a general platform on which cell-surface interactions could be measured and analysed [107]. These measurements involve the screening of ligands for membrane proteins, specifically ion channels and G-protein coupled receptors. The microarrays are also able to be used in nanomedicine, looking at nanoparticle-based drug delivery and how the nanoparticles interact with the tBLMs within the microarray.

Cornell et al. also developed a tBLM based switch sensor in 1997 that utilises the detection of receptors, including antibodies and nucleotides [82]. This switch involved the addition of tethered biotin-conjugated membrane-spanning lipids and tethered *gramicidin-A* ion channels in the inner leaflet of the tBLM. Freely diffusing gramicidin-A monomers were also incorporated into the distal leaflet and were conjugated to a monoclonal antibody. If the gramicidin is free to diffuse in the distal leaflet, they can dimerise with the inner gramicidin monomers, forming an ion channel and the conduction is ‘switched on’. However, if the conjugated antibodies bind with their respective antigens in the distal leaflet, the gramicidin is immobilised, restricting the formation of dimers and the conduction is ‘switched off’. This on/off switch is then able to identify the presence of analytes.

A functionalised tBLM was produced by Andersson et al., 2018, whereby vesicles of pure lipopolysaccharide and lipopolysaccharide/phosphocholine liposomal mixtures were deposited onto a tethering architecture [128]. These tBLMs were then analysed through EIS and neutron reflectivity to identify the lipopolysaccharide within the tBLM structure before adding colistin, an antibiotic that targets Gram-negative bacteria [129]. The interaction of colistin suggested that these functionalised tBLMs may have a use as a screening platform for various antimicrobial compounds [128].

.

1.5 Hypotheses and Aims

As the addition of melimine has been shown to cause a decrease in the integrity of the cytoplasmic membrane in both Gram-positive and Gram-negative bacteria [135], the mechanisms of how this antimicrobial peptide and its derivatives can perturb cell membrane integrity in various ways are brought into question. In this work, I sought to address these issues.

Hypotheses:

- *That the use of advanced lipid bilayer biophysical research techniques can describe the cell membrane interactions of melimine and its associated derivatives.*

- *That through studying their peptide-membrane interactions, the mechanisms of antimicrobial activity can be identified.*

Aims:

1. To use established lipid membrane biophysical techniques including in-silico structural modelling, fluorescent membrane dipole measures, differential scanning calorimetry, neutron reflectometry, dynamic light scattering, electrical impedance spectroscopy and Arrhenius measures of tBLMs to identify the peptide-membrane interactions of melimine and its derivatives.

2. To describe the peptide-membrane interactions of melimine and its derivatives in terms of models of AMP modes of action, including *barrel stave pores, carpet model, interdigitated toroidal pore model, the critical packing parameter (CPP) model* and *surfactant-like peptide model*; as determined using the techniques in **Aim 1**.

3. To correlate membrane activity of melimine and its derivatives with their minimum inhibitory concentration (MIC) values against specific bacterial species.

Through determining the mode of action of melimine and its derivatives, via identifying the peptide-membrane interactions, a deeper understanding of these interactions would be comprehended. This may allow the design of novel cationic peptides that can be tailored

towards better targeting of bacterial cell membranes to combat the growing antimicrobial drug resistance of bacteria.

2 Methods

2.1 Peptide synthesis

Melimine and its derivatives were obtained from Auspep Pty. Ltd. (Vic, Australia). They had been synthesised by conventional solid-phase peptide synthesis protocols.

The peptides were supplied as a trifluoroacetate salt with a purity between 90 and 93%. Their molecular weight was confirmed through mass spectral analysis, and their purity was confirmed through high-performance liquid chromatography (HPLC). These measurements were carried out at Auspep Pty Ltd.

The peptides were dissolved in phosphate-buffered saline (PBS) solution to a concentration of 1mM and stored at 4°C. This stock solution was then used for all experiments.

2.2 tBLMs

2.2.1 Cartridge assembly

The assembly of the tBLMs involves the use of preprepared patterned polycarbonate slides sputter-coated with 100 nM thick 5N5 gold (Figure 2.2.1.2) (SDx Tethered Membranes Pty Ltd, Australia). Slides were then coated in a tethered benzyl-disulfide (tetra-ethyleneglycol)n=2 C20-phytanyl "tethers" and benzyl-disulfide-tetra-ethyleneglycol-OH "spacers" (Figure 2.2.1.1). By adjusting the ratio of tethering molecules to spacer molecules, changes in the tethering densities of the polycarbonate slides could be made. Unless otherwise stated, the ratio of tether molecules to spacer molecules used was 10: 90; this is a tBLM architecture referred to as a "T10".

Pre-coated slides come delivered in the presence of an ethanolic solution. Just prior to tBLM assembly, these are left to air dry, as the ethanol interferes with the adhesive used in the separately supplied cartridge. Slides are then affixed to the base of the cartridge, creating a flow cell (Figure 2.2.1.2 B). The substrate area left for each tBLM to be created within the flow cell is 2.1 mm^2.

Once the slide and cartridge are affixed and assembled (Figure 2.2.1.2 A), lipid membranes are formed over the tethers using a *solvent exchange technique*. This process uses controlled volumes and timing to optimise the formation and ensure complete membrane coverage and formation within each of the six cell chambers.

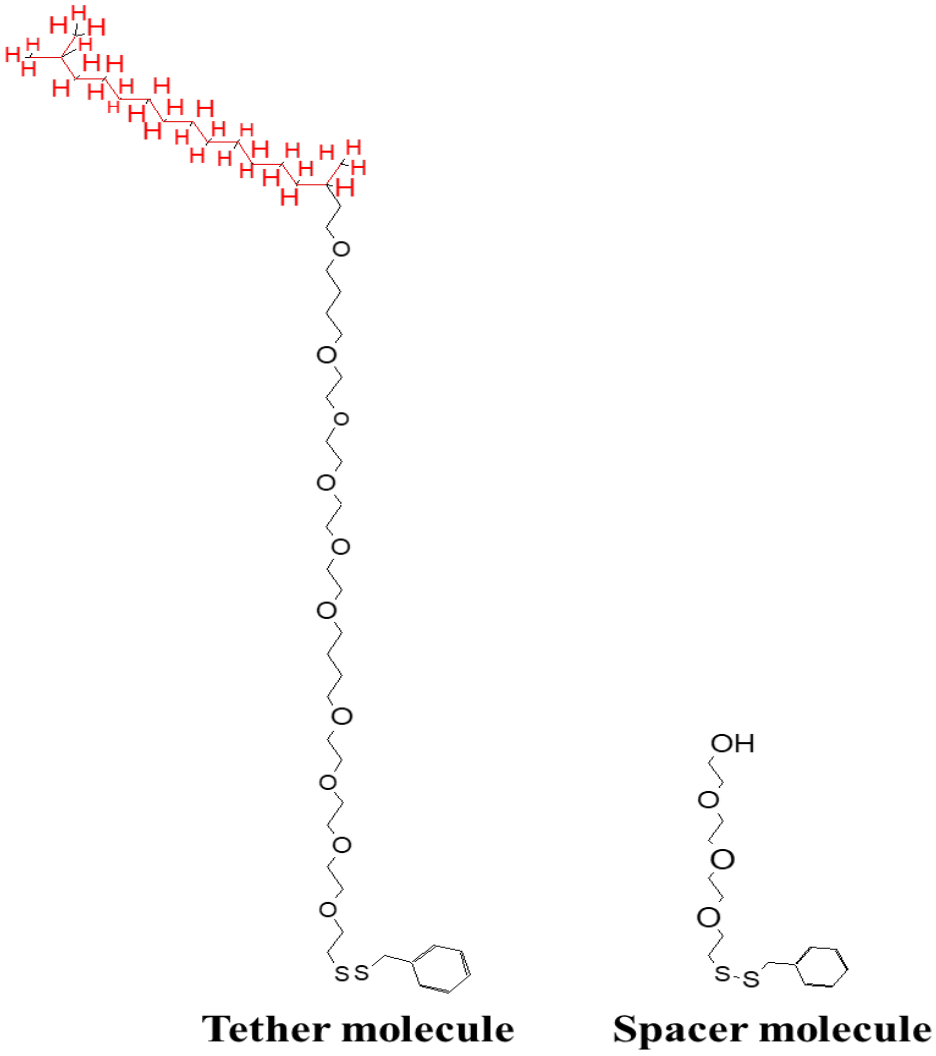

Figure 2.2.1.1: Structures of the tethering and the spacer molecules. The two sulphur moieties on each compound provide the mechanism of attachment to the gold surface via sulphur-gold coordination. The benzene ring attached to the sulphur atoms provides lateral spacing between each compound. The hydrophobic phytanyl group (highlighted in red) is submerged within the lipid bilayer, tethering the membrane in place.

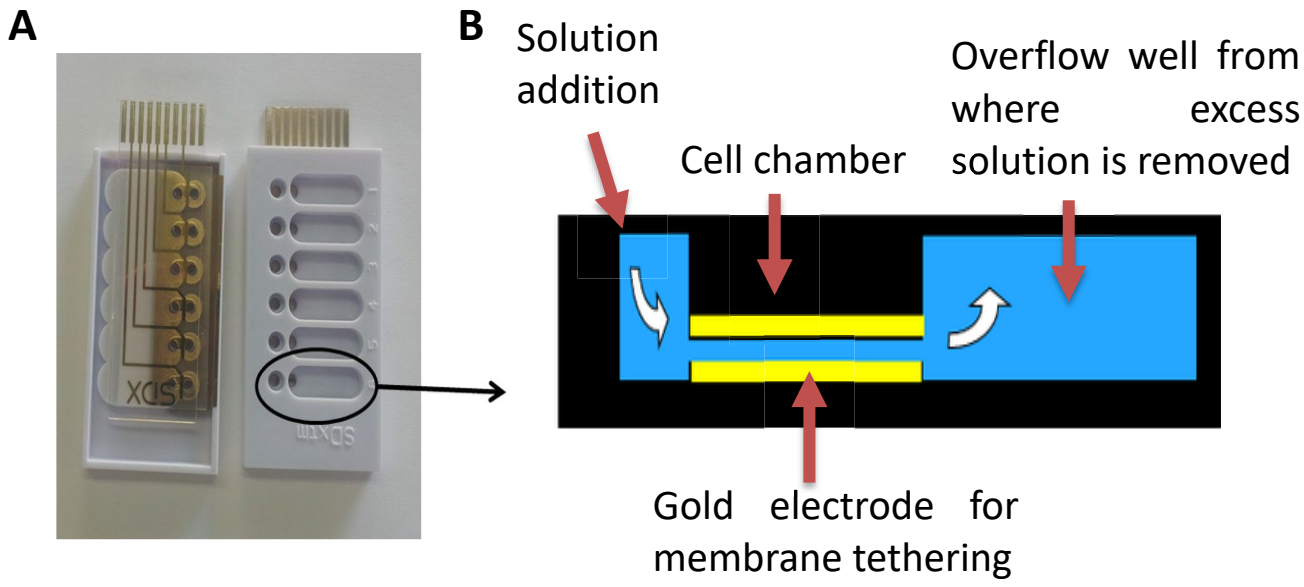

Figure 2.2.1.2: A, An assembled tBLM cartridge from both top and bottom view. Here, the gold electrodes can be seen. **B**, A cross-sectional cartoon view of one well within the tBLM cartridge. Here, yellow shows the location of the gold electrodes. Tether molecules adhere to the bottom gold electrode, with the lipid bilayer forming on these tethers between the two gold layers. Any added solutions flow through the cartridge from left to right in this depiction.

2.2.2 Membrane deposition

In order to create an anchored bilayer, 8 µL of a 3 mM solution of lipids, which are dissolved and stored in ethanol in a mobile phase, are added to each cell chamber. This chamber is 0.1 mm high and holds a volume of 1 µL, so the 2.1 mm^2 electrode surface is entirely covered by the lipid solution. The lipid/ethanol solution is left to incubate for precisely 2 min, after which each cell is washed through with 3 × 400 uL of 100 mM PBS solution. This washing process ensures that any ethanol or excess lipid initially added to the cell is removed. This process is repeated within all of the six cell chambers within the cartridge, so it is possible to run up to six individual experiments in parallel.

The successful creation of a tBLM was determined through EIS measurements. In general, if a membrane showed a conductance value between 0.1 µS – 2 µS and had a capacitance of ~20-

30 nF when using an appropriate circuit to model the data, then the membrane was deemed to be suitable for use in experiments.

2.2.3 Types of lipids used

tBLMs are customisable with regard to the type and mixtures of lipid that are used to form a bilayer. For this project, membranes were typically made from a diphytanyl lipid mixture, composed of two lipids, diphytanyldietherphosphatidylcholine (DPEPC) and glyceroldiphytanylether (GDPE), in a 70%:30% ratio (Figure 2.2.3.1). This lipid mixture provided an optimally sealed membrane that had a consistent average area per molecule[130]. Additional lipids were used to form bilayers in this study, including 1-palmitoyl-2-oleoyl-sn-glycero-3-phosphocholine (POPC) lipids, 1-Palmitoyl-2-oleoyl-sn-glycero-3-phosphoglycerol (POPG) lipids, Lipid A, or LPS and extracted *E.coli* lipids (see Figure 2.2.3.2).

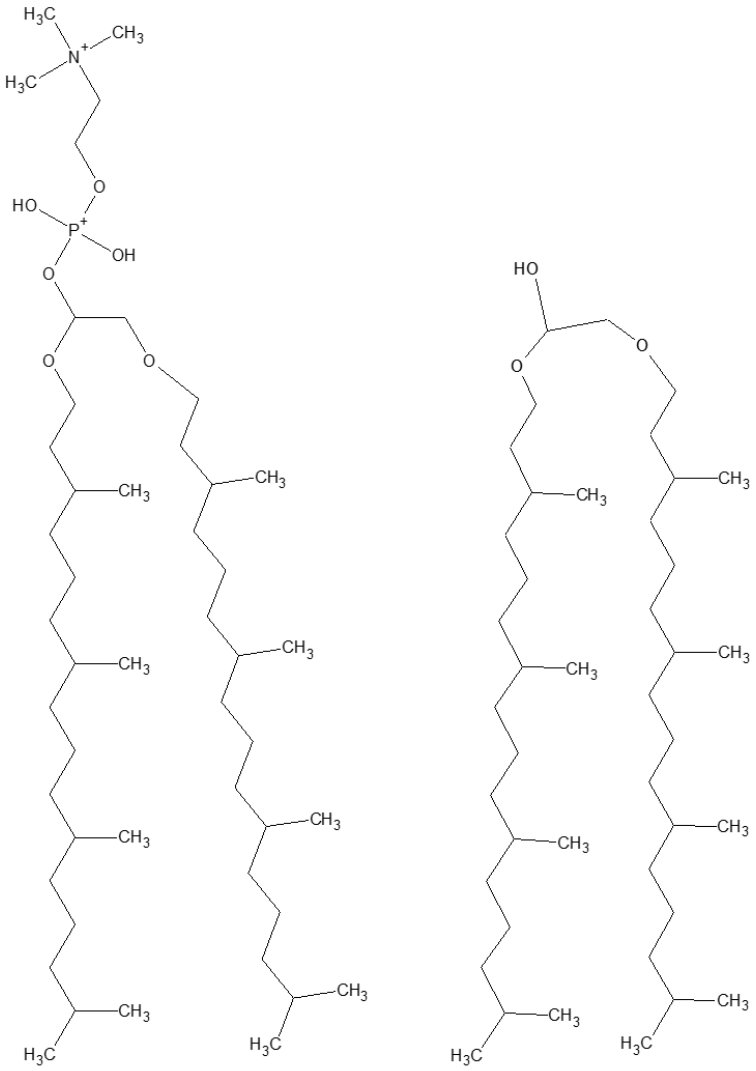

Figure 2.2.3.1: Structures of the lipids used in forming many of the tBLMs in this study. This includes diphytanyldietherphosphatidylcholine (DPEPC) and glyceroldiphytanylether (GDPE).

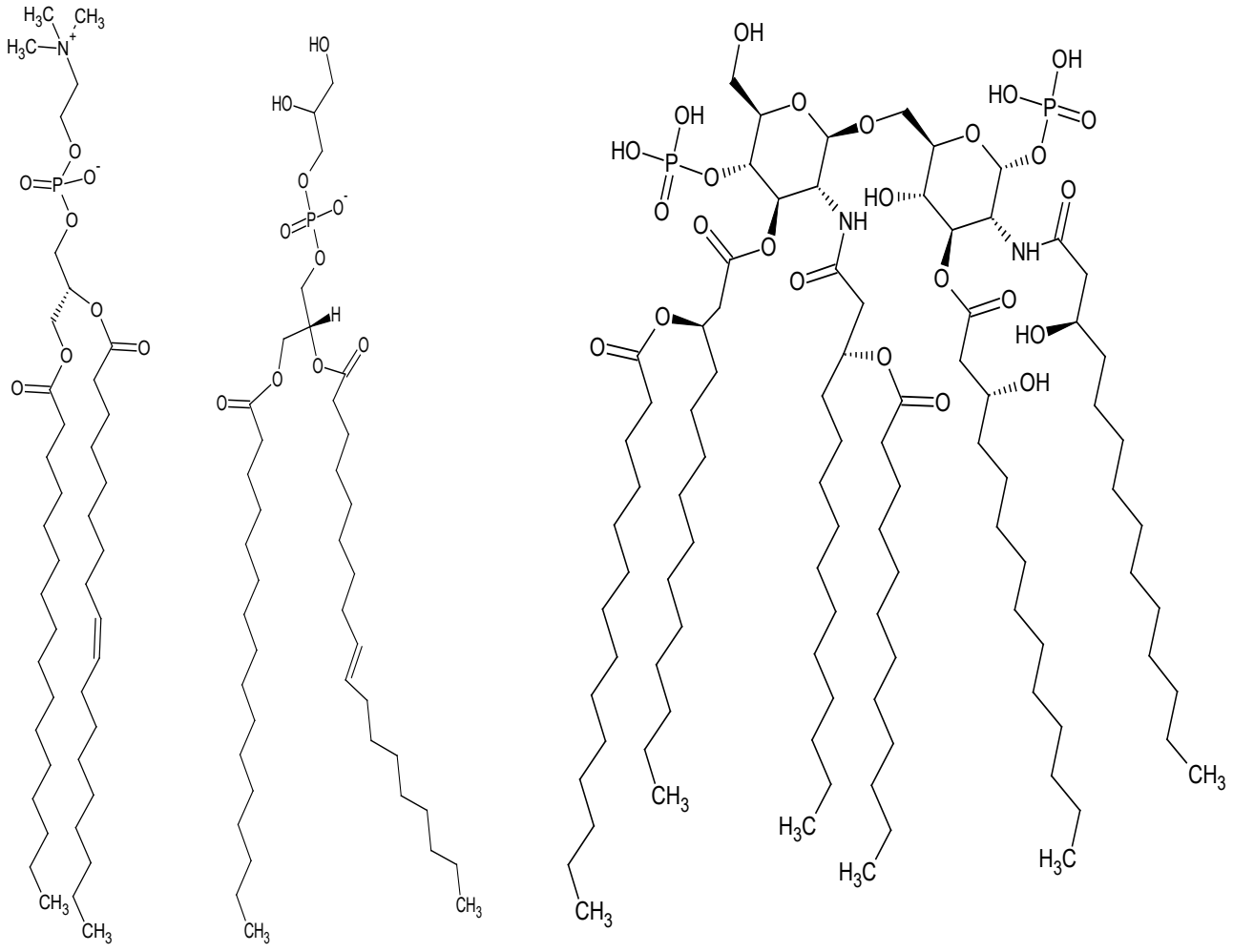

Figure 2.2.3.2: Structures of other lipids used in forming membranes within tBLMs of this study. This includes 1-palmitoyl-2-oleoyl-sn-glycero-3-phosphocholine (POPC), 1-Palmitoyl-2-oleoyl-sn-glycero-3-phosphoglycerol (POPG) and Lipid A.

2.3 Hydropathy Modeling

The modelling of the folding structure of the melimine peptides was carried out using the PEP-FOLD 2.0 software package. Through inputting the peptide sequence in the FASTA format, two different outputs were produced, a local structure prediction profile and 3D models of the predicted structure. The software is limited by requiring that the amino acid sequence be between 9 and 36 amino acids long in order to achieve the best accuracy of predicting the folding pattern [131].

The software's first step is a prediction of the folding pattern based solely on the amino acid sequence. This prediction reconstruction is based on a hidden Markov model (HMM)-derived structural algorithm where proteins are described as a series of overlapping fragments made up of four amino acids. These fragments are stored in a library and used as the basis for peptide reconstruction.

The subsequent 3D modelling step is achieved through the use of two software components. The first component was a greedy algorithm that performed an incremental construction of the structure. After this structure was completed, this greedy algorithm was repeated 50 times to determine the lowest energy conformation for the peptide [132-134].

The second component of the 3D modelling was the *optimized potential for efficient structure prediction* (OPEP) program. OPEP uses a generic protein coarse-grained force field algorithm, which is used to find the lowest energy conformation for a peptide. It inspects local interactions between amino acids and their side chains that affect stereochemistry at neutral pH. These interactions include bond length, bond angle, van der Waals interaction and hydrogen bonds. To achieve the best results, the side chains are simplified and represented as single beads attached to N, H, Cα, C and O atoms that make up the peptide backbone. With the OPEP and the greedy algorithm working together, the structures that the sequence was most likely to form were able to be predicted.

The final output is a local structure prediction profile chart and 10 × 3D models. The chart displays the conformational probability that each fragment would form based on the structural algorithms. These conformations are typically defined as a 'helical conformation', a 'random coil conformation' or as an 'extended' conformation with no specified shape.

2.4 AC impedance

2.4.1 Swept frequency impedance

Swept frequency electrical impedance spectrometry was carried out using a TethaPod™ impedance spectrometer and was operated using TethaQuick™ software (SDx Tethered Membranes Pty Ltd, Australia). For this, a 50 mV peak-to-peak AC excitation was applied to the tBLMs at frequencies of roughly 0.1, 0.2, 0.5, 1, 2, 5, 40, 100, 200, 500, 1000 and 2000 Hz with four frequency steps per decade, and with a zero bias potential. Each frequency was typically measured for 4 seconds. Full frequency sweeps typically took 1-2 min to complete. Depending on the experiment, the frequency range over which the sweeps were performed was adjusted; this involved extending the range from 0.01 Hz to 10,000 Hz, thus increasing the time duration of each sweep.

When the data from the tBLM system is compared to a suitable equivalent circuit (Figure 2.4.1.1), by identifying the electrochemical nature as a network of passive electrical circuit elements, a good estimation of the membrane *conductance* (G_m) and *capacitance* (C_m) is produced. The conductance of a tBLM membrane depicts the ability of the membrane to passage ions back and forth, while the capacitance is inversely proportional to the membrane thickness. The EIS technique used in the present study involved a setup where the membrane was enclosed by two gold electrode surfaces (Figure 2.4.1.1). These electrodes were incorporated into the equivalent circuit with the counter electrode capacitance (C_s) distal to the membrane, and the smaller tethering electrode capacitance (C_{th}) was located directly adjacent to the membrane.

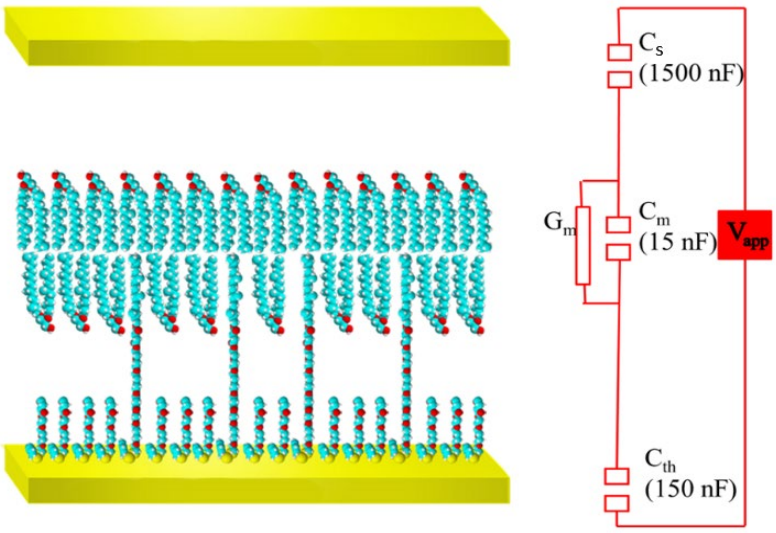

Figure 2.4.1.1: Depiction of a tBLM and an example of an equivalent circuit. (Figure from Cranfield, C.G. et al., 2014) [135] The gold and the membrane are represented by capacitors, with the membrane containing an additional resistive element.

A constant phase element (CPE) in series with a resistor/capacitor network [136] was used to fit the data collected from each sweep (See Figure 2.4.1.2). Fitting was done using a proprietary adaptation of a Levenburg Marquardt fitting routine.

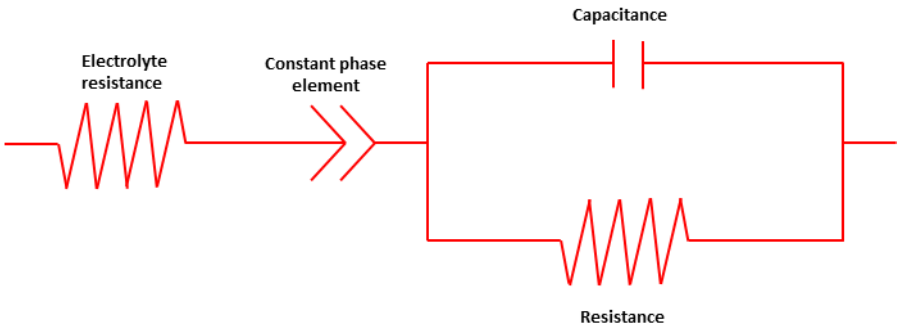

Figure 2.4.1.2: The constant phase element seen with the two arrow symbols is connected in series to the resistor/capacitor network and a resistor representing the electrolyte solution.

Through changing the frequencies of the alternating current, the ions in the solution are able to diffuse back and forth from one electrode to the other across the membrane. Through varying the frequency of the AC signal, the ions diffuse different distances. With high frequencies limiting time between the alternation of the current, the ions have minimal time to diffuse. At these highest frequencies, the resistance of the surrounding solution dominates the impedance as measured with EIS, at the median frequencies, the resistance and capacitance of the lipid bilayer dominate. At lower frequencies, it is the capacitance of the gold that dominates.

Measurements are taken of the impedance of the system and the angle of phase shift between the excitation signal and the measured response. These results are compiled into so-called Bode plots; these plots show a response to the different frequencies used during measurement, giving a comparison of electrical changes across the system. They are typically plotted as impedance vs frequency and phase shift vs frequency; see Figure 2.4.1.3.

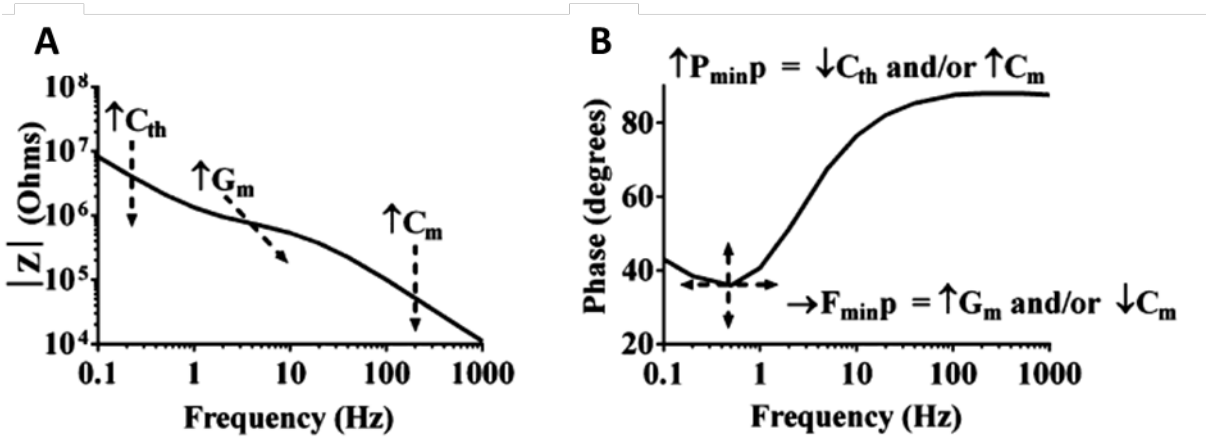

Figure 2.4.1.3: Both **A** and **B** represent typical Bode plots. **A** depicts a characteristic impedance versus frequency plot with a log-log scale. Changes in the slope and of these plots allow for the identification of resistive or capacitive elements across a tBLM architecture. The resistive elements have an ideal slope of '0', and capacitive elements have an ideal slope of '-1' [137, 138]. Changes in the slope and magnitude of the impedance plot at each frequency correlate with changes in different parts of the membrane and the two gold electrodes. These changes can be modelled using an equivalent circuit (e.g. Figure 2.4.1.1). **B** shows a typical phase versus frequency plot on a linear-log scale. This type of plot denotes the admittance of the system and identifies the capacitive (90° phase) and resistive (0° phase) elements of the system through comparing the phase relationship between the excitation signal and the measured response [139]. Thus, the plot allows for the identification of the membrane seen through a low phase angle due to the membrane being a bypass resistor. If a change occurs in the region of the minimum phase (depicted by a cross on the plotted curve above), a change has occurred in either the membrane conductance or capacitance and/or the tethering electrode capacitance. Horizontal shifts to the phase plot in the region of the cross denote a change in the frequency of the minimum phase (FminP); this portrays changes in G_m and/or C_m. A vertical shift indicates a change in the phase of the minimum phase (PminP), describing changes in the C_{th} and/or C_m (Figure from Cranfield et al., 2015) [140].

Through monitoring these changes over time, a picture of the stability of the membrane can be assessed, with any changes in equilibrium contrasted. Upon introducing a new element into the system, such as AMPs, this equilibrium is disrupted. These disruptions are usually seen through changes to the membrane conductance and capacitance. These interactions of peptides with lipid bilayers while using EIS helps identify their intrinsic behaviour. The modulation of membrane conductance and capacitance can determine if a peptide targets membrane or not and can further identify pore-forming or layer rupturing behaviour.

2.4.2 Testing pH effects on membranes

To determine the effect of protonation on the five cationic peptides, the AC impedance technique was used, testing at three different pH value, ~ 5, ~ 7 and ~9. These peptides were tested in both sodium chloride (NaCl) and potassium chloride (KCl) to explore the influence, if any, that these ionic species may have on melimine and its derivatives.

The pH of each solution was adjusted by adding concentrated HCl to make the solution more acidic, or either NaOH or KOH to increase the pH. At the higher pH values, the pH of the solutions was more likely to decrease rapidly due to acidification from outside factors such as atmospheric CO_2 dissolving in the solution. To prevent this, each solution of NaCl and KCl at each pH were kept in an air-tight container prior to use and measurements were undertaken within 5 min of pH adjustment. In addition to this, the pH of each solution was regularly monitored.

Melimine was also tested on POPC and POPG membranes at pH ~ 5, pH ~ 7 and pH ~9. It has been shown that H_3O^+ ions have a dominant effect on conduction [73]. At pH values of 5, 7 and 9, the concentration of H_3O^+ ions range from 10 µM to 1nM. As the pH increases, the positively charged H_3O^+ ions would be less likely to compete with the cationic peptides. For these measurements, the stock 1mM melimine was diluted to 10 µM, using solutions of NaCl at pH ~ 5, pH ~ 7 and pH ~9. Prior to the membrane being tested with the peptide, it was equilibrated with NaCl adjusted to the relevant pH value.

2.5 Dynamic light scattering (DLS)

To determine how the peptides interact with lipid spheroids [141], changes in the spheroid size due to aggregation [142] were measured after the addition of melimine and its derivatives. The dynamic light scattering (DLS) experiments were performed using 1-oleoyl-2-hydroxy-sn-glycero-3-phosphocholine (Lyso PC) lipids 18:1(Avanti Polar Lipids, USA), see Figure 2.5. These single acyl-chain unsaturated lipids were used for their ability to micellize and form into lipid spheroids [141].

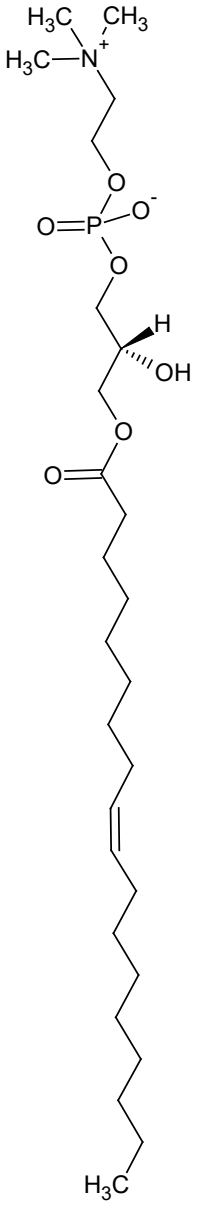

Figure 2.5: Structure of a 1-oleoyl-2-hydroxy-sn-glycero-3-phosphocholine (Lyso PC) lipid.

The lyso PC lipids were used at a concentration of 10mg mL^{-1} before being mixed with each of the five peptides to a ratio of 48.5 lipids per peptide molecule [143, 144]. The lipid/peptide solutions were vortexed for 2 min and further placed on a tube shaker for 15 min to ensure mixing.

For the measurements, a Zetasizer Nano S (Malvern Instruments Ltd., Southborough, UK) was used, which was equipped with a 632.8 nm He−Ne laser (4 mW). This instrument applies a non-invasive backscatter technique with a 173° detection angle. Each of the measurements was run at 25 ± 0.1 °C.

The measurements were taken before, directly after and for 15 min after the addition of the peptides. For each of the three time intervals, 15 scans were completed. These scans were completed with a 20 s interval between each scan. Each set of measurements were repeated three times. This process was then repeated for each of the five peptides. Malvern Instruments Zetasizer software for the Nano, APS and μV(Version 7.03) was used to analyse the average size (nm) and intensity (%).

Through the use of Prism 7.03 (GraphPad Software Inc., La Jolla, CA), an one-way analysis of variance (ANOVA) was carried out, followed by a Tukey multiple comparisons test, to determine if the means of the diameters of the lipid spheroids were the same after the addition of each peptide were statistically different.

2.6 Differential scanning Calorimetry (DSC)

2.6.1 DSC data acquisition

Differential scanning calorimetry (DSC) was used to study how melimine and its derivatives influence the lipid packing during the phase transition of lipid bilayers. Lipid vesicles were formed from 1,2-dimyristoyl-sn-glycero-3-phosphocholine (DMPC); see Figure 2.6.1 below.

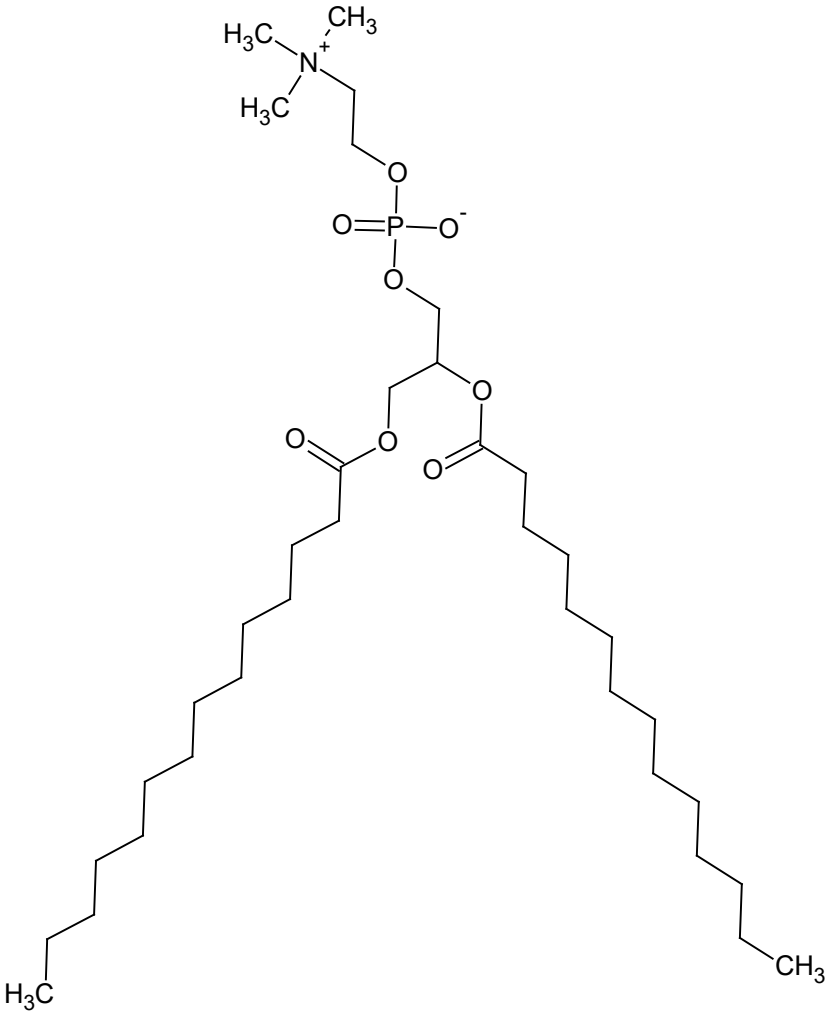

Figure 2.6.1: Structure of 1,2-dimyristoyl-sn-glycero-3-phosphocholine (DMPC) lipid.

For this, dried lipids were weighed and then dissolved in ethanol. The lipids were then dried using nitrogen gas in a round bottom flask, providing an even coating of lipid on the inside surface of the flask. This was followed by rehydration using PBS solution.

DSC measurements were performed using a VP-DSC microcalorimeter (Microcal, Northampton, MA), operated using Origin software. Baseline data were collected using just PBS solution; this baseline was obtained using PBS in both the sample and reference cells of the instrument. The baseline was then subtracted from the lipid sample scans. The measurements were performed at scan rates of 10°C h^{-1}, ranging from 10°C to 65°C. This temperature range allowed for heating or cooling using the inbuilt system. DMPC lipids were chosen as the transition temperature for these lipids is approximately 24°C [145]. This choice allowed for the transition temperature to fall within the heating range. With the DMPC lipids, the peak of the main phase transition occurred over a small temperature range. By slowing the scan rate to just 10°C h^{-1}, more data points were able to be collected. This enabled a better definition of the measured DSC curves, providing enhanced resolution for both the pre-transition and main transition peaks.

Scans were performed on DMPC alone and then repeated with each of the five peptides mixed with DMPC. Ten scans were recorded for each peptide and the DMPC-alone controls; these groups of ten measurements were then averaged into the final thermograms.

2.6.2 DSC Data Fitting

The averaged scans of the replicate groups of thermograms of the phase transition profiles were normalised to the lipid concentration at 3mM, and the averaged PBS baseline scan was then subtracted from each of the peptide profiles.

From the interactions between the DMPC lipids and the melimine derivatives, the thermograms resulted in asymmetrical peaks. Due to this asymmetry, the thermograms were identified as having multiple peaks merged within the thermogram, see Section 3.7.3 [146].

In order to identify enthalpy change, the following equation was employed:

$$C_p = \frac{exp\left\{-\frac{4C_p^{max}T_m^2}{\Delta HT}\left(1-\frac{T}{T_m}\right)\right\}}{\left[1+exp\left\{-\frac{4C_p^{max}T_m^2}{\Delta HT}\left(1-\frac{T}{T_m}\right)\right\}\right]^2} \cdot \frac{4C_p^{max}T_m^2}{T^2} \text{ [146]} \quad (1)$$

This equation was used to fit the data by using non-linear regression. I aimed to fit three parameters, namely the heat capacity, C_p, the temperature of the phase transition, T_m, and the enthalpy change per mole of lipid, ΔH. The deconvolution was carried out using Prism 7.03 (GraphPad Software Inc., La Jolla, CA).

Before deconvolution, to aid the fitting process, initial estimates of ΔH were calculated. This was done by calculating the area under each of the thermograms.

From the regression fitting, the deconvoluted curves were compared to the original data curve by fitting the values received from the regression back into the curve equation. The area under each of the deconvoluted curves of the thermograms was then used to calculate the enthalpy change associated with each of the five peptides.

2.7 Neutron Reflectometry

2.7.1 Membrane measurement with PLATYPUS

The PLATYPUS time-of-flight neutron reflectometer located at the 20 MW OPAL research reactor Australian Nuclear Science and Technology Organisation (ANSTO), Sydney, Australia, was used for this study in order to identify any changes in membrane thickness and any changes in the water volume fractions of the membrane due to the presence of the peptides [73]. The PLATYPUS instrument is located on a cold neutron guide which provides the instrument with a neutron bandwidth ranging from 2.5 – 18.0 Å, with the cut-off being determined by the four instrument disc choppers. See Figure 2.7.1.1 below.

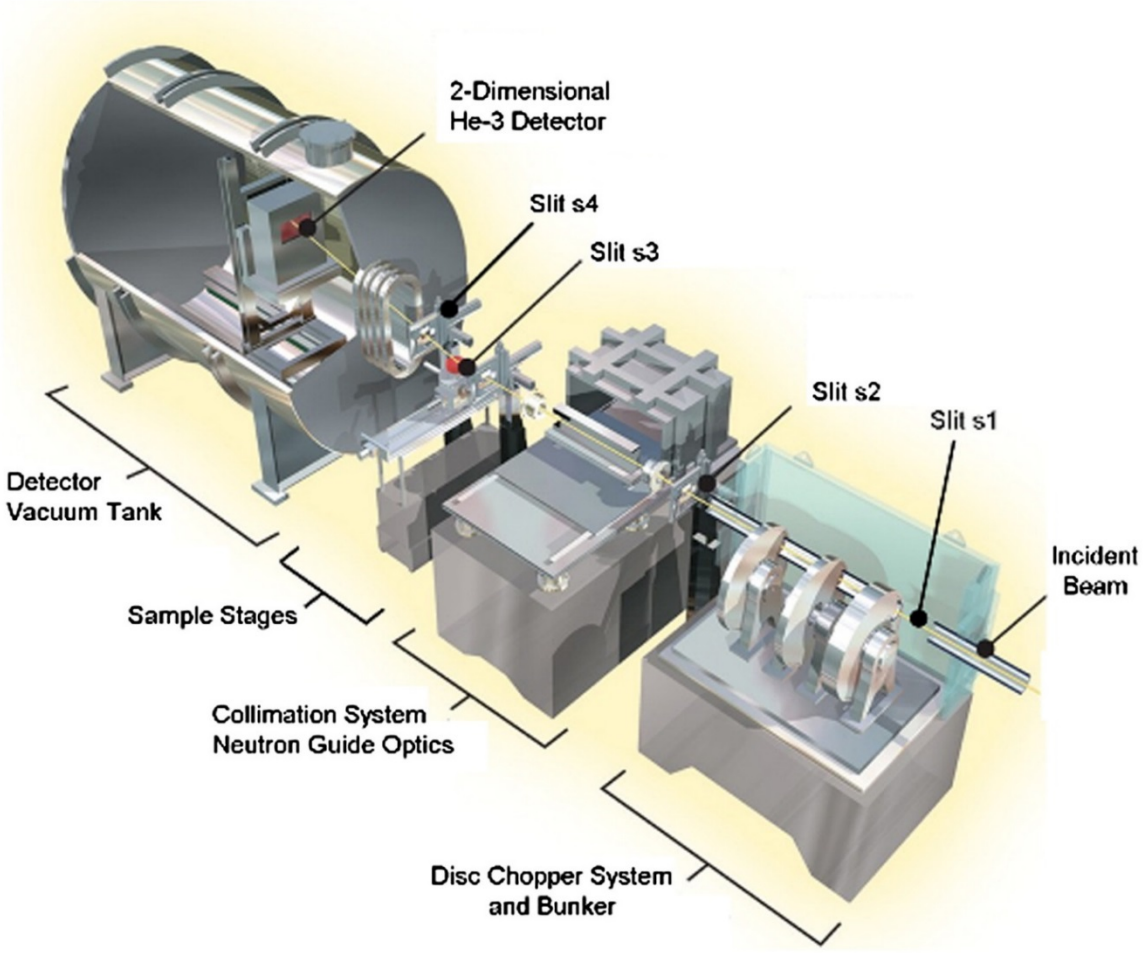

Figure 2.7.1.1: Setup of the Platypus time-of-flight neutron reflectometer. The incident beam of neutrons enters from the right, passing through the four disc choppers before reaching the sample stage and ended up at the detector. Figure from James, M. et al. [147]

For this set of experiments, the first and third choppers were used. The chopper configuration delivered the optimal neutron wavelength range and resolution for measurements with the tethered lipid bilayers.

Once the beam had been optimised for wavelength, it travelled further into the instrument towards the sample chamber. This is the chamber into which the sample, a tethered lipid bilayer, was placed on the sample stage. The sample stage permitted the sample to be moved into and out of the path of the incident neutron beam and to switch between different sample discs as well as for fine adjustment of the location and angle of the sample area for optimal beam alignment in relation to the lipid bilayer.

When scanning, the relevant perfusion chamber was moved in front of the neutron beam and adjusted to its first scanning angle. As the beam passed through the perfusion chamber, some neutrons were scattered off the lipid bilayer and the substrate. The neutrons scatter differently as they pass the nucleus of the atoms comprising the lipid bilayer and the substrate, with different atoms causing the neutrons to scatter different lengths. One major difference lies between hydrogen and deuterium, where there is a large separation in their scattering lengths at $-0.374\ 10^{-12}$ cm and $0.667\ 10^{-12}$ cm, respectively [148]. The scattered neutrons then continued towards the detector, located behind the sample stage. The area of the detector in which the scattered neutrons hit could be used to estimate the angle from which the neutrons scattered from the sample. Through the use of graphing software, these trajectories were mapped and subsequently used to provide information on the structure of the layers of the membrane and the positioning of the peptides within them.

The reflectivity measured with PLATYPUS is the ratio of the reflected beam and incident beam and is measured as a function of Q, the scattering vector. Q is defined as,

$$Q = (4\pi \sin\theta) / \lambda \quad (2)$$

where θ is the scattering angle and λ is the wavelength of the incident radiation.

For these measurements, tethered bilayers were formed on conductive silicon disks that were 50 mm in diameter and 7mm thick. The silicon discs had been sputter-coated with a layer of chromium, followed by a second layer of gold, at the *Melbourne Centre for Nanotechnology*. The sample was then prepared as a tBLM using the method outlined in Section 2.2. In the

preparation, two changes were made. The first was with the substrate that was required for these experiments: the gold layer was coated onto a chromium-silicon disc instead of a polycarbonate slide. The second change was the volume of the mobile lipid phase added to the tethered substrate: the volume of the mobile lipid phase used was 1 mL to accommodate the larger substrate area. The substrate area was covered in tethers without spacer molecules, resulting in 100% tethering density. The lipids used to create the outer leaflet of the bilayer were fully deuterated 1,2-dioleoyl-sn-glycero-3-phosphocholine (DOPC) lipids. The silicon discs were clamped to a bespoke perfusion chamber during the assembly of the tethered bilayer and during measurement at the PLATYPUS sample position.

The difference in scattering length between hydrogen and deuterium provides a way of examining most biological materials. The first way that was employed was through using fully deuterated DOPC lipids (Figure 2.7.1.2) to give neutron contrast between the two leaflets of the membrane. This contrast was improved by surrounding the membrane in bulk solutions of 100 mM PBS in either D_2O, H_2O or an H_2O/D_2O mixture, which mimicked the scattering of the gold layer. Through scanning with each of the three solutions, parts of the system could be hidden, providing the contrast in the scans observe differences in SLD between different sections of the bilayer system. The peptides were also dissolved in solutions of H_2O and D_2O at 10 μM concentration. These solutions were then further mixed when required for the H_2O/D_2O gold matched mixtures.

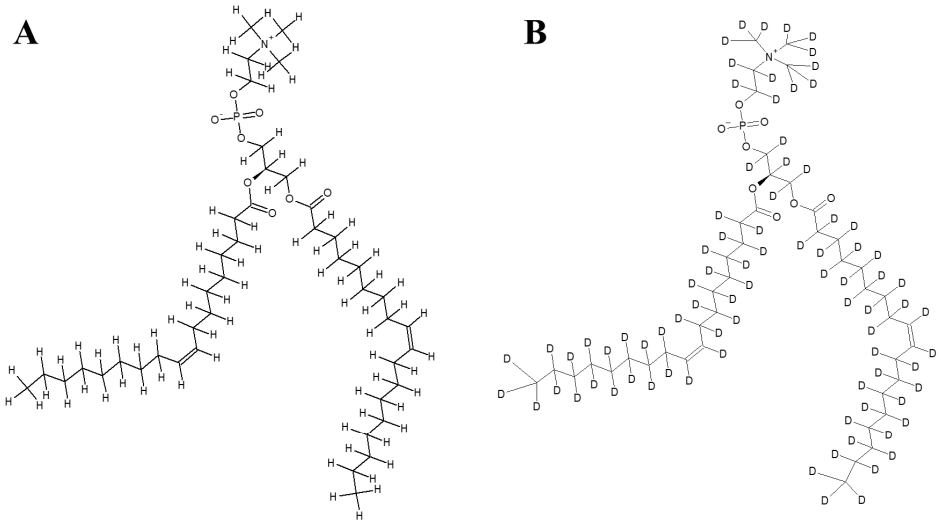

Figure 2.7.1.2: Comparison of DOPC. **A,** DOPC lipid in its normal hydrogenated state. **B,** The hydrogens have been replaced with deuterium.

Additionally, another property of neutrons was used as a source of contrast; that is, the neutron is in one of two nuclear spin states which will interact differently with magnetic materials. The beam of neutrons is polarised using a mirror; this filters out one of two neutrons quantised spin states that are either 'up' or 'down'. The substrate of the tethering setup is replaced with an internal magnetic layer of permalloy underlayer instead of chromium. This underlayer creates an internal reference layer that scatters neutrons differently depending on their spin state [149, 150].

Background scans were taken to measure any background interference, in addition to scans of the silicon substrate used to align the centre of the perfusion chambers on the sample stage with the neutron beam. When measuring each of these contrasts, the membranes were tilted to various angles to cover the required scattering vector (Q) range.

Due to the number of membranes required for testing, two different types of perfusion chambers were used, and each one required different angles for acquiring data. The first type of perfusion chamber was a standard build. For this type of perfusion chamber, solutions of H_2O and D_2O were used as contrasts better to identify the peptide and deuterated lipids within the membrane. An H_2O/D_2O mixture that mimicked the scattering of the gold layer was also used as an additional contrast. The incident angles used in these measurements were 0.5°, 0.85° and 3.8°.

The second type of perfusion chamber was magnetically orientated; for these measurements, the H_2O/D_2O mixture was not used. Instead, only the solutions of H_2O and D_2O were used, and the up spin and down spin of the neutrons were taken into account as they passed through the magnetic field of this perfusion chamber. The polarization of the up spin and down spin neutrons removes the need for a third contrast solution. For these sets of measurements, incident angles of 0.5°, 1.5° and 4.5° were used. [151] [149, 150]

The data from these angles were spliced together after normalisation to the direct beam and background subtraction to produce a single scaled reflectivity dataset for each contrast scan of H_2O, D_2O, or gold matched solutions. These datasets were compiled over a Q range of 0.006 to 0.25 $Å^{-1}$ using the SLIM reduction package[147].

2.7.2 Software

When acquiring and processing the data from PLATYPUS, two software programs were used. The first program is the user interface for the PLATYPUS, called the FIZZY program [147]; it allows the user to interact with the machine with respect to moving the instrument stage, turning the detector acquisition electronics on, and allowing the user to see the detector image in real-time.

Modelling of these data was carried out assuming that the tBLM structure was composed of a series of parallel layers[152]. Three parameters were associated with each layer during the model; these were scattering length density (SLD), layer thickness and interfacial roughness. Data from each contrast were simultaneously fitted whereby the structural parameters of the layers were constrained to be equivalent, but the SLD was allowed to vary with buffer contrast.

For the data fitting process, the layers of the lipid bilayer were assumed to be the outer lipid head groups, the outer lipid tails (both of which had been deuterated), the inner leaflet and tethers due to 100% tethering, and the substrate, consisting of layers of gold, silicon and chromium (Figure 2.7.2). These layers represent the different parameters used in the modelling process. For this study, thickness, roughness and the scattering length densities for the gold, silicon and chromium substrate and the tethers were set at fixed values with the scattering length densities of the outer lipid tails and head groups permitted to change. Changes within

the layers of the outer lipid tails and head groups were expected to show the interactions of each of the five peptide derivatives.

The second item of software was MATLAB with an addon called *RasCAL* (version 1, A. Hughes, ISIS Spallation Neutron Source, Rutherford Appleton Laboratory). This software provides a way to use the least-squares fitting of the neutron reflectivity data, fitting the collected data with an expected model. The reduced reflectivity data collected from PLATYPUS is input and, through the least-squares fitting, reduces the difference between the reflectivity and the layer model using each of the different contrast data sets. The analysis was used to try to distinguish the layer structure of the outer leaflet of the lipid bilayer and to identify the peptides in contrast to the deuterated DOPC lipid layer. The values of roughness, thickness and scattering length densities obtained through the least-squares fitting were then compared through a Markov Chain Monte Carlo-Bayesian analysis to obtain the probability distribution for these values[73, 128].

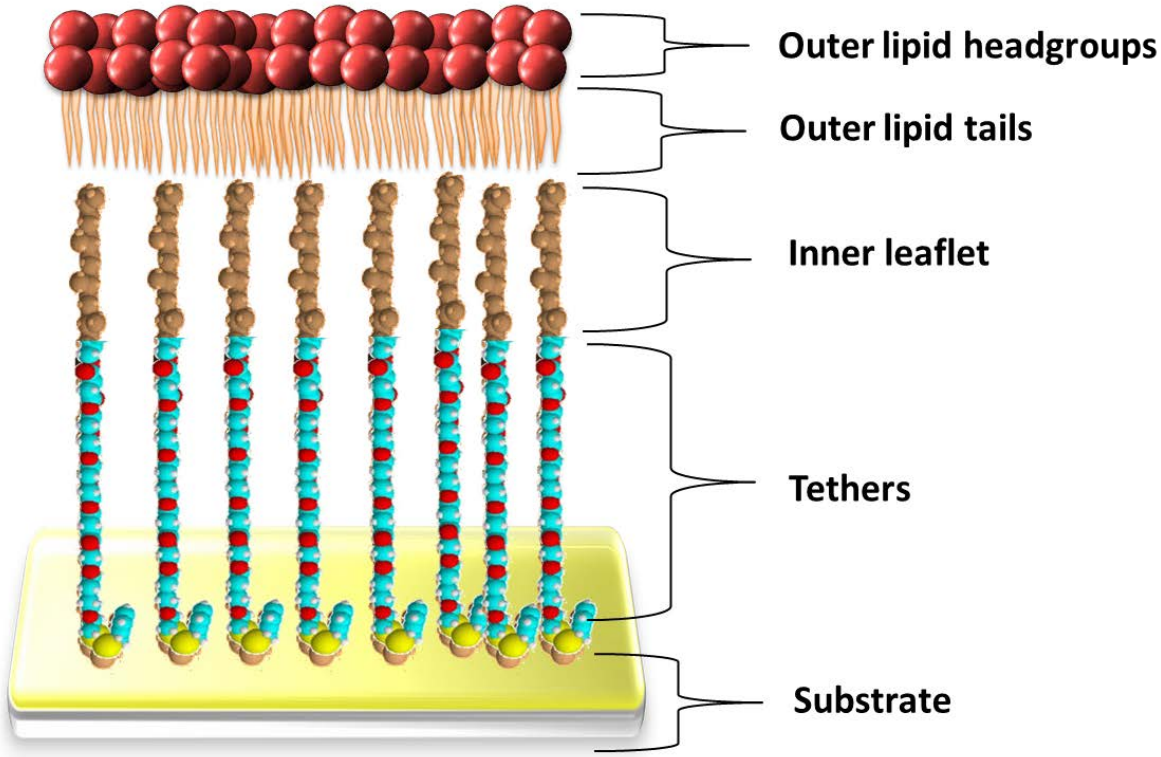

Figure 2.7.2: Schematic of a cross-sectional area of a tBLM, showing the separation of the layers used for the modelling of neutron scattering data for each of the lipid bilayers.

2.8 Activation energy

The *activation energy* describes the energy required for a peptide to overcome or insert into an inherent barrier such as a lipid membrane. One method of obtaining the activation energy for a peptide or compound is through an *Arrhenius plot*. Such plots use the Arrhenius equation to equate temperature and a rate constant. This equation is mostly used in the interpretation of the influence that an increase in temperature has on the speed at which a chemical reaction takes place. The use of Arrhenius plots in science has been fundamental in calculating rates of chemical reactions [153].

The Arrhenius plot shows the effect of temperature on the reaction rate of a chemical reaction. It can be used to model the temperature dependence of diffusion coefficients, the population of crystal vacancies, creep rates, and many other thermally-induced processes/reactions[154]. It has been proposed by Laidler that there was a good chance for these processes to be chemical as they obeyed the Arrhenius law within experimental error and contained activation energies greater than 5 kcal mol^{-1}, which is above the energy barrier threshold that differentiates the energy needed for initiating chemical reactions[153, 154]. This observed result shows that any process may obey the Arrhenius law, whether complex or not, and resulted in estimable activation energy or estimable energy barriers that can be associated with the inner workings of different processes. The use of the Arrhenius equation in conjunction with tBLMs, has been studied before by Valincius et al., 2008 [155]. In this study, I aimed to refine this technique by incorporating more data points to calculate better the activation energy of ion traversal across tBLMs in the presence of melimine and its derivatives.

In order to estimate the changes in energies required to induce the changes in membrane construction due to the presence of melimine and its derivatives, the AC impedance technique was used to monitor conduction changes at various temperatures. To do this, the tBLMs were heated and cooled in a controlled environment when sealed in an insulated chamber.

Initial warming of the chamber was achieved through blowing heated air into it. While this method worked efficiently to heat the membranes, it evaporated the PBS solution within the wells of the tBLM cartridge and led to inconsistent heating of all parts of the chamber. Following this discovery, the chamber was subsequently heated by placing in on top of a heated water bath; thus, heating was achieved by thermal transfer between the water bath and the

insulated chamber. Cooling was achieved by allowing the box to first reach room temperature, with further cooling provided with an air-conditioning unit. Using this method, temperatures ranging from 10 - 32°C were achieved.

Heating and cooling were first measured on a plain membrane to establish a baseline data set and subsequently repeated after the addition of the peptides. Each of the peptide derivatives was first allowed to equilibrate to the temperature within the chamber before being added at a concentration of 10 μM.

When the results are plotted in an Arrhenius plot, where the *K* is plotted against the reciprocal of absolute temperature, a linear graph is observed. The slope of the resulting line is what is then used to estimate the activation energy of the reaction and thus the energy to overcome a barrier to the reaction.

In calculating the energy required for a mole of ions to traverse the membrane, the data were plotted with the natural logarithm of the conductance vs 1000×temperature^{-1}. From this graph, the activation energy was estimated from the resultant slope of the graph, according to the Arrhenius equation below:

$$k = Ae^{\frac{-E_a}{RT}} \qquad (3)$$

In this equation, the rate constant, *k*, is the result of a pre-exponential constant *A*, multiplied by the exponential term containing the activation energy E_a, temperature *T* and the gas constant *R*, with the activation energy and the pre-exponential constant being temperature independent.

The graph of the natural logarithm of the conductance vs 1000×temperature^{-1} gives a slope of:

$$-\frac{E_a}{R}$$

The slope of each graph was estimated using linear regression with the aid of Prism 7 software. From this slope, the activation energy for each peptide was estimated.

2.9 Fluorescence Membrane dipole measures

2.9.1 Extrusion of liposomes

The lipids were extruded to achieve uniformity in vesicle size in suspensions in preparation for fluorescent dipole measurements. For all lipid extrusions, POPC (1-palmitoyl-2-oleoyl-glycero-3-phosphocholine) was used. The mass of dry powdered lipid was first calculated, weighed out to have an end volume of between 2-4mL at 3mM, with the volume that was required varied between each experiment.

The powdered lipid was dissolved in 100 μL of ethanol before drying off with nitrogen gas. This process left an even coating on the glass vial: this glass vial was then placed in a vacuum desiccator overnight, completing the drying process by removing excess ethanol.

Before each experiment, the lipid was then redissolved in buffer solution, either 100 mM phosphate-buffered saline solution (PBS) or 10 mM Tris buffer with 100 mM NaCl. The volume of buffer was added to make solutions to 3mM and sonicated for 2 min to ensure that the lipid had been fully dissolved. An Avanti extruder (Avanti Polar Lipids, Alabama) was used for the extrusion of liposomes. One mL of lipid/buffer solution was loaded into a syringe for each experiment. The solution was passed through 0.1 μM pores of the filter; this was repeated a further 20 times to ensure the homogeneous size distribution of liposomes. The extruded lipids were then diluted from 3 mM to 500 μM.

2.9.2 Dipole potential measurements

In order to determine if there were any changes in the dipole potential of the membranes as a result of the addition of the peptides, an electric field sensitive fluorescent probe molecule, RH451, was used [156]. Measurements were made using a Cary Eclipse Fluorescence Spectrophotometer (Agilent Technologies, Inc, California). The scanning was undertaken at room temperature, across wavelengths from 350 nM to 650 nM., at a scan rate of 600 nm min^{-1}, with data points being collected at every 1 nm. The excitation slit was set to a width of 10nm, and the emission slit was set to 20 nm. The instrument was set to receive emissions at a wavelength of 670 nm. A long-pass filter was included in the set up before the emission slit in order to attenuate the shorter wavelengths of light.

For each set of measurements, 900 µL of extruded lipid in PBS solution was added to the cuvette. An additional 2 µl of RH-421 dye was also added. The dye was at a concentration of 1.5 mM in methanol. For each set of measurements, the first scans were completed with only lipid and dye. To the cuvette, stock peptide solution was added, and scans were completed at each concentration. Scans were undertaken at peptide concentrations (µM) of 2.5, 5, 7.5, 10, 12.5, 15, 17.5 and 20. The volume of the stock solution of peptide that was added to the cuvette for each scan was calibrated against the concentration of peptide in the cuvette and corrected for the increasing volume after each addition. For the PBS control cuvette, PBS solution was added to the cuvette equal to the volume added of the peptide stock solution's volume. For each concentration of peptide, five scans were completed. This set of concentration measurements were repeated for each of the five peptides. A PBS control was measured at an equivalent volume for each concentration measurement.

2.9.3 Ratio of intensities analysis

The ratio of the emission intensities at 440 nm and 540 nm was determined for each sample, I440/I540 [157, 158]. This intensity ratio at 10 µM concentration was compared through one-way ANOVA testing using Prism 7.03 (GraphPad Software Inc., La Jolla, CA) for each peptide to determine the significance of the peptide-membrane interactions in comparison to the PBS control.

3 Results

3.1 Melimine modelling

When exploring the possible interactions that melimine and its derivatives have with lipid bilayers, the peptide structure plays an important role. The software package PEP-FOLD 2.0 [132, 159-162] was used to identify the spatial conformation of amino acid residues of the peptide. For each of the five peptides, a local structure prediction profile and 10 × 3D variations of the predicted structure of each of the melimine peptides were obtained. The local structure prediction profile charts the probability that a structural alphabet (SA) fragment [163, 164], a section of four amino acids representing elementary prototype protein conformations, would form into a particular spatial conformation. These spatial conformations are defined as one of three types, a helical conformation, a random coil conformation and an extended conformation with no specified shape. The 3D peptide structures show the outcome of the completed *greedy* algorithm [131, 134], used to build the peptide sequence in its lowest energy state, and an optimised potential for efficient structure prediction (OPEP) algorithm [165], to limit the roughness of the peptides' energetic landscape. From these two algorithms, ten conformations with the highest probability of forming are presented.

3.1.1 Melimine

The predicted structure is presented in solution [159, 160]. These predicted structures have been compared for several buffers with potassium phosphate, NaCl and trifluoroethanol (TFE). By studying the local structure prediction profile, Figure 3.1.1.1, and comparing this prediction to the amino acid sequence of melimine, a picture of the secondary structure was able to be formed.

TLISWIKNKRKQRPRVSRRRRRRGGRRRR

Starting at the N-terminus, the peptide is predicted to have a structural conformation that is of either random coil or helical in nature, with a 40% likelihood of each.

Between the leucine, the 2nd amino acid residue, and the first arginine residue, the 11th amino acid residue in this peptide sequence, the software predicted with a 60% likelihood that the

peptide was likely to form an α-helical configuration. In the next SA fragment of this peptide, between the first and second arginine's, at the 11th position and 14th positions of the sequence, the arginine, lysine and glutamine were predicted to enter into a random coil configuration with a likelihood of 70-80%. A second α-helical configuration was predicted to encompass over half of the arginine residues from the 14th residue to the 22nd residue. This α-helix conformation persisted until the two glycines (23rd and 24th position) within the peptide (another 60% probability of this conformation). The last four residues from the C-terminus were predicted to be in a random coil configuration with a likelihood above 90%. This prediction was further displayed in the model visualisation shown in Figure 3.1.1.2.

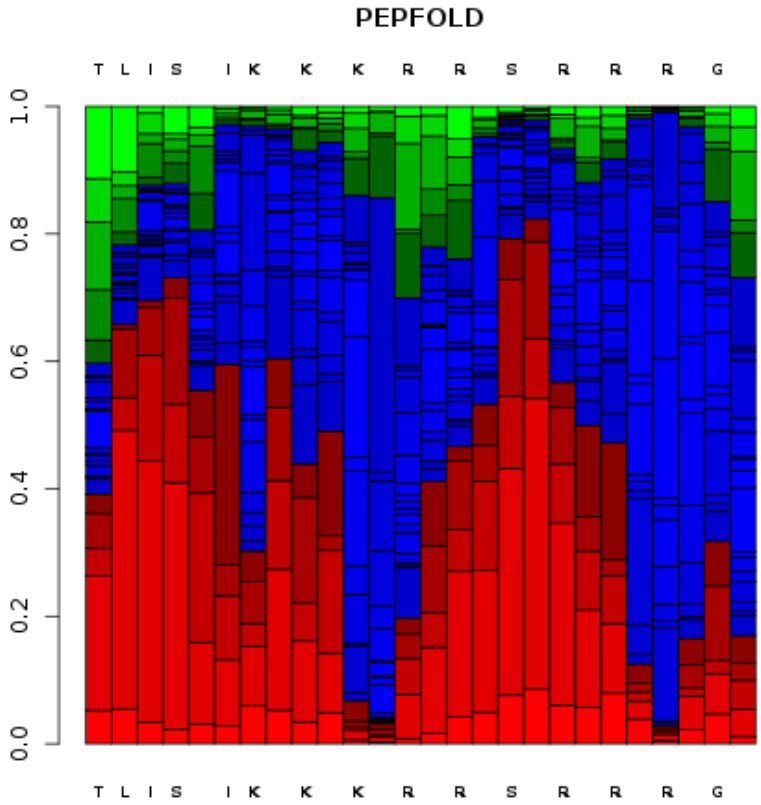

Figure 3.1.1.1: Local structure prediction profile for melimine. Here, the SA fragments of four amino acid residues in length showed the predictions for the structural conformations. The colours represent the three different conformations, helical conformation (red), random coil conformation (blue) and an extended (non-specific) conformation (green). Image collected using PEP-FOLD 2.0 software package [132, 159-162].

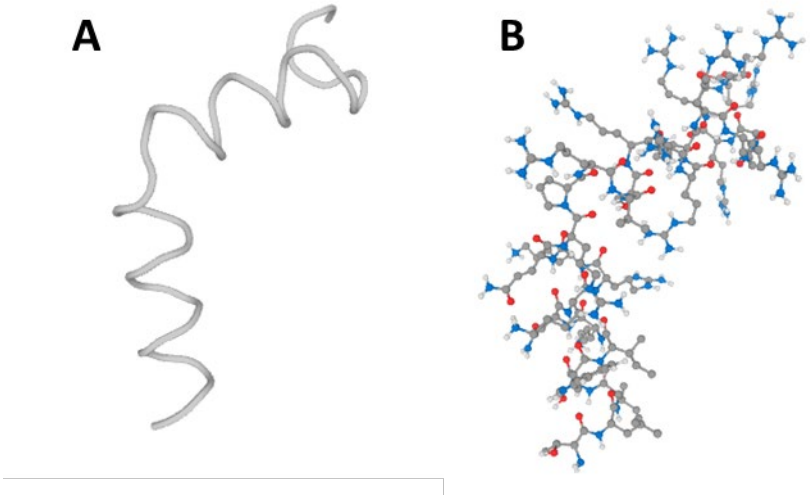

Figure 3.1.1.2: Example of the model visualisation of melimine (one of 10 model outputs) **A**, a cartoon version of the model depicting α-helical structures. **B**, ball and stick model showing side amino acid chains. Image collected using PEP-FOLD 2.0 software package [132, 159-162].

To describe further this peptide, hydrophilicity calculations [166] were undertaken based on the Hopp and Woods scale [167]. This scale measures the hydrophilicity as positive values, with the hydrophobicity having negative values, as seen in Figure 3.1.1.3. Melimine contains a hydrophobic N-terminus region before transitioning into hydrophilic amino acid residues along the rest of the peptide. The coils of melimine contain basic amino acid residues of arginine, and lysine, which are positively charged in solutions around pH 7.

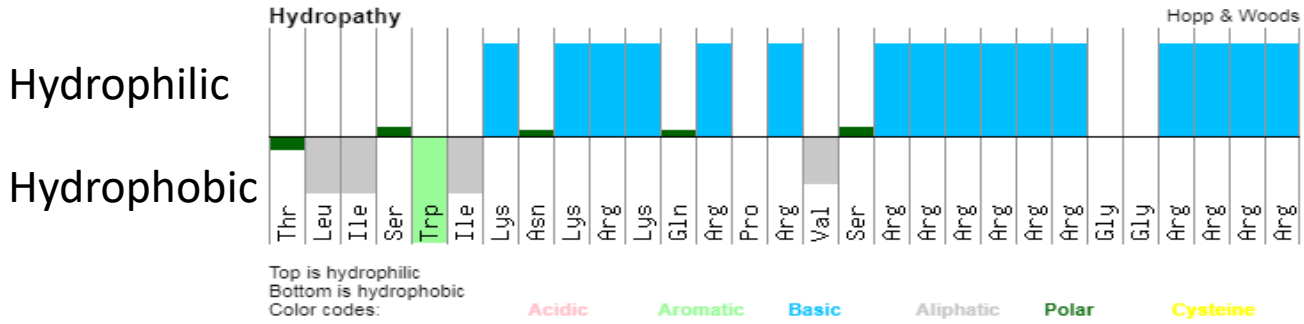

Figure 3.1.1.3: Depiction of the hydrophilicity and hydrophobicity of melimine [166]. The peptide has more hydrophobic residues at the N-terminus and more hydrophilic residues at the C-terminus.

3.1.2 Cys-melimine

Cys-melimine has the same sequence as melimine except for the addition of a cysteine moiety on the N-terminus. Within the prediction profile, this cysteine was predicted to have a high likelihood of being in an extended conformation, at a 60-70% probability, see Figure 3.1.2.1. This extension was prevalent in the 3D model seen in Figure 3.1.2.2 and can be contrasted with the continued coil at the N-terminus of melimine in Figure 3.1.1.2.

In having the same sequence as melimine, cys-melimine contained the helix-hinge-helix formation, with an 80-90% likelihood of being in a random coil conformation, at the 12^{th}-15^{th} residues centred around the proline residue.

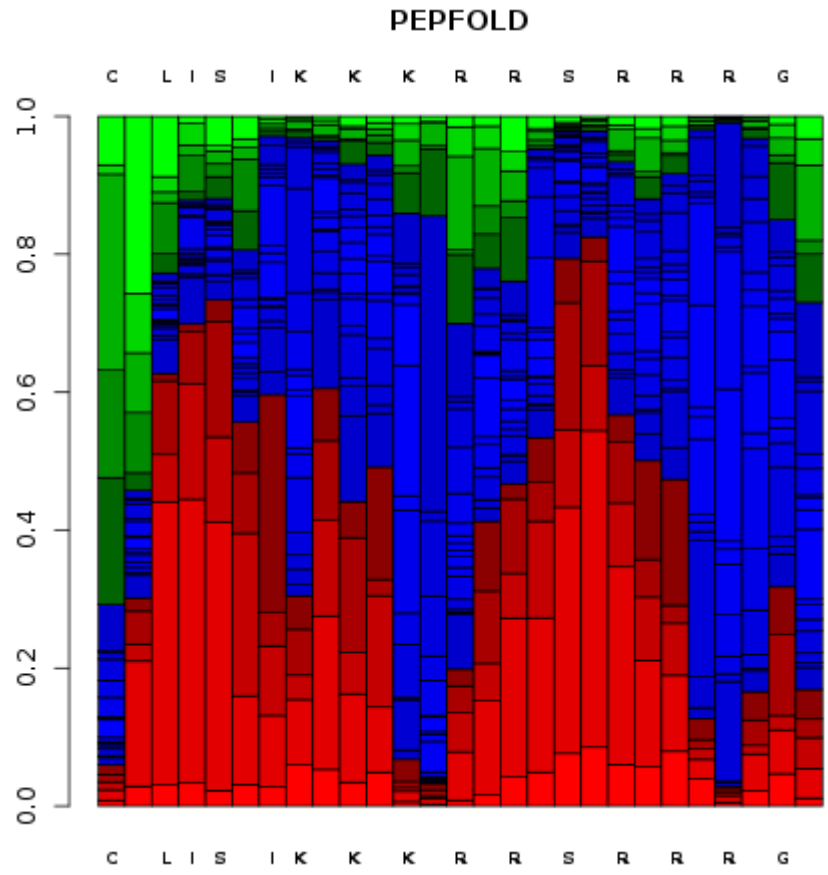

Figure 3.1.2.1: Local structure prediction profile for cys-melimine. The colours represent the three different conformations, helical conformation (red), random coil conformation (blue) and an extended (non-specific) conformation (green). Image collected using PEP-FOLD 2.0 software package [132, 159-162].

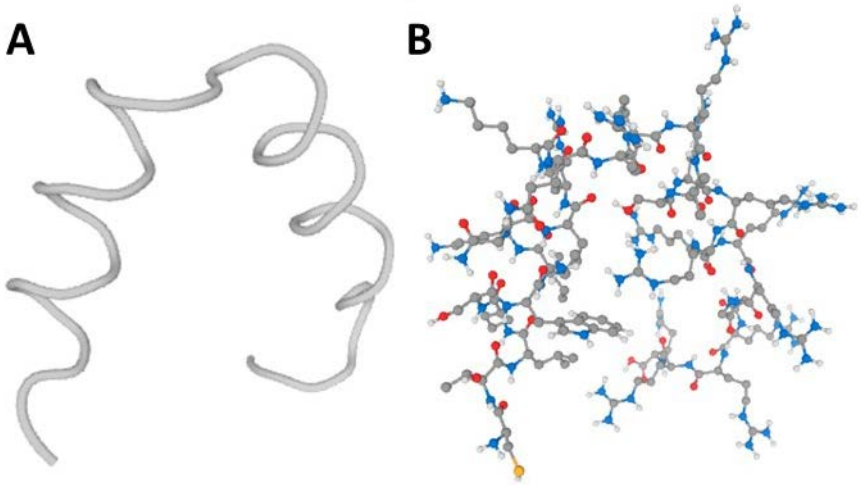

Figure 3.1.2.2: Example of the model visualisation of cys-melimine (one of 10 model outputs) **A**, a cartoon version of the model depicting α-helical structures. **B**, ball and stick model showing side amino acid chains. Image collected using PEP-FOLD 2.0 software package [132, 159-162].

When looking at the hydrophilicity of the peptide, while being the same as melimine, the additional cysteine moiety to the N-terminus of the peptide adds to the hydrophobic nature of this region; see Figure 3.1.2.3.

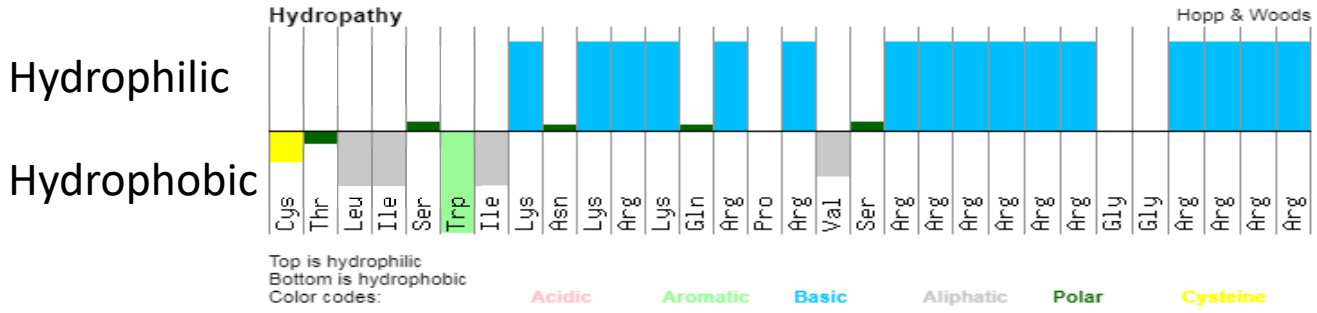

Figure 3.1.2.3: Depiction of the hydrophilicity and hydrophobicity of cys-melimine [166]**.**

3.1.3 Mel4

The truncated peptide mel4 had the shorter peptide sequence shown here:

KNKRKRRRRRRGGRRRR

Using the **PEP-FOLD 2.0** software, mel4 was predicted to form only one α-helical configuration in its structure before terminating in a random coil configuration, as seen in Figure 3.1.3.1. The α-helical structure was predicted to form between the 2nd and nine residues, constituting over half of the peptide, before terminating in a random coil between the 9th and 14th residues at the C-terminus. This prediction can be seen in Figure 3.1.3.2. As mel4 is a truncated version of melimine, it lacks the proline residue associated with the helix-hinge-helix motif.

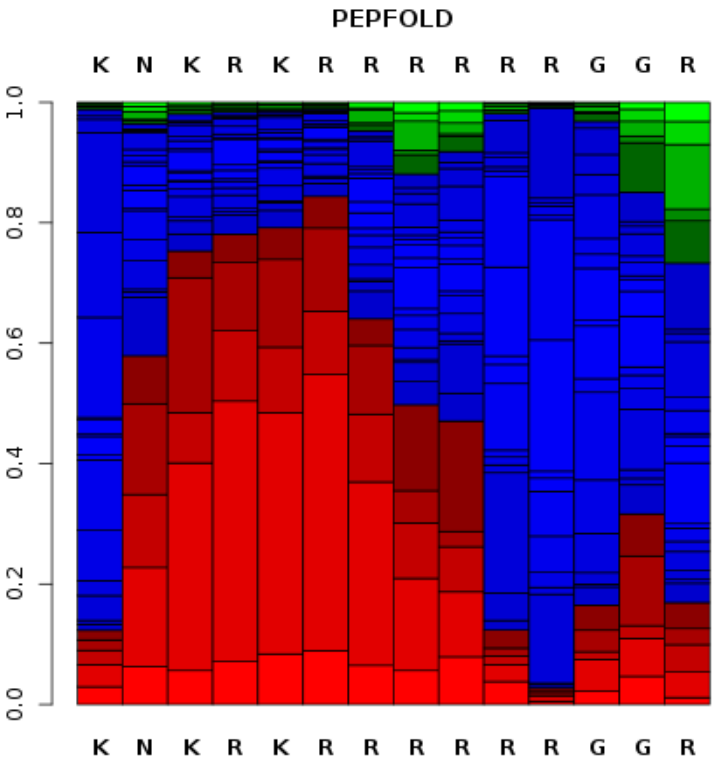

Figure 3.1.3.1: Local structure prediction profile for mel4. The colours represent the three different conformations, helical conformation (red), random coil conformation (blue) and an extended (non-specific) conformation (green). Image collected using PEP-FOLD 2.0 software package [132, 159-162].

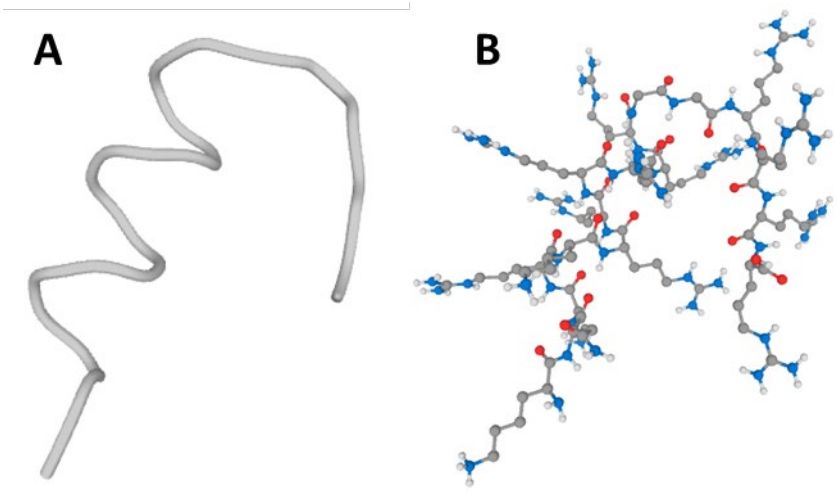

Figure 3.1.3.2: Example of the model visualisation of mel4 (one of 10 model outputs) **A**, a cartoon version of the model depicting α-helical structure. **B**, ball and stick model showing side amino acid chains. Image collected using PEP-FOLD 2.0 software package [132, 159-162].

Mel4, being smaller than melimine but containing a similar number of arginine residues, its charge and hydrophilic nature are spread across the whole peptide, not simply localised at the C-terminus (see Figure 3.1.3.3).

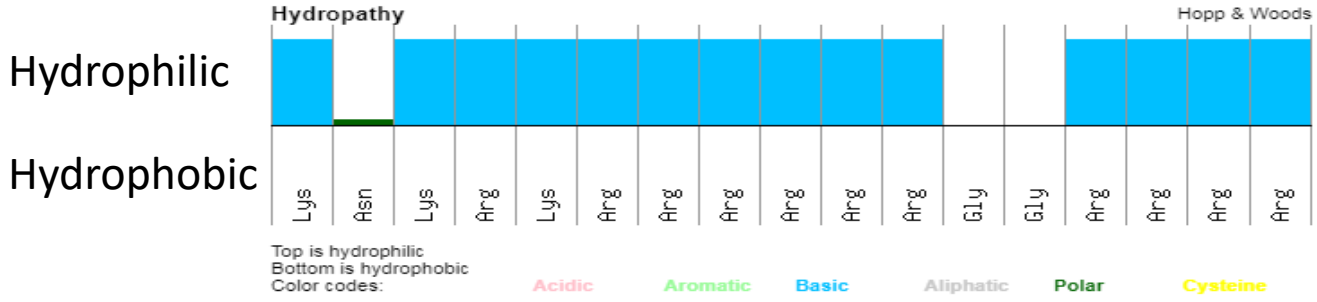

Figure 3.1.3.3: Depiction of the hydrophilicity and hydrophobicity of mel4 [166].

3.1.4 Cys-mel4

Cys-mel4 consists of the same sequence as mel4, with the addition of a cysteine moiety on the N-terminus.

CKNKRKRRRRRRGGRRRR

The peptide is predicted to form the same α-helical structure as mel4, between the 2nd and nine residues before terminating in a random coil between the 9th and 14th residues at the C-terminus (see Figure 3.1.4.1). The added cysteine residue does not have much effect on the overall predicted structure, with it increasing the likelihood of the N-terminus being an extended region, as seen in Figure 3.1.4.2, in much the same way as for cys-melimine.

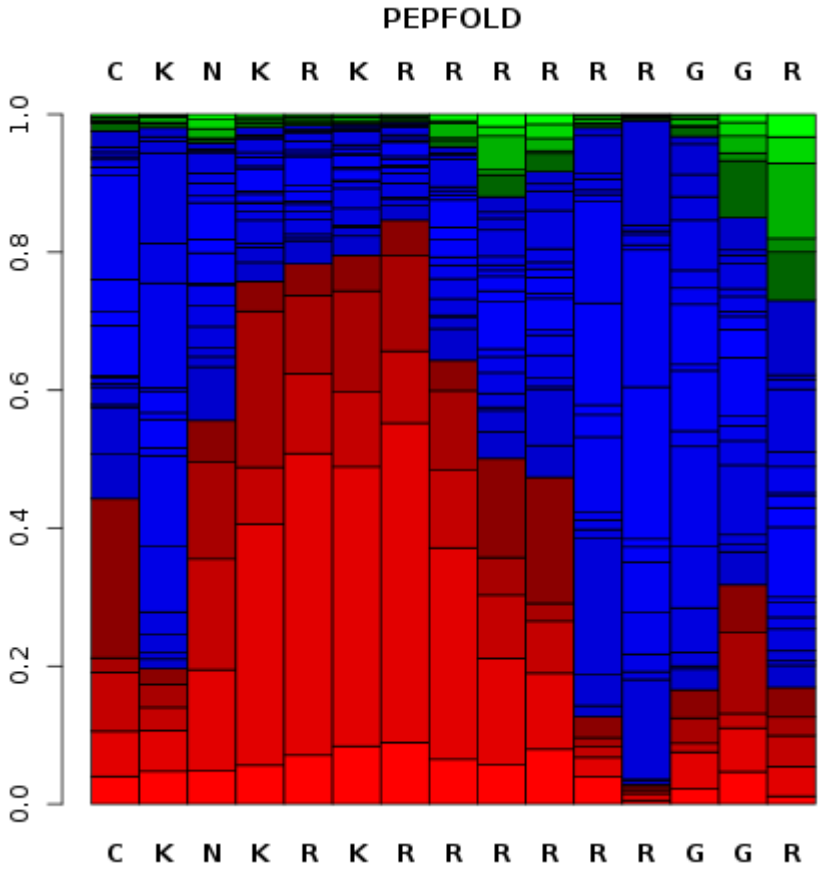

Figure 3.1.4.1: Local structure prediction profile for cys-mel4. The colours represent the three different conformations, helical conformation (red), random coil conformation (blue) and an extended (non-specific) conformation (green). Image collected using PEP-FOLD 2.0 software package [132, 159-162].

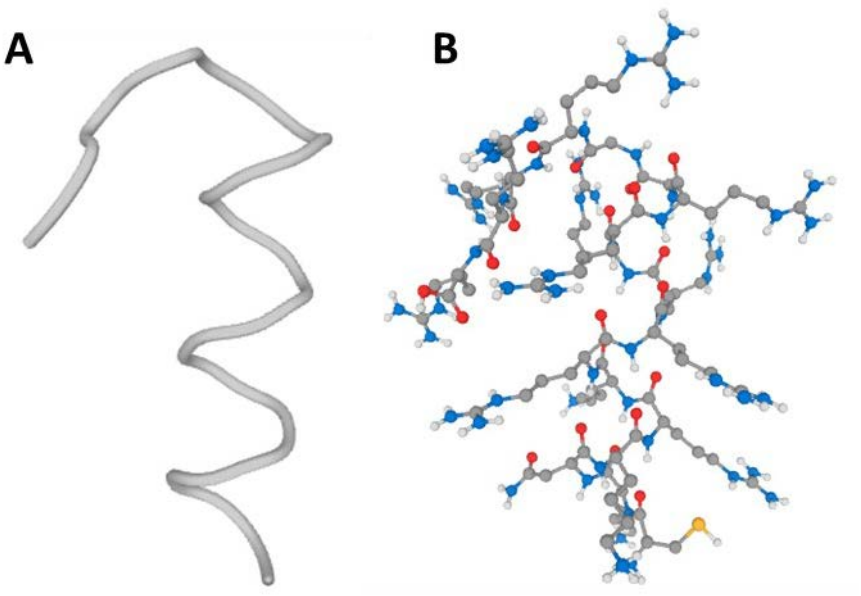

Figure 3.1.4.2: Example of the model visualisation of cys-mel4 (one of 10 model outputs) **A**, a cartoon version of the model depicting α-helical structure. **B**, ball and stick model showing side amino acid chains. Image collected using PEP-FOLD 2.0 software package [132, 159-162].

When studying the hydrophilicity of cys-mel4 in Figure 3.1.4.3, the addition of the cysteine residue at the N-terminus, caused this N-terminus to have a hydrophobic nature. This contrasts against the completely hydrophilic mel4.

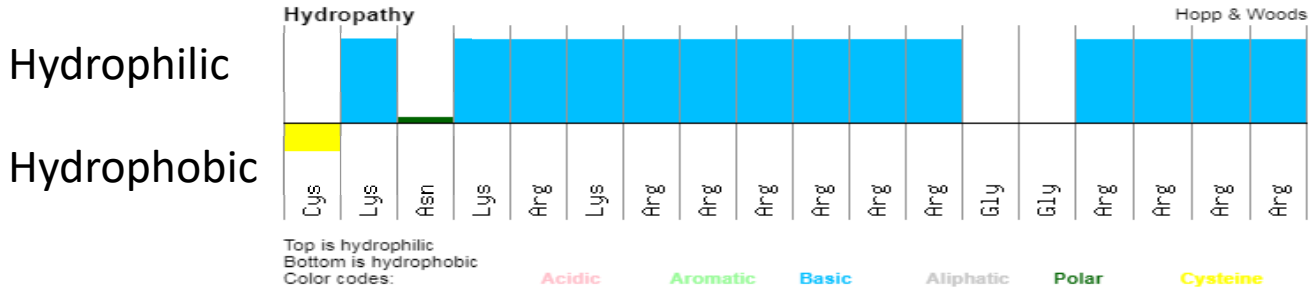

Figure 3.1.4.3: Depiction of the hydrophilicity and hydrophobicity of cys-mel4 [166].

3.1.5 MelAlanine

MelAlanine has the same number of amino acid residues as melimine, but it contains alanine residues that replace the arginine residues in the 18th to the 22nd positions within the sequence:

TLISWIKNKRKQRPRVSAAAAAAGGRRRR

The alanine residues still maintained the α-helix configuration that was seen in both melimine and cys-melimine. The main difference seen after the substitution of alanine residues for arginines was the likelihood of the alanine residues being in a helical conformation slightly reduced by ~5-10% (see Figure 3.1.5.1).

The hinge-helix-hinge structural motif was also present within this peptide (Figure 3.1.5.2) between the 12th to 15th residues, centred around the proline residue in the sequence. While melAlanine contained this helix-hinge-helix motif, it does not have the same antibacterial properties as melimine [40].

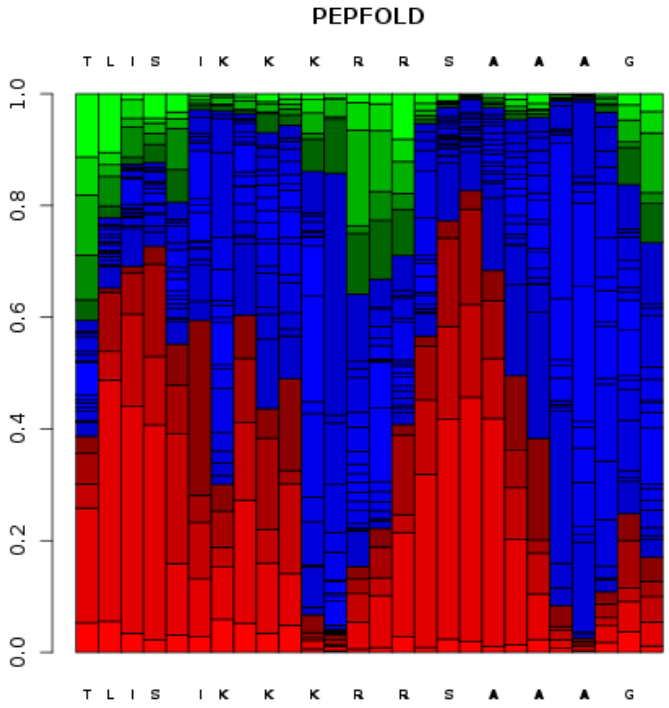

Figure 3.1.5.1: Local structure prediction profile for melAlanine. The colours represent the three different conformations, helical conformation (red), random coil conformation (blue) and an extended (non-specific) conformation (green). Image collected using PEP-FOLD 2.0 software package [132, 159-162].

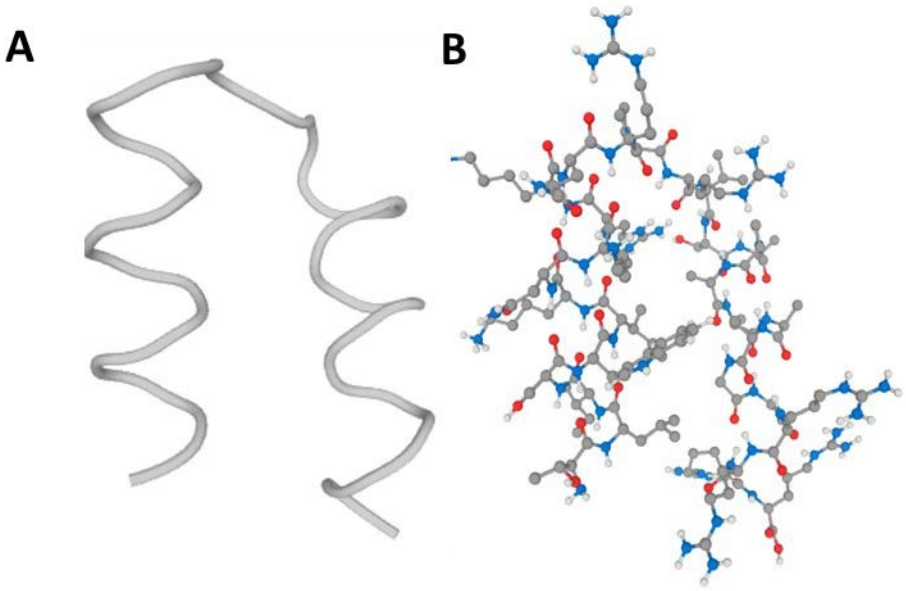

Figure 3.1.5.2: Example of the model visualisation of melAlanine (one of 10 model outputs) **A**, a cartoon version of the model depicting α-helical structures. **B**, ball and stick model showing side amino acid chains. Image collected using PEP-FOLD 2.0 software package [132, 159-162].

The hydrophilicity of melAlanine is in contrast to the melimine (Figure 3.1.1.3.). The replacement of the arginines with the alanine residues reduces the hydrophilicity of this peptide. This is seen in the second coil region between the 18-22nd positions. The alanine residues here have a slight hydrophobic nature, which is quite different from the highly hydrophilic arginine residues present in melimine (Figure 3.1.5.3). See Section 4.1.1 for further discussion on this topic.

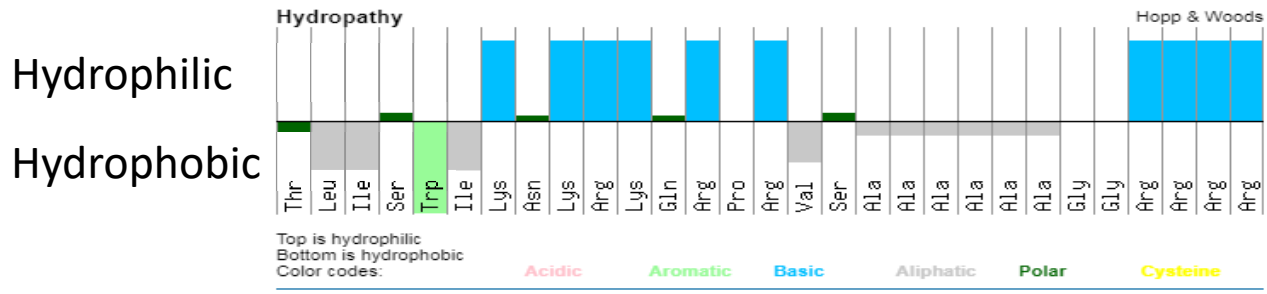

Figure 3.1.5.3: Depiction of the hydrophilicity and hydrophobicity of melAlanine [166].

3.2 Fluoroscopy with RH-421 dye

RH421 dye is an electric field sensitive probe that can be used to measure the dipole that extends from the lipid water interface to the centre of a lipid membrane. When a peptide interacts with the outer leaflet of a lipid bilayer, a change in the local electric field occurs, causing a wavelength shift in the dye [156, 168]. This is used to determine if a peptide such as melimine is membrane active through measuring if the static potential of the membrane is perturbed by adding the peptide to it.

3.2.1 Melimine

In comparing the intensity response of the RH-421 dye, a drop in the peak intensity was seen upon the addition of melimine (see Figure 3.2.1.1). While this change in peak intensity-shift appeared to be significant, the drop in intensity was not reproducible. This was due to a variety of factors that influenced the signal from the dye. The intensity of the response could change due to the dye itself altering the membrane potential or the dipole potential; also, changes in the dye concentration between scans could have influenced the peptide conformation or changed the membrane fluidity [157]. Because of these factors, the ratio of intensities at 440 nm and 540 nm was deduced to be a better measure to determine if there was a shift in the fluorescence intensity of the dye [157, 158].

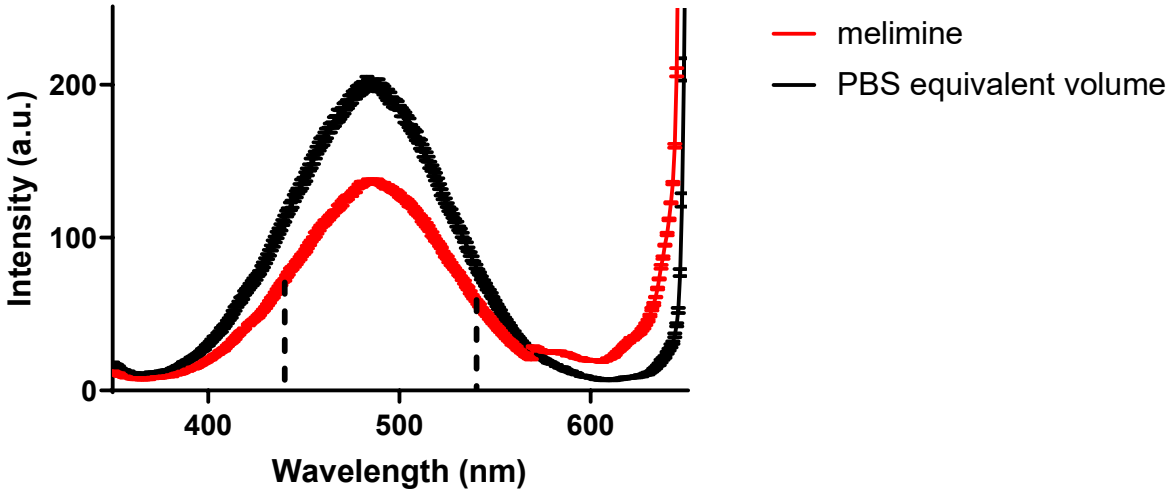

Figure 3.2.1.1: Intensity profile of melimine and PBS at an equivalent volume. Average of five scans at a concentration of 10 μM melimine. Dotted lines show the corresponding intensities at 440 nm and 540 nm, at which where the ratios were calculated.

The ratio of intensity at each concentration were plotted for each measured concentration (see Figure 3.2.1.2). The melimine profile of the intensity ratio showed a decrease in the ratio with increasing melimine concentration. This fall in the ratio between the PBS control and the melimine signified that the peptide was interacting with the lipid membrane headgroups.

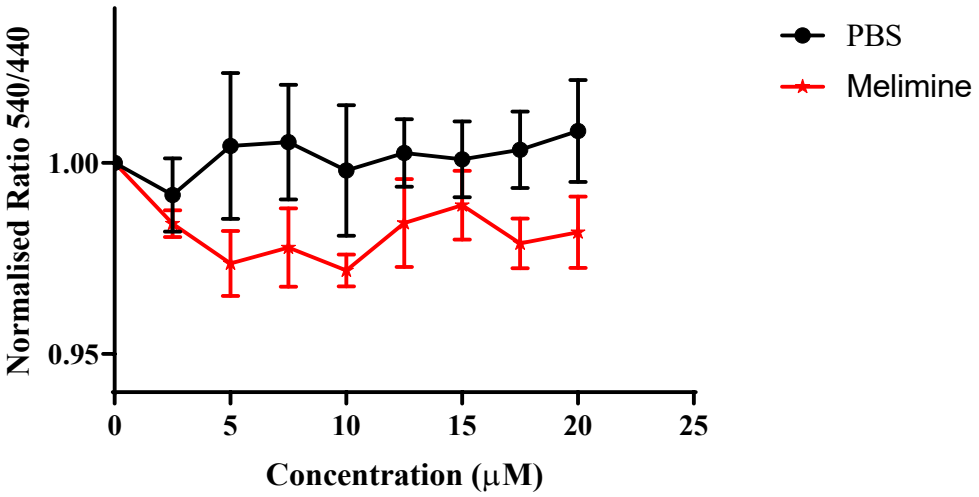

Figure 3.2.1.2: Comparison of the intensity ratios between the PBS control and melimine at increasing concentrations. Average of five scans. Error bars denote the standard deviation.

To determine the significance of the drop, the normalised intensity ratio of the 10 μM value of each scan was plotted, see Figure 3.2.1.3, with a one-way Analysis of Variance (ANOVA) comparing the difference between the peptide and the PBS control at the equivalent volume. Two of the peptide derivatives showed a significant difference in the intensity ratio in comparison to the PBS control, melimine and cys-melimine (Figure 3.2.1.3).

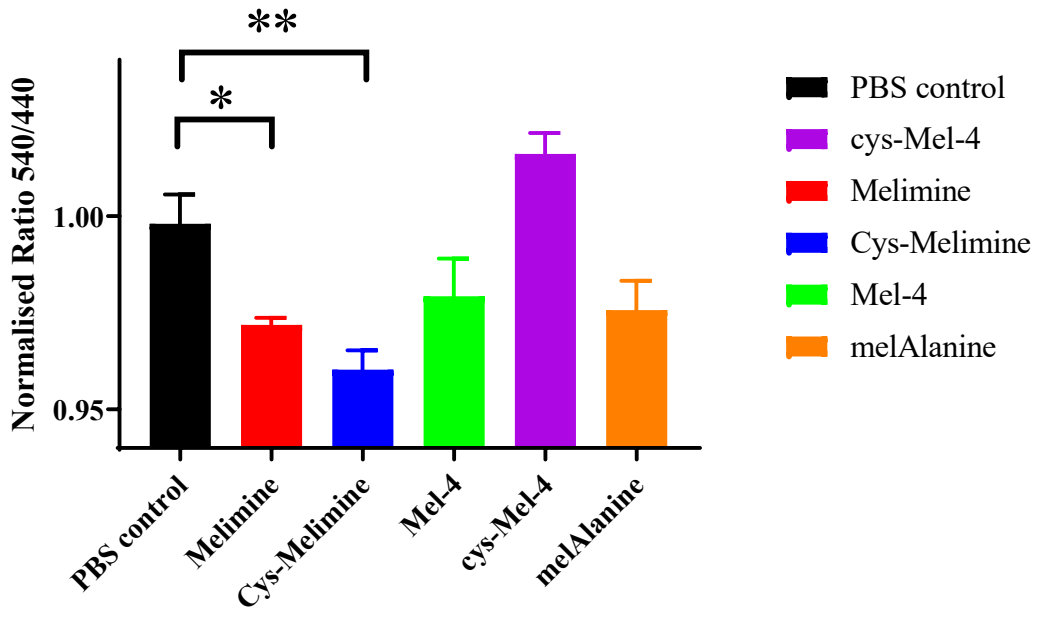

Figure 3.2.1.3: Comparison of the change in the RH-421 fluorescence of melimine and its derivatives at 10 μM against a PBS control at equivalent volume. The error bars represent the standard error of the mean (SEM). One-way ANOVA was conducted determining the statistical difference in terms of a P-value. (*P<0.05, **P<0.01).

From this analysis, a P-value is reported; it tests whether the normalised intensity ratio at 10 μM for each of the peptide derivatives had the same mean as the ratio of the PBS control. In the analysis between the PBS control and melimine, a P-value of 0.0434 was calculated, indicating that the means of the exponential components from the two data sets were statistically different. Due to this significant difference in the intensity of the emitted signal, it was concluded that the interactions of melimine would cause a shift in the dipole potential of the lipid headgroups.

3.2.2 Cys-melimine

The cys-melimine profile of the intensity ratio showed a decrease in the ratio with increasing cys-melimine concentration, with this fall starting at a higher concentration than melimine (see Figure 3.2.2). This was deduced to indicate that cys-melimine bound differently from melimine.

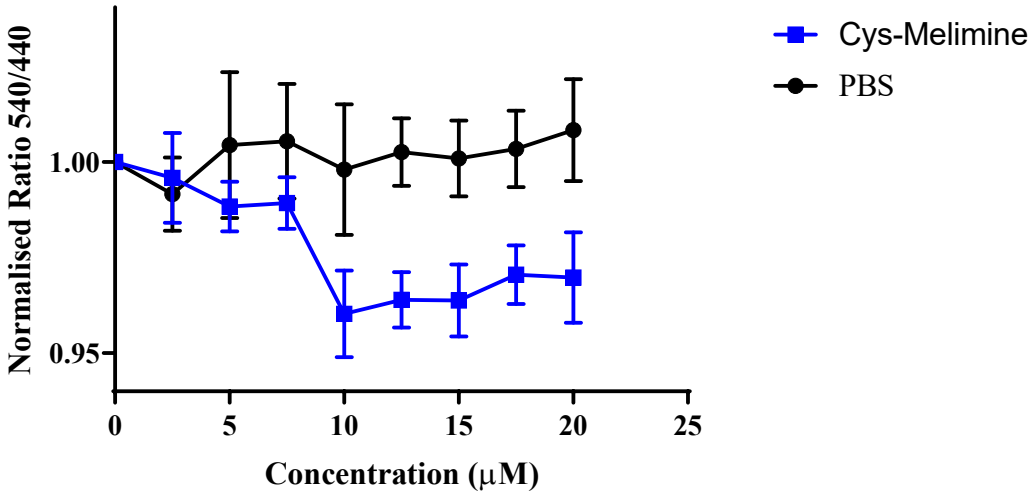

Figure 3.2.2: Comparison of the intensity ratios between the PBS control and cys-melimine. Average of five scans. Error bars denote the standard deviation.

After running the ANOVA analysis on the 10 μM intensity ratios of cys-melimine (see Figure 3.2.1.3), a P-value of 0.002 was calculated; this value was smaller than that for melimine, indicating that the means of 10 μM values of cys-melimine and the PBS control were significantly different. As cys-melimine shows a greater significant difference than melimine, this may indicate that the interactions of cys-melimine have a larger effect in influencing the dipole potential of the lipid headgroups.

3.2.3 Mel4

After plotting the intensity ratios of mel4, the profile showed a gradual decrease in the ratio with increasing concentration, where a slight difference at higher concentrations was seen between the PBS control and the mel4 profiles (see Figure 3.2.3).

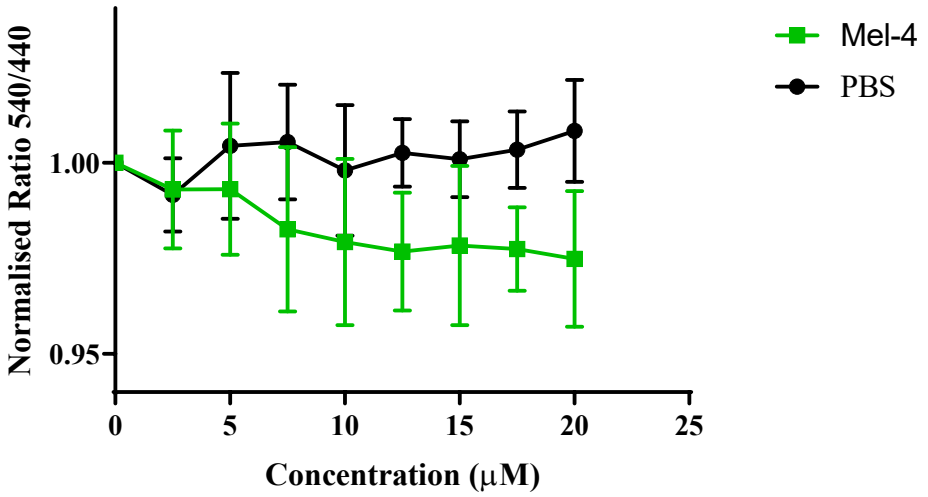

Figure 3.2.3: Comparison of the intensity ratios between the PBS control and mel4. Average of five scans. Error bars denote the standard deviation.

After running the ANOVA analysis on the 10 μM intensity ratios of mel4, plotted in Figure 3.2.1.3 above, a P-value of 0.2060 was reported.

The p-value returned was >0.05, indicating that the means of the intensity ratios at 10 μM and from the means of the PBS control were not statistically different at the level of 95% confidence. In other words, this high P-value indicates that the collected data for mel4 did not appear to be statistically different from the PBS control. This result suggests that the interactions of mel4 had minimal influence over changes in the lipid headgroup dipole potential.

3.2.4 Cys-mel4

After plotting the intensity ratios, the cys-mel4 profile shows the least difference in comparison to the PBS control (see Figure 3.2.4).

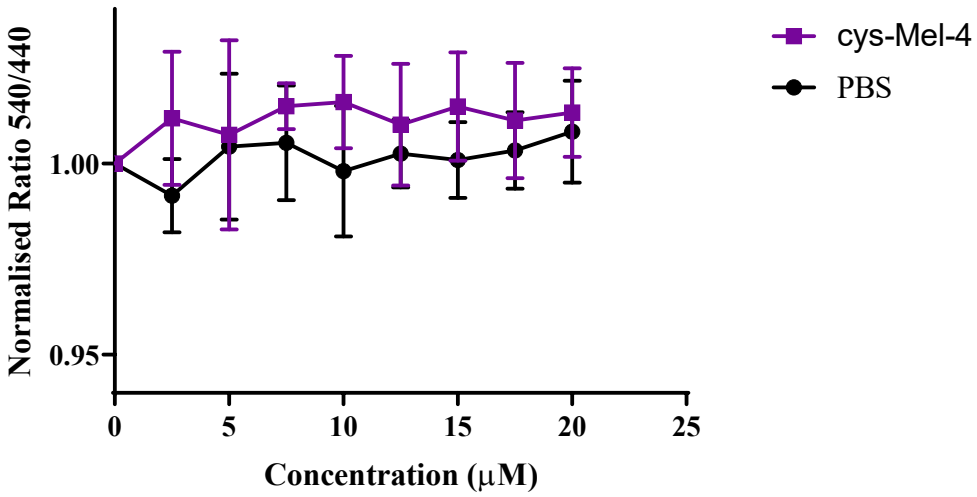

Figure 3.2.4: Comparison of the intensity ratios between the PBS control and mel4. Average of five scans. Error bars denote the standard deviation.

The intensity ratios were plotted against the concentration, with the 10 μM values used to compare to the PBS control (see Figure 3.2.1.3). Following the same ANOVA analysis, a P-value of 0.2311was calculated for cys-mel4 and was larger than 0.05, indicating that the means of the exponential components of both cys-mel4 and the PBS control were not expected to differ. This confirmed that cys-mel4 had minimal influence over the lipid membrane headgroup dipole potential.

3.2.5 MelAlanine

After plotting the intensity ratios, the melAlanine profile showed a decrease in the ratio that was similar to the decrease seen with melimine (see Figure 3.2.5). As melAlanine was designed to be a negative control peptide, this type of interaction was not expected.

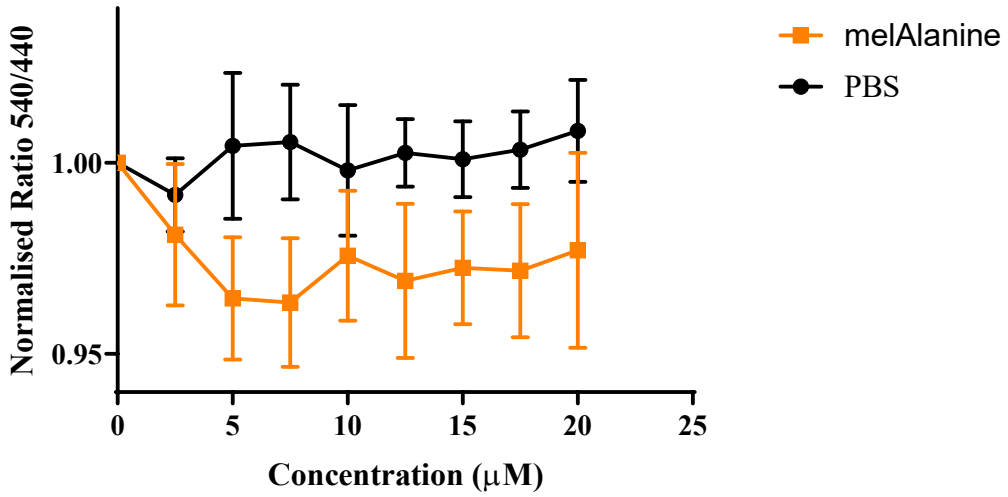

Figure 3.2.5: Comparison of the intensity ratios between the PBS control and mel4. Average of five scans. Error bars denote the standard deviation.

After using the values of the 10 μM intensity ratio in an ANOVA analysis (see Figure 3.2.1.3), the comparison of the means between the melAlanine and the PBS control returned a P-value of 0.1009; this value is smaller than the reported P-values of mel4 and cys-mel4 but was > 0.005. This indicated that means of the 10 μM intensity ratios of melAlanine and the PBS control were not statistically different. This suggested that the influence of melAlanine on the dipole potential of the membrane was smaller than melimine and cys-melimine, which would be consistent with melAlanine being a suitable negative control at this concentration.

ANOVA comparison	P-Value	Significantly different?
PBS vs. melimine	0.0434	Yes
PBS vs. cys-melimine	0.0025	Yes
PBS vs. mel4	0.2060	No
PBS vs. cys-mel4	0.2311	No
PBS vs. melAlanine	0.1009	No

Table 3.2: Summary of the ANOVA analysis comparing each of the peptides to the PBS control.

From the low P-values associated with melimine and cys-melimine, both peptides gave values that were significantly different from the PBS control (see Table 3.2), indicating that they have a small influence over the dipole potential of the membrane. On the other hand, the interactions of mel4, cys-mel4 and melAlanine were not sufficiently large enough to influence the dipole potential of the membrane.

The disruptive capabilities of the dipole potential by melimine and cys-melimine suggested that these peptides had an influence over the lipid packing and the CPP of the membrane, which, although small, still showed that these peptides are *potentially* membrane-active. See Section 4.1.3 for further discussion on this topic.

3.3 Dynamic light scattering (DLS)

Through DLS, the hydrodynamic diameter of lipid spheroids can be measured. When studying interactions between lipids and peptides, DLS provides an alternative, non-invasive method to measure size changes and aggregation of the lipid spheroids using interactions between peptides and membranes [142].

Peptides with an amphipathic structure are known to cause aggregation in electrically neutral charged lipid vesicles [142], with the strength of the aggregation increasing as a peptide forms a stable α-helix [169].

3.3.1 Fusogenic properties of melimine and its derivatives

By measuring the average diameter of the lipid spheroids in each sample, the Lyso-PC spheroids were found to originally have a diameter of 10.19±0.47nm before the addition of the peptides. Lipid spheroids formed from single chain Lyso-PC lipids reported in the literature have diameters of 5-10 nm [170, 171]. The lyso-PC lipids used in these measurements were oleyl (18:1) with a single carbon double bond in the acyl chain: this could bring about a change in the volume and surface area of a vesicle that would influence the CPP resulting in the formation of the larger diameters.

After the addition of each of the five peptides, the lipid spheroids in the samples had undergone aggregation, resulting in the average diameter of the lipid spheroids increasing (see Figure 3.3.1.1). The larger peptides melimine, cys-melimine and melAlanine had interacted in a way that led to the formation of larger aggregates when compared to both mel4 and cys-mel4.

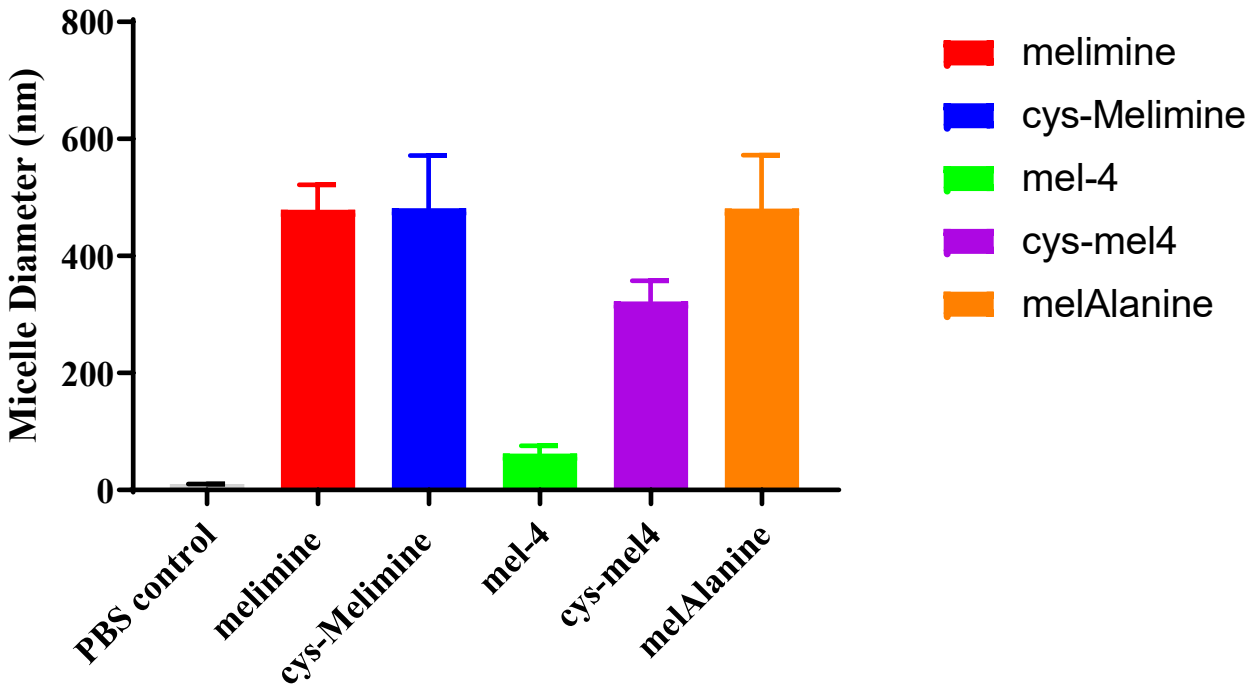

Figure 3.3.1.1: Comparison of the size of the LysoPC lipid spheroids. The average diameters of the lipid spheroids are shown after the addition of each peptide in comparison to the diameter of lipid spheroids with no peptide. The error bars denote the standard deviation from n=15 measurements.

A one-way ANOVA was carried out on these data in order to ascertain if there were significant differences in the change of the size of the lipid spheroids after the addition of each peptide. All peptides, except for mel4, were shown to bring about a statistically different change in diameter from the plain lipid control (see Figure 3.3.1.2). Section 4.1.2 contains further discussion on this topic.

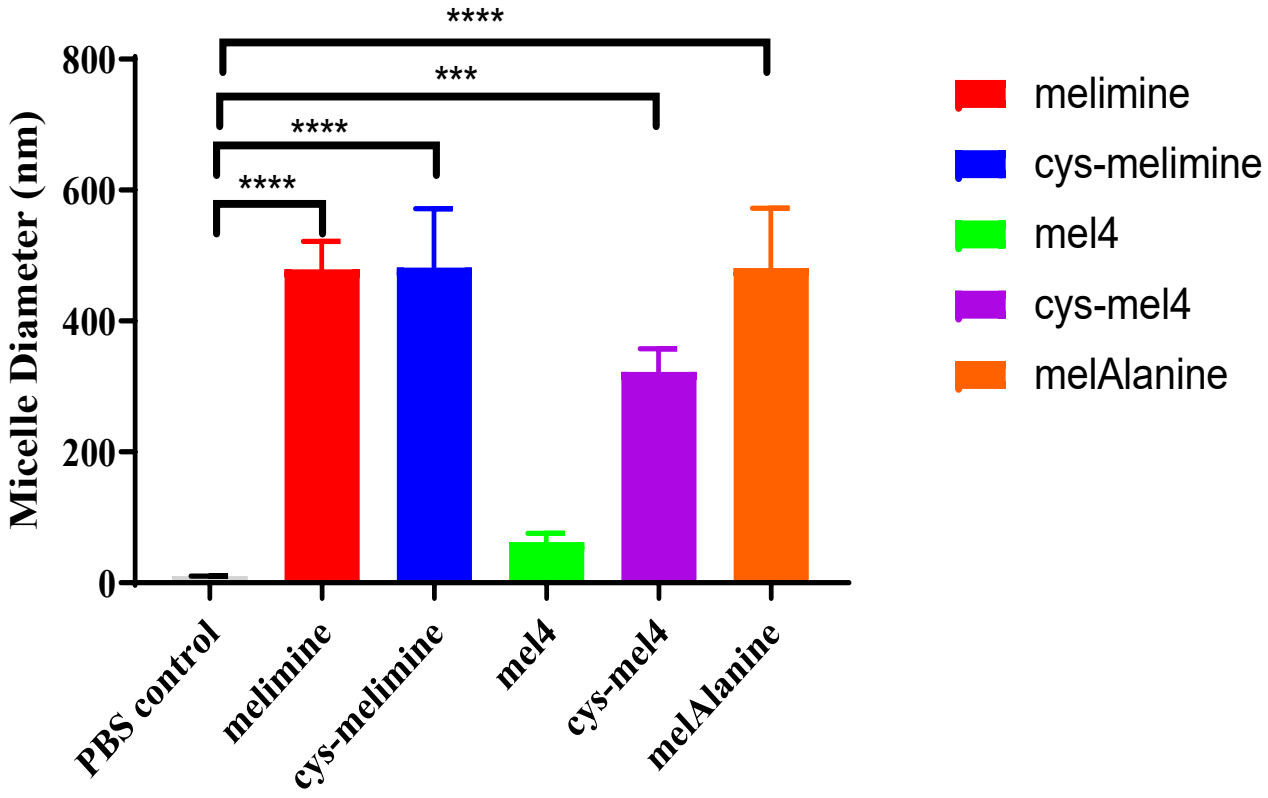

Figure 3.3.1.2: An analysis of variance (ANOVA) was undertaken on this data set, performed using Prism 7.03 (GraphPad Software Inc., La Jolla, CA) [****P-value <0.0001), ***P-value <0.001] Error bars denote the standard deviation from n = 15 measurements.

3.4 Electrical Impedance Spectroscopy (EIS)

As a way to identify how melimine and its derivatives behave when interacting with cell membranes, EIS has been used in conjunction with tBLMs. For these experiments, tBLMs were created by using the method described in Section 2.2. When using this technique to identify changes in membrane conductance and capacitance, a picture can be built up of a peptide's mode of action [67, 74].

3.4.1 Melimine

Due to their prevalence in natural cell membranes of both eukaryotic and prokaryotic organisms [41, 172], zwitterionic phospholipids were first used to identify if melimine caused a conduction response, in particular, phosphatidylcholine (PC) lipids.

Melimine was added at a concentration of 10 µM, in line with its *minimum inhibitory concentration* (MIC) and *minimum bactericidal concentration* (MBC) against various bacterial strains (Table 3.4) [40]. The MIC is the concentration at which a peptide inhibits bacterial growth, while the MBC is the concentration at which 99.9% of bacteria are killed after the addition of the peptide. The peptide was compared against both gram-positive and gram-negative bacterial bio-films, which included *S. Aureus*, *S. epidermidis*, *P.aeruginosa* and *E. coli*.

MIC / MBC (µM)					
	Melimine	cys-Melimine	Mel4	cys-Mel4	MelAlanine
S. aureus 31	17 / 34	8 / 16	27 / 27	26 / 51	>611 / >611
S. aureus 004	17 / 34	8 / 16	53 / 53	26 / 26	>611 / >611
S. aureus 152	17 / 34	8 / 16	426 / 851	26 / 51	>611 / >611
S. epidermidis 013	8.4 / 17	2.1 / 4.2	27 / 27	3.3 / 6.7	>611 / >611
P. aeruginosa 6294	132 / 264	32 / 32	213 / 213	102 / 204	>611 / >611
E. coli ATCC 0157	17 / 17	16 / 16	106 / 213	26 / 51	>611 / >611

Table 3.4: The minimum inhibitory concentrations and the minimum bactericidal concentrations for each peptide derivative used in this study. Various strains of both Gram-positive and Gram-negative bacteria were used. (Table from Berry et al. [40]).

The addition of melimine caused two small changes in the membrane, as identified in the Bode plot shown in Figure 3.4.1 A. The first change was a shift in the impedance magnitude; this is denoted as a decrease in the resistive component of the impedance plot. The capacitive elements showed no change in this plot.

The second change was in the phase component of the Bode plot. This change in the phase was made obvious through a shifting of the area of low phase angle attributed to the membrane (see Figure 1.5.2 B). The minima in the phase plot was shifted along the abscissal direction towards the higher frequency; this increase corresponds to an increase in the membrane conductance.

In the direct measurements of the membrane conductance (see Figure 3.4.1 B) a small increase in the intrinsic conduction was observed across the membrane. This was interpreted as an increase in the ionic permeability, increasing the ease at which ions can traverse the membrane. Melimine was incubated with the membrane for a period of 15 min, to determine if there would be any further interactions, before washing out with 1 mL of PBS. After washing, the conduction of the membrane was unchanged, suggesting that the off-rate for melimine interactions with the membrane was much slower than the on-rate. Furthermore, there was no significant change seen in the membrane capacitance after the addition of melimine (Figure 3.4.1. C).

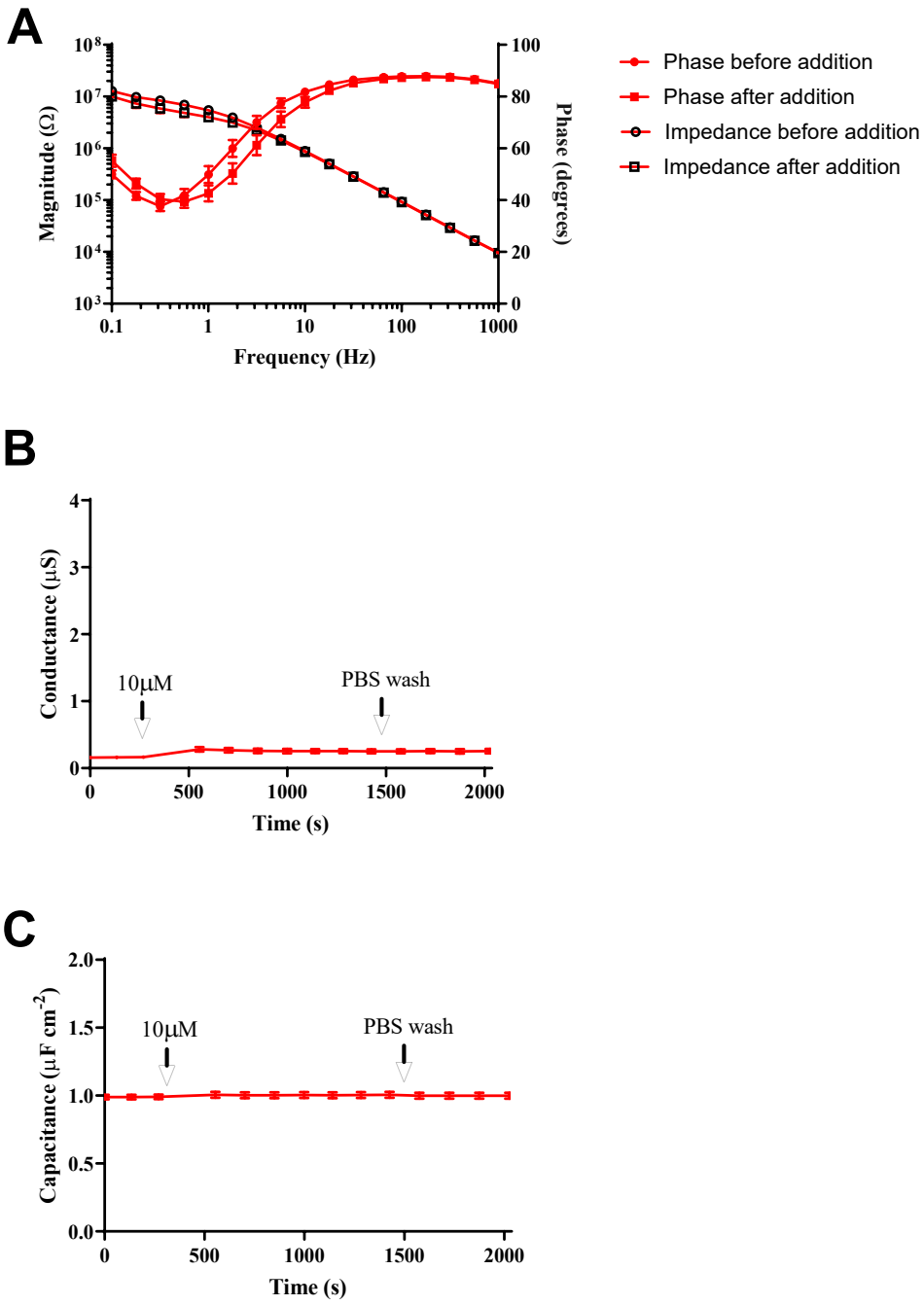

Figure 3.4.1: EIS plots for melimine in diphytanyl lipid tBLMs. **A**, Bode plot of before and after the addition of melimine (n = 3) showing a fit of the data points; the error bars denote the standard error of the mean (SEM) for each measurement. **B**, conductance response in diphytanyl lipid tBLM to the peptide melimine in diphytanyl lipid tBLM (n = 3). The error bars denote the SEM. **C**, capacitance response in diphytanyl lipids to the peptide melimine (n=3). The error bars denote the SEM.

3.4.2 Cys-melimine

3.4.2.1 Action on Zwitterionic Lipid Membranes

Cys-melimine was added to diphytanyl PC lipids at a concentration of 10 μM. After the addition, there was a noticeable shift in the resistive component of the impedance plot. The magnitude decreased as indicated by the arrow in Figure 3.4.2.1 A. The shift of the impedance minimum to a higher frequency reveals a significantly different profile when compared to melimine (Figure 3.4.1 A). The change in the phase plot also indicated more substantial membrane interactions than with seen with melimine. The area of low phase angle was shifted in the abscissal direction to higher frequencies, and in the ordinate direction where the minimum phase angle had increased. The shifting of the phase plot after the addition of cys-melimine was more pronounced than for the interaction of melimine with the tBLM, indicating that cys-melimine had a greater influence on the ionic permeability of the tBLM, it had a greater influence on both the capacitance and conductance of the membrane.

This larger influence was seen in the fitted measurements of the conduction responses of cys-melimine seen in Figure 3.4.2.1. B. These responses revealed that cys-melimine indeed had a greater influence on the ionic permeability than melimine, increasing the conductance approximately 20 times more than melimine.

However, after an initial increase over a period of ~15 min, the conduction of the membrane slowly decreased. After washing the membrane with 1 mL of PBS, the conductance of the membrane further decreased, but it did not return to baseline levels. This elevation from baseline was more pronounced than melimine, probably influenced from greater interactions as seen through the larger initial conduction increase.

Differing from melimine, cys-melimine caused an increase in the capacitance of the tBLM after its addition (Figure 3.4.2.1. C). The increased capacitance is consistent with the membrane becoming thinner due to the presence of the cys-melimine, or there may have been a change in the relative permittivity of the membrane due to the increased water content in the membrane as a result of adding the peptide. After washing with PBS, the capacitance of the membrane decreased but did not return to baseline levels.

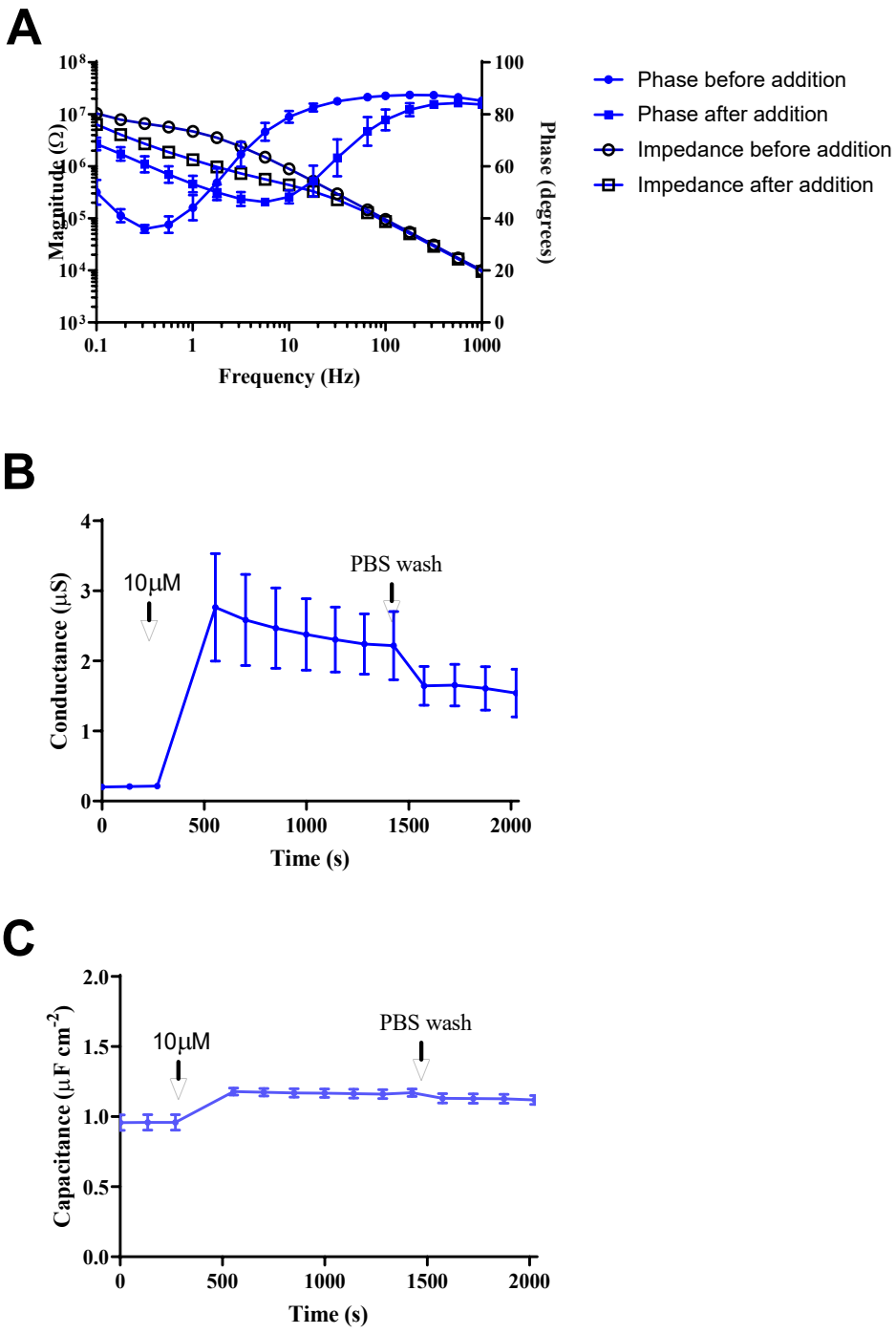

Figure 3.4.2.1: EIS plots for cys-melimine in diphytanyl lipid tBLMs. **A**, Bode plot before and after the addition of cys-melimine (n = 3), showing a fit of the data points. The error bars denote the SEM. **B**, conductance response of diphytanyl lipids to the peptide cys-melimine (n = 3). The error bars denote the SEM.**C**, capacitance response of diphytanyl lipids to the peptide cys-melimine (n = 3). The error bars denote the SEM.

3.4.2.2 Action on Negatively Charged Lipid Membranes

To explore the effect that negatively charged lipids would have on the interactions of cys-melimine, increasing concentrations of negatively charged POPG lipids were used. As cys-melimine interactions showed the largest response in terms of conduction and capacitance changes, as well as having the lowest MIC values (Table 3.4), it was chosen as the focus for testing with negatively charged lipids. This negative charge is reminiscent of that found in many bacterial cell membranes [173-175]. Negatively charged lipids have been used previously in identifying the effects of antimicrobial peptides, such as *PGLa* [135].

To elicit this interaction, a series of tBLMs composed of an increasing amount of POPG lipids were prepared. The POPG lipids were mixed with POPC lipids at relative concentrations (%) of 0, 10, 20 and 30.

As cys-melimine was added to these membranes, a slight shift was observed in the Bode plots. For each increasing concentration of POPG, there was a corresponding shift; an example of this is seen in the Bode plot of 10% POPG in Figure 3.4.2.2. A. In the impedance Bode plot, a small shift occurred to a lower magnitude in the resistive component. The area of low phase angle shifted to a higher minimum and higher frequency. These shifts were of the same form as occurred with diphytanyl lipids, although the range of the shift was smaller.

In the direct conductance measurements, as the concentration of POPG increased within the membrane, a higher negative charge was present. The interaction of cys-melimine produced a more pronounced conductance response with this increase in proportion to the amount of negatively charged lipid in the membrane (see Figure 3.4.2.2).

The effect of this was a step up in the conductance response with an increasing negative charge. This suggested that there may have been an attractive force operating between the positive charges of the amino acid residues of cys-melimine and the negatively charged membrane surface.

Across each of the membranes, the increase of capacitance response was proportionately similar (Figure 3.4.2.2. C). This suggested that cys-melimine was causing only minor changes to the thickness and/or the water content of each of the tBLM membranes.

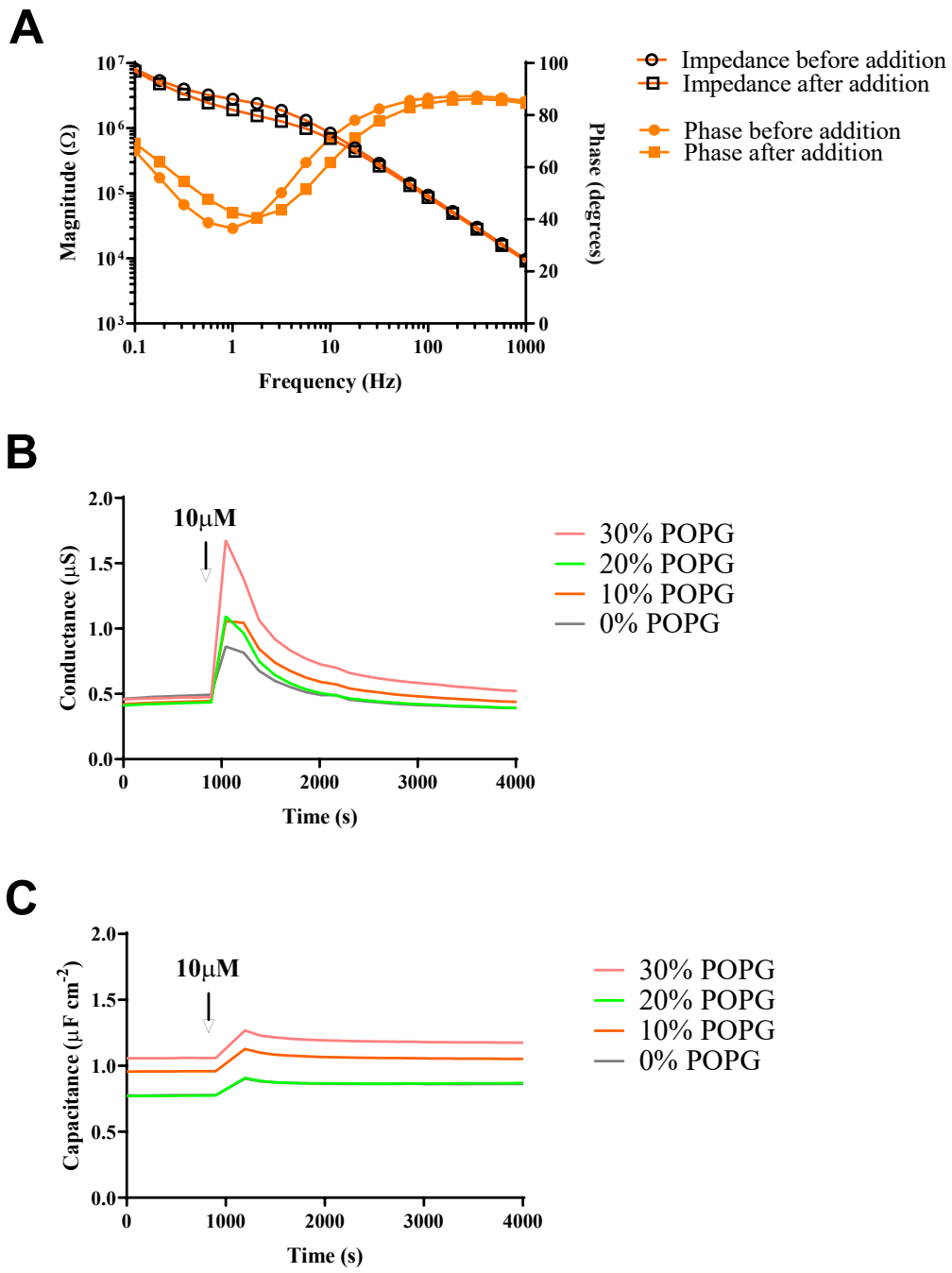

Figure 3.4.2.2: EIS plots for cys-melimine in negatively charged tBLMs. **A**, Bode plot of 10% POPG tBLMs before and after the addition of cys-melimine, showing a fit of the data points. The error bars denote the SEM. **B**, Conductance response of varying concentrations of negatively charged POPG lipids to the peptide cys-melimine. **C**, Capacitance response of varying concentrations of negatively charged POPG lipids to the peptide cys-melimine. The 0% POPG and 20% POPG profiles show overlapping data points.

3.4.3 Mel4

Truncating melimine to produce the peptide mel4 decreases its bactericidal effects (Table 3.4) [40]. After mel4 was added to a tBLM with a diphytanyl lipid membrane at a concentration of 10 μM, no change was observed in the Bode plot (Figure 3.4.3.1. A) with no shift of the impedance or phase angle.

In the direct conductance measurements, an almost negligible response was seen (Figure 3.4.3.1. B). Mel4 also elicited no change in the capacitance of the membrane (Figure 3.4.3.1. C).

Following this, the concentration of mel4 was increased to 30 μM, to match more closely its optimal MIC concentration against the bacterial strains tested [40]; and the experiment was repeated (Figure 3.4.3.2). The interaction at this higher concentration produced a slightly larger conduction response, but this was still smaller than that reported for melimine.

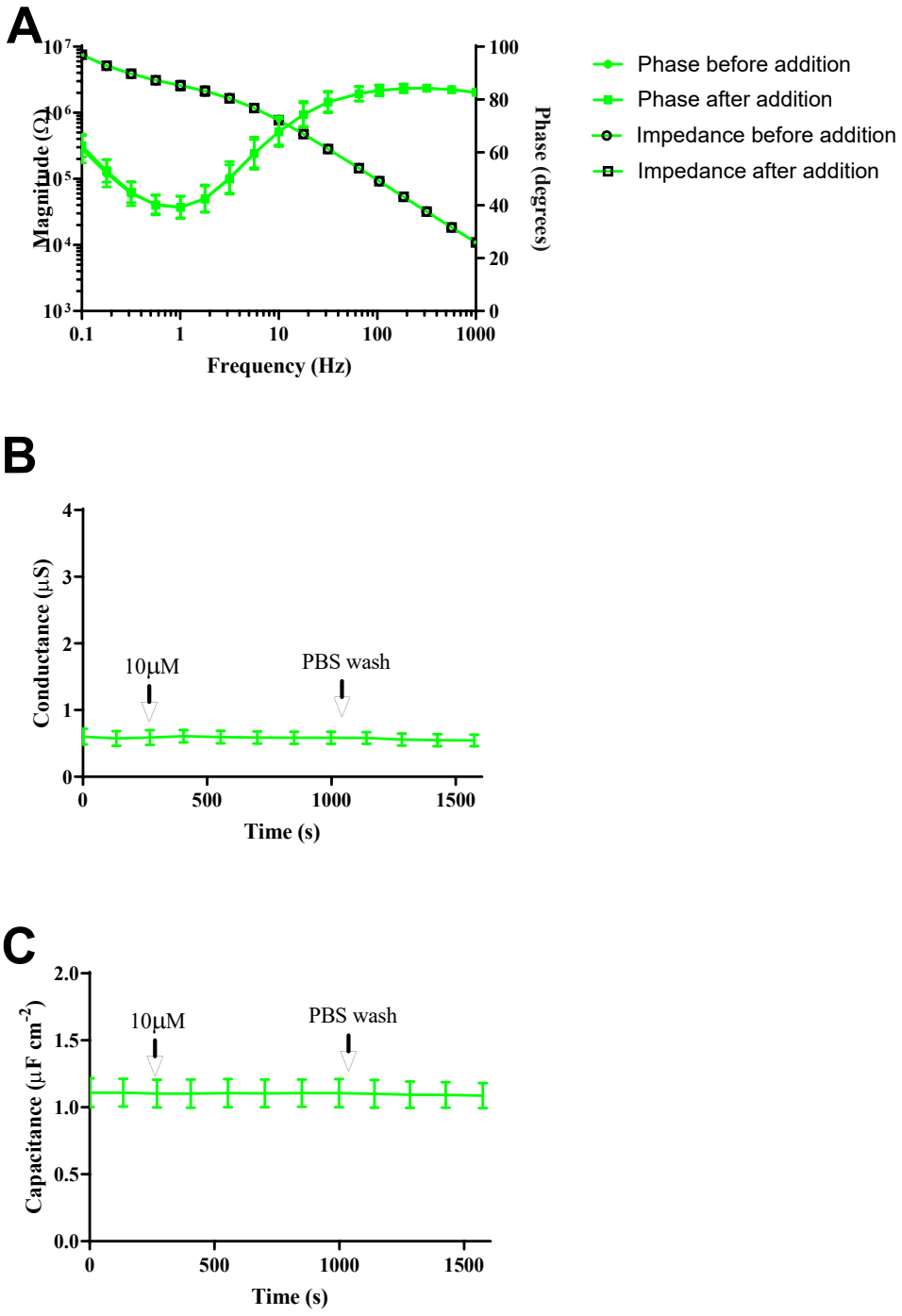

Figure 3.4.3.1: EIS plots for mel4 in diphytanyl lipid tBLMs. **A**, Bode plot of before and after the addition of mel4 (n = 3), showing a fit of the data points. The error bars denote the SEM. **B**, Conductance response of diphytanyl lipids to the peptide mel4 (n=3). The error bars denote the SEM. **C**, Capacitance response of diphytanyl lipids to the peptide mel4 (n=3). The error bars denote the SEM.

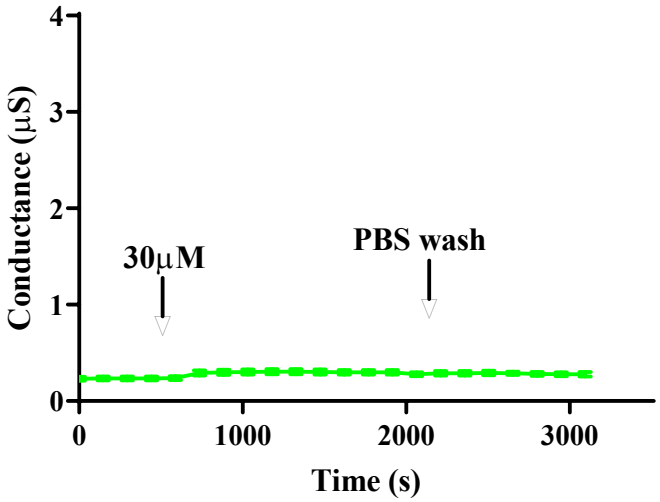

Figure 3.4.3.2: Conductance response of diphytanyl lipids to the peptide mel4 (n = 3) repeated at a higher concentration of 30 μM. The error bars denote the SEM.

3.4.4 Cys-mel4

Cys-mel4 was added to diphytanyl lipid membranes at a concentration of 10 μM. After its addition, the peptide caused a decrease in the conductance (see Figure 3.4.4. B). This decrease was opposite to the effect of the previous three peptides, melimine, cys-melimine and mel4, indicating that cys-mel4 interacts differently with the tBLM. After washing out with 1 mL of PBS, the conduction increased again, but with much variance between repeats (n = 3), suggesting some changes to the lipid bilayer, which may be due to some sort of membrane destabilisation.

The addition of a cysteine residue in cys-mel4 caused a different result to mel4. This effect is also present when comparing melimine to cys-melimine. The difference of one amino acid between the pairs of peptides, melimine and cys-melimine, and mel4 and cys-mel4, has shown a larger difference in the interactions of the peptide with lipid bilayers. The addition of the cysteine residue caused a larger effect but occurred in opposite directions. The conduction increased after the addition of cys-melimine but decreased for cys-mel4.

When recording the capacitance effects (Figure 3.4.4. C), cys-mel4 caused a decrease in the capacitance of the tBLM. This decrease suggested thickening of the membrane and/or a reduction of water within the membrane as a result of the lipids becoming more tightly packed.

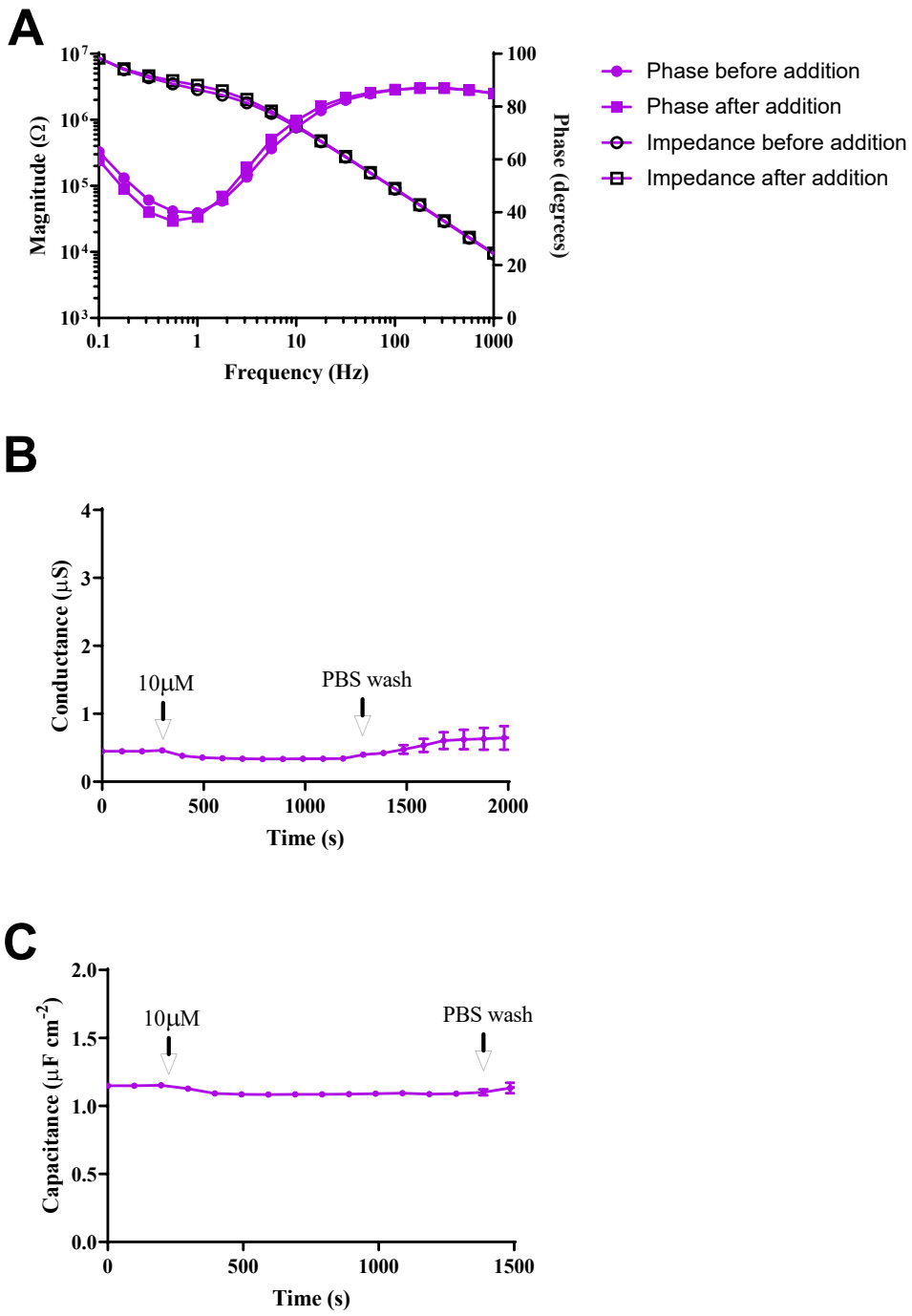

Figure 3.4.4: EIS plots for cys-mel4 in diphytanyl lipid tBLMs. **A**, Bode plot of before and after the addition of cys-mel4 (n = 3), showing a fit of the data points. The error bars denote the SEM, **B**, Conductance response of diphytanyl lipids to the peptide cys-mel4 (n = 3). The error bars denote the SEM. **C**, Capacitance response of diphytanyl lipids to the peptide cys-mel4 (n = 3). The error bars denote the SEM.

3.4.5 MelAlanine

The addition of 10 μM of melAlanine to diphytanyl lipid bilayers in the tBLM apparatus brought about peptide-lipid interactions that induced changes in the output of the instrument that were greater than those of melimine but smaller than for cys-melimine. In the impedance and phase Bode plots (see Figure 3.4.5. A), the magnitude of the resistive component of the impedance plot decreased in magnitude after the addition, while the phase plot depicted a shift of the area of low phase angle in the horizontal direction, to higher frequencies: and in the vertical direction, the minimum phase angle increased. These responses portray similar movements to those of cys-melimine, but in these, the shifting of the Bode plots was less pronounced.

In the direct conductance measurements, melAlanine induced a conduction response that was comparable to those from cys-melimine (Figure 3.4.5 B). The replacement of the arginine residues with alanines in melAlanine has shown to increase the conductance response due to the interactions of this peptide, varying from the minimal response seen with melimine (Figure 3.4.1 B). The conductance initially increased before slowing decreasing throughout a 30 min period. After washing with 1 mL of PBS, the conductance decreased and did not return to initial baseline levels.

The capacitance of the diphytanyl membranes increased slightly with the addition of melAlanine (see Figure 3.4.5. C): this matched the capacitance response of cys-melimine.

MelAlanine had the worst MIC values out of each of the five peptides and is supposed to be the negative control peptide in that it is ineffective at killing bacteria; this contrasts against the lipid-peptide interactions observed. See Section 4.2.1 for further discussion on this topic.

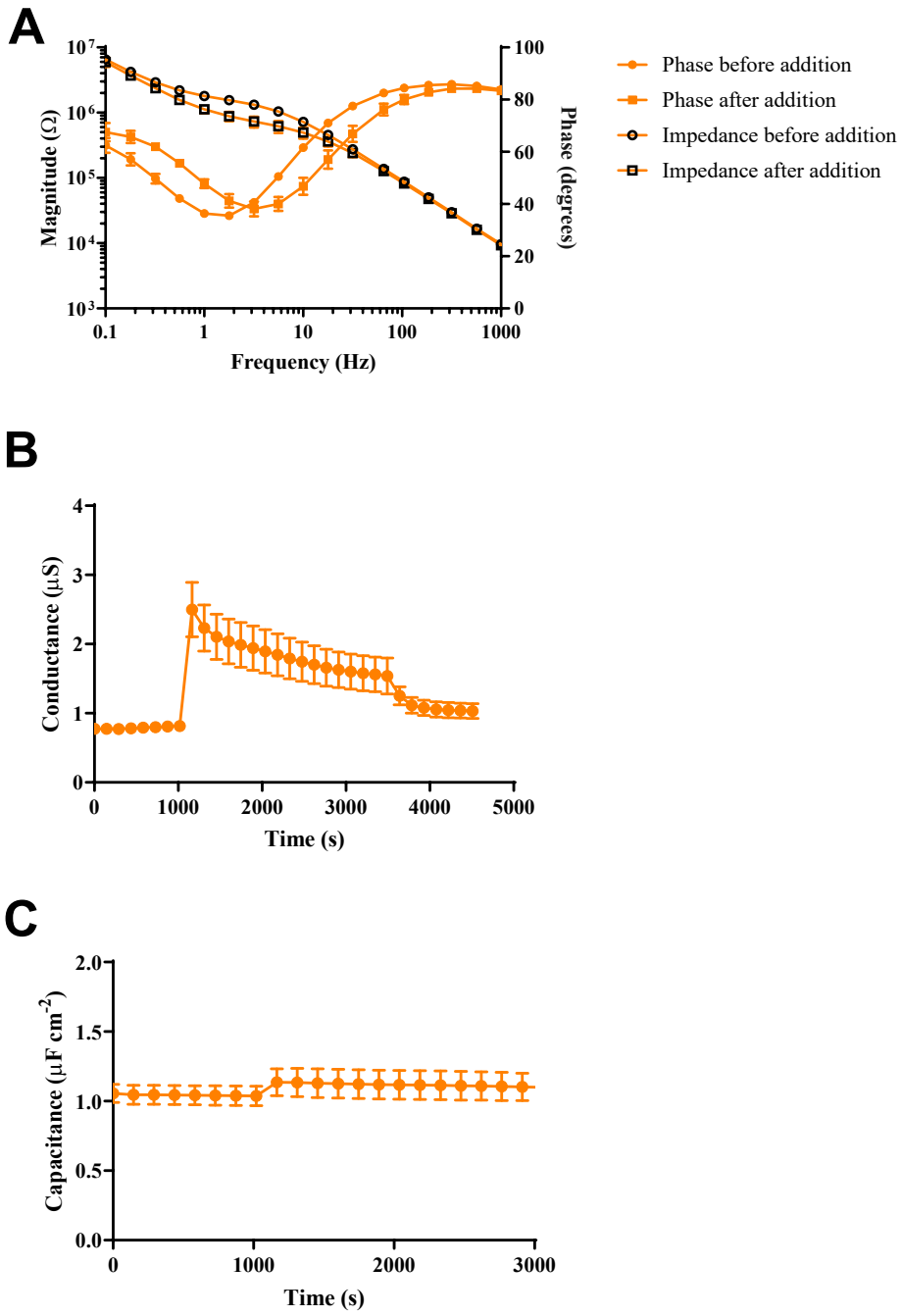

Figure 3.4.5: EIS plots for melAlanine in diphytanyl lipid tBLMs. **A**, Bode plot of before and after the addition of melimine (n = 3). The error bars denote the SEM. **B**, Conductance response of diphytanyl lipids to the peptide melAlanine (n = 3). The error bars denote the SEM. **C**, Capacitance response of diphytanyl lipids to the peptide melAlanine (n = 3). The error bars denote the SEM.

3.4.6 Membranes with bacterial lipids

3.4.6.1 *E. coli* lipids

To further complement the effect that cys-melimine had on POPG lipids, lipids that had been extracted from *E. coli* were also investigated. The interaction of cys-melimine with *E. coli* lipid membranes showed a massive increase in the conductance (Figure 3.4.6.1.1 B), further highlighting the specificity that cys-melimine has with negatively charged membranes. Membranes composed of *E. coli* lipids are difficult to make consistently and are generally unstable, having high baseline conduction values; because of this, it was difficult to obtain reliable, reproducible results.

This instability of the *E. coli* lipids was even more evident in experiments on melimine interactions with the tBLMs. In different measurements (see Figure 3.4.6.1.2. B) there was considerable variation in the baseline conductance, which resulted in inconsistencies in the results, making it hard to determine the true nature of the peptide-tBLM interactions.

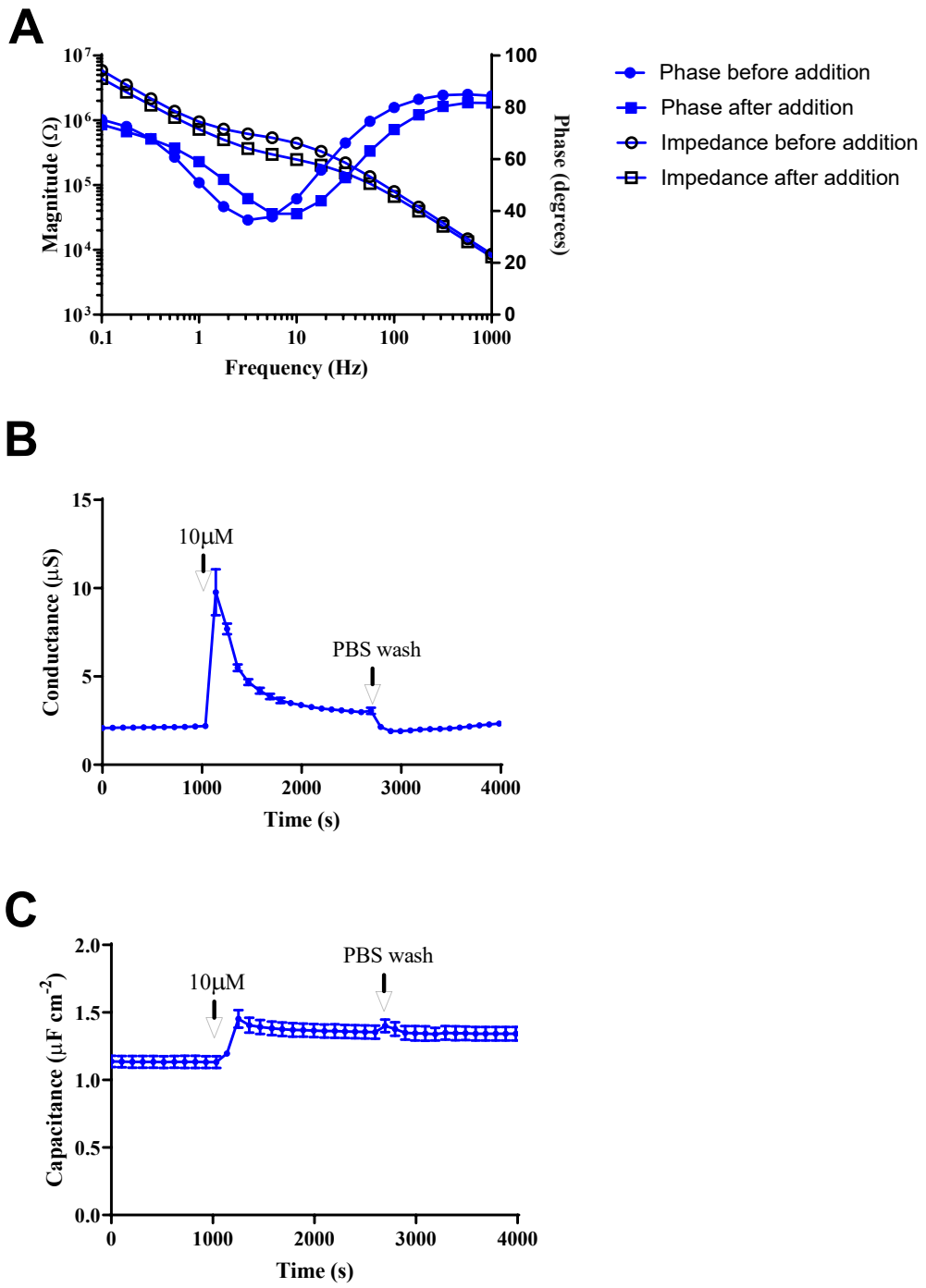

Figure 3.4.6.1.1: EIS plots for cys-melimine in *E.coli* lipid tBLMs. **A**, Bode plot of before and after the addition of cys-melimine (n = 3), showing a fit of the data points. The error bars denote the SEM **B**, Conductance response of *E.coli* lipids to the peptide cys-melimine (n = 3). The error bars denote the SEM. **C**, Capacitance response of *E.coli* lipids to the peptide cys-melimine (n=3). The error bars denote the SEM.

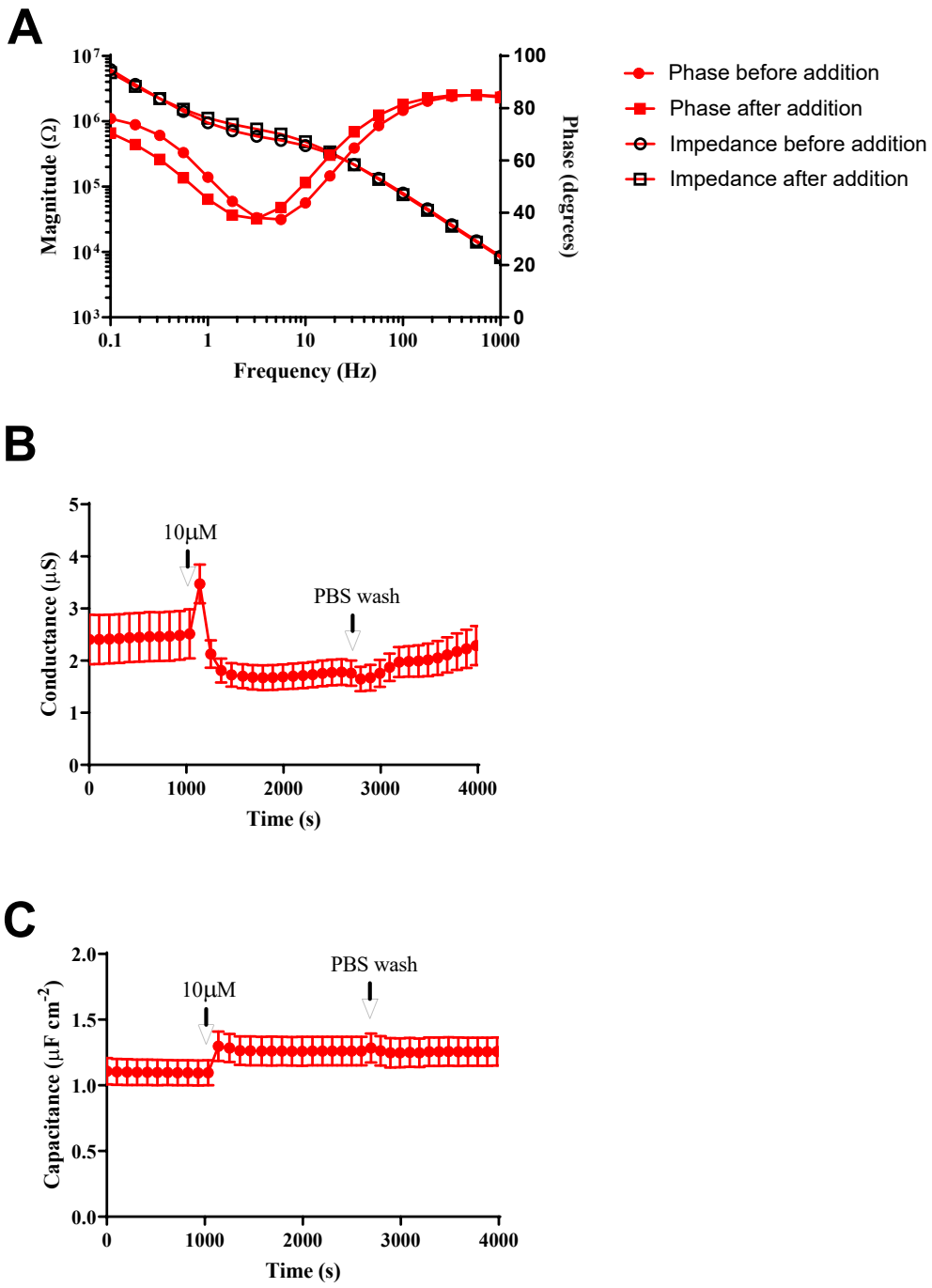

Figure 3.4.6.1.2: EIS plots for melimine in *E.coli* lipid tBLMs**. A**, Bode plot of before and after the addition of melimine (n = 3), showing a fit of the data points. The error bars denote the SEM. **B**, Conductance response of *E.coli* lipids to the peptide melimine (n = 3). The error bars denote the SEM. **C**, Capacitance response of *E.coli* lipids to the peptide melimine (n = 3). The error bars denote the SEM**.**

3.4.6.2 Lipopolysaccharide and Lipid A

In order to improve the stability of the bacterial membranes made from *E. coli* lipids, which were a mix of various lipid types, pure lipopolysaccharide (LPS) and its lipid A moiety were used. As LPS represents the main component of the outer bacterial membrane of a Gram-negative bacterium [176, 177], membranes containing both LPS and Lipid A were produced.

LPS in synthetic membranes yielded a similar outcome to membranes that were produced using the *E. coli* lipids. The LPS membranes showed a lack of stability that resulted in a significant variation of the baseline conductance of each membrane, making it impossible to obtain reliable, reproducible results (Figure 3.4.6.2.1).

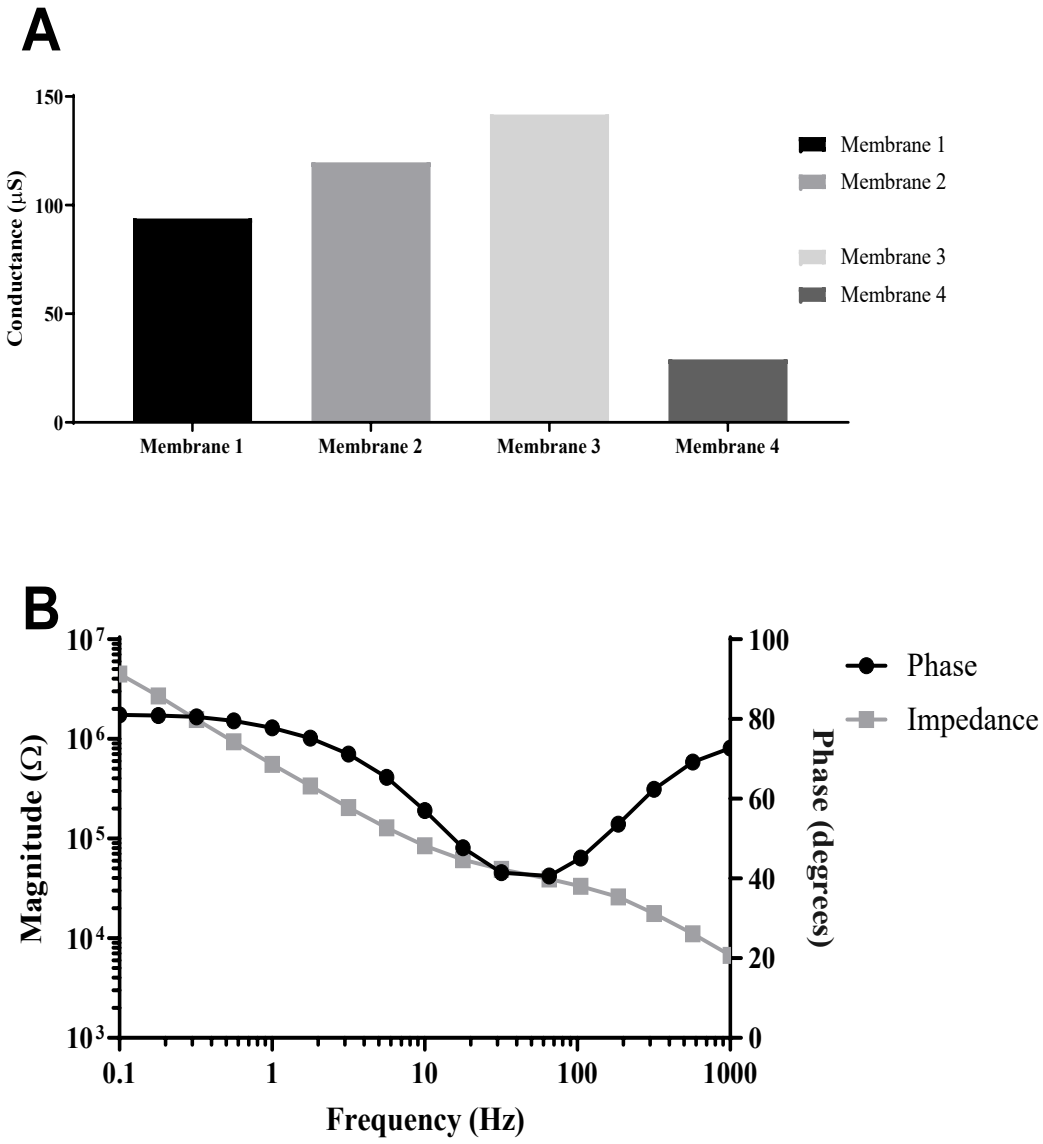

Figure 3.4.6.2.1: EIS plots for lipopolysaccharide tBLMs **A**, Baseline conductance of four lipopolysaccharide membranes. The variation across each well showed no repeatability. **B**, Bode plot of membrane 4 depicts a phase minima at high frequencies, with a fitted data curve.

Lipid A membranes were slightly more stable than the LPS membranes but still lacked reproducibility. Limited conduction and capacitance results were produced using a single membrane (see Figure 3.4.6.2.2.). After the addition of melimine and cys-melimine, a decrease in the conductance response was seen, opposite of the response observed in other

measurements in both the *E. coli* lipids and diphytanyl lipids. Changes in the capacitance response were the same as with the other lipid types.

Whether this result was due to that structure of the lipid, with each lipid packing differently due to its six alkyl chains (see Figure 2.2.3.2.). Alternatively, the results may be due to an artifact in the measurements as these results were not able to be replicated.

From looking at the conductance responses from each of the peptide derivatives, the variations in the data suggested that there may be more than one particular characteristic of the peptides that were influencing the interactions between each peptide and the lipid bilayers. The effect that each peptide has on the transport of ions across lipid bilayers may be due to the molecular shape of the peptides, its charge or its hydrophobicity or hydrophilicity.

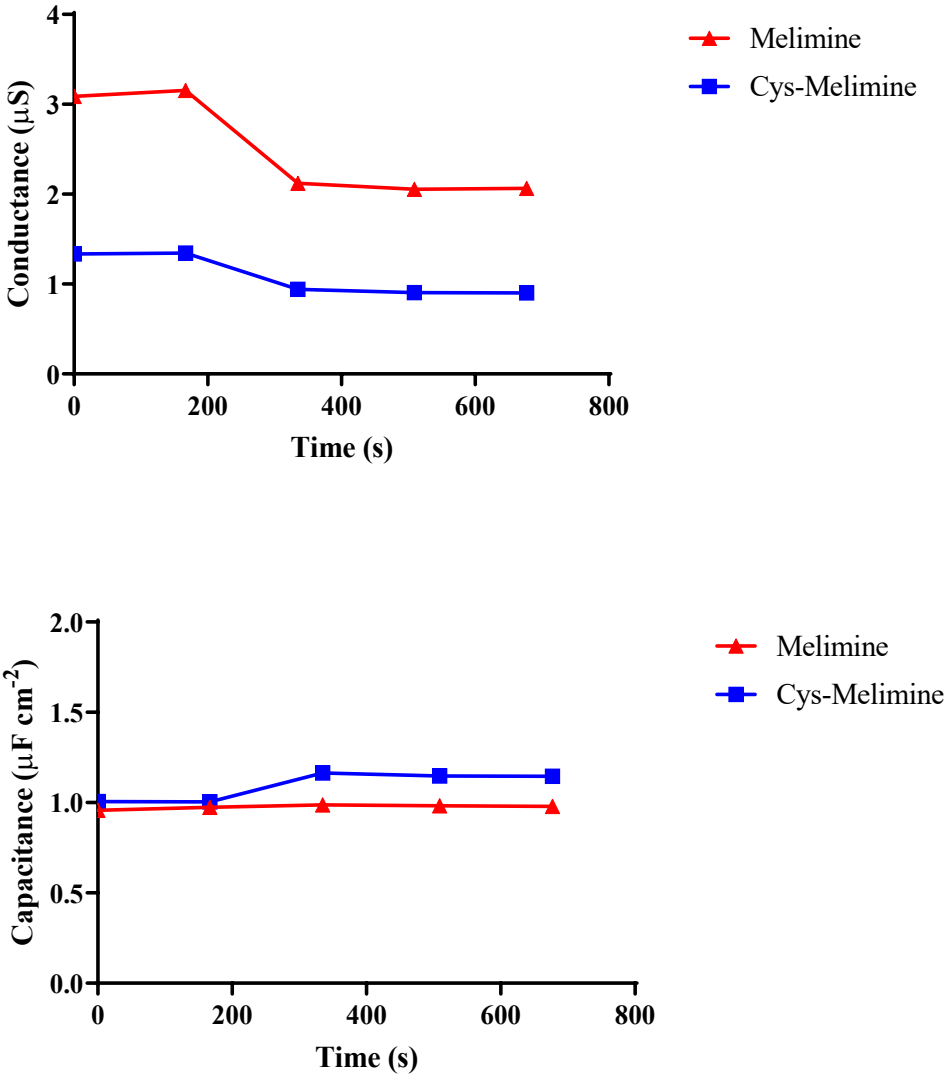

Figure 3.4.6.2.2: A, Conductance response of Lipid A membranes to the peptide melimine. **B**, Capacitance response of Lipid A membranes to the peptide melimine.

3.4.7 Melimine with changes in pH

Recent studies have shown that at high pH values, the area per lipid within a membrane is larger, increasing the spacing between the lipids [73, 178]. By having these larger spaces between the lipids, a peptide may more readily insert into the lipid bilayer.

Melimine was added at a concentration of 10 μM for each of the three pH values tested. At both pH ~ 5 and pH ~ 7 the addition of melimine resulted in a slight increase in the conductance. Still, upon the addition of melimine at pH ~ 9, a reduction in the conductance was observed (see Figure 3.4.7.1.). The capacitance response is similar at each of the three pH values (see Figure 3.4.7.2.), indicating that there was minimal difference in the reaction of the membrane to the addition of melimine at high pH.

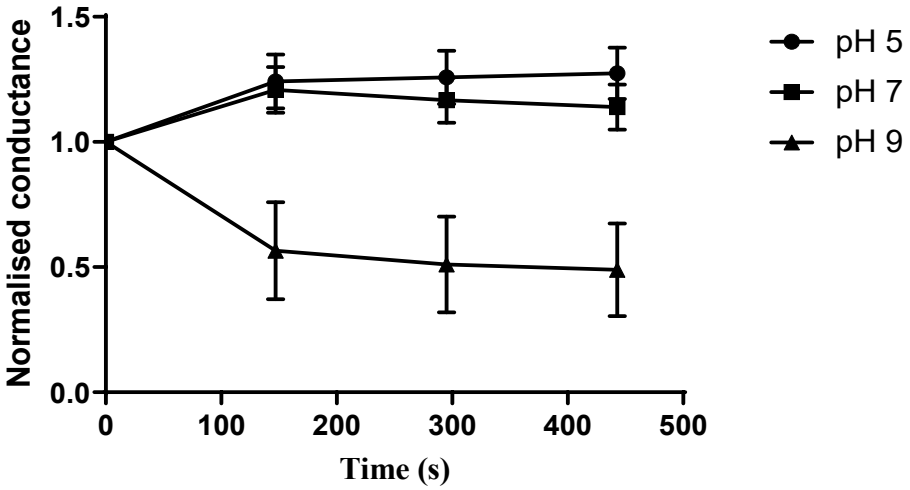

Figure 3.4.7.1: Conductance response of melimine at pH ~ 5,7,9 in zwitterionic membranes (n = 2). The error bars denote the SEM.

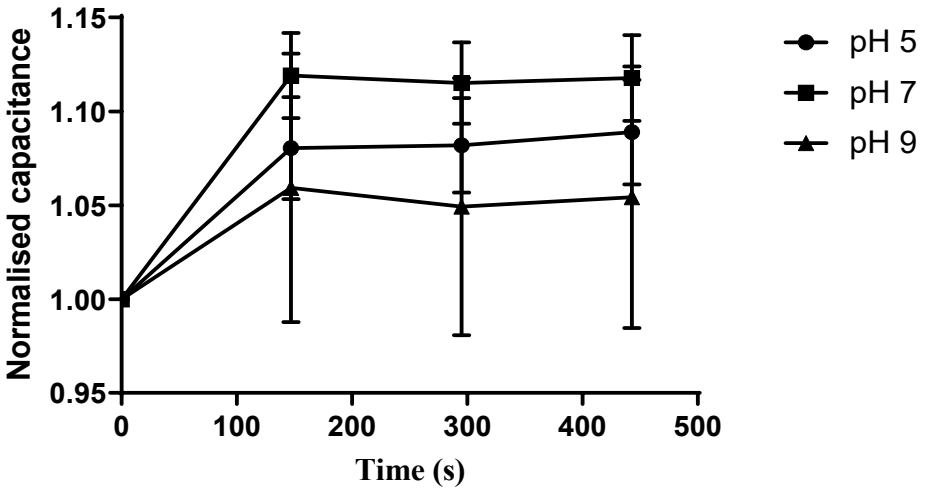

Figure 3.4.7.2: Capacitance response of melimine at pH ~ 5,7,9 in zwitterionic membranes (n = 2). The error bars denote the SEM.

Negatively charged lipids consisting of 30% POPG were tested in comparison. After the addition of melimine at each of the tested pH values, the conductance responses showed a similar trend to that of the zwitterionic lipid membranes, with the conductance decreasing at pH ~ 9 (see Figure 3.4.7.3.). In the capacitance response, seen in Figure 3.4.7.4., at pH ~ 9, there was a small variation to the response seen at the lower pH values. This small response was not consequential enough to indicate a difference in the membrane due to the interactions of melimine across the three pH values. See Section 4.1.4 for further discussion on this topic.

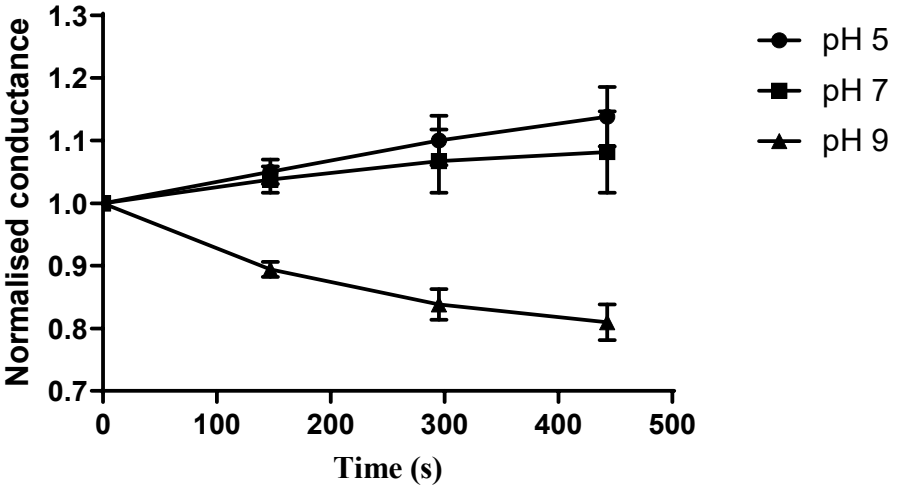

Figure 3.4.7.3: Conductance response of melimine at pH ~ 5,7,9 in negatively charged membranes (n = 2). The error bars denote the SEM.

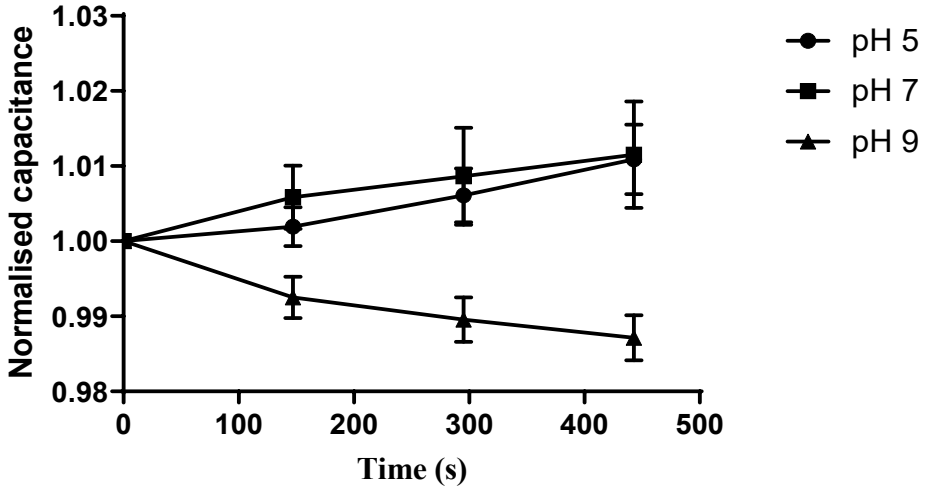

Figure 3.4.7.4: Capacitance response of melimine at pH ~ 5,7,9 in negatively charged membranes (n = 2). The error bars denote the SEM.

3.5 EIS - Arrhenius plots

Here the average energy required for 1 mol of ions to traverse the membrane is determined using the Arrhenius equation, the so-called activation energy. Changes in the activation energy of ion traversal have been used to identify the impact of melimine and its derivatives with the lipid bilayer. These experiments were carried out using EIS techniques with tBLMs over a range of temperatures from 10-35°C. For these experiments, tBLMs were created following the method outlined in Section 2.2.

3.5.1 Melimine

For these measurements, 10 μM of melimine was added to the membrane at ~10°C before heating the membrane and observing the change in the conductance as a function of temperature.

To calculate the activation energy, the slope of a graph of the natural log of the conduction versus reciprocal of absolute temperature was used. The slope of this graph was determined using linear regression (Prism 7.03, GraphPad Software Inc., La Jolla, CA). The resultant line is approximately linear, and the slope is therefore equivalent to: $-\frac{E_a}{RT}$ See Section 1.6.

Conduction measures of membranes without melimine were completed in parallel. From these measures, the slope was calculated to be approximately -10.8 ±0.25 (see Figure 3.5.1.). Using this slope, the activation energy of ion traversal for the membrane architecture used was calculated to be 90 kJ mol^{-1}. Other research has shown activation energies of ion traversals across lipid bilayers for various lipid membranes between 50 - 100 kJ mol^{-1} [155, 179-181]. This discrepancy can be attributed to variations in membrane thickness and lipid composition and the measurement techniques used [179-181].

In the tBLM's where melimine had been added, the resultant slope was slightly lower. The slope was calculated to be approximately -10.5±0.22 (see Figure 3.5.1.). From this slightly lower slope, the activation energy was then calculated to be 87 kJ mol^{-1}. This small reduction

in the activation energy due to the interaction of melimine indicated a change in the lipid membrane such that the membrane is less resistant to the traversal of ions.

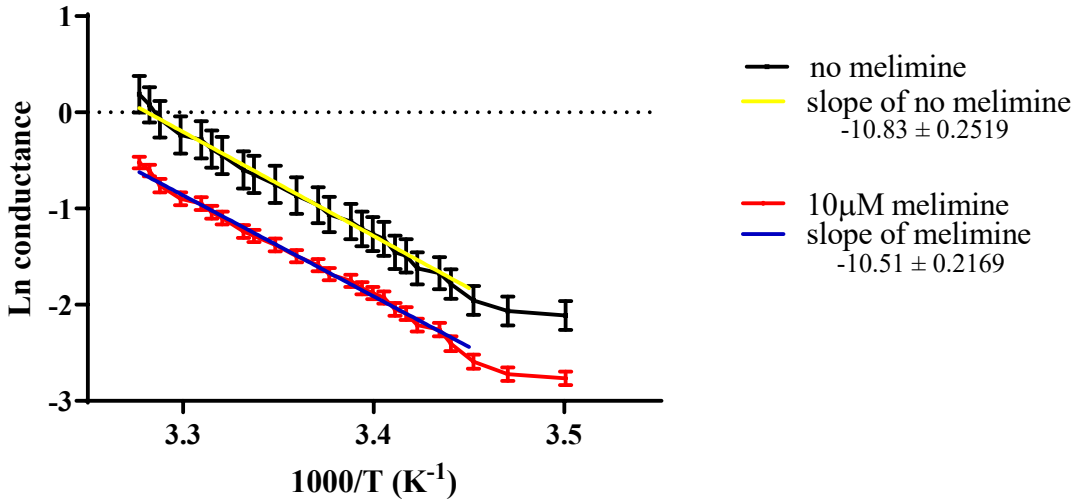

Figure 3.5.1: Arrhenius plot comparing diphytanyl membranes with and without 10 µM melimine. Measurements were completed in parallel, with n=3 for both sets of measurements. The error bars denote the SEM.

3.5.2 Cys-melimine

For cys-melimine-tBLM activation energies, the data collected was plotted in the same manner as outlined in Section 3.5.1, with a linear regression used to calculate the slope.

From these measurements, with the membranes where no cys-melimine was added, the slope was calculated to be approximately -9.4±0.28, see Figure 3.5.2. Using this slope, the activation energy of ion traversal was calculated to be 82 kJ mol^{-1}.

In the tBLM's where cys-melimine had been added, the resultant slope showed more considerable variation with a significantly reduced slope in comparison to the tBLMs without the peptide. The slope was calculated to be approximately -6.1±0.15; see Figure 3.5.2. From this slope, the activation energy was then calculated to be 51 kJ mol^{-1}.

The addition of cys-melimine resulted in a significant drop in the activation energy of ion traversal of approximately 38%, which was significantly larger than that caused by melimine. Though the activation energy that was calculated for cys-melimine showed a significant reduction compared to that of a peptide free membrane, it is still higher than that reported for ion channels such as those produced by gramicidin-A [182].

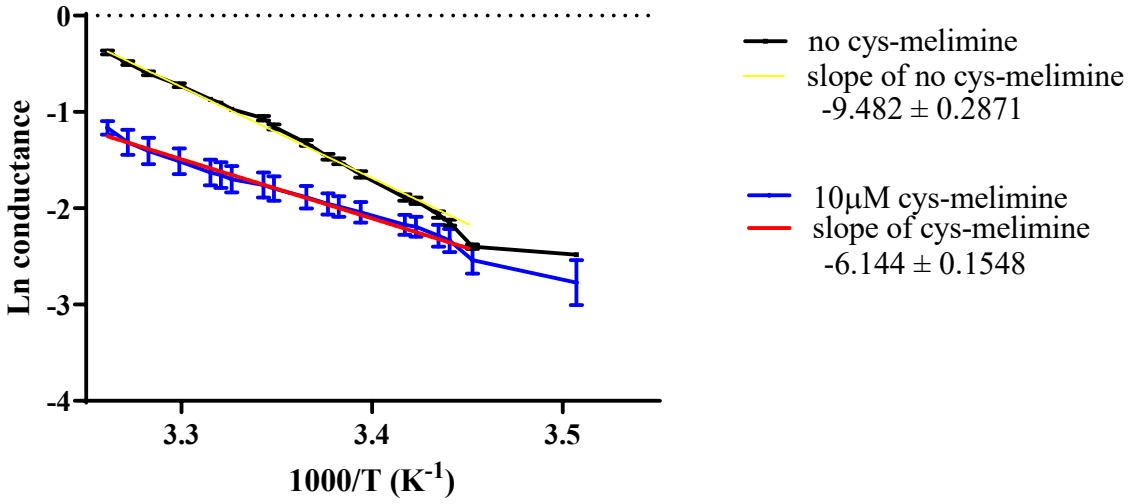

Figure 3.5.2: Arrhenius plot comparing diphytanyl membranes with and without 10 µM cys-melimine. Measurements were completed in parallel, with n=3 for both sets of measurements. The error bars denote the SEM.

3.5.3 Mel4

The data collected for mel4 activity measures were plotted in the same manner as outlined above in Section 3.5.1, with linear regression used to calculate the slope.

From these measurements, the slope was calculated to be approximately -8.9±0. 95 for mel4-free tBLMs, see Figure 3.5.3. Using this slope, the activation energy of ion traversal was calculated to be 74 kJ mol^{-1}.

In the tBLM's where mel4 had been added, the slope was calculated to be 9.6±0.49 (see Figure 3.5.3.). From this slope, the activation energy was then calculated to be 80 kJ mol^{-1}. This activation energy of the membrane after the addition of mel4 appears to be greater than the

activation energy of the membrane without the addition of peptide. The error margin in the slope of the Arrhenius plot is larger for mel4, leading to overlapping in the activation energy of ion traversal, see Table 3.5. With the overlap in the activation energy that showed minimal difference, mel4 may cause no change in the passage of ions, which is in agreement with the EIS conductance measures in Section 3.4.3.

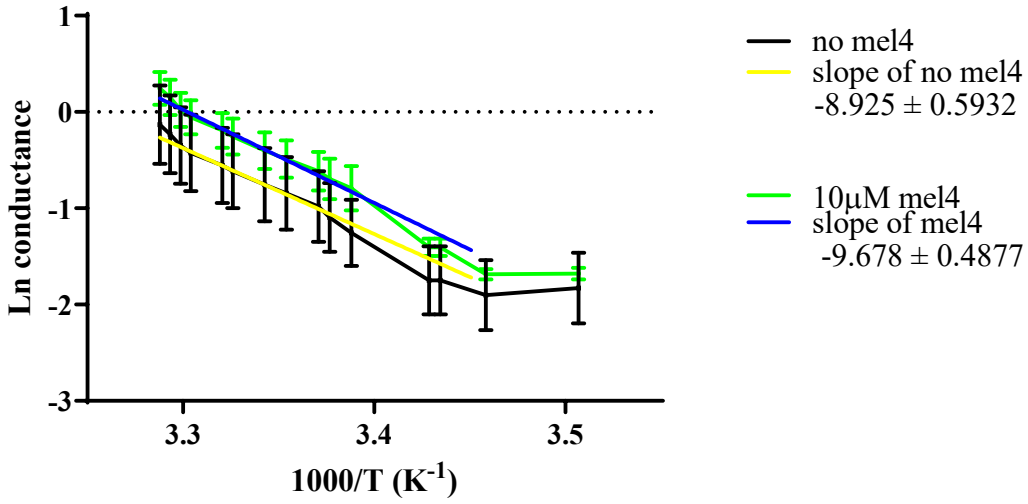

Figure 3.5.3: Arrhenius plot comparing diphytanyl membranes with and without 10 µM mel4. Measurements were completed in parallel, n=3 for both sets of measurements. The error bars denote the SEM.

3.5.4 Cys-mel4

The data collected was plotted in the same manner as outlined above in Section 3.5.1, with linear regression used to calculate the slope.

From these measurements, the slope was calculated to be approximately -10.1±0.29, for cys-mel4 free membranes, see Figure 3.5.4. Using this slope, the activation energy of ion traversal was calculated to be 83 kJ mol^{-1}.

In the tBLM's where cys-mel4 had been added, the slope was calculated to be approximately -9.4±0.25; see Figure 3.5.4. From this slope, the activation energy was then calculated to be 78 kJ mol^{-1}.

This peptide showed similar activity to melimine, interacting in a way that slightly lowered the activation energy of ion traversal, increasing the degrees of freedom of the ions by influencing the lipid packing of the lipid bilayer.

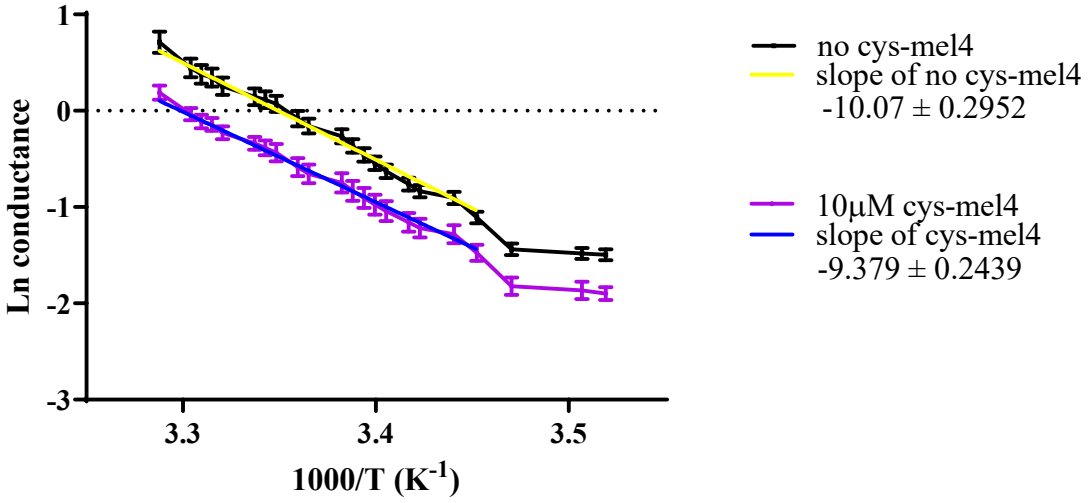

Figure 3.5.4: Arrhenius plot comparing diphytanyl membranes with and without 10 µM cys-mel4 comparing the natural log conductance versus the reciprocal of absolute temperature. Measurements were completed in parallel, n=3 for both sets of measurements. The error bars denote the SEM.

3.5.5 MelAlanine

For these measurements, melAlanine was added to the tBLMs and cooled to ~10°C before heating the membrane and observing the change in the conductance as a function of temperature. The data collected was plotted in the same manner as outlined above in Section 3.5.1, with linear regression used to calculate the slope.

From these measurements, the slope of the control tBLMs was -13.4±0.88; see Figure 3.5.5. After calculating the activation energy of ion traversal, the PBS control returned activation energy of 111 kJ mol^{-1}.

After the addition of melAlanine, a decreased slope of -11.6±0.66 was reported, with the activation energy being calculated to be 94 kJ mol^{-1}. This was a 15% reduction in the activation energy across the membranes after the addition of the peptide. The magnitude of this reduction is greater than the change caused by melimine but smaller than the effect of cys-melimine.

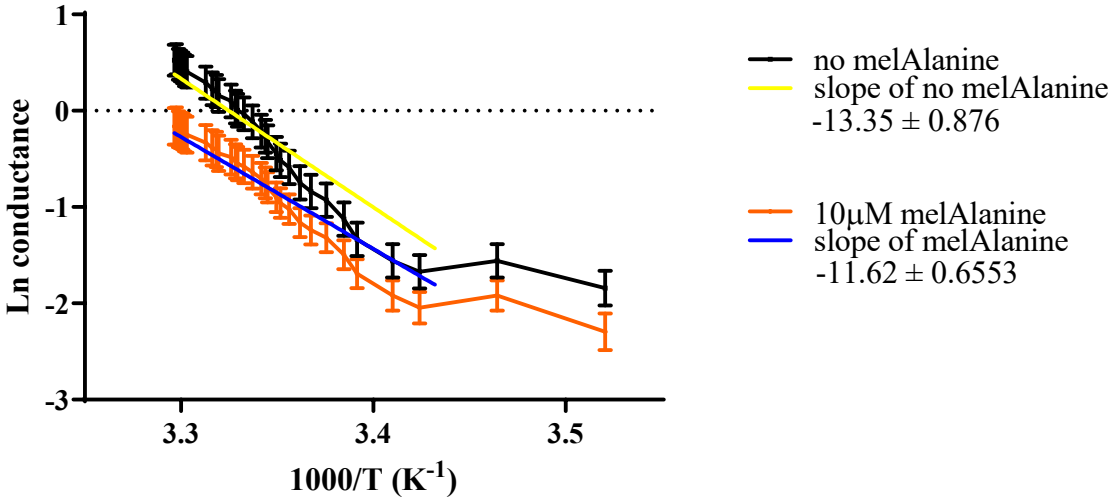

Figure 3.5.5: Arrhenius plot comparing diphytanyl membranes with and without 10 μM melAlanine. Measurements were completed in parallel, n=3 for both sets of measurements. The error bars denote the SEM.

Melimine and its derivatives have been shown to lower the energy requirements for the passage of ions across the lipid bilayers membranes, see Table 3.5. This level of reduction in the activation energy is considerably smaller than that of pore formers such as gramicidin-A, Staphylococcus aureus α-toxin and the capsaicin Ion Channel, VR1 [182-184]. This suggests that melimine and its derivatives are not forming pores within the membrane but instead permit the passage of ions by some other mechanism, possibly by causing the widening of intrinsic pores in the lipid bilayer. See Section 4.1.6 for further discussion on this topic.

	Activation energy of membrane with no peptide (kJ mol^{-1})	Activation energy of membrane with peptide (kJ mol^{-1})	Percentage change (%)
Melimine (10 µM)	90 ± 2.1	87 ± 1.8	-3
Cys-melimine (10 µM)	82 ± 2.4	51 ± 1.3	-38
Mel4 (10 µM)	74 ± 4.9	80 ± 4.1	8
Cys-mel4 (10 µM)	83 ± 2.5	78 ± 2	-6
MelAlanine (10 µM)	111 ± 7.3	94 ± 5.4	-15

Table 3.5: Percentage change of the activation energies of ion traversal after the addition of melimine and its derivatives.

3.6 Neutron Reflectometry

Neutron reflectivity can provide information on the structure of lipid bilayers that are normal to the membrane plane [185]. As neutrons are pass through the lipid bilayer, neutrons can scatter off the lipid bilayer structure. By determining the neutron scattering length densities and fitting them to a model of tBLM chemistry layers, it is hoped that structural changes within the lipid bilayer caused by the insertion of the melimine peptides can be identified.

3.6.1 Melimine

These measurements were completed using a tBLM substrate using magnets to create a magnetic guide for the cold neutron source. By using this and making use of the contrasts provided by the up spin and down spin neutrons, there was a reduced need for buffer exchange, requiring one less contrast solution, limiting the washing of the membrane and reducing the chance of removing peptide from the lipid bilayer[149, 150].

Measurements were first undertaken on a deuterated DOPC bilayer to provide background measurements; these measurements were completed in contrast solutions of PBS buffer in both H_2O and D_2O. These measurements were repeated on the same bilayers after 10 μM melimine was added.

During the fitting process, the contrast datasets were compared before and after the addition of melimine. The roughness and scattering length densities of the outer lipid headgroups and outer lipid tails were left unconstrained during the least-squares fitting. This allowed for the outer leaflets of each measurement of the bilayer to be independently fitted, allowing for the comparison of any differences between the leaflets as a result of the addition of melimine. From this fitting process, the reduced reflectometry data and the modelled layered fit for the bilayers did not converge. This prevented the determination of the roughness or scattering length densities for the outer lipid headgroups and outer lipid tails, preventing the Bayesian analysis from being performed.

During this fitting process, it was noticed that there was not much change before and after the addition of peptides in the reflectivity profiles, see Figure 3.6.1. Within the D_2O contrast, the

addition of the non-deuterated melimine should have caused a more significant change in the reflectivity of the neutrons that were scattering off the bilayer, but this was not the case. The reflectivity profiles before and after the addition of melimine show no difference in the reflectivity. This suggests that melimine is not aggregating within the bilayer.

It can also be said that there is no additional water inside the bilayer due to the addition of melimine. This additional water would be observable in the H_2O contrast, with the hydronium in the water scattering neutrons differently from the deuterium in the lipids.

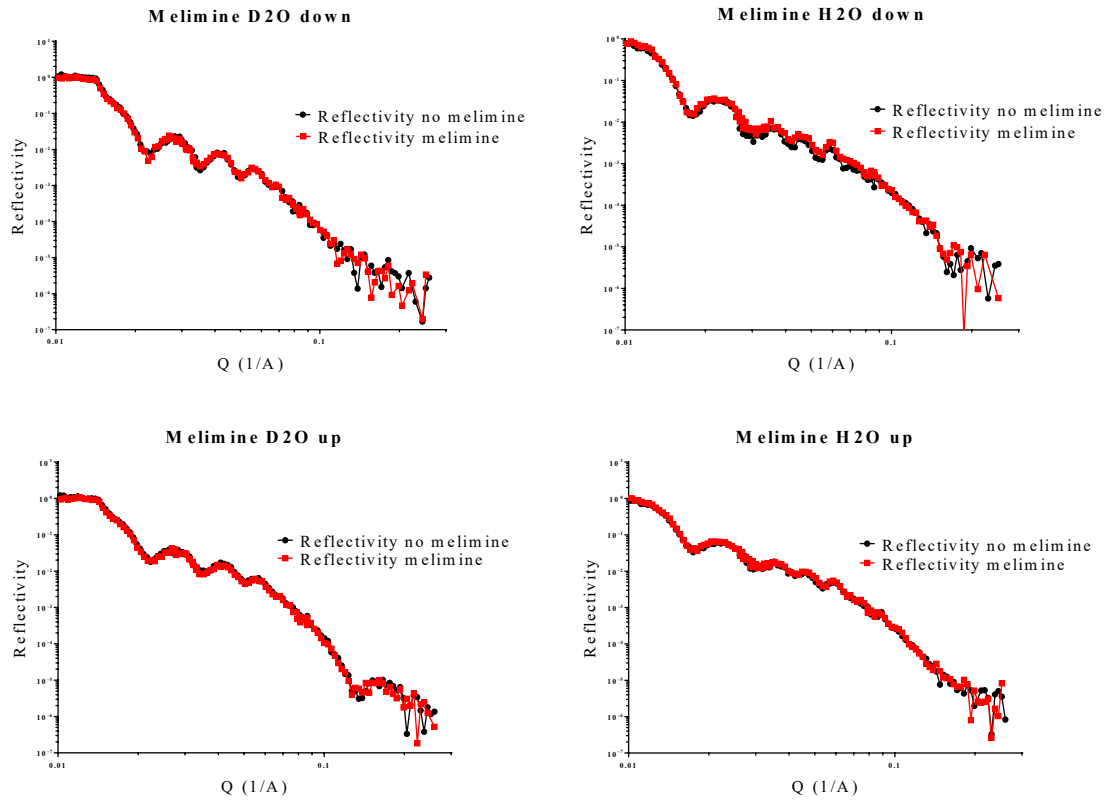

Figure 3.6.1: Reflectivity data profiles showing the different contrast scans of melimine in D_2O and H_2O for both up spin and down spin neutron measurements. Reflectivity has been plotted against Q, the scattering vector, defined in Section 2.7.1.

3.6.2 Cys-melimine and mel4

Measurements of cys-melimine and mel4 were completed in the same manner as with melimine. The result of adding these peptides to their respective membrane resulted in the same result as observed with the addition of melimine, with no significant changes observed.

In Figure 3.6.2.1 and Figure 3.6.2.2, the reflectivity profiles of membranes after the addition of each peptide, cys-melimine and mel4, were overlapped with the reflectivity profiles of the membranes before this addition where minimal differences were observed.

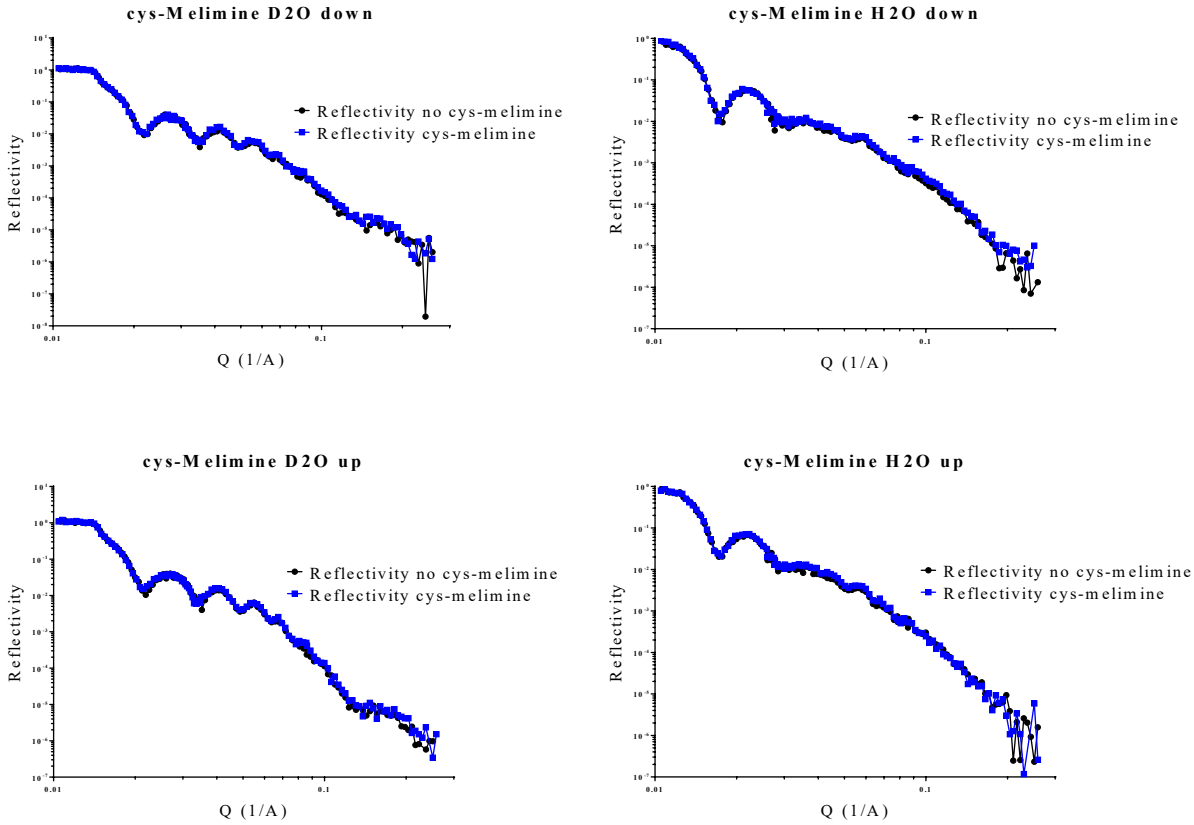

Figure 3.6.2.1: Reflectivity data profiles showing the different contrast scans of cys-melimine in D_2O and H_2O for both up spin and down spin neutron measurements. Reflectivity has been plotted against Q, the scattering vector.

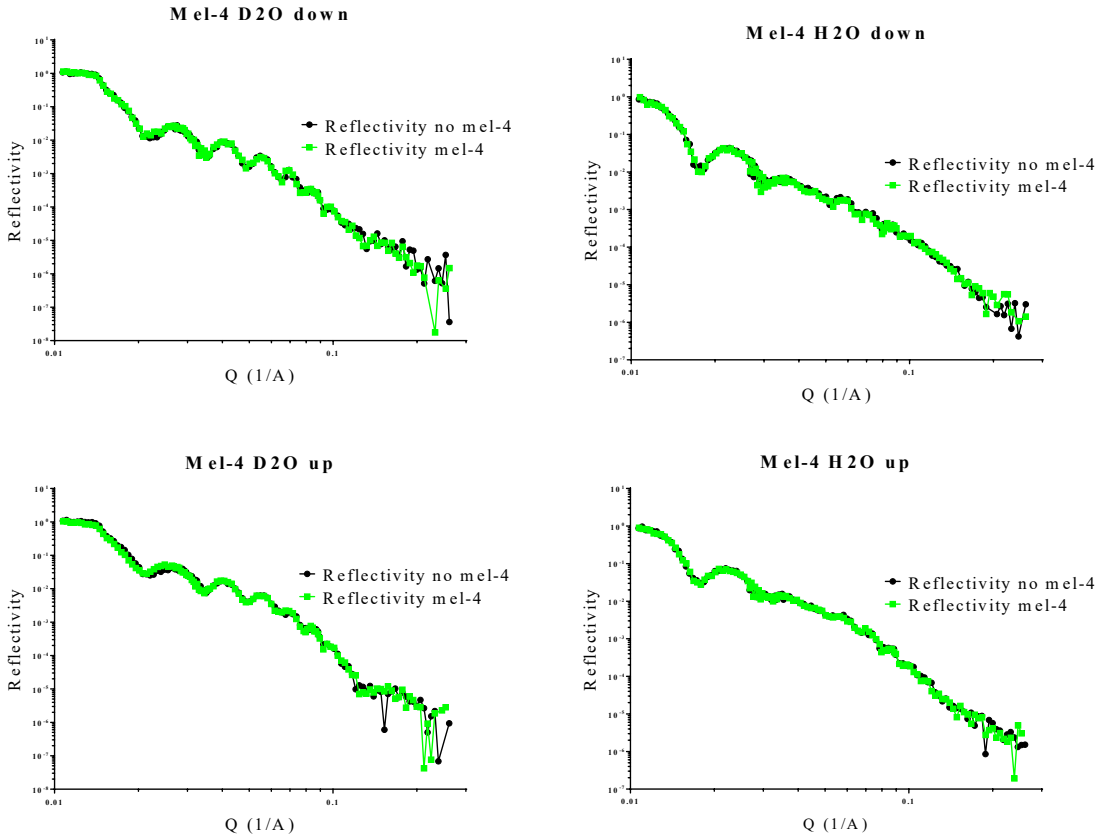

Figure 3.6.2.2: Reflectivity data profiles showing the different contrast scans of mel4 in D_2O and H_2O for both up-spin and down-spin neutron measurements. Reflectivity has been plotted against Q, the scattering vector.

3.6.3 Cys-mel4 and melAlanine

The measurements of both cys-mel4 and melAlanine differed from the other peptides. For these measurements, due to limited availability, the chromium substrates were used without polarising the neutrons; this required the use of an additional mixed D_2O/H_2O contrast.

With the addition of both cys-mel4 and melAlanine, some observable differences in the reflectivity profiles were noted between the before and after measurements for these two peptides.

Upon further examination, it was identified that the contrast solutions had been contaminated; as such, there was D_2O or H_2O mixing with the pure contrasts. This mixing may have been due to a problem with the HPLC pump, affecting the flushing of the solutions from the cells containing the membranes. This contamination of the solutions can be seen predominantly in the critical edge of the reflectivity profiles between 0.01-0.02 Q. This can be seen in the D_2O and H_2O measurements of cys-mel4, see Figure 3.6.3.1, and the H_2O measurements of melAlanine, see Figure 3.6.3.2. Due to time constraints, repeat measurements were unable to be taken.

Apart from the disruption to the reflectivity profiles due to the contrast contamination, no other significant changes were detected, suggesting similar interactions to the other peptides. Still, a complete comparison was not able to be completed.

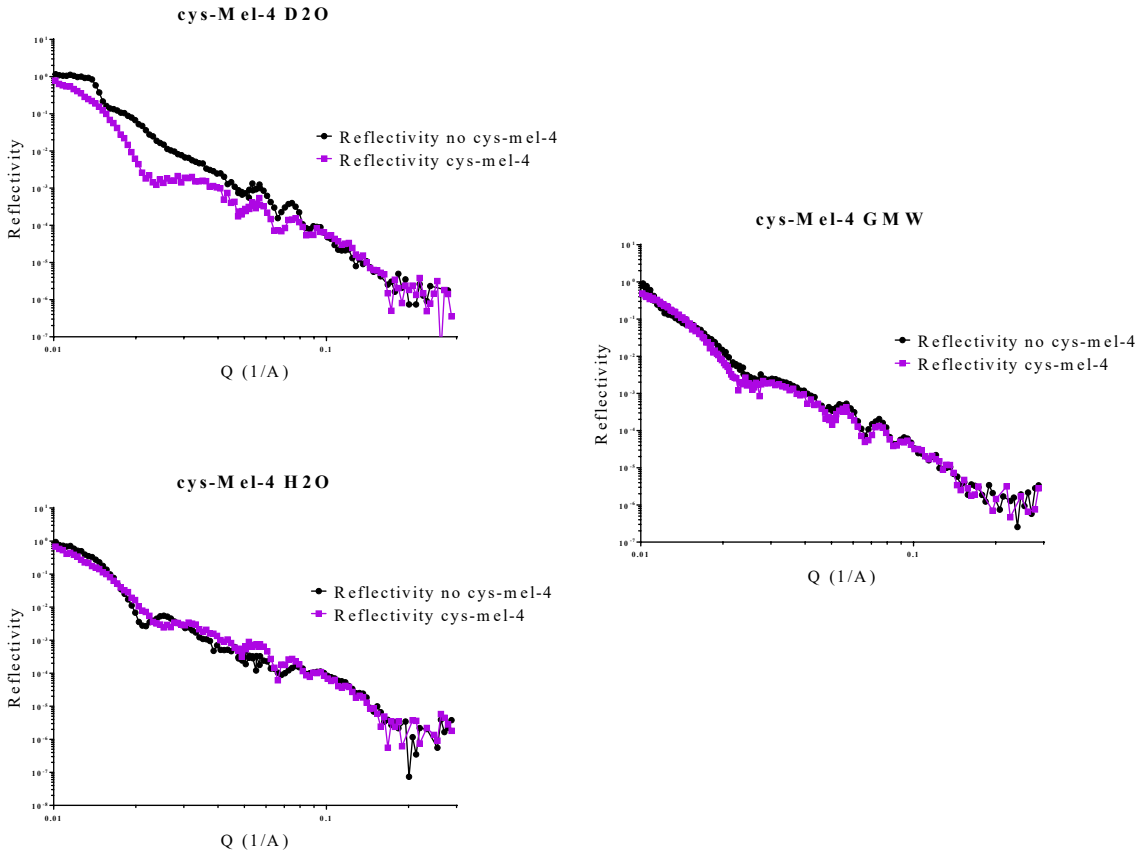

Figure 3.6.3.1: Reflectivity data profiles showing the different contrast scans of cys-mel4 in D2O, H2O and GMW contrast measurements. Reflectivity has been plotted against Q, the scattering vector.

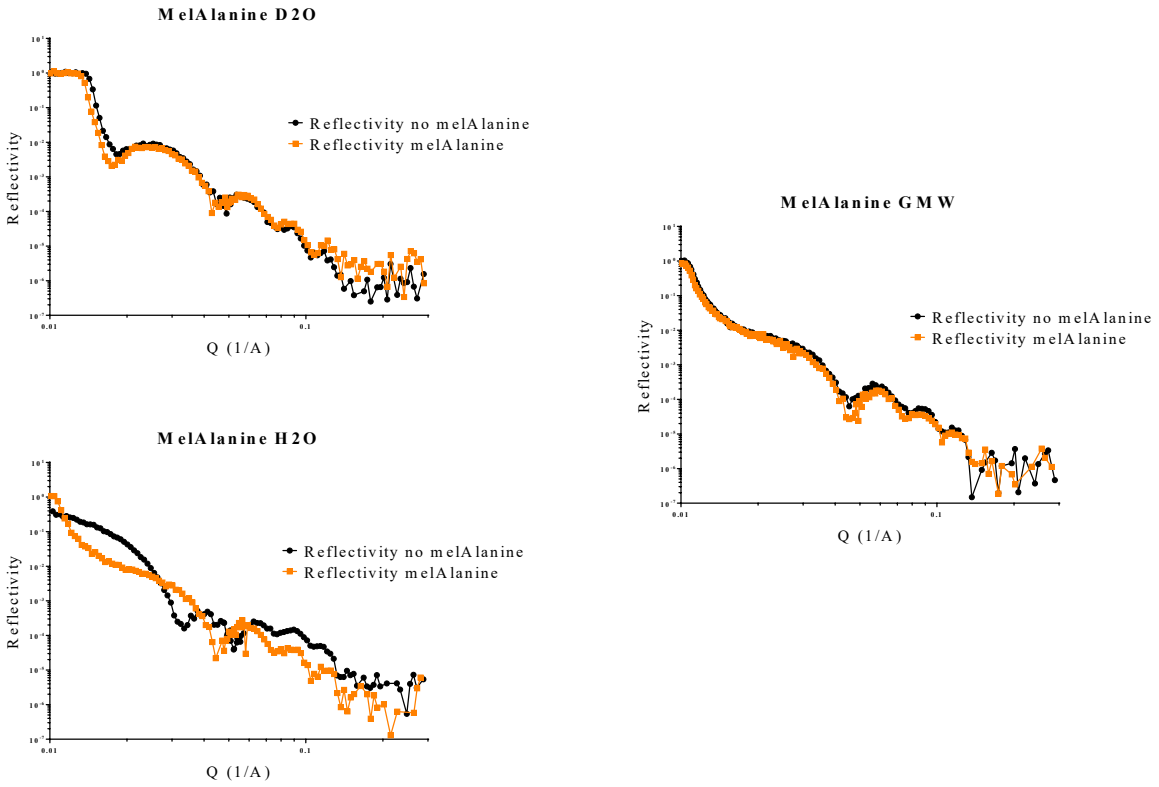

Figure 3.6.3.2: Reflectivity data profiles showing the different contrast scans of melAlanine in D_2O, H_2O and GMW contrast measurements. Reflectivity has been plotted against Q, the scattering vector.

3.7 Differential scanning calorimetry

Through changes in temperature, lipids undergo phase transitions whereby the hydrocarbon chains experience changes in their fluidity and mobility. These transition temperatures differ for each lipid type, varying due to differences in the tail length, a saturation of the tails and head group hydration. Upon introducing a peptide, this process can be disrupted. DSC can, therefore, provide an insight into the changes in the lipid packing as a result of this interaction.

3.7.1 Melimine

Upon heating the DMPC vesicles, we can see an increase in the heat capacity of the system. These increases correspond to the phase transitions of the lipid bilayers, see Figure 3.7.1.1. The main phase transition occurs at 24.1°C, with the pre-transition temperature occurring at 13.7°C. From determining the area under each of these peaks, the calorimetric enthalpy of these transitions was calculated [186]. The enthalpy of the main phase transition was calculated to be 23.89 KJ mol^{-1}, and the enthalpy for the pre-transition was calculated to be 4.02 KJ mol^{-1}.

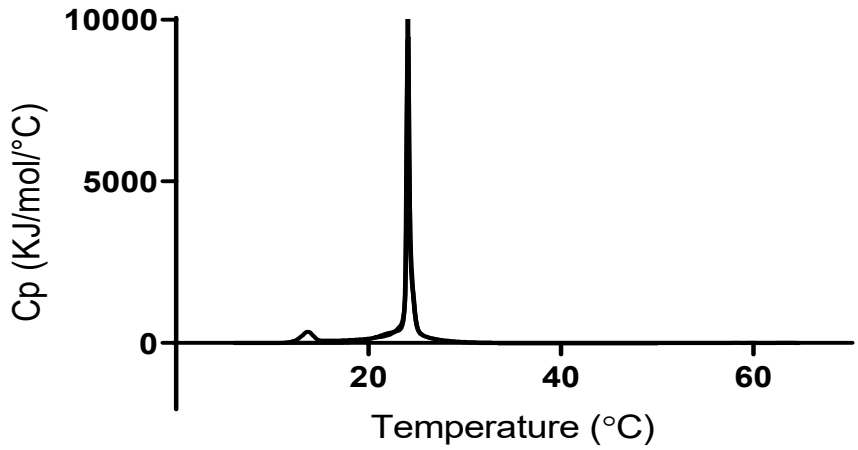

Figure 3.7.1.1: Thermogram of DMPC vesicles, showing an increase in the heat capacity coinciding with the pre-transition and the main phase transition.

In the thermogram, after the addition of 10 μM melimine, changes were observed when compared to the thermogram without the peptide (see Figure 3.7.1.2.). The first difference is a shift in the temperature at which the lipids are undergoing the phase transition. The membranes with melimine are undergoing this phase transition at a lower temperature, 23°C (see Figure 3.7.1.2.).

This decrease in the main transition temperature could be attributed to greater van der Waals interactions between neighbouring lipids within the lipid bilayer, with the melimine most likely occupying regions of the bilayer that are still in the liquid-crystalline phase [187, 188].

The enthalpy of the transition was slightly increased after the addition of melimine, from 23.89 KJ mol^{-1} to 24.52 KJ mol^{-1}. This combined effect was attributed to having impurities in the bilayer, i.e. melimine, as the lipid packing had been disrupted, reducing the lipid order parameter, increasing the entropy and decreasing the transition temperature [188].

The main transition peak of the melimine thermogram can be seen to have broadened. This broadening was due to the membrane becoming homogeneous with the addition of the peptide, with the interactions between the lipids and melimine hindering the ease at which the lipids were able to go through the phase transition, requiring more time to undergo the complete phase transition [188, 189].

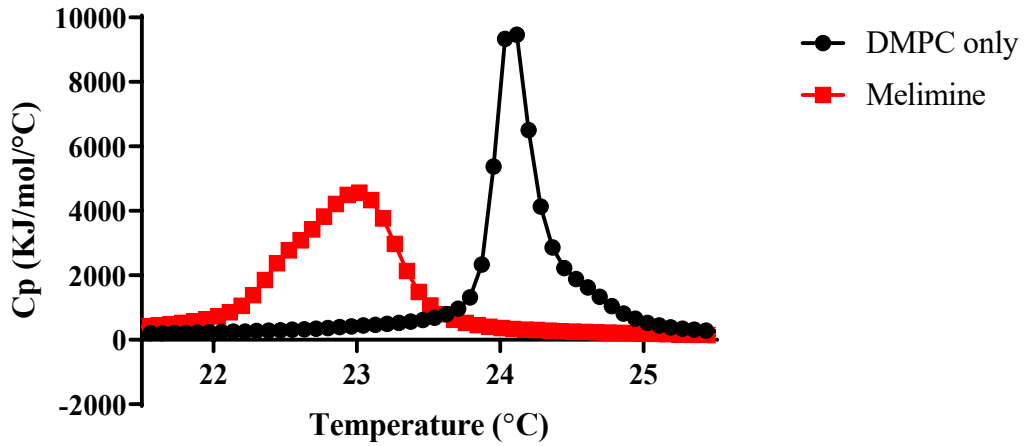

Figure 3.7.1.2: Thermogram of the main phase transition of DMPC lipid vesicles with and without 10 μM melimine.

The peak signifying the pre-transition of the membrane can be seen to have shifted in a similar manner as the peak at the main transition, see Figure 3.7.1.3. The pre-transition peak, after the addition of melimine, resulted in the scanning densitometry transition temperature decreasing to 8.8 °C, with an enthalpy of 1.09 KJ mol^{-1}.

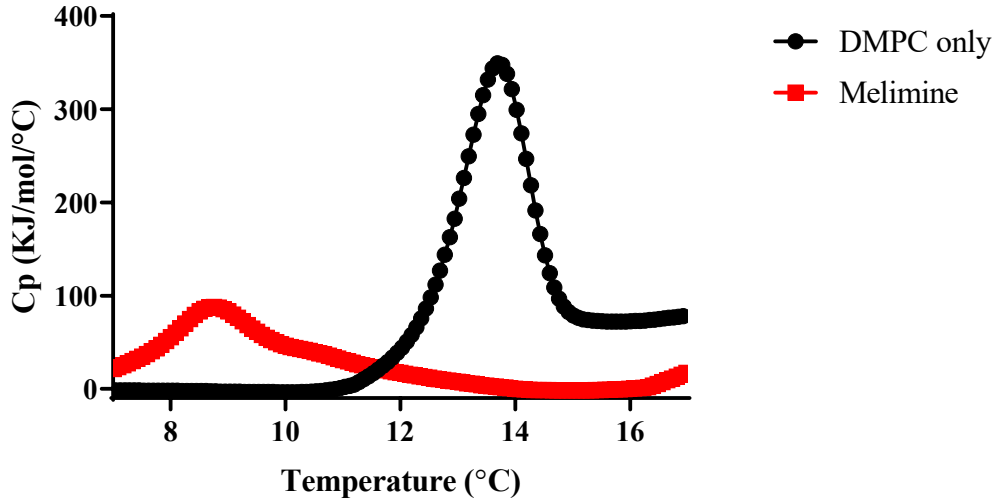

Figure 3.7.1.3: Thermogram of the pre-transition of DMPC lipid vesicles with and without 10 μM melimine.

3.7.2 Cys-melimine

After the addition of 10 μM cys-melimine to the DMPC vesicles, the resultant thermogram showed a broadening of the peak and a shift in the main phase transition temperature to lower temperatures, though slightly smaller than the temperature shift caused by melimine (see Figure 3.7.2.1.). The temperature of the main transition peak, at 23.8°C, shifted from the 24.1°C of the pure DMPC lipid phase transition. This was attributed to an increase in the van der Waals interactions between the neighbouring lipids within the bilayer. The transition peak was also observed to have broadened, similar to melimine, showing that the impurities in the membrane caused by the cys-melimine were also hindering the ability of the lipids to undergo the phase transition.

The enthalpy of the transition was calculated to be 22.26 KJ mol^{-1}, which is smaller than the energy required for only DMPC lipids and, having the opposite effect than that of melimine, indicated that while the membrane is less cooperative, the order parameter is not reduced.

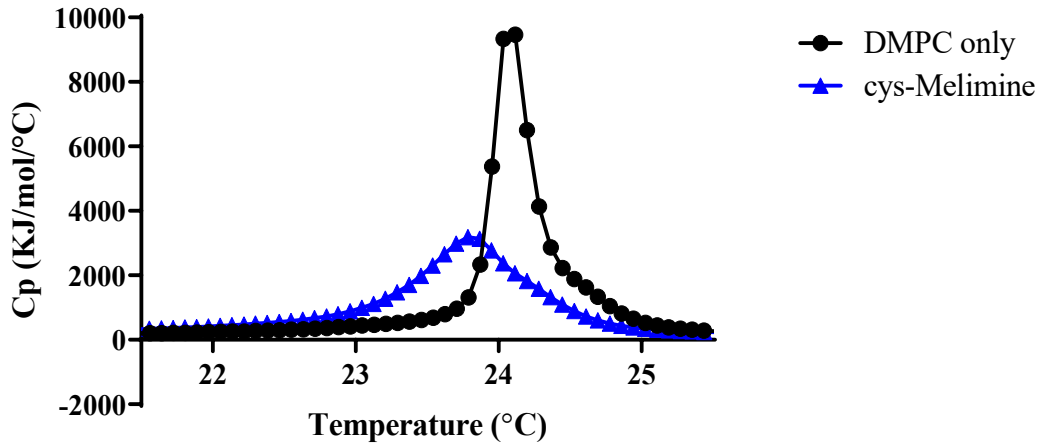

Figure 3.7.2.1: Thermogram of the main phase transition of DMPC lipid vesicles with and without 10 µM cys-melimine.

The peak signifying the pre-transition of the membrane shifted in a similar manner as the peak at the main transition (see Figure 3.7.2.2.). The pre-transition peak after the addition of melimine resulted in the transition temperature decreasing to 11.8°C with the enthalpy calculated to be 1.21 KJ mol^{-1}.

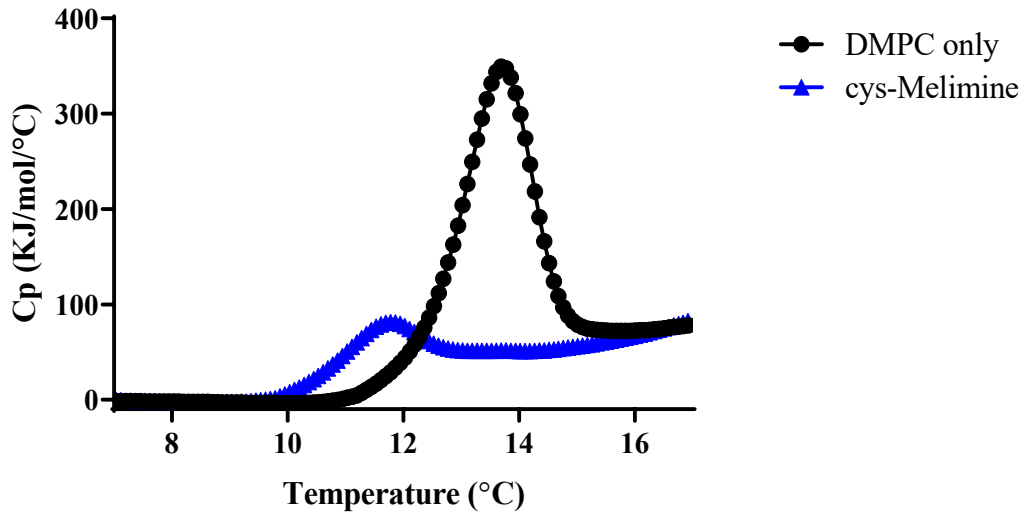

Figure 3.7.2.2: Thermogram of the pre-transition of DMPC lipid vesicles with and without 10 μM cys-melimine.

3.7.3 Mel4

The addition of 10 μM mel4 into the DMPC vesicles did not cause a change to the temperature at which the main peak phase transition occurred. However, the thermogram during the main phase transition exhibited an additional peak at 24.5°C (see Figure 3.7.3.1.), suggesting a delay with some regions of the bilayer as the lipids underwent their phase transition.

The enthalpy of the phase transition for mel4 was calculated to be 26.28 KJ mol^{-1}. This enthalpy was much higher than the enthalpy of DMPC lipids alone. The proposed delay of the regions of lipids might explain this increased enthalpy as there would be two populations of lipids undergoing separate phase transitions.

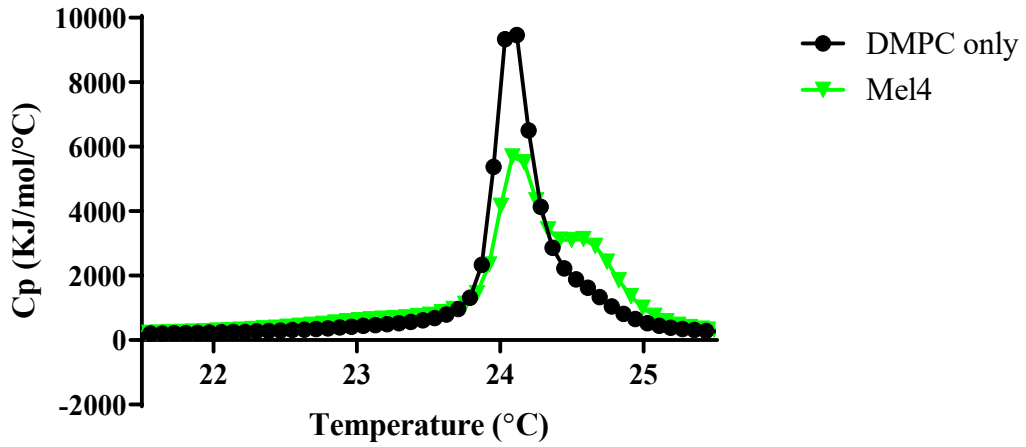

Figure 3.7.3.1: Thermogram of the main phase transition of DMPC lipid vesicles with and without 10 µM mel4.

Minimal changes are observed between the thermograms with and without mel4 during the pre-transition (see Figure 3.7.3.2.). The transition temperature after the addition of mel4 was 13.8°C, an increase of 0.1°C compared to the pre-transition temperature of the DMPC vesicles with lipid only. The enthalpy of the pre-transition did decrease after the addition of mel4. It was calculated to be 3.14 KJ mol^{-1}. This reduction indicates that mel4 was influencing the packing of the lipids within the membrane. However, this reduction was less than the effect of melimine and may be due to mel4 being truncated, possessing a shorter sequence.

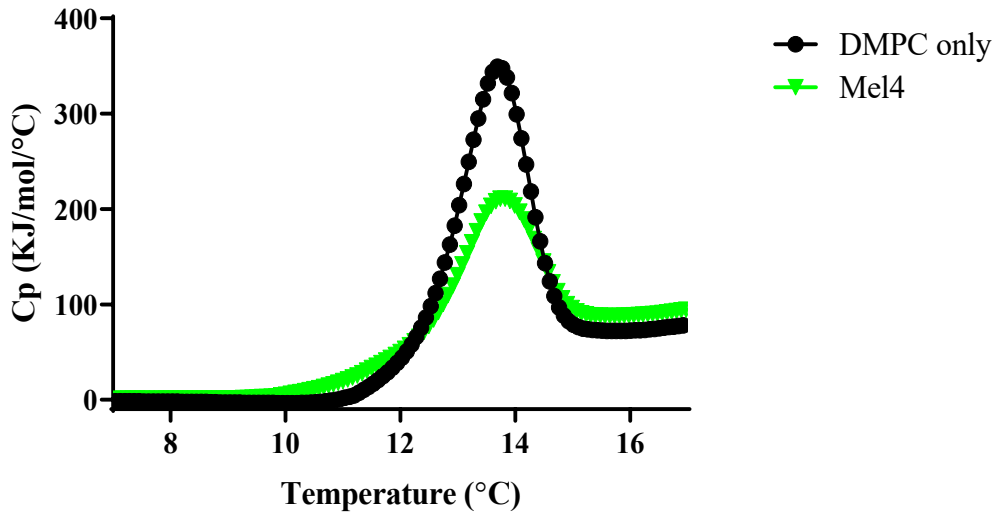

Figure 3.7.3.2: Thermogram of the pre-transition of DMPC lipid vesicles with and without 10 μM mel4.

3.7.4 Cys-mel4

The thermogram, after the addition of 10 μM cys-mel4, showed no significant changes in comparison to the thermogram with DMPC lipid (see Figure 3.7.4.1.). The main phase transition temperature for cys-mel4 is 24°C had a decrease of 0.1°C compared to the main phase transition temperature of the DMPC lipid thermogram.

The enthalpy of the cys-mel4 thermogram was calculated to be 23.85 KJ mol^{-1} and showed no change compared to the enthalpy of the control. These minimal changes suggested that cys-mel4 had a little effect on the lipid packing of the lipid bilayer.

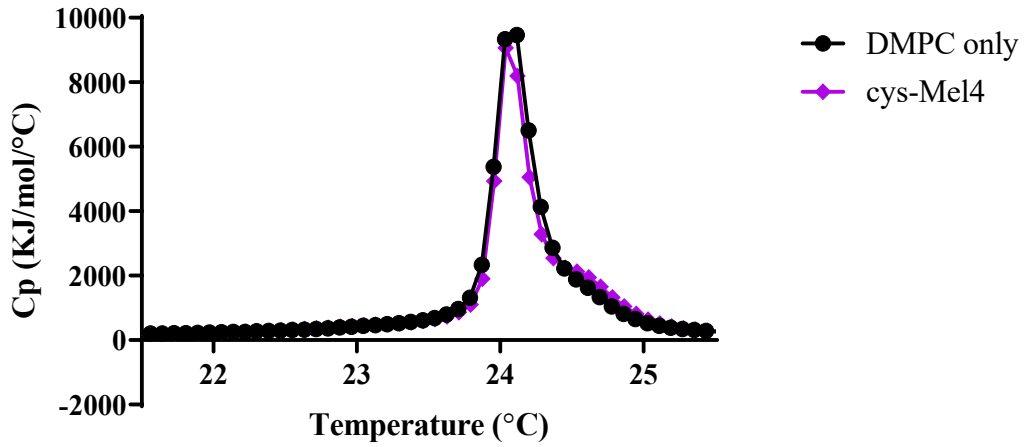

Figure 3.7.4.1: Thermogram of the main phase transition of DMPC lipid vesicles with and without 10 μM cys-mel4.

The pre-transition of the cys-mel4 thermogram showed small differences in comparison to the DMPC only thermogram (see Figure 3.7.4.2.). The pre-transition temperature increased to 13.9°C after the addition of cys-mel4, and the enthalpy of the pre-transition of the cys-mel4 membrane was calculated to be 3.43 KJ mol^{-1}, showing a small reduction when compared to the DMPC only control. The decrease of the enthalpy seen in the increase in the transition temperature is most likely due to the impurity of cys-mel4 existing within the lipid bilayer.

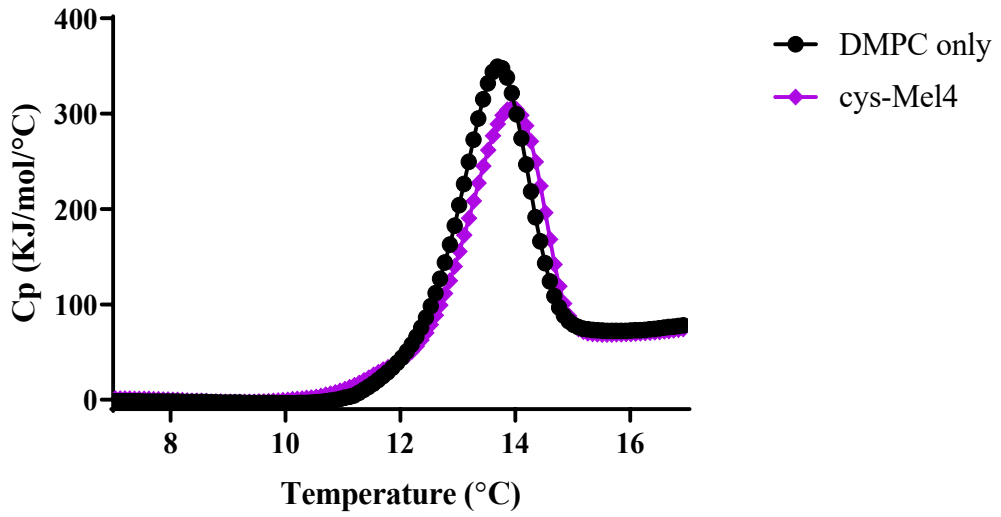

Figure 3.7.4.2: Thermogram of the main phase transition of DMPC lipid vesicles with and without 10 μM cys-mel.

3.7.5 MelAlanine

The introduction of melAlanine into the bilayer resulted in changes that were opposite to that of melimine (see Figure 3.7.5.1.). The thermogram of the melAlanine addition showed a slight increase in the transition temperature to 24.3°C with a narrowing of the peak width. The enthalpy was also reduced and was calculated to be 18.66 KJ mol^{-1}. This indicated that melAlanine caused a reduction in the vans der Waals interactions between neighbouring lipids within the bilayer and caused the lipids to go through the phase transition within a narrower temperature range.

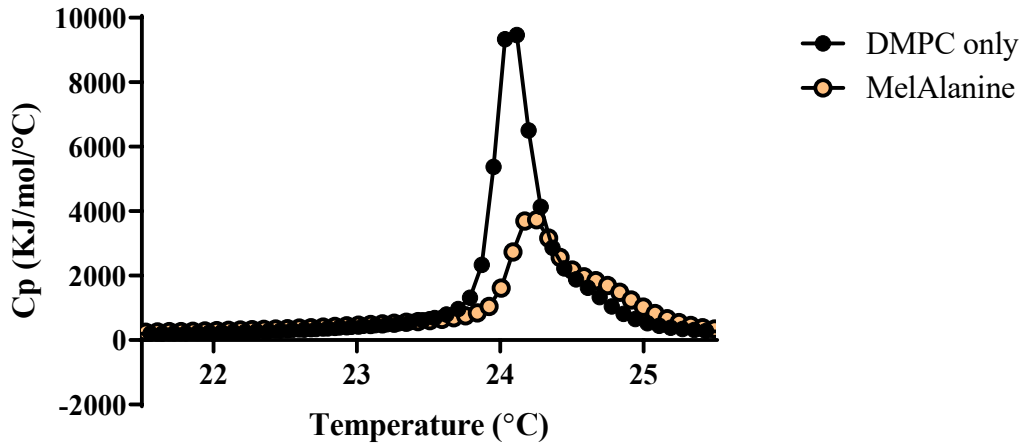

Figure 3.7.5.1: Thermogram of the main phase transition of DMPC lipid vesicles with and without 10 μM melAlanine.

The pre-transition of the melAlanine thermogram also showed an increase in the transition temperature to 14.3°C (see Figure 3.7.5.2.). The enthalpy of the pre-transition was calculated to be 2.3 KJ mol^{-1}. This was a reduction when compared to the DMPC only pre-transition. This decrease in the enthalpy was greater than the decrease caused by mel4 and cys-mel4, but smaller than the effect of melimine and cys-melimine. This relatively midrange reduction may be due to the size of melAlanine being the same as melimine. However, the charge of melAlanine is smaller than the other four peptides, and the hydrophobicity of the alanine residues differs from the arginines. This change in the charge and the hydrophobicity would have influenced the interactions between melAlanine and the lipids within the bilayer, changing the way that the lipids would have packed when compared to the other peptides. This was seen in the increase in the transition temperature and narrower peak width.

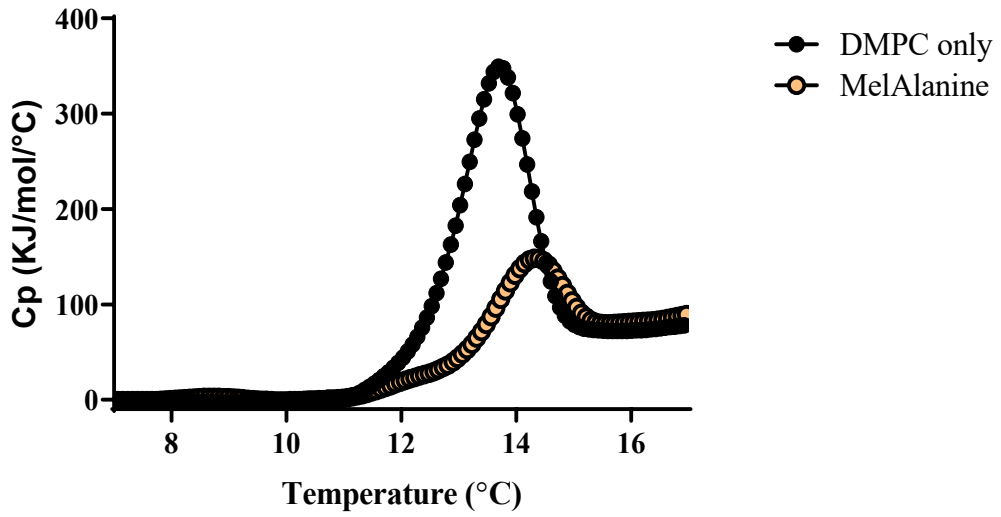

Figure 3.7.5.2: Thermogram of the main phase transition of DMPC lipid vesicles with and without 10 μM melAlanine.

3.7.6 Summary

Melimine and its derivatives have been shown to interact with lipids within the bilayer in a way that influences the packing through changes in the phase transitions of lipid bilayers (Table 3.7). See Section 4.1.5 for further discussion on this topic.

	Transition temperature (°C)	**Transition enthalpy (kJ mol^{-1}) ΔH**	**Pre-transition temperature (°C)**	**Pre-transition enthalpy (kJ mol^{-1})**
Lipid only	24.1	23.89	13.7	4.02
Melimine	23	24.52	8.8	1.09
Cys-melimine	23.8	22.26	11.8	1.21
Mel4	24.1	26.28	13.8	3.14
Cys-mel4	24	23.85	13.	3.43
MelAlinine	24.3	18.66	14.3	2.3

Table 3.7: Summary of the enthalpies and transition temperatures of melimine and its derivatives.

4 Discussion

This work set out to use advanced biophysical research techniques such as in-silico structural modelling, fluorescent membrane dipole measures, differential scanning calorimetry, neutron reflectometry, dynamic light scattering and electrical impedance spectroscopy of tBLMs to describe the cell membrane interactions of melimine and its associated derivatives. An EIS tBLM technique modelled on the Arrhenius equation was also developed to record the activation energies of ion transport across the tBLMs in response to melimine and its derivatives. Further, the data collected through the aforementioned techniques were used to describe the interactions of melimine and its derivatives according to the CPP model, which, given the size of the peptides, appears to best explain the interactions of these molecules with lipid bilayers. The minimal interaction with the membranes observed in this study is in contrast to *in vivo* bacterial dye release measures of melimine that originally suggested a pore-forming action [30].

Technique		Melimine	Cys-melimine	Mel4	Cys-mel4	MelAlanine
MIC		Low	Low	Low-med	Low	High
Fluorescence dipole measures	Significantly different to peptide free	Yes P = 0.043*	Yes P = 0.003**	No P = 0.206	No P = 0.231	No P = 0.101
DLS	Significantly different to peptide free	Yes P < 0.0001 ****	Yes P < 0.0001 ****	No P = 0.867	Yes P < 0.0003***	Yes P < 0.0001 ****
EIS	Δ conductance (μS) [μS cm^{-2}]	0.115 ± 0.02 [0.0055 ± 0.0002]	2.55 ± 0.74 [0.121 ± 0.035]	0.02 ± 0.02 [0.001 ± 0.001]	-0.081 ± 0.015 [0.0039 ± 0.0007]	1.68 ± 0.38 [0.08 ± 0.018]
	Δ capacitance (μF cm^{-2})	0.0146 ± 0.004	0.22 ± 0.03	0	-0.035 ± 0.005	0.098 ± 0.028
EIS Arrhenius	Percentage change (%) in E_a	-3	-38	8	-6	-15
Neutron Reflectometry	Structural change detected	No	No	No	No	No
DSC	Δ temp (°C)	-1.1	-0.3	0	-0.1	0.2
	Δ enthalpy (kJ mol^{-1})	0.63	-1.63	2.39	-0.04	-5.23

Table 4.1: Summary of the results in response to each peptide at 10 μM. Green boxes indicate a marked difference compared to a no-peptide control. Red boxes indicate little or no difference compared to control.

4.1 Melimine and its derivatives: membrane interactions

4.1.1 Impact of the peptide structure

The in-silico modelling of melimine, cys-melimine and melAlanine has shown that the peptide contains two α-helical conformations, connected by random coiling, see Figure 3.1.2. This random coiling occurs around the proline residue, as would be expected. The proline bend present in the structure is similar to the structure seen in peptides like Pardaxin [190], Apolipoprotein A-I [191], magainin II, caerin 1.1, and clavanin [192, 193]. This bend has also been identified in melittin, which shares sequence homology with melimine [190]. This structure with the proline bend between two helices has been designated a *helix-hinge-helix* motif [191, 194, 195].

This proline hinge has been shown to be a factor in antibacterial activity [190] and to increase antimicrobial cell penetration [196, 197]. For example, loss of this hinge motif reduces the cytolytic activity of modified pardaxin and reduces the ability of modified *buforin II* to penetrate the membrane of cells, resulting in an accumulation of the peptide on the cell surface. While the helix-hinge-helix motif has been shown to increase peptides antibacterial activity, its exact mode of action with the addition of the hinge is unknown [190]. It has been postulated that the increased flexibility provided by the hinge is what allows for optimal orientation and increased insertion of the hydrophobic regions of the helical regions of these types of peptides [193, 194].

In addition to the hinge induced from proline, glycine has also been shown to induce a similar hinge [196]. The two glycine residues within melimine's sequence structure, at positions 24 and 25, have been identified as the most likely point where the second helix terminates; this may correlate with a second hinge of the peptide were it longer.

Through the use of EIS with melimine, cys-melimine and melAlanine, the increased conduction measurements do not show any impact due to the proline hinge, with melimine showing minimal conductance change, see Figure 3.4.1.

The impact of the proline hinge is also not prevalent in Arrhenius measures. This can be noted in the percentage change of the activation energy of ion traversal, seen in Table 3.5, for melimine, cys-melimine and melAlanine.

The added cysteine moiety within the cys-derivatives of melimine may have additional interactions, which may lead to disulfide-bridges forming between these peptides in solution. However, both cys-melimine and cys-mel4 were examined using high-resolution nanoelectrospray ionization mass spectrometry [40]. This was used to determine whether disulfide-bridged homodimers were forming in solution. They found that only monomeric forms of the two peptides were present.

4.1.2 Fusogenic properties

Results from the DLS measurements showed that the interactions of melimine and its derivatives led to an increase in the diameter of lipid spheroids, suggesting that the peptides promote the fusing of these lipid complexes (Figure 3.3.1.2).

Studies have shown that the interaction between peptides and lipid membranes may lead to the aggregation of vesicles, particularly by charged peptides or ones that have hydrophobic properties [142, 169, 198]. Peptides with an α–helix component have been shown to destabilise lipid bilayers and influence the fusogenicity of the peptides [198-200]. With melimine, cys-melimine and melAlanine having a second α-helical coil segment in their predicted structures, as shown in the in-silico modelling in Section 3.1, this may be correlated to an increased fusogenic potential, as seen in the resultant lipid spheroids size in comparison to mel4 and cys-mel4, in Figure 3.3.1.1.

The angle of the insertion, as influenced by the interactions of the dipole potential of each peptide with the lipid bilayer, may also lead to changes in the fusogenic properties of the peptides and, as such, change the aggregation of lipid spheroids [201]. The dipole moment of the lipids would influence the peptide, changing the insertion angle, ranging from parallel to perpendicular to the membrane, with studies showing that α-helices inserted at angles between these planes cause more significant disruptions to the packing of lipids [202-204]. Additionally, the proline hinge found in the three larger peptides studied here may also cause changes to the angle of insertion as it alters the degrees of freedom of the second α-helix component of these peptides.

Studies have also shown that changes in lyso PC lipids within bacterial membranes, such as the density of lipid packing, have been shown to affect membrane resistance [205] and lipid membranes' permeability [206]. The interaction of melimine and its derivatives with the lyso PC lipids within a bacterial membrane may lead to better insertion due to this increased permeability, thus further disrupting lyso PC lipids' packing leading to changes in ionic transport across bacterial membranes.

4.1.3 Fluorescent dipole meaurements

To what degree the dipole of the lipid head groups existing between the phosphate to nitrogen atoms is affected by the insertion of the peptide was explored by determining the spectral changes of the fluorophore RH-421 [15]. Of the five peptides, melimine and cys-melimine caused a significant decrease of the lipid headgroup dipole potential (Table 3.2 and 4.1).

Within the membrane, the total dipole signal is constituted from three components [207, 208]. The first reported component is the transmembrane potential that arises due to differences in the salt concentrations on each side of the membrane, such as the Nernst potential. The second reported component arises from a surface potential from the accumulation of ions that are attracted to the charged lipid head groups. The third reported component of the membrane dipole originates from the alignment of the membrane lipids and the alignment of water molecules at the membrane-water interface [201]. Of the total dipole signal, the third component is a dominant factor in determining the total electric field strength, as it is greater in strength by one to two orders of magnitude [207, 208].

As each of the peptide derivatives interacts with the membrane surface, the hydration layer of the membrane may be affected. This interaction would lead to a decrease in the membrane dipole through the disruption of the hydrogen bonds between the water molecules and the lipid head groups and the disassociation of the water molecules from the lipid bilayer [201]. The changes in this water content across the membrane headgroups can be measured by identifying changes in the capacitance measures when using electrical impedance spectroscopy; It is tempting to compare the capacitance measure with the fluorescence dipole measures, but in reality, they are comparing different things.

The interactions between the peptides, particularly melimine and cys-melimine (see Table 3.2 and 4.1) and the lipid bilayer may cause the lipids to shift to accommodate the peptide insertion and or have a significant impact on the hydration state of the lipid headgroups; in this case, the magnitude of the membrane dipole is also affected. The dipole of the lipid head groups, existing between the phosphate to nitrogen atoms, has been reported to be perpendicular to the lipids and parallel to the membrane in the absence of electrolytes [209]. It is uncertain, however, whether the presence of ions would cause a change to the orientation of this dipole moment as the previous studies that suggested a parallel arrangement of the headgroups with the bilayer were performed in pure water.

Regardless, shifting of the orientation of these lipids by the insertion of melimine or cys-melimine seems to cause a significant change in the dipole potential across the membrane headgroups, Figures 3.2.1.2 and 3.2.2.1. These two peptides, being untruncated, have a greater length than mel4 and cys-mel4, suggesting that the increased length of these peptides allows for greater interactions with the lipid headgroups, disrupting the dipole. Charge attraction to the membrane may also allow for increased disruption of the dipole of the headgroups, as melimine and cys-melimine possess the highest charge of all of the peptide derivatives (Table 1.2), with the untruncated, reduced charged, melAlanine, showing a less significant interaction with the lipid headgroups.

The dipole of the membrane has been shown to influence the angle of insertion of some peptides, either increasing or decreasing the angle of insertion [201, 210]. The angle of insertion can then have an effect on the fusogenic properties of the membrane [201]. This can be seen with melimine and cys-melimine, influencing both the fusogenic and the dipole potential of these membranes.

The dipole moment of each peptide would also have a direct influence on the magnitude of the dipole across the membrane, with the orientation of the peptide having some impact as it inserts into the membrane. If the insertion of this peptide with its dipole is such that its alignment is in contrast to the membrane dipole, then the magnitude of the membrane dipole will be altered [201]. While melimine and cys-melimine were shown to alter the magnitude of the dipole of the membrane, it is important to realise that the overall downshift of the magnitude of the

membrane dipole is minimal, suggesting that these two peptides are only causing minimal disruptions to the lipid packing and the hydrogen bonds between the water and the membrane.

4.1.4 pH-induced membrane response

The decrease in the conductance response at pH = 9 in both zwitterionic and negatively charged membranes may be due to changes in the protonation state of the side chains of some of the amino acid residues in the melimine sequence. Arginine and lysine both report a pKa value for their side chains at high pH values. Arginine reports a pKa of approximately 12, and lysine reports a value of approximately 10 [211]. While these pK_a values are above the measured pH values used, J.K.Thibado *et al.,* 2016*,* have shown that while the side chains of the arginine residues will not change at these measured pH values, the side chains of lysine residues undergo deprotonation at pH values between 6.5–8.0 [212].

Melimine contains three lysine residues in the first α-helix coil in its sequence. If the lysine side chains are undergoing deprotonation at pH = 9, the peptide would be experiencing changes in its charge and its hydrophobicity. This may lead to changes to its structural conformation around the lysine residues within the peptide. These changes may then limit its ability to insert into the membrane.

4.1.5 Lipid phase transition disruption

Adding impurities into a membrane, such as an antimicrobial peptide, as it is undergoing its phase transition would generally lead to a reduction in the cooperativity of the membrane (the ease at which the lipids go through the phase transition) through a disruption in the lipid packing [188]. As this packing is disrupted, the measured enthalpy of the phase transition decreases and the temperature at which the transition occurs is decreased [188]. The effect of these impurities is more prominent when observing the pre-transition, leading to a loss of the pre-transition peak due to disruption of the lipid packing after a peptide has interacted with the bilayer core [213, 214].

The insertion of melimine and cys-melimine caused the main phase transition temperature to slightly decrease, indicating these two untruncated peptides caused a more noticeable change in the packing of the lipid bilayer [187-189]. Melimine, cys-melimine, mel4 and melAlanine caused small changes to the enthalpy of the phase transition (see Table 4.1). Small changes in the enthalpy of the main transition have been shown to indicate minimal disruption of the hydrocarbon chain packing of DMPC membranes [215]. This is because the enthalpy of the phase transition arises from the disruption of the van der Waals interactions between the chains as they undergo melting through the phase transition. The minimal differences in the enthalpy caused by the addition of melimine and its derivatives (see Table 3.7) suggest that these peptides only minimally interact with the lipid membrane [215, 216]. MelAlanine caused a greater decrease in the enthalpy (Table 3.7). The alanine residues in the second helix result in the peptide being more hydrophobic; this might allow for more interactions with the hydrophobic chains in comparison to the other peptides.

The presence of the second overlapping transition peak for mel4, see Figure 3.7.3.1, may have arisen from differing temperatures at which the lipids are undergoing the phase transition due to separation into areas of lipid that are interdigitated with the peptide, where the hydrocarbon chains are shielded from water by the mel4 and regions of lipid only [217]. This peptide-lipid interdigitation has also been observed with the bee venom peptide, melittin, in PC lipids [217].

A decrease in the pretransition was observed for each of the five peptide derivatives. The three untruncated peptides resulted in a more substantial reduction of the pretransition. Still, the pretransition was not completely removed at the peptide concentrations used; this is suggesting that melimine and its derivatives are only causing minor packing defects within the lipid headgroups (Figures 3.7.1.3, 3.7.2.2, 3.7.3.2, 3.7.4.2, 3.7.5.2). This is in contrast to a study by C. Mollay, 1976, whereby the introduction of the bee venom peptide, melittin, into a lipid membrane at a lipid to peptide ratio of 250:1 almost completely removed the pre-transition [218]. Melimine and its derivatives were added at a lower concentration, at a lipid to peptide ratio of 300:1. Other peptides at higher concentrations have been shown to completely remove the pretransition, this includes Temporin-SHa and Gramicidin S, at a lipid to peptide ratio of 100:1 [219, 220], and two novel peptides derived from human and chicken lysozyme at a lipid to peptide ratio of 25:1 [221]. The disappearance of the pretransition may also be due to the use of the faster rate of increasing the temperature during their measurements, as the

pretransition has been shown to be a slower process, thereby making it harder to interpret the changes with rapid scanning [187, 222].

4.1.6 Ion traversal energy barrier of membranes

The activation energy of ions traversing across the lipid bilayer is similar to determining the energetic barrier. The interaction of peptides with a lipid bilayer leads to a change in the energy barrier; as such, a decrease in the activation energy would show that the energy barrier restricting the flow of ions has been decreased.

Compared to pores like gramicidin A, Staphylococcus aureus α-toxin and the capsaicin ion channel, VR1, whose activation energy for ion traversal has been reported as 38.9kJ mol^{-1} [182], 15.9kJ mol^{-1} [183], and 29.3 kJ mol^{-1} respectively [184], the activation energy in the presence of melimine and its derivatives are still significantly higher. Though for gramicidin A and the α-toxin, this activation energy measurement was done in black lipid membranes formed from monoglyceride or egg phosphatidylcholine, and the activation energy of the capsaicin ion channel was calculated based on data collected using patch-clamp electrophysiology techniques. This makes direct comparisons with the tBLM Arrhenius energy measurements used here tenuous.

Valincius et al., 2008 reported a change in the activation energy of ion traversal to be 100 kJ mol^{-1} for DOPC tethered lipid bilayers without any compounds added [155]. This is consistent with the membranes in this study, before the addition of melimine and its derivatives, where activation energies in the range of 74-111 kJ mol^{-1} were found (Table 3.5).

The addition of the amyloid β-peptides oligomers by Valincius et al. caused the barrier energy of the bilayer to drop to 36.8 kJ mol^{-1}. This decrease was much larger than the barrier decrease caused by melimine, mel4, cys-mel4 and melAlanine, which caused changes in the range of 3-17 kJ mol^{-1} (Table 3.5). Considerations need to be made for the different tBLM architectures used in the study by Valincius et al. compared to the study presented here. Their study used DOPC lipids on a T30 tethering architecture, whilst this study used a mixture of diphytanyl lipids on a T10 tethering architecture. Further, this study used a collected greater number of temperature points used in calculating the resultant slope of the Arrhenius plots.

The interactions of cys-melimine have a more considerable influence on the energy barrier of the lipid bilayer than melimine and the other three derivatives, from 82 kJ mol^{-1} to 51 kJ mol^{-1}, which suggests that the interactions of cys-melimine are significantly lowering the energy barrier of the lipid bilayer.

With cys-melimine causing the most substantial change to the energy barrier of the membrane and melAlanine, while the disruption was smaller, was still larger than the other derivatives, this correlates with the EIS data presented in Section 3.4 and the number of their relative hydrophobic amino acid residues.

Overall the five peptides, melimine and its derivatives, have a small influence on the energy barrier of lipid bilayers. This suggests that the interactions of these peptides, while increasing the ion conduction, are not forming pores.

4.2 Model for Membrane Disruption

4.2.1 Membrane penetration

Despite having a low MIC (Table 3.4), the small conductance response suggests that the bactericidal effects of melimine are not caused by either cell lysis or through a surfactant-like effect (e.g. the carpet modal). If melimine had interacted in a way similar to these modes of action, the membrane would have ruptured, leading to the membrane falling apart and the disappearance of the phase minima of each Bode plot (Figures 3.4.1.1.1 A, 3.4.2.1.1 A, 3.4.3.1 A, 3.4.4.1 A, and 3.4.5.1 A). With the Bode plots remaining stable after the addition of each peptide, no evidence of this effect was seen. Further, from the reflectivity profiles (Figures 3.6.1.1, 3.6.2.1, 3.6.2.2, 2.6.3.1 and 2.6.3.2), before and after the addition of melimine and its derivatives show no difference in the reflectivity. This is suggesting that melimine is not inducing significant changes in membrane morphology.

Furthermore, if an increase in membrane packing that leads to a small or negative conductance response were to be the cause of low MIC values, this would be evident in the DSC results. Of the peptide derivatives, melimine, mel4 and cys-mel4 show a small conductance response, with the Δconductance response of cys-mel4 being negative. The interactions of these three peptides would also have caused an increase in the ΔT of the main transition due to the closer packing of the phospholipids. The data shows that the melimine caused a decrease in the main transition temperature, while mel4 caused no change to the transition temperature and cys-mel4 caused only a minor increase, see Table 3.7. This suggests that it is unlikely increased phospholipid packing is the cause of the low MIC values due to these peptides.

When compared to ion channel-forming peptides and proteins such as gramicidin A and α-hemolysin [101, 136], the conductance response of each of these peptides is considerably smaller, suggesting that they are not forming ion channels spanning across the membrane, such as a barrel-stave pore. The activation energy of ion traversal through the membranes in the presence of melimine and its derivatives was also determined to be lower than what would be expected for an ion channel (See discussion in Section 4.1.6 above).

That I did not detect any changes to the acyl chains morphology using neutron reflectometry, suggests that melimine and its derivatives are not present in this region. Yet, the resolution of the neutron reflectometry may not be sufficient enough to detect any changes within the

headgroup region of the lipid bilayer. Accounting for the changes in membrane conduction then must be as a result of interactions at the water-lipid interface. From the types of peptide-membrane models presented in Section 1.1.2, only the CPP model seems to be supported by the data.

4.2.2 Peptide charge

In the presence of negatively charged lipids such as POPG, cationic peptides induce a greater membrane conduction response (Figure 3.4.2.2). It has been hypothesised that membrane disruption due to charge attraction of cationic peptides is the cause of their antimicrobial activity; this phenomenon is well understood and has been reported previously [135, 223-230]. In the structure of these peptides, melAlanine is the same size as melimine and cys-melimine but contains differences in its charge and hydrophobicity. Melimine and mel4, while having a difference in size, have a similar charge. The only difference between melimine and cys-melimine, and mel4 and cys-mel4, is the presence of the hydrophobic cysteine residue. While melAlanine has a smaller charge than all peptides, the alanine residues add to its hydrophobic nature, increasing its membrane-disruptive properties. As melAlanine has a high MIC value against bacteria (see Table 3.4)., it brings into question whether the correlation between peptide charge and low MICs against bacteria is a result of a membrane disruption mechanism. That the truncated, highly charged, less hydrophobic peptides had induced minimal membrane-disruptive changes whilst maintaining low MIC values against bacteria lends credence to this supposition.

4.2.3 Summary

In summary, the data suggests that the actions of these compounds against bacteria are unlikely to be as a result of any lipid bilayer lytic response or through the formation of a barrel stave pore. This lends credence to the CPP toroidal pore model being the better fit for identifying a mode of action for melimine and its derivatives. This would be either through the compounds forming part of the lipidic toroidal pore in an interdigitated pattern, or they are causing disruptions in the CPP across the bilayer and inducing or modulating toroidal pores within the membrane [67, 73]. The melAlanine data with its MIC values (Table 3.4) indicating that it does not kill bacteria, combined with its high conductance response, enforces an idea that these peptides are not causing bacterial cell death through pore-forming.

4.3 Antimicrobial properties

A large volume of the literature assumes that there is a strong link between membrane attraction and insertion [135, 223-234]. For melimine and its derivatives, which are highly positively charged peptides, have net charges ranging from +10 to +16 at neutral pH. This would suggest that the peptides have a strong affinity for binding to membranes. The results in this study have shown that these peptides are not inserting into membranes and forming pores yet are still active against both gram-positive and gram-negative bacteria in weakening the integrity of bacterial cytoplasmic membranes [30].

For the exact mode of action of melimine and its derivatives, it is feasible that these peptides are targeting other components of bacterial cell membranes. There is an increasing number of AMPs that are being shown not to be membrane targeting. Two peptides, nisin and pep5, have been shown to activate the enzyme autolysin, which breaks down the components of the peptidoglycan barrier within bacterial membranes, leading to eventual cell lysis [18, 235]. It is conceivable that such an antimicrobial mechanism could be mistaken for being membrane targeting experimentally. Indolicidin has been shown to inhibit the synthesis of both DNA and RNA [236, 237]. Three other peptides, pyrrhocoricin, drosocin and apidaecin, have been linked with binding to DnaK, reducing the ATPase activity and preventing molecular chaperone functions such as protein folding [18, 238, 239].

The porin channel OmpF allows for passive diffusion of small molecules across the outer LPS membrane of *E. coli*. If melimine and its derivatives are small enough, this may be a possible method of traversing the outer membrane of bacteria. Alternatively, a study by Lamichhane et al., 2012, has shown that arginine-rich peptides caused blockages of OmpF protein pores [240]. As melimine and its derivatives, excluding melAlanine, are arginine-rich, their actions might be attributed to interactions with such bacterial porins rather than membrane interactions as was initially postulated. Studying the possible interactions of these peptides with the porin pores was beyond the scope of this thesis.

5 Conclusions

The novel peptide melimine and its derivatives were examined with a variety of sophisticated biophysical techniques to characterise their interactions with lipid membranes.

Aim 1 of this project was to study the properties of melimine and its derivatives through established lipid membrane biophysical techniques. The results of these experiments are summarised under the heading of each technique (see Table 4.1 above).

Each of the techniques used in this study were chosen to characterise the interactions of these peptides with lipid membranes. Other techniques were considered for identifying the interactions, such as nuclear magnetic resonance (NMR), quartz crystal microbalance with dissipation (QCM-D), and surface plasmon resonance (SPR). The use of QCM-D was attempted using liposomal deposition techniques [241, 242]. Unfortunately, uniformity of lipid deposition was difficult to achieve, and the results were inconsistent (data not shown).

Solid-state NMR with lipids may have provided additional orientation and positional information [243-245]. However, a large amount of each peptide would have been required to use this technique, and the data would have required elaborate 'interpretation' to relate the results to peptide activity against bacteria. Like QCM-D, SPR would provide information on the binding affinity and kinetics of the peptides within the bilayer [246]. Nevertheless, the technique can provide additional information about models of peptide-membrane interactions.

In comparing the peptide-membrane interactions of melimine and its derivatives against models of AMP modes of action (**Aim 2**), it was clear that only the critical packing parameter model fitted the data. This model suggested that the peptide-membrane interactions led to steric alterations of lipid bilayers, causing a modulation in the size of intrinsic toroidal pores within the membranes [73]. Though this model accounts for changes in membrane conduction, it does not explain the mechanism(s) of antimicrobial actions of the peptides (**Aim 3**).

After examining the interactions of melimine and its derivatives through the various biophysical techniques, it is concluded that, while these peptides are active against both Gram-positive and Gram-negative bacteria in having small minimum inhibitory concentrations (MICs), they do not traverse membranes or form pores in them. A potential mode of action of

melimine and its derivatives involves targeting extracellular components of bacterial cell membranes. As melimine and its derivatives are active against bacteria when bound to surfaces such as contact lenses [29], this adds credence to an extracellular interaction.

To understand further the antimicrobial mode of action of melimine and its derivatives, testing these peptides while bound to a surface, such as gold nanoparticles, could reveal additional insights into their mechanisms of bactericidal action. Also, introducing these peptides into bacterial cell membrane components, such as porin channels, may bring about a deeper understanding of their antimicrobial mechanism(s).

References

1. Fleming, A., *On the Antibacterial Action of Cultures of a Penicillium, With Special Reference to Their Use in the Isolation of B. Influenzæ.* British Journal of Experimental Pathology, 1929. **10**(3): p. 226-236.

2. Abraham, E.P., et al., *Further Observations on Penicillin* The Lancet, 1941. **238**(6155): p. 177-189.

3. Chain, E., et al., *Penicillin as a Chemotherapeutic Agent.* The Lancet, 1940. **236**(6104): p. 226-228.

4. Florey, M.E., et al., *General and Local Administration of Penicillin.* The Lancet, 1943. **241**(6239): p. 387-397.

5. Abraham, E.P. and E. Chain, *An Enzyme from Bacteria able to Destroy Penicillin.* Nature, 1940. **146**: p. 837.

6. Sabath, L.D., et al., *A New Type of Penicillin Resistance of Staphylococcus Aureus.* The Lancet, 1977. **309**(8009): p. 443-447.

7. Banno, H., et al., *Characterization of Multidrug-Resistant Group B Streptococci with Reduced Penicillin Susceptibility Forming Small Non-Beta-Hemolytic Colonies on Sheep Blood Agar Plates.* Journal of Clinical Microbiology, 2014. **52**(6): p. 2169-2171.

8. Willyard, C., *The Drug-resistant Bacteria that Pose the Greatest Health Threats.* Nature News, 2017. **543**(7643): p. 15.

9. Ganz, T. and R.I. Lehrer, *Antimicrobial Peptides of Vertebrates.* Current Opinion in Immunology, 1998. **10**(1): p. 41-44.

10. Brown, K.L. and R.E.W. Hancock, *Cationic Host Defense (Antimicrobial) Peptides.* Current Opinion in Immunology, 2006. **18**(1): p. 24-30.

11. Bulet, P., et al., *Antimicrobial Peptides in Insects; Structure and Function.* Developmental & Comparative Immunology, 1999. **23**(4–5): p. 329-344.

12. D'Herelle, F., *On an Invisible Microbe Antagonistic Toward Dysenteric Bacilli: Brief Note by Mr. F. D'Herelle, Presented by Mr. Roux. 1917.* Research in Microbiology, 1917. **158**(7): p. 553-4.

13. Chopra, I. and M. Roberts, *Tetracycline Antibiotics: Mode of Action, Applications, Molecular Biology, and Epidemiology of Bacterial Resistance.* Microbiology and Molecular Biology Reviews, 2001. **65**(2): p. 232-260.

14. Winstanley, T.G. and J.G.M. Hastings, *Penicillin-aminoglycoside Synergy and Post-antibiotic Effect for Enterococci.* Journal of Antimicrobial Chemotherapy, 1989. **23**(2): p. 189-199.

15. Whitford, D., *Proteins: Structure and Function*. 2013: John Wiley & Sons.

16. Powers, J.-P.S. and R.E.W. Hancock, *The Relationship Between Peptide Structure and Antibacterial Activity.* Peptides, 2003. **24**(11): p. 1681-1691.

17. Shai, Y., *Mechanism of the Binding, Insertion and Destabilization of Phospholipid Bilayer Membranes by α-helical Antimicrobial and Cell Non-selective Membrane-lytic Peptides.* Biochimica et Biophysica Acta (BBA) - Biomembranes, 1999. **1462**(1–2): p. 55-70.

18. Brogden, K.A., *Antimicrobial Peptides: Pore Formers or Metabolic Inhibitors in Bacteria?* Nature Reviews Microbiology, 2005. **3**(3): p. 238-250.

19. Reddy, K.V.R., R.D. Yedery, and C. Aranha, *Antimicrobial Peptides: Premises and Promises.* International Journal of Antimicrobial Agents, 2004. **24**(6): p. 536-547.

20. Zhang, S., et al., *Spontaneous Assembly of a Self-complementary Oligopeptide to Form a Stable Macroscopic Membrane.* Proceedings of the National Academy of Sciences, 1993. **90**(8): p. 3334-3338.

21. Gräfe, U., *CIBA Foundation Symposium 186: Antimicrobial Peptides. VIII + 283 S., 35 Abb., 22 Tab. Chichester-New York-Brisbane-Toronto-Singapore 1994. John Wiley & Sons. £ 47.50. ISBN: 0-471-95025-4.* Journal of Basic Microbiology, 1995. **35**(2): p. 72-72.

22. Montville, T. and Y. Chen, *Mechanistic Action of Pediocin and Nisin: Recent Progress and Unresolved Questions.* Applied Microbiology and Biotechnology, 1998. **50**(5): p. 511-519.

23. Bierbaum, G., et al., *Engineering of a Novel Thioether Bridge and Role of Modified Residues in the Lantibiotic Pep5.* Applied and Environmental Microbiology, 1996. **62**(2): p. 385-92.

24. Märki, F., et al., *Mode of Action of the Lanthionine-containing Peptide Antibiotics Duramycin, Duramycin B and C, and Cinnamycin as Indirect Inhibitors of Phospholipase A2.* Biochemical Pharmacology, 1991. **42**(10): p. 2027-2035.

25. Wiedemann, I., et al., *Specific Binding of Nisin to the Peptidoglycan Precursor Lipid II Combines Pore Formation and Inhibition of Cell Wall Biosynthesis for Potent Antibiotic Activity.* Journal of Biological Chemistry, 2001. **276**(3): p. 1772-1779.

26. Craik, D.J., et al., *Discovery, Structure and Biological Activities of the Cyclotides.* Current Protein and Peptide Science, 2004. **5**(5): p. 297-315.

27. Lindholm, P., et al., *Cyclotides: A Novel Type of Cytotoxic Agents* Molecular Cancer Therapeutics, 2002. **1**(6): p. 365-369.

28. Ireland, David C., Michelle L. Colgrave, and David J. Craik, *A Novel Suite of Cyclotides From Viola odorata: Sequence Variation and the Implications for Structure, Function and Stability.* Biochemical Journal, 2006. **400**(1): p. 1-12.

29. Willcox, M.D., et al., *A Novel Cationic-peptide Coating for the Prevention of Microbial Colonization on Contact Lenses.* Journal of Applied Microbiology, 2008. **105**(6): p. 1817-25.

30. Rasul, R., et al., *Interaction of the Antimicrobial Peptide Melimine With Bacterial Membranes.* International Journal of Antimicrobial Agents, 2010. **35**(6): p. 566-572.

31. Hancock, R.E., *Cationic Peptides: Effectors in Innate Immunity and Novel Antimicrobials.* The Lancet Infectious Diseases, 2001. **1**(3): p. 156-164.

32. de Planque, M.R., et al., *Interfacial Anchor Properties of Tryptophan Residues in Transmembrane Peptides Can Dominate Over Hydrophobic Matching Effects in Peptide−Lipid Interactions.* Biochemistry, 2003. **42**(18): p. 5341-5348.

33. Scott, M.G., H. Yan, and R.E. Hancock, *Biological Properties of Structurally Related α-helical Cationic Antimicrobial Peptides.* Infection and Immunity, 1999. **67**(4): p. 2005-2009.

34. Scott, M.G., M.R. Gold, and R.E. Hancock, *Interaction of cationic peptides with lipoteichoic acid and gram-positive bacteria.* Infection and immunity, 1999. **67**(12): p. 6445-6453.

35. Dutta, D., N. Kumar, and M. DP Willcox, *Antimicrobial Activity of Four Cationic Peptides Immobilised to Poly-hydroxyethylmethacrylate.* Biofouling, 2016. **32**(4): p. 429-438.

36. Chen, R., et al., *Synthesis, Characterization and In Vitro Activity of a Surface-attached Antimicrobial Cationic Peptide.* Biofouling, 2009. **25**(6): p. 517 - 524.

37. Dutta, D., J. Ozkan, and M.D.P. Willcox, *Biocompatibility of Antimicrobial Melimine Lenses: Rabbit and Human Studies.* Optometry & Vision Science, 2014. **91**(5): p. 570-581.

38. Dutta, D., et al., *Activity of a Melimine Derived Peptide Mel4 Against Stenotrophomonas, Delftia, Elizabethkingia, Burkholderia and Biocompatibility as a Contact Lens Coating.* Contact Lens and Anterior Eye, 2017. **40**(3): p. 175-183.

39. Chen, R., et al., *Characterization of Chemoselective Surface Attachment of the Cationic Peptide Melimine and Its Effects on Antimicrobial Activity.* Acta Biomater, 2012. **8**(12): p. 4371-9.

40. Berry, T., et al., *Lipid Membrane Interactions of the Cationic Antimicrobial Peptide Chimeras Melimine and Cys-Melimine.* Langmuir, 2018. **34**(38): p. 11586-11592.

41. Sohlenkamp, C. and O. Geiger, *Bacterial Membrane Lipids: Diversity in Structures and Pathways.* FEMS Microbiology Reviews, 2016. **40**(1): p. 133-159.

42. Russell, N.J. and N. Fukunaga, *A Comparison of Thermal Adaptation of Membrane Lipids in Psychrophilic and Thermophilic Bacteria.* FEMS Microbiology Reviews, 1990. **6**(2-3): p. 171-182.

43. Kates, M., *Influence of Salt Concentration on Membrane Lipids of Halophilic Bacteria.* FEMS Microbiology Reviews, 1986. **2**(1-2): p. 95-101.

44. de Rosa, M., et al., *A C25, C25 Diether Core Lipid from Archaebacterial Haloalkaliphiles.* Microbiology, 1983. **129**(8): p. 2333-2337.

45. Mykytczuk, N., et al., *Cytoplasmic Membrane Fluidity and Fatty Acid Composition of Acidithiobacillus Ferrooxidans in Response to pH Stress.* Extremophiles, 2010. **14**(5): p. 427-441.

46. Semeniuk, A., et al., *A Bifunctional Glycosyltransferase From Agrobacterium Tumefaciens Synthesizes Monoglucosyl and Glucuronosyl Diacylglycerol Under Phosphate Deprivation.* Journal of Biological Chemistry, 2014. **289**(14): p. 10104-10114.

47. Rahman, M.M., et al., *The Membrane Phospholipids of Neisseria Meningitidis and Neisseria Gonorrhoeae as Characterized by Fast Atom Bombardment Mass Spectrometry.* Microbiology, 2000. **146**(8): p. 1901-1911.

48. Kikuchi, S., I. Shibuya, and K. Matsumoto, *Viability of an Escherichia coli pgsANull Mutant Lacking Detectable Phosphatidylglycerol and Cardiolipin.* Journal of Bacteriology, 2000. **182**(2): p. 371-376.

49. Guerin, M.E., et al., *New Insights Into the Early Steps of Phosphatidylinositol Mannoside Biosynthesis in Mycobacteria PimB' Is an Essential Enzyme of Mycobacterium Smegmatis.* Journal of Biological Chemistry, 2009. **284**(38): p. 25687-25696.

50. Jackson, M., D.C. Crick, and P.J. Brennan, *Phosphatidylinositol is an Essential Phospholipid of Mycobacteria.* Journal of Biological Chemistry, 2000. **275**(39): p. 30092-30099.

51. Morii, H., et al., *Ubiquitous Distribution of Phosphatidylinositol Phosphate Synthase and Archaetidylinositol Phosphate Synthase in Bacteria and Archaea, Which Contain Inositol Phospholipid.* Biochemical and Biophysical Research Communications, 2014. **443**(1): p. 86-90.

52. Arondel, V., C. Benning, and C.R. Somerville, *Isolation and Functional Expression in Escherichia Coli of a Gene Encoding Phosphatidylethanolamine Methyltransferase (Ec 2.1. 1.17) From Rhodobacter Sphaeroides.* Journal of Biological Chemistry, 1993. **268**(21): p. 16002-16008.

53. Boumann, H.A., et al., *Ladderane Phospholipids in Anammox Bacteria Comprise Phosphocholine and Phosphoethanolamine Headgroups.* FEMS Microbiology Letters, 2006. **258**(2): p. 297-304.

54. Serricchio, M. and P. Bütikofer, *An Essential Bacterial-type Cardiolipin Synthase Mediates Cardiolipin Formation in a Eukaryote.* Proceedings of the National Academy of Sciences, 2012. **109**(16): p. E954-E961.

55. Zhou, P., et al., *Simultaneous Analysis of Cardiolipin and Lipid A From Helicobacter Pylori by Matrix-assisted Laser Desorption/ionization Time-of-flight Mass Spectrometry.* Molecular BioSystems, 2012. **8**(3): p. 720-725.

56. González-Silva, N.n., et al., *The Dioxygenase-encoding olsD Gene From Burkholderia Cenocepacia Causes the Hydroxylation of the Amide-linked Fatty Acyl Moiety of Ornithine-containing Membrane Lipids.* Biochemistry, 2011. **50**(29): p. 6396-6408.

57. Benning, C. and C. Somerville, *Identification of an Operon Involved in Sulfolipid Biosynthesis in Rhodobacter Sphaeroides.* Journal of Bacteriology, 1992. **174**(20): p. 6479-6487.

58. Güler, S., B. Essigmann, and C. Benning, *A Cyanobacterial Gene, sqdx, Required for Biosynthesis of the Sulfolipid Sulfoquinovosyldiacylglycerol.* Journal of Bacteriology, 2000. **182**(2): p. 543-545.

59. Vences-Guzmán, M.Á., et al., *Agrobacteria Lacking Ornithine Lipids Induce More Rapid Tumour Formation.* Environmental Microbiology, 2013. **15**(3): p. 895-906.

60. Jorasch, P., et al., *A UDP Glucosyltransferase From Bacillus Subtilis Successively Transfers Up to Four Glucose Residues to 1, 2-diacylglycerol: Expression of ypfP in Escherichia Coli and Structural Analysis of Its Reaction Products.* Molecular Microbiology, 1998. **29**(2): p. 419-430.

61. Benning, C., Z.-H. Huang, and D.A. Gage, *Accumulation of a Novel Glycolipid and a Betaine Lipid in Cells of Rhodobacter Sphaeroides Grown Under Phosphate Limitation.* Archives of Biochemistry and Biophysics, 1995. **317**(1): p. 103-111.

62. Martínez-Carmona, M., Y.K. Gun'ko, and M. Vallet-Regí, *Mesoporous Silica Materials as Drug Delivery: "The Nightmare" of Bacterial Infection.* Pharmaceutics, 2018. **10**(4): p. 279.

63. Ehrenstein, G. and H. Lecar, *Electrically Gated Ionic Channels in Lipid Bilayers.* Quarterly Reviews of Biophysics, 1977. **10**(1): p. 1-34.

64. Yang, L., et al., *Barrel-stave Model or Toroidal Model? A Case Study on Melittin Pores.* Biophysical Journal, 2001. **81**(3): p. 1475-1485.

65. Sato, H. and J.B. Feix, *Peptide–membrane Interactions and Mechanisms of Membrane Destruction by Amphipathic α-helical Antimicrobial Peptides.* Biochimica et Biophysica Acta (BBA) - Biomembranes, 2006. **1758**(9): p. 1245-1256.

66. López-Meza, J., et al., *Antimicrobial Peptides: Diversity and Perspectives for Their Biomedical Application*. 2011.

67. Alghalayini, A., et al., *The Use of Tethered Bilayer Lipid Membranes to Identify the Mechanisms of Antimicrobial Peptide Interactions with Lipid Bilayers.* Antibiotics, 2019. **8**(1): p. 12.

68. Pouny, Y., et al., *Interaction of Antimicrobial Dermaseptin and Its Fluorescently Labeled Analogs With Phospholipid Membranes.* Biochemistry, 1992. **31**(49): p. 12416-12423.

69. Matsuzaki, K., et al., *An Antimicrobial Peptide, Magainin 2, Induced Rapid Flip-Flop of Phospholipids Coupled with Pore Formation and Peptide Translocation.* Biochemistry, 1996. **35**(35): p. 11361-11368.

70. Hallock, K.J., D.-K. Lee, and A. Ramamoorthy, *MSI-78, an Analogue of the Magainin Antimicrobial Peptides, Disrupts Lipid Bilayer Structure via Positive Curvature Strain.* Biophysical Journal, 2003. **84**(5): p. 3052-3060.

71. Sokolov, Y., et al., *Membrane Channel Formation by Antimicrobial Protegrins.* Biochimica et Biophysica Acta (BBA)-Biomembranes, 1999. **1420**(1-2): p. 23-29.

72. Wiedman, G., et al., *The Electrical Response of Bilayers to the Bee Venom Toxin Melittin: Evidence for Transient Bilayer Permeabilization.* Biochimica et Biophysica Acta (BBA)-Biomembranes, 2013. **1828**(5): p. 1357-1364.

73. Cranfield, C.G., et al., *Evidence of the Key Role of H3O+ in Phospholipid Membrane Morphology.* Langmuir, 2016. **32**(41): p. 10725-10734.

74. Cranfield, C.G., et al., *Kalata B1 and Kalata B2 Have a Surfactant-Like Activity in Phosphatidylethanolomine Containing Lipid Membranes.* Langmuir, 2017. **33**(26): p. 6630-6637.

75. Yu, T.T., et al., *Design, Synthesis and Biological Evaluation of N-Sulfonylphenyl glyoxamide-Based Antimicrobial Peptide Mimics as Novel Antimicrobial Agents.* ChemistrySelect, 2017. **2**(12): p. 3452-3461.

76. Giacometti, A., et al., *In Vitro Activities of Membrane-active Peptides Against Gram-positive and Gram-negative Aerobic Bacteria.* Antimicrobial Agents and Chemotherapy, 1998. **42**(12): p. 3320-3324.

77. Oren, Z., J. Hong, and Y. Shai, *A Comparative Study on the Structure and Function of a Cytolytic α-helical Peptide and Its Antimicrobial β-sheet Diastereomer.* European Journal of Biochemistry, 1999. **259**(1-2): p. 360-369.

78. Mendez, E., et al., *Primary Structure and Inhibition of Protein Synthesis in Eukaryotic Cell-free System of a Novel Thionin, γ-hordothionin, From Barley Endosperm.* European Journal of Biochemistry, 1990. **194**(2): p. 533-539.

79. Bart, P.H.J.T., P.A.C. Bruno, and T. Karin, *Mode of Action of Plant Defensins Suggests Therapeutic Potential.* Current Drug Targets - Infectious Disorders, 2003. **3**(1): p. 1-8.

80. Israelachvili, J.N., S. Marčelja, and R.G. Horn, *Physical Principles of Membrane Organization.* Quarterly Reviews of Biophysics, 1980. **13**(02): p. 121-200.

81. Heather, E.F. and J.B. Paula, *The Biological Significance of Lipid–protein Interactions.* Journal of Physics: Condensed Matter, 2006. **18**(28): p. S1281.

82. Cornell, B.A., et al., *A Biosensor That Uses Ion-channel Switches.* Nature, 1997. **387**(6633): p. 580.

83. Neher, E. and B. Sakmann, *The Patch Clamp Technique.* Scientific American, 1992. **266**(3): p. 44-51.

84. Ries, R.S., et al., *Black Lipid Membranes: Visualizing the Structure, Dynamics, and Substrate Dependence of Membranes.* The Journal of Physical Chemistry B, 2004. **108**(41): p. 16040-16049.

85. Blodgett, K.B., *Monomolecular Films of Fatty Acids on Glass.* Journal of the American Chemical Society, 1934. **56**(2): p. 495-495.

86. Langmuir, I., *Mechanical Properties of Monomolecular Films.* Journal of the Franklin Institute, 1934. **218**(2): p. 143-171.

87. Zasadzinski, J., et al., *Langmuir-Blodgett Films.* Science, 1994. **263**(5154): p. 1726-1733.

88. Lasic, D. and D. Papahadjopoulos, *Liposomes Revisited.* Science, 1995. **267**(5202): p. 1275-1276.

89. Sharma, A. and U.S. Sharma, *Liposomes in Drug Delivery: Progress and Limitations.* International Journal of Pharmaceutics, 1997. **154**(2): p. 123-140.

90. Pinchuk, I., et al., *Evaluation of Antioxidants: Scope, Limitations and Relevance of Assays.* Chemistry and physics of lipids, 2012. **165**(6): p. 638-647.

91. Hamill OP, S.B., *A Cell-free Method for Recording Single Channel Currents From Biological Membranes.* The Journal of Physiology, 1981. **312**: p. 41-42.

92. Hamill, O.P., et al., *Improved Patch-clamp Techniques for High-resolution Current Recording From Cells and Cell-free Membrane Patches.* Pflugers Archiv, 1981. **391**(2): p. 85-100.

93. Fischmeister, R., R. Ayer, Jr., and R. DeHaan, *Some Limitations of the Cell-attached Patch Clamp Technique: a Two-electrode Analysis.* Pflügers Archiv, 1986. **406**(1): p. 73-82.

94. Aguila, F., *Patch-clamp*, patch2.jpg, Editor. 2000: https://www.ipmc.cnrs.fr/~duprat/neurophysiology/patch.htm.

95. MDougM, *Black Lipid Membrane*, B.l. membrane.svg, Editor. 2009: Wikimedia Commons.

96. Tamm, L.K. and H.M. McConnell, *Supported Phospholipid Bilayers.* Biophysical Journal, 1985. **47**(1): p. 105-113.

97. Ndeye Rokhaya, F., et al., *Phase Behavior and Structure Properties of Supported Lipid Monolayers and Bilayers in Interaction with Silica Nanoparticles*. 2013.

98. Lang, H., C. Duschl, and H. Vogel, *A New Class of Thiolipids for the Attachment of Lipid Bilayers on Gold Surfaces.* Langmuir, 1994. **10**(1): p. 197-210.

99. Vockenroth, I., et al., *Stable Insulating Tethered Bilayer Lipid Membranes.* Biointerphases, 2008. **3**(2): p. FA68-FA73.

100. Vockenroth, I.K., et al., *Formation of Tethered Bilayer Lipid Membranes Probed by Various Surface Sensitive Techniques.* Biointerphases, 2009. **4**(2): p. 19-26.

101. Cranfield, C., et al., *The Assembly and Use of Tethered Bilayer Lipid Membranes (tBLMs)*, in *Methods in Membrane Lipids*. 2015, Springer. p. 45-53.

102. Knoll, W., et al., *Functional Tethered Lipid Bilayers.* Reviews in Molecular Biotechnology, 2000. **74**(3): p. 137-158.

103. Dietrich, C., L. Schmitt, and R. Tampé, *Molecular Organization of Histidine-tagged Biomolecules at Self-assembled Lipid Interfaces Using a Novel Class of Chelator Lipids.* Proceedings of the National Academy of Sciences, 1995. **92**(20): p. 9014-9018.

104. Heyse, S., et al., *Covalent Attachment of Functionalized Lipid Bilayers to Planar Waveguides for Measuring Protein Binding to Biomimetic Membranes.* Protein Science, 1995. **4**(12): p. 2532-2544.

105. Beyer, D., et al., *Influence of Anchor Lipids on the Homogeneity and Mobility of Lipid Bilayers on Thin Polymer Films.* Angewandte Chemie International Edition in English, 1996. **35**(15): p. 1682-1685.

106. Prashar, J., et al., *Making Lipid Membranes Even Tougher.* Journal of Materials Research, 2007. **22**(8): p. 2189-2194.

107. Deng, Y., et al., *Fluidic and Air-Stable Supported Lipid Bilayer and Cell-Mimicking Microarrays.* Journal of the American Chemical Society, 2008. **130**(19): p. 6267-6271.

108. Vockenroth, I.K., et al., *Tethered Bilayer Lipid Membranes With Giga-ohm Resistances.* Electrochemistry Communications, 2008. **10**(2): p. 323-328.

109. Wang, X., et al., *A Facile Approach for Assembling Lipid Bilayer Membranes on Template-stripped Gold.* Langmuir, 2010. **26**(23): p. 18239-18245.

110. Rossi, C. and J. Chopineau, *Biomimetic Tethered Lipid Membranes Designed for Membrane-protein Interaction Studies.* European Biophysics Journal, 2007. **36**(8): p. 955-965.

111. Naumann, R., et al., *The Peptide-tethered Lipid Membrane as a Biomimetic System to Incorporate Cytochrome C Oxidase in a Functionally Active Form.* Biosensors and Bioelectronics, 1999. **14**(7): p. 651-662.

112. Richter, R.P., J.L.K. Him, and A. Brisson, *Supported Lipid Membranes.* Materials Today, 2003. **6**(11): p. 32-37.

113. Giess, F., et al., *The Protein-Tethered Lipid Bilayer: A Novel Mimic of the Biological Membrane.* Biophysical Journal, 2004. **87**(5): p. 3213-3220.

114. Marquês, J.T., R.F.M. de Almeida, and A.S. Viana, *Lipid Bilayers Supported on Bare and Modified Gold – Formation, Characterization and Relevance of Lipid Rafts.* Electrochimica Acta, 2014. **126**: p. 139-150.

115. Rebaud, S., O. Maniti, and A.P. Girard-Egrot, *Tethered Bilayer Lipid Membranes (tBLMs): Interest and Applications for Biological Membrane Investigations.* Biochimie, 2014. **107, Part A**: p. 135-142.

116. Hartman, K.L., et al., *Supported Lipid Bilayers as Dynamic Platforms for Tethered Particles.* Nanoscale, 2015. **7**(1): p. 66-76.

117. Janshoff, A. and C. Steinem, *Mechanics of Lipid Bilayers: What Do We Learn From Pore-spanning Membranes?* Biochimica et Biophysica Acta (BBA) - Molecular Cell Research, 2015. **1853**(11, Part B): p. 2977-2983.

118. Tun, T.N. and A.T.A. Jenkins, *An Electrochemical Impedance Study of the Effect of Pathogenic Bacterial Toxins on Tethered Bilayer Lipid Membrane.* Electrochemistry Communications, 2010. **12**(10): p. 1411-1415.

119. Junghans, A. and I. Köper, *Structural Analysis of Tethered Bilayer Lipid Membranes.* Langmuir, 2010. **26**(13): p. 11035-11040.

120. Andersson, J., et al., *Synthesis and Characterization of Novel Anchorlipids for Tethered Bilayer Lipid Membranes.* Langmuir, 2017. **33**(18): p. 4444-4451.

121. Kinsky, S.C. and R.A. Nicolotti, *Immunological Properties of Model Membranes.* Annual Review of Biochemistry, 1977. **46**(1): p. 49-67.

122. Littman, D.R., S.E. Cullen, and B.D. Schwartz, *Insertion of Ia and H-2 Alloantigens into Model Membranes.* Proceedings of the National Academy of Sciences, 1979. **76**(2): p. 902-906.

123. Seelig, J. and A. Seelig, *Lipid Conformation in Model Membranes and Biological Membranes.* Quarterly Reviews of Biophysics, 1980. **13**(1): p. 19-61.

124. Traeubl, H. and E. Sackmann, *Crystalline-liquid Crystaline Phase Transition of Lipid Model Membranes. III. Structure of a Steroid-lecithin System Below and Above the Lipid-phase Transition.* Journal of the American Chemical Society, 1972. **94**(13): p. 4499-4510.

125. Budvytyte, R., et al., *Structure and Properties of Tethered Bilayer Lipid Membranes With Unsaturated Anchor Molecules.* Langmuir, 2013. **29**(27): p. 8645-8656.

126. Hoiles, W., et al., *An Engineered Membrane to Measure Electroporation: Effect of Tethers and Bioelectronic Interface.* Biophysical Journal, 2014. **107**(6): p. 1339-1351.

127. Krishna, G., et al., *Tethered Bilayer Membranes Containing Ionic Reservoirs: the Interfacial Capacitance.* Langmuir, 2001. **17**(16): p. 4858-4866.

128. Andersson, J., et al., *A Tethered Bilayer Lipid Membrane That Mimics Microbial Membranes.* Physical Chemistry Chemical Physics, 2018. **20**(18): p. 12958-12969.

129. Nation, R.L. and J. Li, *Colistin in the 21st Century.* Current Opinion in Infectious Diseases, 2009. **22**(6): p. 535.

130. Ltd, S.T.M.P. *SDx Tethered Membranes*. 2019 [cited 2019.

131. Maupetit, J., P. Derreumaux, and P. Tuffery, *A Fast Method for Large-scale De Novo Peptide and Miniprotein Structure Prediction.* Journal of Computational Chemistry, 2010. **31**(4): p. 726-38.

132. Maupetit, J., P. Derreumaux, and P. Tuffery, *PEP-FOLD: An Online Resource for De Novo Peptide Structure Prediction.* Nucleic Acids Research, 2009. **37**(Web Server issue): p. W498-503.

133. Tuffery, P. and P. Derreumaux, *Dependency Between Consecutive Local Conformations Helps Assemble Protein Structures From Secondary Structures using Go Potential and Greedy Algorithm.* Proteins: Structure, Function, and Bioinformatics, 2005. **61**(4): p. 732-740.

134. Tuffery, P., F. Guyon, and P. Derreumaux, *Improved Greedy Algorithm for Protein Structure Reconstruction.* Journal of Computational Chemistry, 2005. **26**(5): p. 506-513.

135. Cranfield, C.G., et al., *Transient Potential Gradients and Impedance Measures of Tethered Bilayer Lipid Membranes: Pore-forming Peptide Insertion and the Effect of Electroporation.* Biophysical Journal, 2014. **106**: p. 182-189.

136. Cranfield, C.G., T. Bettler, and B. Cornell, *Nanoscale Ion Sequestration to Determine the Polarity Selectivity of Ion Conductance in Carriers and Channels.* Langmuir, 2014. **31**(1): p. 292-298.

137. Vockenroth, I.K., et al., *Functional Incorporation of the Pore Forming Segment of AChR M2 Into Tethered Bilayer Lipid Membranes.* Biochimica et Biophysica Acta (BBA) - Biomembranes, 2007. **1768**(5): p. 1114-1120.

138. Macdonald, J.R., *Impedance Spectroscopy.* Annals of Biomedical Engineering, 1992. **20**(3): p. 289-305.

139. Raguse, B., et al., *Tethered Lipid Bilayer Membranes: Formation and Ionic Reservoir Characterization.* Langmuir, 1998. **14**(3): p. 648-659.

140. Cranfield, C.G., T. Bettler, and B. Cornell, *Nanoscale Ion Sequestration to Determine the Polarity Selectivity of Ion Conductance in Carriers and Channels.* Langmuir, 2015. **31**(1): p. 292-298.

141. Carnie, S., J.N. Israelachvili, and B.A. Pailthorpe, *Lipid Packing and Transbilayer Asymmetries of Mixed Lipid Vesicles.* Biochimica et Biophysica Acta (BBA) - Biomembranes, 1979. **554**(2): p. 340-357.

142. Domingues, M.M., et al., *What Can Light Scattering Spectroscopy Do for Membrane-active Peptide Studies?* Journal of Peptide Science: an Official Publication of the European Peptide Society, 2008. **14**(4): p. 394-400.

143. Parente, R., S. Nir, and F. Szoka, *pH-dependent Fusion of Phosphatidylcholine Small Vesicles. Induction by a Synthetic Amphipathic Peptide.* Journal of Biological Chemistry, 1988. **263**(10): p. 4724-4730.

144. Trivedi, V., et al., *Fusion Induced Aggregation of Model Vesicles Studied by Dynamic and Static Light Scattering.* Chemistry and Physics of Lipids, 2000. **107**(1): p. 99-106.

145. Caffrey, M. and J. Hogan, *LIPIDAT: A Database of Lipid Phase Transition Temperatures and Enthalpy Changes. DMPC Data Subset Analysis.* Chemistry and Physics of Lipids, 1992. **61**(1): p. 1-109.

146. Garcia, A., et al., *Polar Interactions Play an Important Role in the Energetics of the Main Phase Transition of Phosphatidylcholine Membranes.* ACS Omega, 2019. **4**(1): p. 518-527.

147. James, M., et al., *The Multipurpose Time-of-flight Neutron Reflectometer "Platypus" at Australia's OPAL Reactor.* Nuclear Instruments and Methods in Physics Research Section A: Accelerators, Spectrometers, Detectors and Associated Equipment, 2011. **632**(1): p. 112-123.

148. Jacrot, B. and G. Zaccai, *Determination of Molecular Weight by Neutron Scattering.* Biopolymers: Original Research on Biomolecules, 1981. **20**(11): p. 2413-2426.

149. Le Brun, A.P., et al., *Monitoring the Assembly of Antibody-binding Membrane Protein Arrays Using Polarised Neutron Reflection.* European Biophysics Journal, 2008. **37**(5): p. 639-645.

150. Holt, S.A., et al., *An Ion-channel-containing Model Membrane: Structural Determination by Magnetic Contrast Neutron Reflectometry.* Soft Matter, 2009. **5**(13): p. 2576-2586.

151. Wacklin, H.P., *Neutron Reflection From Supported Lipid Membranes.* Current Opinion in Colloid & Interface Science, 2010. **15**(6): p. 445-454.

152. Abelès, F., *La Théorie Générale des Couches /minces.* Journal de Physique et le Radium, 1950. **11**(7): p. 307-309.

153. Laidler, K.J., *The Development of the Arrhenius Equation.* Journal of Chemical Education, 1984. **61**(6): p. 494.

154. Laidler, K.J., *Unconventional Applications of the Arrhenius law.* Journal of Chemical Education, 1972. **49**(5): p. 343.

155. Valincius, G., et al., *Soluble Amyloid β-oligomers Affect Dielectric Membrane Properties by Bilayer Insertion and Domain Formation: Implications for Cell Toxicity.* Biophysical journal, 2008. **95**(10): p. 4845-4861.

156. Garcia, A., et al., *Cholesterol Depletion Inhibits Na+, K+-ATPase Activity in a Near-native Membrane Environment.* Journal of Biological Chemistry, 2019. **294**(15): p. 5956-5969.

157. Clarke, R.J. and D.J. Kane, *Optical Detection of Membrane Dipole Potential: Avoidance of Fluidity and Dye-induced Effects.* Biochimica et Biophysica Acta (BBA)-Biomembranes, 1997. **1323**(2): p. 223-239.

158. Berkovich, A.K., E.P. Lukashev, and N.S. Melik-Nubarov, *Dipole Potential as a Driving Force for the Membrane Insertion of Polyacrylic Acid in Slightly Acidic Milieu.* Biochimica et Biophysica Acta (BBA)-Biomembranes, 2012. **1818**(3): p. 375-383.

159. Shen, Y., et al., *Improved PEP-FOLD Approach for Peptide and Miniprotein Structure Prediction.* Journal of Chemical Theory and Computation, 2014. **10**(10): p. 4745-4758.

160. Thevenet, P., et al., *PEP-FOLD: An Updated De Novo Structure Prediction Server for Both Linear and Disulfide Bonded Cyclic Peptides.* Nucleic Acids Research, 2012. **40**(Web Server issue): p. W288-93.

161. Alland, C., et al., *RPBS: A Web Resource for Structural Bioinformatics.* Nucleic Acids Research, 2005. **33**(suppl_2): p. W44-W49.

162. Néron, B., et al., *Mobyle: A New Full Web Bioinformatics Framework.* Bioinformatics, 2009. **25**(22): p. 3005-3011.

163. Camproux, A.-C., R. Gautier, and P. Tuffery, *A Hidden Markov Model Derived Structural Alphabet for Proteins.* Journal of Molecular Biology, 2004. **339**(3): p. 591-605.

164. Camproux, A. and P. Tuffery, *Hidden Markov Model-derived Structural Alphabet for Proteins: the Learning of Protein Local Shapes Captures Sequence Specificity.* Biochimica et Biophysica Acta (BBA)-General Subjects, 2005. **1724**(3): p. 394-403.

165. Maupetit, J., P. Tuffery, and P. Derreumaux, *A Coarse-grained Protein Force Field for Folding and Structure Prediction.* Proteins: Structure, Function, and Bioinformatics, 2007. **69**(2): p. 394-408.

166. *Peptide Property Calculator*. 1/5/2018]; Available from: http://www.innovagen.com/proteomics-tools

167. Hopp, T.P. and K.R. Woods, *Prediction of Protein Antigenic Determinants From Amino Acid Sequences.* Proceedings of the National Academy of Sciences, 1981. **78**(6): p. 3824-3828.

168. Garcia, A., et al., *The Voltage-sensitive Dye RH421 Detects a Na+, K+-ATPase Conformational Change at the Membrane Surface.* Biochimica et Biophysica Acta (BBA)-Biomembranes, 2017. **1859**(5): p. 813-823.

169. Vagt, T., et al., *Membrane Binding and Structure of De Novo Designed α-Helical Cationic Coiled-Coil-Forming Peptides.* ChemPhysChem, 2006. **7**(6): p. 1361-1371.

170. Tasis, D., et al., *Diameter-selective Solubilization of Carbon Nanotubes by Lipid Micelles.* Journal of Nanoscience and Nanotechnology, 2008. **8**(1): p. 420-423.

171. Stangl, M., et al., *Detergent Properties Influence the Stability of the Glycophorin A Transmembrane Helix Dimer in Lysophosphatidylcholine Micelles.* Biophysical Journal, 2012. **103**(12): p. 2455-2464.

172. Da Costa, T. and M. Ito, *PHOSPHOLIPIDS| Physiology.* 2003.

173. Loder, T. and P. Liss, *Control by Organic Coatings of the Surface Charge of Estuarine Suspended Particles 1.* Limnology and Oceanography, 1985. **30**(2): p. 418-421.

174. Van Loosdrecht, M., et al., *The Role of Bacterial Cell Wall Hydrophobicity in Adhesion.* Applied and Environmental Microbiology, 1987. **53**(8): p. 1893-1897.

175. Jucker, B.A., H. Harms, and A. Zehnder, *Adhesion of the Positively Charged Bacterium Stenotrophomonas (Xanthomonas) Maltophilia 70401 to Glass and Teflon.* Journal of Bacteriology, 1996. **178**(18): p. 5472-5479.

176. Raetz, C. and W. Dowhan, *Biosynthesis and Function of Phospholipids in Escherichia Coli.* Journal of Biological Chemistry, 1990. **265**(3): p. 1235-1238.

177. Raetz, C.R., et al., *Lipid a Modification Systems in Gram-negative Bacteria.* Annual Review of Biochemistry, 2007. **76**: p. 295-329.

178. Deplazes, E., et al., *The Effect of H3O+ on the Membrane Morphology and Hydrogen Bonding of a Phospholipid Bilayer.* Biophysical Reviews, 2018. **10**(5): p. 1371-1376.

179. Vodyanoy, I. and J.E. Hall, *Thickness Dependence of Monoglyceride Bilayer Membrane Conductance.* Biophysical Journal, 1984. **46**(2): p. 187-193.

180. Janas, T. and H.T. Tien, *Influence of Dolichyl Phosphate on Permeability and Stability of Bilayer Lipid Membranes.* Biochimica et Biophysica Acta (BBA)-Biomembranes, 1988. **939**(3): p. 624-628.

181. Janas, T., T. Chojnacki, and E. Swiezewska, *The Effect of Undecaprenol on Bilayer Lipid Membranes.* Acta Biochimica Polonica, 1994. **41**(3): p. 351-358.

182. Ginsburg, S. and D. Noble, *The Activation Enthalpies for Ion Conductance Systems in Lipid Bilayer Membranes.* The Journal of Membrane Biology, 1974. **18**(1): p. 163-176.

183. Belmonte, G., et al., *Pore Formation by Staphylococcus Aureus Alpha-toxin in Lipid Bilayers.* European Biophysics Journal, 1987. **14**(6): p. 349-358.

184. Liu, B., K. Hui, and F. Qin, *Thermodynamics of Heat Activation of Single Capsaicin Ion Channels VR1.* Biophysical Journal, 2003. **85**(5): p. 2988-3006.

185. King, G.I. and S.H. White, *Determining Bilayer Hydrocarbon Thickness from Neutron Diffraction Measurements using Strip-function Models.* Biophysical Journal, 1986. **49**(5): p. 1047-1054.

186. McElhaney, R.N., *The Use of Differential Scanning Calorimetry and Differential Thermal Analysis in Studies of Model and Biological Membranes.* Chemistry and Physics of Lipids, 1982. **30**(2-3): p. 229-259.

187. Yashar, V.B., et al., *Interaction of Trans-parinaric Acid With Phosphatidylcholine Bilayers: Comparison With the Effect of Other Fluorophores.* Biochimica et Biophysica Acta (BBA)-Biomembranes, 1987. **904**(1): p. 117-124.

188. Biltonen, R.L. and D. Lichtenberg, *The Use of Differential Scanning Calorimetry as a Tool to Characterize Liposome Preparations.* Chemistry and Physics of Lipids, 1993. **64**(1-3): p. 129-142.

189. Chiu, M.H. and E.J. Prenner, *Differential Scanning Calorimetry: an Invaluable Tool for a Detailed Thermodynamic Characterization of Macromolecules and Their Interactions.* Journal of Pharmacy and Bioallied Sciences, 2011. **3**(1): p. 39.

190. Oren, Z. and Y. Shai, *A Class of Highly Potent Antibacterial Peptides Derived from Pardaxin, A Pore-Forming Peptide Isolated from Moses Sole Fish Pardachirus marmoratus.* European Journal of Biochemistry, 1996. **237**(1): p. 303-310.

191. Wang, G., J.T. Sparrow, and R.J. Cushley, *The Helix-hinge-helix Structural Motif in Human Apolipoprotein AI Determined by NMR Spectroscopy.* Biochemistry, 1997. **36**(44): p. 13657-13666.

192. van Kan, E.J., et al., *Membrane Activity of the Peptide Antibiotic Clavanin and the Importance of Its Glycine Residues.* Biochemistry, 2001. **40**(21): p. 6398-6405.

193. Pukala, T.L., et al., *Investigating the Importance of the Flexible Hinge in Caerin 1.1: Solution Structures and Activity of Two Synthetically Modified Caerin Peptides.* Biochemistry, 2004. **43**(4): p. 937-944.

194. Galanth, C., et al., *Mechanism of Antibacterial Action of Dermaseptin B2: Interplay Between Helix−hinge−helix Structure and Membrane Curvature Strain.* Biochemistry, 2008. **48**(2): p. 313-327.

195. Hsu, C.-H., et al., *Structural Characterizations of Fusion Peptide Analogs of Influenza Virus Hemagglutinin Implication of the Necessity of a Helix-hinge-helix Motif in Fusion Activity.* Journal of Biological Chemistry, 2002. **277**(25): p. 22725-22733.

196. Lee, J.K., et al., *A Proline-hinge Alters the Characteristics of the Amphipathic α-helical AMPs.* PLoS One, 2013. **8**(7): p. e67597.

197. Park, C.B., et al., *Structure–activity Analysis of Buforin II, a Histone H2A-derived Antimicrobial Peptide: the Proline Hinge Is Responsible for the Cell-penetrating Ability of Buforin II.* Proceedings of the National Academy of Sciences, 2000. **97**(15): p. 8245-8250.

198. Martin, I., et al., *Correlation Between Fusogenicity of Synthetic Modified Peptides Corresponding to the NH2-terminal Extremity of Simian Immunodeficiency Virus gp32 and Their Mode of Insertion Into the Lipid Bilayer: an Infrared Spectroscopy Study.* Journal of Virology, 1994. **68**(2): p. 1139-1148.

199. Lear, J.D. and W.F. DeGrado, *Membrane Binding and Conformational Properties of Peptides Representing the NH2 Terminus of Influenza HA-2.* Journal of Biological Chemistry, 1987. **262**(14): p. 6500-6505.

200. Wharton, S., et al., *Membrane Fusion by Peptide Analogues of Influenza Virus Haemagglutinin.* Journal of General Virology, 1988. **69**(8): p. 1847-1857.

201. Cladera, J., et al., *Characterization of the Sequence of Interactions of the Fusion Domain of the Simian Immunodeficiency Virus With Membranes Role of the Membrane Dipole Potential.* Journal of Biological Chemistry, 1999. **274**(42): p. 29951-29959.

202. Epand, R.M. and R.F. Epand, *Relationship Between the Infectivity of Influenza Virus and the Ability of Its Fusion Peptide to Perturb Bilayers.* Biochemical and Biophysical Research Communications, 1994. **202**(3): p. 1420-1425.

203. Durell, S.R., et al., *What Studies of Fusion Peptides Tell Us About Viral Envelope Glycoprotein-mediated Membrane Fusion.* Molecular Membrane Biology, 1997. **14**(3): p. 97-112.

204. Epand, R.F., et al., *Membrane Orientation of the SIV Fusion Peptide Determines Its Effect on Bilayer Stability and Ability to Promote Membrane Fusion.* Biochemical and Biophysical Research Communications, 1994. **205**(3): p. 1938-1943.

205. Zutphen, H.v. and L. Van Deenen, *The Effect of Lysolecithin on the Electrical Resistance of Lecithin Bilayer Membranes.* Chemistry and Physics of Lipids, 1967. **1**(4): p. 389-391.

206. Lee, Y. and S.I. Chan, *Effect of Lysolecithin on the Structure and Permeability of Lecithin Bilayer Vesicles.* Biochemistry, 1977. **16**(7): p. 1303-1309.

207. Stowasser, C., *The Dipole Potential of Lipid Membranes—an Overview*. 2008, Citeseer.

208. Clarke, R.J., *The Dipole Potential of Phospholipid Membranes and Methods for Its Detection.* Advances in Colloid and Interface Science, 2001. **89**: p. 263-281.

209. Büldt, G., et al., *Neutron Diffraction Studies on Selectively Deuterated Phospholipid Bilayers.* Nature, 1978. **271**(5641): p. 182-184.

210. Zhan, H. and T. Lazaridis, *Influence of the Membrane Dipole Potential on Peptide Binding to Lipid Bilayers.* Biophysical Chemistry, 2012. **161**: p. 1-7.

211. Schmidt, C.L., P.L. Kirk, and W. Appleman, *The Apparent Dissociation Constants of Arginine and of Lysine and the Apparent Heats of Ionization of Certain Amino Acids.* Journal of Biological Chemistry, 1930. **88**(1): p. 285-293.

212. Thibado, J.K., et al., *Influence of High pH and Cholesterol on Single Arginine-containing Transmembrane Peptide Helices.* Biochemistry, 2016. **55**(45): p. 6337-6343.

213. Henzler-Wildman, K.A., et al., *Perturbation of the Hydrophobic Core of Lipid Bilayers by the Human Antimicrobial Peptide LL-37.* Biochemistry, 2004. **43**(26): p. 8459-8469.

214. Jain, M.K. and N.M. Wu, *Effect of Small Molecules on the Dipalmitoyl Lecithin Liposomal Bilayer: III. Phase Transition in Lipid Bilayer.* The Journal of Membrane Biology, 1977. **34**(1): p. 157-201.

215. Abrunhosa, F., et al., *Interaction and Lipid-induced Conformation of Two Cecropin− Melittin Hybrid Peptides Depend on Peptide and Membrane Composition.* The Journal of Physical Chemistry B, 2005. **109**(36): p. 17311-17319.

216. Alves, I.D., et al., *The Interaction of Cell-penetrating Peptides With Lipid Model Systems and Subsequent Lipid Reorganization: Thermodynamic and Structural Characterization.* Journal of Peptide Science: an Official Publication of the European Peptide Society, 2009. **15**(3): p. 200-209.

217. Sevcsik, E., et al., *How Lipids Influence the Mode of Action of Membrane-active Peptides.* Biochimica et Biophysica Acta (BBA)-Biomembranes, 2007. **1768**(10): p. 2586-2595.

218. Mollay, C., *Effect of Melittin and Melittin Fragments on the Thermotropic Phase Transition of Dipalmitoyllecithin and on the Amount of Lipid-bound Water.* FEBS Letters, 1976. **64**(1): p. 65-68.

219. Abbassi, F., et al., *Solution Structure and Model Membrane Interactions of Temporins-SH, Antimicrobial Peptides From Amphibian Skin. A NMR Spectroscopy and Differential Scanning Calorimetry Study.* Biochemistry, 2008. **47**(40): p. 10513-10525.

220. Prenner, E.J., et al., *Differential Scanning Calorimetric Study of the Effect of the Antimicrobial Peptide Gramicidin S on the Thermotropic Phase Behavior of Phosphatidylcholine, Phosphatidylethanolamine and Phosphatidylglycerol Lipid Bilayer Membranes.* Biochimica et Biophysica Acta (BBA)-Biomembranes, 1999. **1417**(2): p. 211-223.

221. Hunter, H.N., et al., *The Interactions of Antimicrobial Peptides Derived From Lysozyme With Model Membrane Systems.* Biochimica et Biophysica Acta (BBA)-Biomembranes, 2005. **1668**(2): p. 175-189.

222. Lentz, B., E. Freire, and R. Biltonen, *Fluorescence and Calorimetric Studies of Phase Transitions in Phosphatidylcholine Multilayers: Kinetics of the Pretransition.* Biochemistry, 1978. **17**(21): p. 4475-4480.

223. Schweizer, F., *Cationic Amphiphilic Peptides with Cancer-selective Toxicity.* European Journal of Pharmacology, 2009. **625**(1-3): p. 190-194.

224. Ganz, T., *Fatal Attraction Evaded: How Pathogenic Bacteria Resist Cationic Polypeptides.* Journal of Experimental Medicine, 2001. **193**(9): p. F31-F34.

225. LaRock, C.N. and V. Nizet, *Cationic Antimicrobial Peptide Resistance Mechanisms of Streptococcal Pathogens.* Biochimica et Biophysica Acta (BBA)-Biomembranes, 2015. **1848**(11): p. 3047-3054.

226. Hale, J.D. and R.E. Hancock, *Alternative Mechanisms of Action of Cationic Antimicrobial Peptides on Bacteria.* Expert Review of Anti-infective Therapy, 2007. **5**(6): p. 951-959.

227. Glukhov, E., et al., *Basis for Selectivity of Cationic Antimicrobial Peptides for Bacterial Versus Mammalian Membranes.* Journal of Biological Chemistry, 2005. **280**(40): p. 33960-33967.

228. Kichler, A., A.J. Mason, and B. Bechinger, *Cationic Amphipathic Histidine-rich Peptides for Gene Delivery.* Biochimica et Biophysica Acta (BBA)-Biomembranes, 2006. **1758**(3): p. 301-307.

229. Sand, S.L., et al., *Plantaricin A, a Cationic Peptide Produced by Lactobacillus Plantarum, Permeabilizes Eukaryotic Cell Membranes by a Mechanism Dependent on Negative Surface Charge Linked to Glycosylated Membrane Proteins.* Biochimica et Biophysica Acta (BBA)-Biomembranes, 2013. **1828**(2): p. 249-259.

230. Bechinger, B., *Rationalizing the Membrane Interactions of Cationic Amphipathic Antimicrobial Peptides by Their Molecular Shape.* Current Opinion in Colloid & Interface Science, 2009. **14**(5): p. 349-355.

231. Wu, M. and R.E. Hancock, *Improved Derivatives of Bactenecin, a Cyclic Dodecameric Antimicrobial Cationic Peptide.* Antimicrobial Agents and Chemotherapy, 1999. **43**(5): p. 1274-1276.

232. Illya, G. and M. Deserno, *Coarse-grained Simulation Studies of Peptide-induced Pore Formation.* Biophysical journal, 2008. **95**(9): p. 4163-4173.

233. Liu, X., et al., *Mechanism of Anticancer Effects of Antimicrobial Peptides.* Journal of Fiber Bioengineering and Informatics, 2015. **8**(1): p. 25-36.

234. Su, Y., S. Li, and M. Hong, *Cationic Membrane Peptides: Atomic-level Insight of Structure–activity Relationships From Solid-state NMR.* Amino Acids, 2013. **44**(3): p. 821-833.

235. Bierbaum, G. and H. Sahl, *Autolytic System of Staphylococcus Simulans 22: Influence of Cationic Peptides on Activity of N-acetylmuramoyl-L-alanine Amidase.* Journal of Bacteriology, 1987. **169**(12): p. 5452-5458.

236. Marchand, C., et al., *Covalent Binding of the Natural Antimicrobial Peptide Indolicidin to DNA Abasic Sites.* Nucleic Acids Research, 2006. **34**(18): p. 5157-5165.

237. Subbalakshmi, C. and N. Sitaram, *Mechanism of Antimicrobial Action of Indolicidin.* FEMS Microbiology Letters, 1998. **160**(1): p. 91-96.

238. Otvos, L., et al., *Interaction Between Heat Shock Proteins and Antimicrobial Peptides.* Biochemistry, 2000. **39**(46): p. 14150-14159.

239. Kragol, G., et al., *The Antibacterial Peptide Pyrrhocoricin Inhibits the ATPase Actions of DnaK and Prevents Chaperone Assisted Protein Folding.* Biochemistry, 2001. **40**: p. 3016-3026.

240. Lamichhane, U., et al., *Peptide Translocation Through the Mesoscopic Channel: Binding Kinetics at the Single Molecule Level.* European biophysics journal, 2013. **42**(5): p. 363-369.

241. Mechler, A., et al., *Specific and Selective Peptide-membrane Interactions Revealed Using Quartz Crystal Microbalance.* Biophysical journal, 2007. **93**(11): p. 3907-3916.

242. Wang, K.F., et al., *Characterization of Supported Lipid Bilayer Disruption by Chrysophsin-3 using QCM-D.* The Journal of Physical Chemistry B, 2011. **115**(51): p. 15228-15235.

243. Marcotte, I., et al., *Interaction of Antimicrobial Peptides From Australian Amphibians With Lipid Membranes.* Chemistry and Physics of Lipids, 2003. **122**(1-2): p. 107-120.

244. Lau, T.-L., et al., *Amyloid-β Peptide Disruption of Lipid Membranes and the Effect of Metal Ions.* Journal of Molecular Biology, 2006. **356**(3): p. 759-770.

245. Sani, M.-A., A.P. Le Brun, and F. Separovic, *The Antimicrobial Peptide Maculatin Self Assembles in Parallel to Form a Pore in Phospholipid Bilayers.* Biochimica et Biophysica Acta (BBA)-Biomembranes, 2020. **1862**(5): p. 183204.

246. Kinouchi, H., M. Onishi, and H. Kamimori, *Lipid Membrane-binding Properties of Daptomycin using Surface Plasmon Resonance.* Analytical Sciences, 2013. **29**(3): p. 297-301.